VELAMMAL MEDICAL COLLEGE
HOSPITAL AND RESEARCH INSTITUTE
MADURAI - 625009

Details of papers published in the journals notified on UGC – CARE list in the UGC website 2021

S.N	UGC website/ Scopus/ Web of Science/ PubMed	Publication type	Publication title	Author name	Journal name	Year
1.	Scopus	Original article	Inferior Alveolar Nerve Canal Segmentation by Local Features based Neural Network Model	Maheswari, P.U., Banumathi,A., Ulaganathan, G., Yoganandha, R	IET Image Processing	2021
2.	34447159	Original article	Potential Antibacterial efficacy of garlic extract on Staphylococcusaureus, E.coli&K.Pneumoniae: Anin vitro study	Abidullah M, Jadhav P, Sujan SS, Shrimanikandan AG, Reddy CR, Wasan RK	Journal of pharmacy and bioallied sciences	2021
3.	34447191	Original article	Anaesthetic Efficacy of Lidocaine&Articaine in inferior alveolar nerve block complainedwith buccal infiltration in patients with irreversible pulpitis	Gandhi SA, Das S, Das A, Agnihotri Y, Mohan RV, Dasu Subramanian VR	Journal of pharmacy and bioallied sciences	2021
4.	33332556	Original article	Vanishing left bundle branch potential during physiological pacing	Ponnusamy SS	Europace	2021
5.	33205843	Original article	Uncommon modes of initiation of 'A on V' narrow QRS tachycardia: What are the mechanisms?	Bansal R, Vadivelu R, Lokhandwala Y	Pacing and clinical electrophysiology : PACE	2021
6.	32452718	Original article	Impact of plaque burden and composition on	Reddy S, Rao K R, Kashyap JR, Kadiyala	Acta cardiologica	2021

Dean
Velammal Medical College Hospital and Research Institute
'Velammal Village'
Madurai-Tuticorin Ring Road
Anuppanadi, Madurai (TN)-625 009

			coronary slow flow in ST-segment elevation myocardial infarction undergoing percutaneous coronary intervention: intravascular ultrasound and virtual histology analysis	V, Reddy H, Malhotra S, Daggubati R, Kumar S, Soni H, Kaur N, Kaur J, Ramalingam V		
7.	33068721	Case Reports	Ventricular tachycardia as the presenting feature in two patients with cardiac lipoma and cardiac fibroma	Vadivelu R, Bohora S, Bachani N, Sharma R, Panicker G, Lokhandwala Y	Indian pacing and electrophysiology journal	2021
8.	34466272	Review article	How to implant His bundle and Left bundle branch pacing leads – Tips and Pearls	Ponnusamy SS, Vijayaraman P	Cardiac failure review	2021
9.	33865523	Original article	How significant is the radiation exposure during electrophysiology study and ablation procedures for supraventricular tachycardia?	Bagchi A, Vadivelu R, Rathi C, Chavan BG, Lokhandwala Y	Indian heart journal	2021
10.	34157426	Original article	QRS alternans during right ventricular pacing while ablating a concealed left sided accessory pathway	Bansal R, Vadivelu R, Sternick EB, Lokhandwala Y	Indian pacing and electrophysiology journal	2021
11.	34252793	Review article	Electrocardiography guided left bundle branch pacing	Ponnusamy SS, Vijayaraman P	Journal of Electrocardiology	2021
12.	33812829	Original article	Left bundle branch block induced cardiomyopathy: Insights from left bundle branch pacing	Ponnusamy SS, Vijayaraman P	JACC. Clinical electrophysiology	2021

Dean
Velammal Medical College Hospit
and Research Institute
'Velammal Village'
Madurai-Tuticorin Ring Road
Anuppanadi, Madurai (TN)-625 009

13.	33858179	Original article	Template Beat: A novel marker for left bundle branch capture during physiological pacing	Ponnusamy SS, Ganesan V, Syed T, Balasubramanian S, Vijayaraman P	Circulation. Arrhythmia and electrophysiology	2021
14.	32623624	Original article	Mid-term Feasibility, safety and outcomes of left bundle branch pacing – single center experience	Ponnusamy SS, Muthu G, Kumar M, Bopanna D, Anand V, Kumar S.	Journal of interventional cardiac electrophysiology : an international journal of arrhythmias and pacing	2021
15.	33484212	Original article	Cardiac troponin release following left bundle branch pacing	Ponnusamy SS, Patel NR, Naperkowski A, Subzposh FA, Vijayaraman P.	Journal of cardiovascular electrophysiology	2021
16.	33714396	Original article	Feasibility, safety and outcomes of left bundle branch pacing in octogenarians	Ponnusamy SS, Bopanna D, Syed T, Muthu G, Kumar S.	Indian heart journal	2021
17.	33602393	Original article	Left bundle branch area pacing for cardiac resynchronization therapy: Results from international LBBAP collaborative study group	Pugazhendhi Vijayaraman, ShunmugaSundaram Ponnusamy, Óscar Cano, Parikshit S. Sharma, Angela Naperkowski, Faiz A. Subsposh, Pawel Moskal, Agnieszka Bednarek, Alexander R.	JACC: Clinical Electrophysiology	2021

Dean
Velammal Medical College Hospital
and Research Institute
'Velammal Village'
Madurai-Tuticorin Ring Road
Anuppanadi, Madurai (TN)-625 009

				Dal Forno, Wilson Young, Sudip Nanda, Dominik Beer, Bengt Herweg, Marek Jastrzebski		
18.	34339851	Original article	Left bundle branch optimized cardiac resynchronization therapy: results from an international LBBAP collaborative study group	Jastrzębski M, Moskal P, Huybrechts W, Curila K, Sreekumar P, Rademakers LM, Ponnusamy SS, Herweg B, Sharma PS, Bednarek A, Rajzer M, Vijayaraman P	Heart Rhythm	2021
19.	34332877	Original article	Bundle branch re-entrant ventricular tachycardia during left bundle branch pacing	Ponnusamy SS, Vijayaraman P	JACC: Clinical Electrophysiology	2021
20.	34245402	Original article	Unmasking of left bundle branch potential in left bundle branch block during physiological pacing	Ponnusamy SS, Vijayaraman P	Journal of interventional cardiac electrophysiology : an international journal of arrhythmias and pacing	2021
21.	34245478	Case report	Late dislodgement of left bundle branch pacing lead and successful extraction	Ponnusamy SS, Vijayaraman P	Journal of cardiovascular electrophysiology	2021

Dean
Velammal Medical College Hospital
and Research Institute
'Velammal Village'
Madurai-Tuticorin Ring Road
Anuppanadi, Madurai (TN)-625 009

VELAMMAL MEDICAL COLLEGE
HOSPITAL AND RESEARCH INSTITUTE
MADURAI - 625009

22.	34080102	Original article	Segmental fascicular block during physiological pacing	Ponnusamy SS, Vijayaraman P	Journal of interventional cardiac electrophysiology : an international journal of arrhythmias and pacing	2021
23.	34035980	Original article	Left Posterior Fascicular Pacing	Ponnusamy SS, Syed T, Kumar S	The Journal of innovations in cardiac rhythm management	2021
24.	32918667	Original article	Unmasking of pathological Q waves by left bundle branch pacing	Ponnusamy SS, Vijayaraman P	Journal of interventional cardiac electrophysiology: an international journal of arrhythmias and pacing	2021
25.	33146852	Original article	Concealed left bundle branch potential during physiological pacing	Ponnusamy SS, Vijayaraman P	Journal of interventional cardiac electrophysiology: an international journal of arrhythmias and pacing	2021

Dean
Velammal Medical College Hospital
and Research Institute
'Velammal Village'
Madurai-Tuticorin Ring Road
Anuppanadi, Madurai (TN)-625 009

Received: 21 July 2021 | Revised: 23 September 2021 | Accepted: 25 October 2021

DOI: 10.1049/ipr2.12375

IET Image Processing

The Institution of Engineering and Technology WILEY

ORIGINAL RESEARCH PAPER

Inferior alveolar nerve canal segmentation by local features based neural network model

P. Uma Maheswari[1] | A. Banumathi[2] | G. Ulaganathan[3] | R. Yoganandha[4]

[1] Research Scholar, Department of ECE, Thiagarajar College of Engineering, Madurai, Tamil Nadu, India

[2] Department of ECE, Thiagarajar College of Engineering, Madurai, Tamil Nadu, India

[3] Department of Oral and Maxillofacial Surgery, CSI College of Dental Science and Research, Madurai, Tamil Nadu, India

[4] Department of Craniofacial Surgery, Dentistry & Implantology, Velammal Medical College Hospital & Research Institute, Madurai 15, Tamil Nadu, India

Correspondence
P. Uma Maheswari, Research Scholar, Department of ECE, Thiagarajar College of Engineering, Madurai, Tamil Nadu, India.
Email: umamahes.p@gmail.com

Funding information
Council of Scientific & Industrial Research, Grant/Award Number: 08/237(0015)/2018-EMR-I

Abstract

The detection of Inferior Alveolar Nerve Canal (IAC) plays major and crucial role in dental surgical procedures to avoid damage to IAC during the course of treatment. Exact visualization and detection of IAC is necessary for precise surgery planning to prevent IAC damage. The proposed method comprises of three stages namely, novel edge enhancement, candidate classification and candidate pixel clustering to detect the IAC. For better visualization of IAC, initially the edges of dental OPG images are enhanced using a novel structural filter. Candidate regions are selected from the enhanced image by the proposed Multi Hidden Layer Extreme Learning Machine Artificial Neural Network (MELMANN) model driven by combined regional features such as Histogram of Gradients (HOG), Local Binary Pattern (LBP) and Gray Level Co-occurrence Matrix (GLCM). Consequently the candidate region pixels are clustered by a Self-Organising Map-based Neural Network (SOM - NNC) along with active contour method to detect the IAC completely. Experimental results show that this method effectively delineated the IAC with the Dice coefficient of 0.854 ± 0.05.Therefore, the proposed method has high potential in clearly visualizing IAC to avoid neurological sensory disorders in oral and maxillofacial surgery and implantology and it provides better prediagnostic approach to the surgeons.

1 | INTRODUCTION

The dentists deal with a wide range of complex issues related to densely innervated territory during surgery. One of the core sensory nerves in the maxillofacial region is the Inferior Alveolar Nerve (IAN) which needs additional attention at the time of surgery to avoid serious medical complications. IAN navigates through the Inferior Alveolar Nerve Canal (IAC) and supply sensation to teeth, delicate tissues, and other muscles. Since the IAN is located within the IAC, it can be analysed as part of the IAC's radiographic evaluation. Damage to IAC results in partial numbness in the lower lip, tongue, chin and buccal mucosa or complete loss of sensation, spontaneous, stimulus-evoked pain, allodynia, neuropraxia, neurotmesis, axonotmesis and hyperalgesia [1, 2]. In most cases, total recovery of IAC injury takes 6 to 8 weeks, but it can take up to 24 months in serious cases. So it is mandatory that the dental implants and other dental surgeries have to be planned based on location of IAC to avoid such complications [3, 4].

Ashok Ramadorai et al. [5] have audited the third molar sites and have observed distorted sensation of the IAN after the surgery. Gerardo La et al. [6] have reported 8.4% of nerve damage happens during third molar surgery. Alteration of sensation is one of the serious difficulties that happen after implant placement in the posterior mandible. The prevalence of such a complication has been accounted as high as 13% [7].This difficulty may be perhaps the most undesirable encounter for both the patient and the dental specialist, so every preventative measure should be taken to evade it. While injury to the IAC during the procedures of dental and oral and maxillofacial surgery is a serious complication, it is more significant to understand how to treat it. Since its structure isn't well defined and also connects to adjacent hollow spaces it is difficult to detect the outline of IAC. Figure 1a and b shows few samples of dental OPG images from

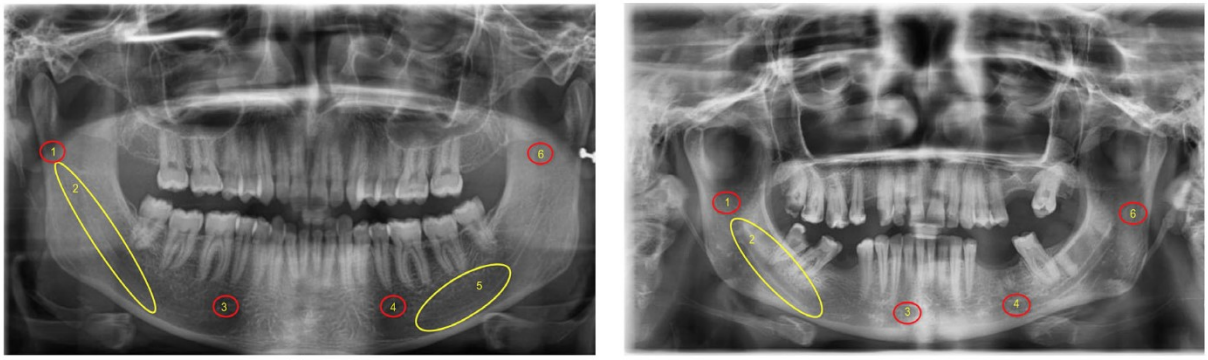

FIGURE 1 (a, b). 1,6—Mandible Foramen, 3,4—Mental Foramen, 2—Structure of IAC, 5—Deficient portion in IAC in panoramic dental OPG images

the dataset, with the entire structure of the IAC labelled as 2, incomplete/deficient portion of IAC labelled as 5, and mandible and mental foramen regions are labelled as (3,4) and (1,6). In a dental image-based surgical planning like implant placement, third molar surgery, muscle implantation, and lower dentistry procedure performed in Oral and maxillofacial treatment centres/clinics, the dental surgeon must pre-diagnose the dental images obtained from various imaging modalities. In all these treatments, prime importance has to be given in segmenting or detecting the position of Inferior Alveolar Nerve Canal (IAC) in posterior mandibular surgical procedures. Any misjudgement in the segmenting the IAC results in nerve injury to the patients while the doctor performs treatment. So, IAC segmentation of IAC plays vital role in an implant osteotomy or implant placement. Despite the huge success rate in the surgery of dental implantology, several complications have been recorded at the time of surgery in the following situations.

- Deficient information about IAC due to imaging modality.
- Improper detection of IAC region in panoramic dental image.
- Poor understanding of the anatomy of the mandibular region.

Therefore a solution based on medical image processing is required to visualize, locate or detect IAC so that the anatomical structure of the mandibular region is understood properly. In this paper, Section 2 presents the literature on IAC detection. Section 3 deals with the methods utilized in the execution of the automatic IAC detection technique which comprises preprocessing, HOG,LBP, and GLCM based feature extraction, MELM based ANN(Artificial Neural Network) classification and SOM (Self Organizing Maps)-based ANN clustering with chan vese active contour. Section 4 presents the performance results of feature-based classifier and Section 5 gives the conclusion of the study.

2 | LITERATURE REVIEW

During the installation of dental implants, injury to the inferior alveolar nerve might be a significant problem. Clinicians must recognise and rule out common etiological variables that cause nerve damage. To avoid nerve sensory abnormalities, adequate presurgery planning, quick diagnosis, and treatment are essential. In the treatment of inferior alveolar nerve injury caused by endodontic sealer extrusion, a non-surgical method comprising prednisone and pregabalin is a promising alternative. Alternatively, surgical procedures would require a traditional two-dimensional panoramic radiograph, known as an orthopantomogram (OPG), which is the most commonly utilised imaging modality for assessing third molars and their proximity to the mandibular canal. Previous research have established that definite radiographic features on OPGs, such as narrowing of the mandibular canal, darkening of the root, discontinuity of the white line, are risk factors for IAN injuries. To avoid injury to the alveolar nerve, it becomes necessary to localize/segment IAC.

Several automated and semi-automated techniques have been introduced earlier and have mainly focused on segmenting or identifying IAC region based on the anatomical and computer extraction method using CBCT and OPG images such as active appearance model [8, 9], adaptive region growing [10, 11], gradient vector flow line tracking snake model [12], adaptive diffusion flow active contour [13], level set method [14], line tracking algorithm [15, 16], and modified Dijkstra's algorithm [17, 18]. The outcomes of all these works depend heavily on seed point segmentation, which result in imperfect IAC delineation and is validated on a small dataset. Research on IAC detection can be categorized into anatomical and computerized image processing methods.

2.1 | Anatomical methods

Identifying the location of Mandibular Foramen (MF) plays an important role in IAC detection as the position of IAC varies with respect to MF and Mental Foramen. Narayan et al. [19] investigated the position of the MF concerning the anatomical planes over the ramus of the mandible and also the one-fourth on the medial surface of the ramus of the mandible to locate the IAC. Similarly, two bony landmarks relative to MF are examined to assist the procedures of Inferior Alveolar Nerve Block (IANB) [20]. Dentists can also use internal oblique ridge,

Sigmoid notch, inferior border, and temporo mandibular joints as a reference point for planning different techniques of IANB. Four different types of IAC positions are identified in 96 dried mandible regions using radiographic images [21]. Pogrel et al. investigated the arrangement of IAC in 8 preserved human hemi mandibles to avoid surgical complications [22]. Kieser et al. examined 107 cadaveric edentulous mandible regions and concluded that the IAN was located in the lower mandible for more than 70% of the humans [23]. Kim et al. revealed the topography of IAC in 3D mandibular canal reconstruction [24]. These methods identify the position of IAC by analysing edentulous mandible region foramen details. This may lead to incorrect analysis about the location of IAC.

2.2 | Image processing methods

Image processing methods use dental images taken from different imaging modalities to analyse risk factors related to dental treatments. Researchers and doctors have suggested various segmentation methods to overcome the risk factors in dentistry. Semi-automatic land marking for jaw tissue segmentation and an active appearance model for IAC detection in 2D slices in CT data have been proposed [8, 9]. Yau et al. [10] proposed a semi-automatic method for the identification of IAC using region growing in 2D slice mandible images and extended work of this technique has been presented by Zachow et al. [11]. Gabriella Tognola et al. [12] presented a 3D reconstruction of mandibular nerve by gradient vector flow snake method and Chadaporn Keatmanee et al. [13] developed an adaptive diffusion flow active contour model for IAC segmentation. Hanssen et al. [14] suggested a level set approach for segmenting IAC in CBCT data. Toshiaki Kondo et al. [15] presented a 3D line tracking model for computer based IAC extraction and the fast marching based line tracking was developed to segment the IAC [16]. Stein et al. [17] developed a balloon inflation method and Dijkstra algorithm for segmenting the IAC in CT data. Kainmueller et al. [18] suggested a combined technique of statistical shape modelling and Dijkstra's optimization algorithm locate the nerve in a 3D image. A statistical texture feature-based IAN identification in panoramic radiographic images are proposed [25]. Morphological skeletonization and Hough transform-based IAC detection in CBCT images are presented [26]. The majority of previous studies on IAC identification needed user interference, such as the indication of the IAC initial seed points location or as a manual trace. These algorithms also fail in the case of mandibular osteoporosis.

Even with advanced imaging technology such as CT, CBCT and OPG, distinguishing/segmenting the IAC from surrounding structures can always be challenging. Although CBCT, CT and OPG (Orthopantomogram) have shown to be comparable to standard imaging modalities for depicting the IAC, the appearance of this structure can vary substantially, within the same person. Most existing algorithms were primarily concerned with locating the foramen on CT [8–11] and CBCT [13, 14] images in order to segment the IAC path. If there is insufficient information in the imaging, detecting foramen itself is a difficult task. Statistical shape and texture model and Dijkstra's method cannot specifically segment the tissue with weak boundary because the pixel inside the region and on the boundary will have similar intensity. When cross-sectional images are analysed individually, the distinction of the canal from its surroundings becomes less obvious towards the mental foramen region. The radiographic appearance usually involves a radiolucent zone lined by superior and inferior borders. The cortication of the canal is variable, which may explain why in some cases the IAC is not well-visualized. Therefore, the aim of this study was to determine the IAC under poor visibility.

The main reason for IAN damage is the improper localization of the Inferior Alveolar nerve Canal (IAC) and improper understanding of the anatomy of the mandibular region. This paper attempts to provide quality improvement of IAC edges and localization of IAC using feature driven neural network and clustering based approach. The major contributions are

- Proposal of a non-foramen based IAC segmentation.
- Introduction of a definite novel structural mechanism to enhance ROI.
- Selection and fusion of complimentary features like HOG, LBP and GLCM for IAC classification.
- Pixel based feature discrimination by MELMANN.
- SOM-NNC based weak structures (IAC) localization.
- Performance comparison of proposed classification with state of art techniques.

3 | METHODOLOGY

The flow diagram of the proposed local feature driven ANN model for IAC localization in dental OPG images is shown in Figure 2. The dental OPG images are enhanced by a novel filtering element. The shape and texture features are analysed by HOG, LBP and GLCM and these features are fused to get the hybrid feature vectors for candidate classification performed by MELMANN. Then the input image is clustered with the help of classified candidate IAC pixels using SOM and active contour model for IAC detection.

3.1 | Pre-processing

The resolution of dental OPG is not as detailed as intra-oral radiographs and the soft tissue regions are not clearly shown to the observer. Non uniform illumination also affects the quality of OPG images. To overcome this issue and to enhance the soft tissue regions in OPG images, a novel structural filtering technique in Fourier space domain is designed.

This is attained by summing up the top hat filtered image $T(I_d)$ with original image $I_d(m, n)$ and subsequently subtract that image with bottom hat filtered image $B(I_d)$ is shown in (1)–(4).

$$T\ (I_d) = I_d\ (m, n) - \ (I_d\ (m, n)\ oSF) \tag{1}$$

$$B\ (I_d) = (I_d\ (m, n) \bullet SF) - \ I_d\ (m, n) \tag{2}$$

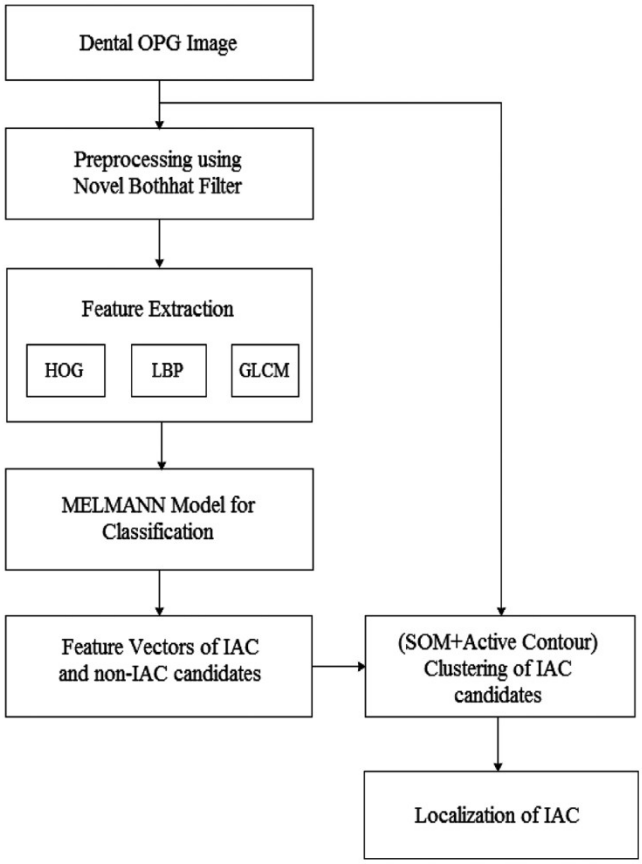

FIGURE 2 Flow diagram of proposed (local feature based neural network) methodology

0	1	1	0	0
1	0	1	1	0
1	1	0	1	1
0	1	1	0	1
0	0	1	1	0

FIGURE 3 Novel structural filter (SF)

where o represents the opening operation and • represents the closing operation

$$T_{I_d}(I_d) = I_d\ (m,n) + T(I_d) \tag{3}$$

$$E\ (m,n) = T_{I_d}\ (I_d) - B(I_d) \tag{4}$$

Subsequently, a novel structural filter (SF) as shown in Figure 3 similar to the nerve canal structure is presented and this is convolved with the original image to emphasize the edges of IAC region $E(m,n)$.

This technique highlights both bright structures and dark structures in an image without losing the essential information.

3.2 | Feature extraction

The IAC region is distinguished by its shape and soft tissue structure, so features extracted using a mixture of HOG [27, 28], LBP [29, 30], and GLCM [31] are considered for classification. The HOG descriptor describes explicates the structure or the shape of an object. Shape of the IAC region and the mandibular region looks anatomically similar and gives out same result. So to overcome this issue, apart from using HOG for extracting shape features subsequently, LBP and GLCM for texture feature to identify the IAC perfectly. The combination of these approaches significantly reduces the training and execution time compared to other state of art techniques.

3.2.1 | Histogram of gradient (HOG)

HOG gives good results to identify objects even from the cluttered background without using any segmentation algorithm. Hence it is highly suitable for the analysis of dental OPG images. HOG can give both edge magnitude and direction by extricating the gradient and orientation of the edges [27]. The significant benefit of HOG is to localize the shape and object appearance in an image. The shape in an image is expressed by the distribution of edge directions or intensity gradients [28].

Initially, the image $E_b(m,n)$is alienated into small connected regions called cells, and a histogram of gradient directions is computed for each pixel within the cell. The horizontal gradient 'g_m'by convolving the image with 1D Kernel $(1D\ kernel)_h$ as by Equation (5) and the vertical gradient 'g_n'by convolving the image with 1D Kernel$(1D\ kernel)_v$ as by (6)

$$g_m = E_b\ (m,n) * (1D\ kernel)_h \tag{5}$$

$$g_n = E_b\ (m,n) * (1D\ kernel)_v \tag{6}$$

Then the magnitude of gradient (HOG_{mg}) and the directional (orientation) (HOG_D) are calculated by using (7) and (8)

$$HOG_{mg} = \sqrt{{g_m}^2 + {g_n}^2} \tag{7}$$

$$HOG_D = arctan\ g_n/g_m \tag{8}$$

Pixel orientation for each pixel in the cell is calculated and values are updated in the orientation bin ranging from 0 to 180 with the step of 20. Orientation bin values are computed by subtracting the orientation value with the bin value and divide the value with the difference between the bins. The orientation bin value is multiplied with the magnitude value to get the values of the histogram of gradients for each cell. All the gradient bin values in each row are assigned to represent the whole image features F_{HOG} and normalize the gradient $(F_{HOG})_N$ to reduce the lighting variations. The maximum value of each normalized

feature value is taken into account as one of the feature vector for classification by (9)

$$HOG_{max} = \max\left((F_{HOG})_N\right) \tag{9}$$

3.2.2 | Local binary pattern (LBP)

Shape features alone do not provide enough information for identifying the object in an image. Texture feature also has to be considered for better identification of object and that is achieved by LBP. This operator converts an image into an image with integer labels that characterize the image's small-scale representation. It is a simple and structured texture operator which labels the pixels of an image by thresholding the neighbourhood of every pixel and the result is taken as a binary number [29].

The first step for creating the LBP feature vectors is to divide the preprocessed dental OPG image into cells. For every pixel in a cell, match up to each pixel of its eight neighbours. Consider the pixels along a circle, where the centre pixel's value is equal and greater than the neighbours value, assign "1". Otherwise, assign "0". This provides an 8-digit binary number and converts that number into decimal form [30]. Subsequently, compute the histogram over the cell and normalize it. Then concatenate the histograms of all the cells. This gives a feature vector for the entire preprocessed dental OPG image. This histogram can be seen as a feature vectored image. Given a pixel in the image$E_b(m, n)$, and LBP code is calculated by comparing it with its neighbours using (10)

$$E_b(LBP_{P,R}) = \sum_{p=0}^{p-1} s(g_p - g_c)2^p, \tag{10}$$

$$\text{where } s(x) = E_b(x) = \begin{cases} 1, & x \geq 0 \\ 0, & x < 0 \end{cases}$$

where 'g_c'is the gray value of the central pixel, 'g_p' is the intensity value of its neighbouring pixels, 'P' is the number of involved neighbours, and 'R' is the radius of the neighbourhood. For an image $E_b(m, n)$, the maximum value in LBP is taken as the feature $LBP_{max}$and that is given as one of the input feature vectors for classification using (11)

$$LBP_{max} = \max\left(E_b(LBP_{P,R})\right) \tag{11}$$

3.2.3 | Gray level co-occurrence matrix (GLCM)

LBP provides local textural details of an image as the texture of IAC region also has to be analysed in terms of spatial relationship between the pixels and that is achieved by Gray-level co-occurrence matrices (GLCM) [31]. It extracts the second-order textural information from an image. The combination of textural information significantly improves the identification rate than when they are used independently. The GLCM of an image is characterized as a matrix of frequencies at which two pixels, isolated by a specific vector, arise in the image. The allocation of the GLCM matrix depends on the spatial and angular association flanked by pixels. Varying the image vector results in taking out different texture characteristics of the image. In this work, the texture features calculated using GLCM are contrast(C_{E_b}), correlation(CC_{E_b}) with mean 'μ', Energy(E_{E_b}), homogeneity(H_{E_b}). These parameters are calculated for each block $E_b(m, n)$ in the preprocessed dental OPG images and it is taken as the final feature vector given for classification. It is given in (12)–(15).

$$C_{E_b} = \sum_{m,n=0}^{N-1} E_{b(m,n)}(m-n)^2 \tag{12}$$

$$CC_{E_b} = \sum_{m,n=0}^{N-1} E_{b(m,n)}\,(m-\mu)\,(n-\mu)\,/\sigma^2 \tag{13}$$

$$H_{E_b} = \sum_{m,n=0}^{N-1} E_{b(m,n)}/1 + (m-n)^2 \tag{14}$$

$$E_{E_b} = \sum_{m,n=0}^{N-1} \left(E_{b(m,n)}\right)^2 \tag{15}$$

3.3 | Classification using MELMANN model

The feature fusion allows thoroughly describing IAC image features and producing compact representation of incorporated image features to improve the detection accuracy. The features derived from HOG, LBP, and GLCM are fused together and used as a function vector by an MELM-based ANN Classifier to distinguish candidate IAC and non-IAC regions. ANN is a bunch of input, intermediate, and output layers in which weight is allied with each layer. Learning of neural organization is performed by changing the weight of the associated layer. It can be categorized as a recurrent network and feed-forward network [32].

Extreme Learning Machines (ELM) belongs to feed forward neural networks with a single layer or multiple layers of randomly assigned hidden nodes and the output weights of hidden nodes are usually learned in a single step, which is a basic need for linear model learning [33].However, the proposed algorithm uses MELMANN [34] with multiple hidden layers is shown in Figure 4. The learning time of MELM chiefly depends on calculating the Moore-Penrose inverse matrices of the hidden layer output analytically with randomly chosen weights and bias. Despite the fact that MELM takes a long time to run, its experimental findings on regression and common classification problems have shown that it outperforms other ELM variants in terms of average accuracy.

The proposed MELMANN algorithm uses feed forward network with the following modelling parameters to classify the candidate IAC and non-IAC region. Continuous log-sigmoidal function is chosen as activation function for the network architecture. Testing a different number of neurons in the hidden layer produces the best architecture. The (6 – 20 – 2) architecture was chosen for this problem because it offers reliable

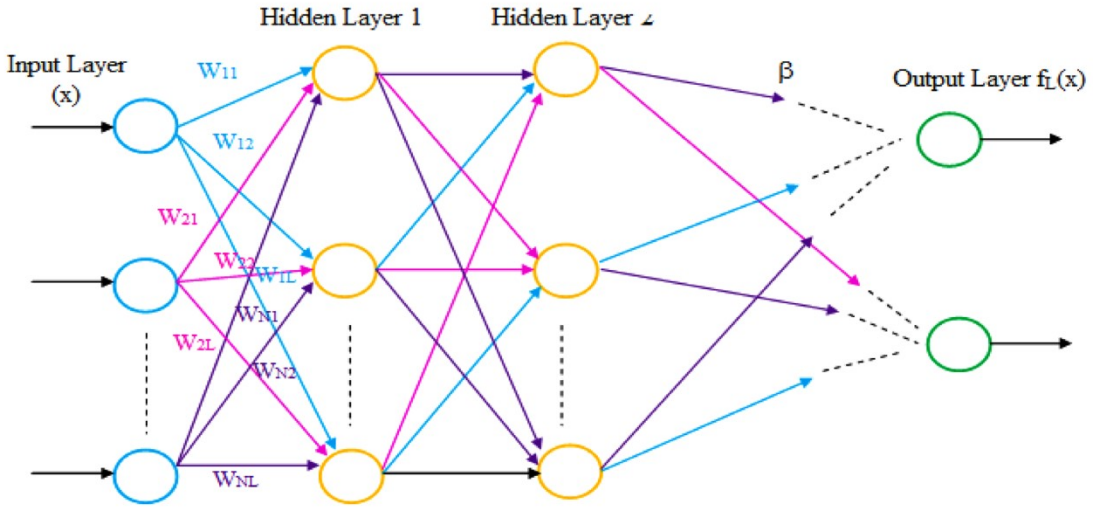

FIGURE 4 MELMANN model

TABLE 1 The MELMANN network modelling parameters

Training algorithm	Transfer function	Network architecture	Training data	Verifying data	Testing data
MELMANN	Continuous Log –Sigmoid	6 - 20 - 2	17248	3234	3234

results (6 input function – 20 hidden layers – 2 outputs) is shown in Table 1.

For classifying the candidate IAC region and non-IAC region, the input samples and the labelled samples are chosen for training sample dataset. Let the training sample dataset be represented as $\{X, T\} = \{(x_j \ldots\ldots., x_N), T\}$where the input samples are $X = (x_1, x_2, x_3, x_4, x_5, x_6) = (HOG_{max}, LBP_{max}$,Contrast, Correlation, Energy, Homogeneity) and the labelled samples are (T) (candidate IAC region and Non-IAC region). Each hidden layer has multiple hidden neurons 'L' with continuous log – sigmoid activation function $g(x)$. The weights 'w' between the input layer and the first hidden layer and the bias 'b' of the first hidden neurons are initialized. For 'N' distinct samples the MELM with zero error is modelled as

$$f_L(x) = \sum_{i=1}^{L} \beta_{ij} H_i = \sum_{i=1}^{L} \beta_{ij}\, g_i\left(w_{ij} * x_j + b_i\right) = T(j = 1, 2, \ldots\ldots N) \tag{16}$$

where 'L' is a number of hidden units, 'N' is a number of training samples and 'β' is the weight vector between the hidden layer and the output. The hidden layer is calculated by

$$H_1 = g_1\ (w_{11} * x_1 + b) \tag{17}$$

where H is the hidden layer and it is expressed in (18)

$$H_i = \begin{pmatrix} g_i(w_{11} * x_1 + b_1) & \cdots & g_i(w_{1L} * x_1 + b_L) \\ \vdots & \ddots & \vdots \\ g_i(w_{N1} * x_N + b_1) & \cdots & g_i(w_{NL} * x_N + b_L) \end{pmatrix}_{N\ X\ L} \tag{18}$$

Then the weight between the hidden layer and the training data matrix for the output is calculated and it is defined in (19)

$$H_i\, \beta_{ij} = T \tag{19}$$

$\beta_{ij}$is calculated by changing the above (19) as

$$\beta_{ij} = H_i^T\, T \tag{20}$$

'β' and 'T' are expressed as

$$\beta_{ij} = \begin{pmatrix} \beta_{11}^T \\ \\ \beta_{LN}^T \end{pmatrix}_{L\ X\ m} \qquad T = \begin{pmatrix} t_1^T \\ \\ t_L^T \end{pmatrix}_{N\ X\ m}$$

The predictable output of the second layer is then determined by (21) and the process is repeated from (18) to (20) to determine the estimated output of the subsequent layers.

$$H_2 = T{\beta_{LN}}^T \tag{21}$$

The final output 'T'classifies the candidate IAC and non IAC region.

3.4 | Clustering by SOM-NNC

Detection of IAC mainly depends on the neighbourhood values located around the nerve features classified by MELMANN. SOM-NNC [35] provides best clustering output

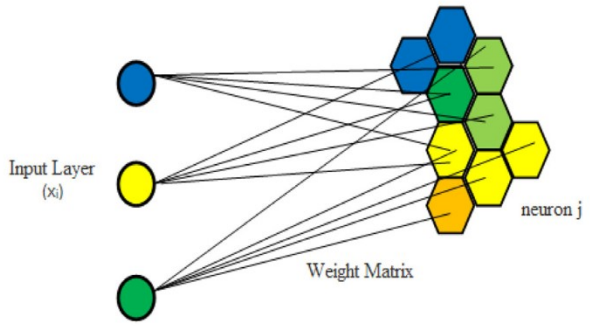

FIGURE 5 Clustering by SOM-NNC model

by the neighbourhood values located around the candidate IAC region. SOM is a matrix of neurons that adjust to the topological state of a dataset, permitting us to picturize large datasets and recognize potential clusters is shown in Figure 5. It learns the classified feature datasets of the candidate IAC region by repeatedly moving its neurons closer to the candidate IAC pixel points. It is used here to cluster the candidate IAC pixels from the Nerve feature datasets.

The weights (w_{ij}) are initialized for each neuron j. For each input pixel x (located in candidate IAC region) and each neuron j, (neighbouring pixel of candidate IAC region) are computed the Euclidean distance by (22).

$$D(j)_{min} = \sqrt{\sum_{i=1}^{m} (x_i - w_{ij})^2} \tag{22}$$

For winner neuron j (i.e., pixels) weight within a specified neighbourhood of J (candidate IAC region) weight is updated by (23)

$$W_{ij}\ (new) = W_{ij}\ (old) + \alpha(x_j - W_{ij}\ (old)) \tag{23}$$

The radius of the topological neighbourhood are reduced at specified times and update the learning rate α. Now there is one neuron with optimum output per each input pixel and that neuron acts as a hit value. The higher the hits value, the neuron represents more input pixels. Every neuron of SOM represents a group of input feature patterns in a 2D map. Now the input feature patterns (pixels for image) can be clustered through clustering the neurons themselves. To combine these clusters and give complete region of IAC chan vese active contour model is utilized.

4 | RESULTS AND DISCUSSION

In this work, a dataset with 220 dental OPG images has been used to assess the performance of candidate feature classification and candidate pixel clustering to identify the IAC region properly. The dataset contains 124 male OPG images available in the age range of 35 to 60 and 96 female OPG images available in the age range of 40 to 65.The algorithm is trained on an NVIDIA supported Intel i3 processor with 4GB of RAM and it is evaluated on MATLAB 2020a platform. The sample dental OPG images were collected from CSI College of Dental Sciences and Research, Madurai, TN, India. The sizes of the images are in different ranges such as 397 × 730, 395 × 735, 402 × 737, etc. Pseudonymization was used on all of the dental OPG images such as OPG1, OPG12 etc. The sample dental OPG images shown in Figure 6a–d (OPG4, OPG18, OPG84, OPG157) are 538 × 266, 300 × 150, 987 × 511, and 1197 × 621 respectively.

Delineation of IAC from these images is more important in the prediagnostic process for appropriate assessment in dental implantology. But, it is difficult to distinguish the IAC region from other gum regions as it has less variation in the intensity level possessed by those regions. Hence to differentiate the IAC region, it is enhanced by bothhat filtering with new structural filter, which has sharpened the IAC region without suppressing the other important details.

The resultant edge enhanced image in the spatial domain is shown in Figure 7a–c. Table 2 shows the performance metrics calculated for the enhanced images. From the analysis, it is observed that the proposed enhancement technique gives better performance than the CLAHE technique. The Mean Square Error (MSE) is the error between the enhanced image and the original image. The proposed method gives less MSE value compared to the CLAHE technique. MSE is indirectly proportional to the PSNR (Peak Signal to Noise ratio). Hence, the higher the PSNR value implies better the quality of an image. Higher cross-correlation value (0.7–0.8), structural similarity index measure value (0.6–0.8), and structural content value (0.8–0.9) of the proposed method indicates the enhanced image maintains the structural information of the original image. The proposed method improves the edge details of the dental OPG image while still maintaining the finer features, according to the experimental results.

After the enhancement with bothhat filtering technique, 220 images from the database were separated into two exclusive sets, 80% is used for training and 20% is used for testing in MELMANN.

Each input image is divided into 32 × 32 blocks. The magnitude and orientation value is calculated for each cell (8 × 8) in the block and it is shown in Figure 8. HOG descriptor algorithm provides 36-D concatenated vectors of all its cells and normalized to an L^2 unit length. Each cell is a 9-bin histogram of HOG and each block contains a feature of nearly 1 × 324 feature vector by HOG to differentiate different structures located in the dental OPG image. The maximum value in each feature block is taken as the HOG feature. It ranges from 0.2–0.4 for the candidate non-IAC region and 0.3–0.45 for the candidate IAC region. Both mandible and IAC regions are furnishing similar feature ranges from 0.3–0.4 because both are having a similar shape shown in Figure 8. So each block in OPG image needs to be further analysed by the different feature vectors. That analysis is done by local texture feature extractor as LBP and the second order texture feature extractor as GLCM. In LBP, the gradient information is depicted as the local binary pattern and it is shown in Figure 9a–c. For the same block used in HOG,

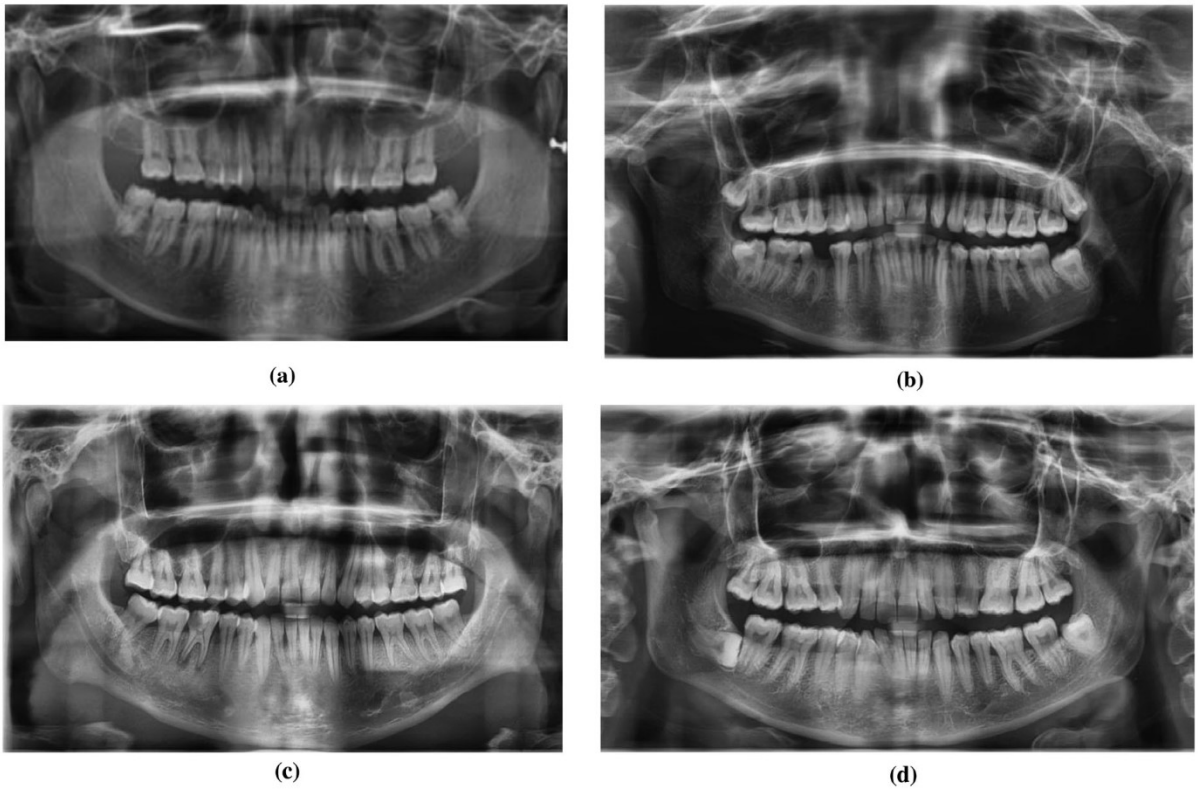

FIGURE 6 (a–d) Sample input images

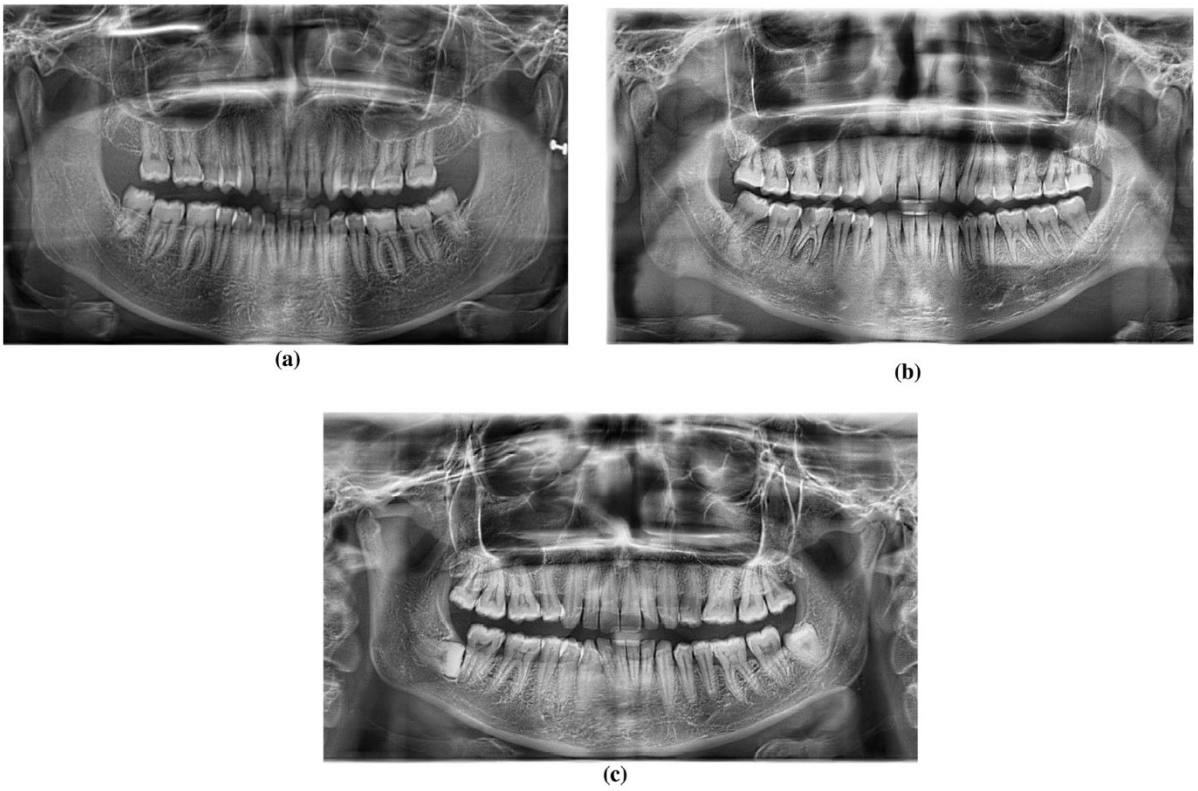

FIGURE 7 (a–c) Preprocessed image by a novel filtering element

TABLE 2 Comparison with CLAHE method

Method	Image	PSNR (db)	SNR	MSE	Cross correlation	MD	NAE	NK	SC	SSIM
Proposed Method (Both Hat with new structuring element)	OPG4	15.3831	10.2031	1882.6719	0.7243	138	0.2775	0.9749	0.9524	0.6774
	OPG18	16.1667	10.7237	1571.8651	0.8042	94	0.2893	1.0791	0.8903	0.6707
	OPG32	15.5575	9.7993	1808.5599	0.7770	134	0.3562	1.1747	0.8635	0.6615
	OPG76	17.6768	9.1247	1641.4653	0.8952	96	0.3897	1.0123	0.8914	0.8757
CLAHE technique	OPG4	11.9615	7.3686	4139.3229	0.6184	223	0.4088	0.9908	0.7320	0.2676
	OPG18	13.5174	8.5309	2892.9514	0.7610	166	0.3883	1.1042	0.7115	0.3352
	OPG32	11.2284	6.4323	4900.4786	0.6464	206	0.5812	1.2266	0.5317	0.2572
	OPG76	12.6154	8.1320	3862.0216	0.6612	189	0.4894	1.0023	0.6141	0.2475

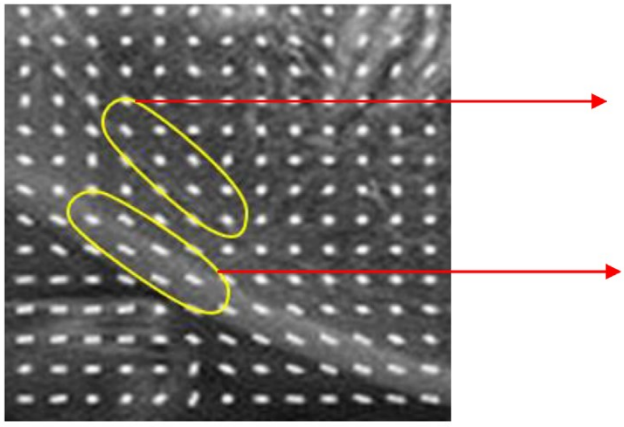

IAC region								
HOG_g	273	162	167	146	123	190	157	97
HOG_θ	87°	155°	154°	28°	63°	32°	76°	73°
Non-IAC region								
HOG_g	273	162	167	146	123	190	157	97
HOG_θ	87°	155°	154°	28°	63°	32°	76°	73°

FIGURE 8 HOG feature map embossed image (HOG_g, HOG_θ)

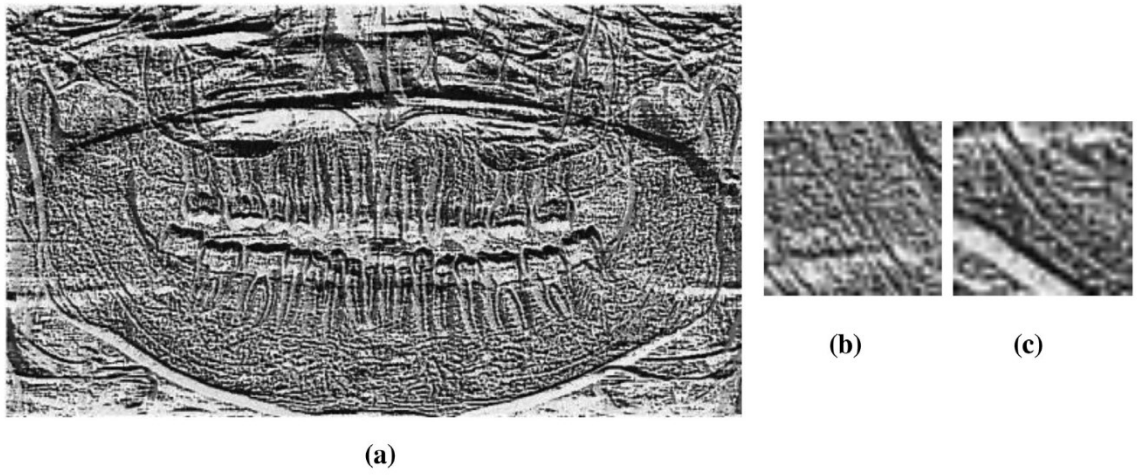

FIGURE 9 (a) Feature extracted image of input images using LBP (b, c) LBP taken for (32 × 32) block in an image

LBP gives around 1 × 177 feature vectors and the maximum value in that block was considered as the best feature.

The maximum value for the candidate IAC ranges from 8–13 and the non-IAC ranges from 14–25. This gives better classification results, and it describes the vast majority gives four different feature values as Contrast, Correlation, Energy, and Homogeneity and it clearly shows candidate IAC region has different information than the non-IAC region. The candidate IAC region in the dental OPG image differs since it is packed with soft tissues.

So from Table 3, the low contrast value ranges from 2100 to 2400, low correlation from 0.71 to 0.75, high energy from 0.2200 to 0.2300, low homogeneity from 0.80 to 0.82 for the

TABLE 3 GLCM texture output

Non-IAC image	GLCM								Texture Output
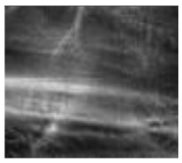	44	101	1	0	0	0	0	0	Contrast = 5916 Correlation = 0.8763 Energy = 0.1224 Homogeneity = 0.8560
	92	1474	549	19	0	0	0	0	
	11	587	3614	792	24	0	0	0	
	1	21	855	2242	561	38	1	0	
	0	0	40	576	1225	313	21	0	
	0	0	1	39	314	318	94	2	
	0	0	0	1	21	93	142	0	
	0	0	0	0	0	1	1	0	
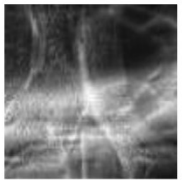	152	82	0	0	0	0	0	0	Contrast = 5748 Correlation = 0.9290 Energy = 0.0775 Homogeneity = 0.8573
	80	1660	373	7	0	0	0	0	
	1	399	1349	356	14	0	0	0	
	0	7	374	1109	354	18	0	0	
	0	0	26	330	834	370	24	0	
	0	0	1	31	352	1062	385	13	
	0	0	0	0	19	376	494	97	
	0	0	0	0	1	19	86	89	
IAC image	0	0	0	0	0	0	0 0		Contrast = 2288 Correlation = 0.7143 Energy = 0.2278 Homogeneity = 0.8132
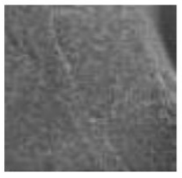	0	19	32	0	0	0	0	0	
	0	29	828	248	2	0	0	0	
	0	0	144	3008	844	2	0	0	
	0	0	2	793	1727	82	0	0	
	0	0	0	1	88	35	0	0	
	0	0	0	0	0	0	0	0	
	0	0	0	0	0	0	0	0	
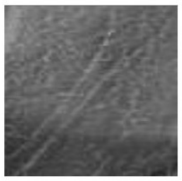	0	0	0	0	0	0	0	0	Contrast = 2166 Correlation = 0.7379 Energy = 0.2203 Homogeneity = 0.8034
	0	46	57	0	0	0	0	0	
	0	44	1200	294	1	0	0	0	
	0	0	228	2098	473	1	0	0	
	0	0	3	445	615	16	0	0	
	0	0	0	3	14	13	0	0	
	0	0	0	0	0	0	0	0	
	0	0	0	0	0	0	0	0	

IAC region because of high information contained in that region and the high contrast from 5700 to 5900, high correlation from 0.87 to 0.92, low energy range is from 0.07 to 0.13, high homogeneity from 0.85 to 0.87 for the non-IAC region. It shows features involved with GLCM in candidate IAC and non-IAC region are differing extremely each other and providing unique information about the IAC. The combination of shape and texture based feature vectors gives better classification output rather than using the features separately. A total of 98 blocks have been extracted from each input image and 21,560 blocks have been produced for the 220 image. From each block 6 features are calculated and fed as an input sample (21,560 × 6) and 20 hidden layers are chosen to classify the candidate IAC and non-IAC region. When the shape and texture features are considered separately the outcome of the classifier gives less accuracy. To solve this, the different combinations of HOG, LBP, and GLCM feature vectors are analysed. Experimentation was carried out using the features individually and with their combinations.

A combination of features compared with the accuracy is shown in Figure 10. Table 4 shows the combination of features attained the overall accuracy of 96%. The overall gain of 7% is achieved when it is analysed with all the features.

Maximum of 96% accuracy in epoch 7 with less cross-entropy of 0.16533 is obtained by considering the six feature vectors namely, max of HOG, max of LBP and contrast, correlation, energy and homogeneity in GLCM and achieved and which is depicted as a validation curve in Figure 11. Table 5

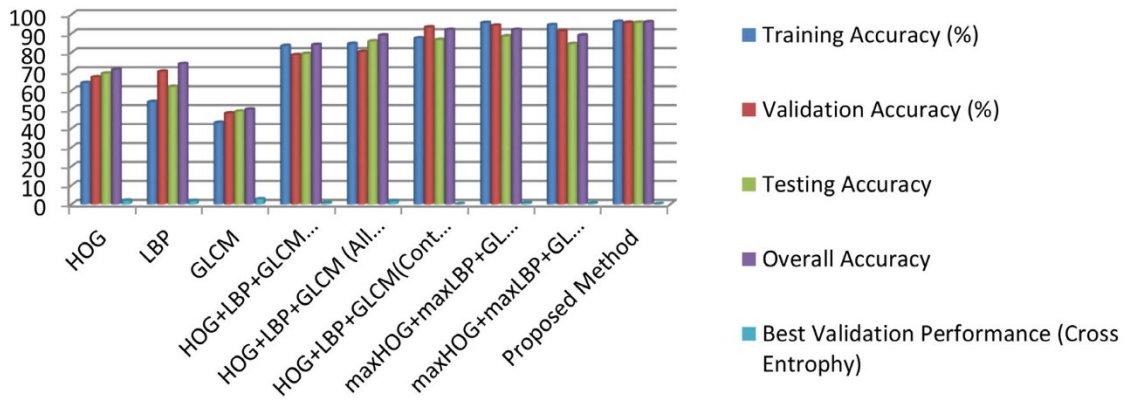

FIGURE 10 Combination of features vs accuracy

TABLE 4 Performance comparison of MELMANN classification by combination of shape and texture features

Combination of features	Training accuracy (%)	Validation accuracy (%)	Testing accuracy (%)	Overall accuracy (%)	Best validation performance (cross entropy)
HOG	64	67	69	71	1.98
LBP	54	70	62	74	1.789
GLCM	43	48	49	50	2.689
HOG+LBP+GLCM (Contrast)	83.5	78.7	79.3	84	0.6943
HOG+LBP+GLCM (All features)	84.6	80.4	85.9	89	1.5467
HOG+LBP+GLCM (Contrast, Correlation, Energy, Homogeneity)	87.5	93.3	86.7	92	0.18079
maxHOG+maxLBP+GLCM (Contrast)	95.6	94.2	88.5	92	0.68959
maxHOG+maxLBP+GLCM(All features)	94.5	91.2	84.5	89	0.5305
Proposed Method maxHOG+maxLBP+GLCM (Contrast, Correlation, Energy, Homogeneity)	96.2	95.7	95.7	96	0.16533

TABLE 5 Performance of the proposed method tested with other classifiers

	Naïve bayes (%)	KNN (%)	SVM (%)	Decision tree (%)	Ensemble (%)	Proposed algorithm (%)
maxHOG+maxLBP+GLCM (Contrast, Correlation, Energy, Homogeneity)	78	89	90	84	80	**95.7**
Cross validation	79.5	88.6	89	85	83	**94**

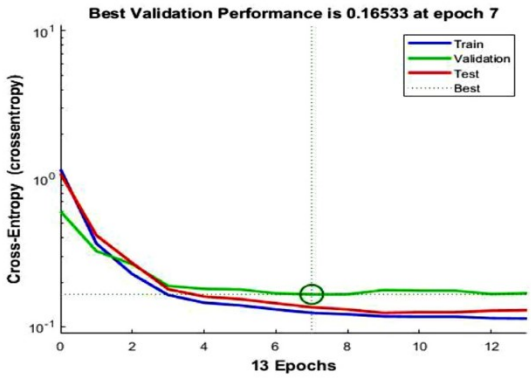

FIGURE 11 Validation curve (cross entropy vs epochs)

gives the performance evaluation of different classification techniques. The proposed method gives the cross validation accuracy of 94% compared with other machine learning methods. The proposed technique takes lesser time to classify the candidate nerve feature vectors.

Figure 12a and b shows the original image and enhanced IAC pixels superimposed in the original image. The nerve feature vectors are clustered by SOM-NNC with an active contour that locates the appropriate IAC region and is shown in Figure 12c. Figure 12d depicts the detected IAC region superimposed in Figure 12c and e presents the boundary of the IAC region by subtracting the dilated IAC with a detected IAC region. Figure 12f shows the detected IAC region superimposed by boundary pixels of an IAC portrayed in Figure 12e.

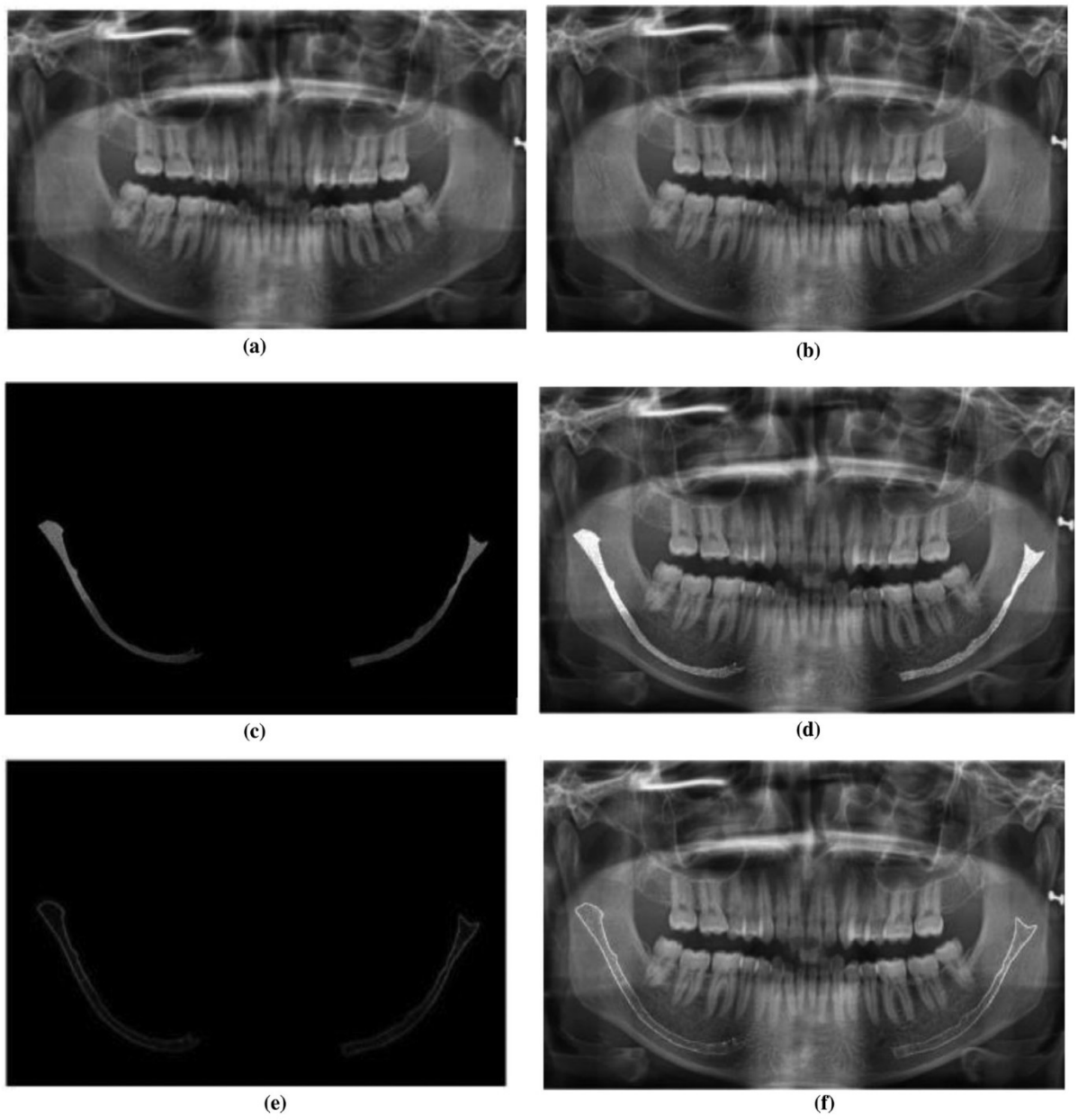

FIGURE 12 (a) Original Image. (b) Original Image + Enhanced IAC pixels superimposed. (c) Detected IAC region (SOM-active contour). (d) Detected IAC superimposed on (b). (e) Edge detected IAC region using subtracted dilated image from original image. (f) Edge detected IAC region superimposed on (b)

The proposed method is compared with the existing algorithms in terms of average distance error and standard deviation distance error and it shows the proposed method has located the IAC with minimum error and takes lesser time. The result shows the feature driven ANN model achieves better dice coefficient compared with deep learning method is shown in Table 6. It shows that the proposed method outperforms and reaches the dice coefficient of 0.854 ± 0.13 with average and standard deviation distance of 0.43 and 0.60 with less processing time of 1.526 ± 04. The experimental results justify that the proposed method can help the dental surgeon at the time of dental implantology as it locates the IAC with maximum accuracy.

5 | CONCLUSION

A novel edge enhancement with the feature driven ANN model has been proposed for automatic IAC detection in dental OPG images. This method involves three stages: OPG image enhancement, feature extraction, candidate classification, and candidate clustering. A novel filtering based preprocessing technique has been utilized here to enhance the IAC region. The feature utilized here is the shape and texture of the candidate IAC and non-IAC region. A parametric model has been used to classify the candidate features. After the feature extraction, the clustering technique has been used to segment the IAC region

TABLE 6 Performance comparison of proposed IAC segmentation method with the existing techniques (line tracking algorithm [16] and deep learning method [36, 37]

Parameter / method	Line tracking algorithm [16] (local dataset)	Deep learning method [36] (local dataset)	Deep learning method [37] (local dataset)	Proposed method
DE_{avg} (mm)	0.70	0.56	0.62	0.43
DE_{std} (mm)	0.65	0.70	0.80	0.60
Time (s)	2.36 ± 0.14	—	—	1.526 ± 0.4
Dice coefficient (%)	—	0.827 ± 0.09	0.60	0.854 ± 0.13

accurately. Experiments on this database justify the viability of this approach.

The proposed algorithm achieves better visibility of weak structures by novel structural filtering mechanism. The discrimination of pixels inside and boundary of IAC is analysed by complimentary features. The proposed method can also be used to estimate the distance between the root apex of the third molar and the IAC boundary. This provides further information to the surgeon's in the dentistry. However, it is intricate to apply the proposed method in circumstances where the IAC shape is partly occluded as there is not adequate information accessible to characterize the IAC. This problem can be addressed by experimenting with the database having more number of occluded images. Extension of this work involves experimenting the proposed algorithm in a more diverse and increased size database, which could be done by collecting dental images from different imaging modalities.

FUNDING INFORMATION

This research work was supported and funded by the Council of Scientific & Industrial Research (CSIR)–Human Resource Development Group (SRF File no.: 08/237(0015)/2018-EMR-I).

CONFLICT OF INTEREST

All co-authors have seen and agree with the manuscript's contents, and there is no financial interest to report.

DATA AVAILABILITY STATEMENT

Data available on request from the corresponding author.

ORCID

P. Uma Maheswari https://orcid.org/0000-0003-2564-6580

REFERENCES

1. Agbaje, J.O., Van de Casteele, E., Hiel, M., Verbaanderd, C., Lambrichts, I., Politis, C.: Neuropathy of trigemical nerve branches after oral and maxillofacial treatment. J. Maxillofac. Surg. 15, 321–327 (2016)
2. Azorin, J.F.M.-L., Andres, G.S., Valenzuela Molina, R.P., Muries, C.A., Panadero, R.A.: Prevention and treatment of IAN injuries: A literature review. JBR J. Interdiscip. Med. Dent. Sci. 2(3), 1000123 (2014). ISSN:2376-032X
3. Mahon, N., Stassen, L.F.A.: Post-extraction inferior alveolar nerve neurosensory disturbances- A guide to their evaluation and practical management. J. Irish Dent. Assoc. 60(5), 241–250 (2014)
4. Shin, Y., Roh, B.-D., Kim, Y., Kim, T., Kim, H.: Accidental injury of the inferior alveolar nerve due to the extrusion of calcium hydroxide in endodontic treatment: A case report. Restor. Dent. Endodont. 41(1), 63–67 2016). ISSN 2234–7666
5. Ramadorai, A., Tay, A.B.G., Vasanthakumar, G., Lye, W.K.: Nerve injury after surgical excision of mandibular third molars under local anesthesia. An audit. J. Maxillofac. Oral Surg. 18(2), 307–313. (2019)
6. La Monaca, G., Vozza, I., Giardino, R., Annibali, S., Pranno, N., Cristalli, M.P.: Prevention of neurological injuries during mandibular third molar surgery: Technical notes. Ann. Stomatol. 8, 45–52 (2017)
7. Alhassani, A.A., AlGhamdi, A.S.T.: Alveolar nerve injury in implant dentistry: Diagnosis, causes, prevention, and managemen. J. Oral Implantol. XXXVI(Five), 401–406 (2010)
8. Rueda, S., Alcañiz, M.: An approach for the automatic cephalometric landmark detection using mathematical morphology and active appearance models. Med. Image Comput. Comput. Assist. Interv. 9(Pt 1), 159–166 (2006)
9. Rueda, S., Gil, J.A., Pichery, R., Alcañiz, M.: Automatic segmentation of jaw tissues in CT using active appearance models and semi-automatic landmarking. Med. Image Comput. Comput. Assist. Interv. 9(Pt 1), 167–174 (2006)
10. Yau, H.T., Lin, Y.K., Tsou, L.S., Lee, C.Y.: An adaptive region growing method to segment inferior alveolar nerve canal from 3D medical images for dental implant surger. Comput.-Aided Des. Appl. 5(5), 743–752 (2008)
11. Zachow, S.,Lamecker, H., Elsholtz, B., Stiller, M.: Is the course of the mandibular nerve deducible from the shape of the mandible? Int. J. Comput. Assist. Radiol. Surg. 1(1), 415–417 (2006)
12. Tognola, G., Parazzini, M.,Pedretti, G., Ravazzani, P., Grandori, F., Pesatori, A., Norgia, M.,Svelto, C.: Gradient-vector-flow snake method for quantitative image reconstruction applied to mandibular distraction surgery. IEEE Trans. Instrum. Meas. 58(7), 2087–2093 (2009)
13. Keatmanee, C., Makhanov, S.S., Kotani, K., Kondo, T., Thongvigitmanee, S.S.: Inferior alveolar canal segmentation in cone beam computed tomography images using an adaptive diffusion flow active contour model. In: 14th IAPR International Conference on Machine Vision Applications (MVA). Tokyo, Japan, pp. 57–60 (2015)
14. Hanssen, N., Burgielski, Z., Jansen, T., Lievin, M., Ritter, L., von Rymon Lipinski, B., Keeve, E.: Nerves - Level sets for interactive 3D segmentation of nerve channels. In: 2nd IEEE International Symposium on Biomedical Imaging: Macro to Nano. Arlington, VA, Vol. 1, pp. 201–204 (2004)
15. Kondo, T., Ong, S.H., Foong, K.W.: Computer-based extraction of the inferior alveolar nerve canal in 3-D space. Comput. Methods Programs Biomed. 76(3), 181–91 (2004)
16. Kim, G., Lee, J., Lee, H., Seo, J., Koo, Y.-M., Shin, Y.-.G. & Kim, B.: Automatic extraction of inferior alveolar nerve canal using feature-enhancing panoramic volume rendering. IEEE Trans. Biomed. Eng. 58, 253–264 (2011)
17. Stein, W., Hassfeld, S., Muhling, J.: Tracing of thin tubular structures in computer tomographic data. Comput. Aided Surg. 3, 83–88 (1998)
18. Kainmueller, D., Lamecker, H., Seim, H., Zinser, M., Zachow, S.: Automatic extraction of mandibular nerve and bone from cone-beam CT data. Med. Image Comput. Comput. Assist. Interv. 12(Pt 2), 76–83 (2009)

19. Narayan, R.K., Ghosh, S.K.: Morphological analysis of mandibular foramen through anatomical planes: Implications for inferior alveolar nerve block. Anat. Sci. Int. 95(2), 209–218 (2020)
20. Sandhya, K., Singh, B., Lugun, N., Prasad, R.: Localization of mandibular foramen relative to landmarks in East Indian mandibles. Indian J. Dent. Res. 26, 571 (2015)
21. Heasman, P.A.: Variation in the position of the inferior dental canal and its significance to restorative dentistry. J. Dent. 16(1), 36–39 (1988)
22. Pogrel, M.A., Dorfman, D., Fallah, H.: The anatomic structure of the inferior alveolar neurovascular bundle in the third molar region. J. Oral. Maxillofac. Surg. 67(11), 2452–2454 (2009)
23. Kieser, J., Paulin, M., Law, B.: Intrabony course of the inferior alveolar nerve in the edentulous mandible. Clin. Anat. (New York, N.Y.) 17, 107–111 (2004)
24. Kim, S.T., Hu, K., Song, W.-C., Kang, M.-K., Park, H.-D., Kim, H.-J.: Location of the mandibular canal and the topography of its neurovascular structures. J. Craniofac. Surg. 20, 936–939 (2009)
25. Karthikeyan, T., Manikandaprabhu, P.: A novel approach for inferior alveolar nerve (IAN) injury identification using panoramic radiographic image. Biomed. Pharmacol. J. 8(1), 307–314 (2015)
26. Bahrampour, E., Zamani, A., Kashkouli, S., Soltanimehr, E., Ghofrani Jahromi, M., Sanaeian Pourshirazi, Z.: Accuracy of software designed for automated localization of the inferior alveolar nerve canal on cone beam CT images. Dentomaxillofac. Radiol. 45(2), 20150298 (2016)
27. Li, B., Cheng, K., Yu, Z.: Histogram of oriented gradient based gist feature for building recognition. Comput. Intell. Neurosci. 2016, 6749325 (2016)
28. Patwary, M.J.A., Parvin, S., Akter, S.: Significant HOG-histogram of oriented gradient feature selection for human detection. Int. J. Comput. Appl. 132, 20–24 (2015)
29. Cai, Y., Xu, G., Li, A., X.W.: A novel improved local binary pattern and its application to the fault diagnosis of diesel engine. Shock Vib. 15, 9830162 (2020)
30. Abdul, Z.K., Al-Talabani, A., Abdulrahman, A.O.: A new feature extraction technique based on 1D local binary pattern for gear fault detection. Shock Vib. 2016, 8538165 (2020)
31. Mall, P.K., Singh, P.K., Yadav, D.: GLCM based feature extraction and medical X-ray image classification using machine learning techniques. In: IEEE Conference on Information and Communication Technology(CICT). Allahabad, India (2019)
32. Bala, R., Kumar, D.: Classification using ANN: A review. Int. J. Comput. Intell. Res. 13(7), 1811–1820 (2017). ISSN 0973–1873
33. Shuxia, L., Wang, X., Zhang, G., Zhou, X.: Effective algorithms of the moore-penrose inverse matrices for extreme learning machine. Intell. Data Anal. 19(4), 743–760 (2015)
34. Xiao, D., Li, B., Mao, Y.: A multiple hidden layers extreme learning machine method and its application. Math. Prob. Eng. 10, 4670187 (2017)
35. Chi, D.: Self-organizing map-based color image segmentation with k-means clustering and saliency map. Int. Scholarly Res. Not. 18, 393891 (2011)
36. Vinayahalingam, S., Xi, T., Bergé, S., Maal, T., de Jong, G.: Automated detection of third molars and mandibular nerve by deep learning. Scientific Reports 9(1), (2019). https://doi.org/10.1038/s41598-019-45487-3
37. Kwak, G.H., Kwak, E.-J., Song J.M., Park, H.R., Jung, Y.-H., Cho, B.-H., Hui, P., Hwang, J.J.: Automatic mandibular canal detection using a deep convolutional neural network. Scientific Reports. 10(1), (2020). https://doi.org/10.1038/s41598-020-62586-8

How to cite this article: Maheswari, P.U., Banumathi, A., Ulaganathan, G., Yoganandha, R.: Inferior alveolar nerve canal segmentation by local features based neural network model. IET Image Process. 16, 703–716 (2022). https://doi.org/10.1049/ipr2.12375

Original Article

Potential Antibacterial Efficacy of Garlic Extract on *Staphylococcus aureus*, *Escherichia coli,* and *Klebsiella pneumoniae*: An *In vitro* Study

Mohammed Abidullah, Pradnya Jadhav[1], S. Sri Sujan[2], Ayyapa Gandhi Shrimanikandan[3], Chukka Rakesh Reddy[4], Raj Kumar Wasan[5]

Department of Dental and Biomedical Sciences, Faculty of Dentistry, Al Baha University, Al Baha, Saudi Arabia, [1]Department of Public Health Dentistry, Government Dental College and Hospital, Aurangabad, Maharashtra, [2]Department of Oral and Maxillofacial Surgery, KIMS Dental College and Hospital, Amalapuram, Andhra Pradesh, [3]Department of Dentistry and Craniofacial Surgery, Velammal Medical College Hospital and Research Institute, Madurai, Tamil Nadu, [4]Department of Conservative Dentistry and Endodontics, SVS Institute of Dental Sciences, Mahabubnagar, Telangana, [5]Department of Microbiology, Genesis Institute of Dental Sciences and Research, Ferozpur, Punjab, India

ABSTRACT

Background: Garlic has been recommended by many ancient medicines such as the Chinese and the Indian medicine to cure respiratory and digestive issues along with treating microbial infestation and leprosy. The therapeutic effects encompass many advantages in the field of cardiovascular system, antibiotics, anticancer, anti-inflammatory, and hormone-like effects. **Aims and Objective:** The present study was carried out to evaluate the garlic antibacterial effect against clinical isolates of *Staphylococcus aureus*, *Escherichia coli,* and *Pneumoniae* from patients attending referral hospital. **Materials and Methods:** The isolation of bacteria was done from pus sample collected from referral hospital, Bedar, Karnataka, with sterile swabs. The study samples were inoculated under aseptic conditions on culture media such as nutrient agar, blood agar, and MacConkey agar plates and isolated the pathogen bacteria such as *E. coli*, *Klebsiella pneumoniae,* and *S. aureus*. The garlic bulbs were peeled off and then ligated using pestle simultaneously with addition of minor quantity of H_2O for preparation of plant extract and study the antimicrobial effect of garlic on these bacteria. **Results:** The result showed that garlic extracts have a high range of antibacterial effect against both Gram-negative (*E. coli* and *K. pneumoniae*) and Gram-positive bacteria *Staphylococcus*. **Conclusion:** The present study observations revealed that garlic makes large clear zones in comparison to the currently available antibiotics used in the study. The potentiality of the garlic can be utilized in the field of antibacterial agents. It can be prepared in the form of tablets in the best concentrations and affordable dosages so that it can be used as medicine against these pathogenic organisms.

Keywords: *Escherichia coli, garlic, Klebsiella pneumonia, Staphylococcus aureus*

Submitted: 17-Oct-2020
Revised: 27-Nov-2020
Accepted: 15-Dec-2020
Published: 05-Jun-2021.

Introduction

Garlic is an herb which is grown across the globe and known well for its anti-infective properties. It falls in family: *Amaryllidaceae*, order, *Asparagales,* and Kingdom: Plantae.[1,2] The botanical name of garlic is "*Allium sativum*" deriving it from the Celtic word "all," which stands for burning or stinging, and the Latin "sativum" stands for planted or cultivated.[2] It has a long traditional history as medicinal plant, started with a direction of preparing a medicinal remedy written in a cuneiform character in about 3000 BC to present date formulation of tablets. Scientific

Access this article online

Quick Response Code:

Website: www.jpbsonline.org

DOI: 10.4103/jpbs.JPBS_681_20

Address for correspondence: Dr. Mohammed Abidullah, Department of Dental and Biomedical Sciences, Faculty of Dentistry, Al Baha University, Al Baha, Saudi Arabia.
E-mail: mdabid2512@gmail.com

How to cite this article: Abidullah M, Jadhav P, Sujan SS, Shrimanikandan AG, Reddy CR, Wasan RK. Potential antibacterial efficacy of garlic extract on *Staphylococcus aureus*, *Escherichia coli*, and *Klebsiella pneumoniae*: An *In vitro* study. J Pharm Bioall Sci 2021;13:S590-4.

investigations of various garlic preparations began in 1939.[1]

Naturally occurring plants play a pivotal role in developing the ancient medicine as it has many therapeutic properties which in previous time in the absence of good diagnostic tools contribute immensely in alleviating patient's pain and improving the social well-being.[3] The therapeutic properties range from the beneficial effects on the cardiovascular system, central nervous system, anticancer effect, anti-inflammatory, antibiotics, and immunity-boosting effect.[4] These extracts are nothing but the by-products which are released during the secondary metabolism of the plants. The availability of these herbal medicine is in many forms such as the powder, liquid, or mixtures which are formulated in paste and ointment forms.[2] The ancient traditional science utilizes these properties and adopts indigenous methods to maintain health system.[5] They also used it for prevention, diagnosis, and treatment of the diseases by accumulating the knowledge, skills, and practices derive from the concepts of different cultures that are acknowledged to maintain health.[6] In underdeveloped and developing countries, a big segment of population put their belief in the traditional form of medicine to cure any kind of illness and improve the health.[7] Garlic (*A. sativum*) is one of the very selected variety of plant species on which lot of research has been carried out to explore its medical propertied qualities and apply it for cure of various health issues including cancer.[3,4,7,8]

Garlic growth is by vegetative reproduction rather than sexual reproduction (seed) producing the individual cloves which contain bulbs having the same genetic properties as the original clove. The earliest evidence of these medicinal plant extract was mention in Avesta, a Zoroastrian book complied during the 6th century along with its detail description in the civilization of Sumerian and Egypt. Indian and Chinese's ancient civilization also recommended the use of garlic for curing respiratory ailment, digestive issues, leprosy, and parasitic infestation.[7] Al Qanoon Fil Tib (The canon of medicine) suggested that the garlic can be powerful curative effect in a condition such as arteritis, toothache, chronic cough, constipation, insect bites, and gynecologic disease.[9] There is ample of epidemiologic instances that elaborates many good health benefits of garlic based on the experimental and clinical investigations.[10,11]

Latest studies carried out in Ethiopia suggested that garlic has been a common medicine used in its traditional medicine for treating infectious diseases such as tuberculosis, sexually transmitted disease, and wounds. Apart that, it serves as a main culinary preparation and applications.[8-10] We carried out this study to evaluate the antibacterial effect of garlic against clinical isolates of *Staphylococcus aureus*, *Escherichia coli,* and *Pneumoniae*.

Materials and Methods

Isolation of bacteria

For bacteria isolation, pus samples were collected by sterile swabs from inpatients and outpatients of different wards of referral Hospital, Bedar, Karnataka, for a period of 6 months from July 2019 to December 2019 in accordance with standard protocols and ethical guidelines. Skin, nasal wounds, ears, legs, internal organs (lungs, kidney, and bladder), and catheters served as samples for collection of pus samples.

Pus samples were preserved in Cary Blair transport medium and transported to the S. B, Patil Dental College, Department of Oral Pathology and Microbiology, Bedar, Karnataka, for the Gram stain and culturing procedure. The samples were inoculated under aseptic conditions on nutrient agar, blood agar (5% sheep blood), and MacConkey agar plates, incubated aerobically at 35°C–37°C for 24–48 h. For primary identification and characterization of isolates were performed on the basis of Gram staining, microscopic characteristics, colony characteristic, and secondary identification were done with the help of biochemical tests such as tripal sugar iron agar, hydrogen sulfide test, carbohydrate fermentation test, phenylalanine deaminase test, methyl red test, nitrate reduction test, urease test, Vogesproskauer, citrate utilization test, and indole test using standard microbiological methods.

Preparation of plant extract

Fresh garlic extract preparation from the plant's bulbs was taken from the local market. The garlic bulbs were peeled, weighed (50 g), and cleaned. The peeled garlic bulbs were then ligated using pestle with simultaneously addition of small quantity of water. This extract was considered as the 100% concentration of the extract and used for antimicrobial effect on isolated bacteria.

Antibacterial sensitivity test

The antibacterial activity test of the crude extract of garlic against clinical isolated bacteria such as *E. coli*, *Klebsiella pneumoniae,* and *S. aureus* was carried out by the Agar diffusion method.[11,12] *E. coli*, *K. Pneumoniae,* and *S. aureus* were inoculated on a nutrient agar plate with the help of sterile cotton swab. Then prepared the wells in the center of Petri plate with the help of puncher. After inoculation of bacteria, 10 µl garlic extract was added with the help of micropipette, and then incubated at 35°C–37°C for 24 h. After 24 h the diameter of the ring was measured.

Statistical analysis

One-way ANOVA was used to compare the mean values as a measure of test of significance. A $P < 0.05$ was considered statistically significant.

Results

The results of the susceptibility of the test organisms against the garlic extracts showed that isolates of *S. aureus*, *E. coli,* and *K. pneumoniae* were sensitive to the concentration of 10 µl garlic of agar media in using diffusion method. In addition, larger clear zones were observed against *Staphylococcus* its 28 mm and then 2nd largest clear zone on *E. coli* that is 27 mm and *K. pneumoniae* also show good clear zone 22 mm at 10 µl concentration against among microorganisms [Table 1, Graph 1 and Figures 1-3]. A $P = 1.000$ was found, and there was no statistically significant difference between the three groups.

Discussion

Naturally occurring species such as garlic and other herbs produce secondary metabolites which are useful for health, but simultaneously these bioactive compounds can cause adverse reactions in the body such as allergy, cardiovascular system (CVS) problem, dermatitis, and bleeding unless there are used under controlled protocol and guidelines.[11,12] However, to confirm the therapeutic use, further studies are needed to find out its efficacy and potential side effects.[6,9]

This research mainly concentrates on the antibacterial effect against multidrug-resistant human pathogen *E. coli*, *K. pneumoniae,* and *S. aureus* with their respective inhibition zone.[12,13] Minimum inhibitory concentration or high zone of inhibition elaborates the bacterial susceptibility or bacterial reaction to the antibiotic used.[14,15]

The extract of the garlic contains a varied range of antimicrobial/antibacterial potential which are effective against Gram-negative organisms (*E. coli* and *K. pneumoniae*) and Gram-positive bacterial *Staphylococcus*.[12-15] The organism which is very stubborn such as the antibiotic-resistant bacterial and their toxic by-product can also be countered with the help of these garlic extracts.[13] The components which bring about this effect are the allicin which mainly inhibits the growth of bacteria by inhibiting the DNA and protein synthesis partially along with RNA inhibition synthesis as the primary target.[16] In addition, there are various studies that have been carried out which suggest the allicin potential to stop the RNA synthesis speed by trapping the RNA peptides chain reaction and amplify the antibacterial.[17]

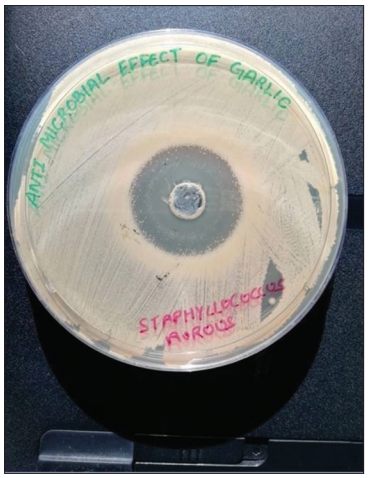

Figure 1: Effect of garlic on *Staphylococcus aureus*

Figure 2: Effect of garlic on *Klebsiella pneumonia*

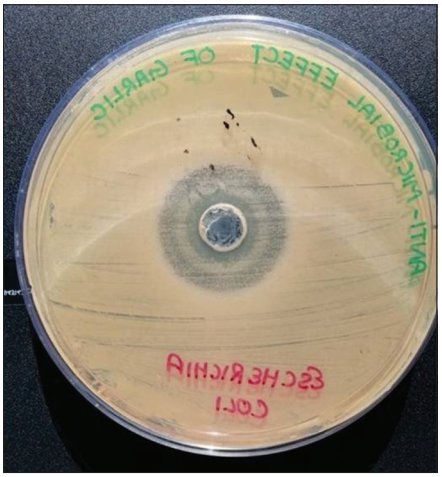

Figure 3: Effect of garlic on *Escherichia coli*

S. aureus organism membrane consists of lipid, which gives it protection.[7] Allicin, a component of garlic, has the ability to penetrate this membrane and consequently influences the RNA mechanism, lysis of membrane along

Table 1: Antibiotic sensitivity test results

Concentration of garlic (µl)	Diameter of clear zone (in mm) on nutrient agar and macConkey agar			*P*
	Escherichia coli	*Klebsiella pneumoniae*	*Staphylococcus aureus*	
10	27	22	28	1 (NS)

NS: Not significant

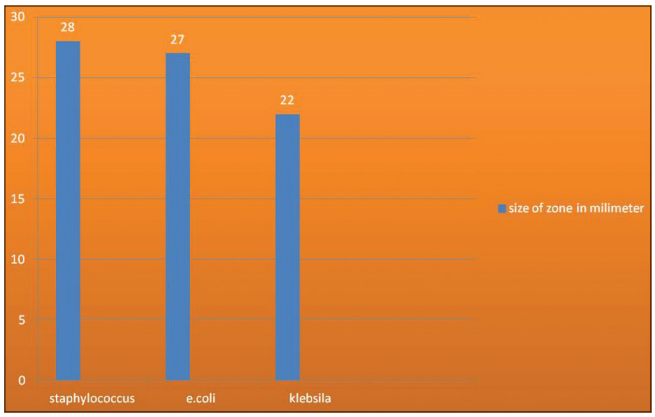

Graph 1: Antibiotic sensitivity test results

with bactericidal effect.[12-16] The effect of inhibition against the growth of these microorganisms relates to the fact that *E. coli* and *K. pneumoniae* are made up of 20% of lipid while *S. aureus* 2% lipid.[7,18]

Findings of the current study are concordant with the studies conducted by Jehan *et al*.,[2] Onyeagba *et al*.,[3] Shaloo *et al*.,[4] Nkang *et al*.,[14] Deresse,[15] Abebe,[16] Yadav *et al*.,[17] Aliy,[18] and Shokrzadeh and Ebadi.[19]

Therefore, the garlic extract is more potent against *S. aureus* and the resistant species of *S. aureus*. As the antibiotic resistance has become challenging scenarios in current medical practice, so in such cases, these findings of garlic and its extracts come as a boon to the patients and medical field.[19]

Conclusion

The present study results suggest that the garlic exhibits a large clear zone compare to the currently available antibiotics used in the study. Garlic can be used as an effective antibacterial agent formulating it in the form of tablets in the best concentrations and affordable dosages so that it can serve as a medicine against these pathogenic microorganisms. In this era of drug-resistant bacteria, we need to get our research strengths in usage of alternative medicine that has a past strong record in treating various disease pathogens with the help of these naturally occurring herbs.

Financial support and sponsorship

Nil.

Conflicts of interest

There are no conflicts of interest.

References

1. Weiss RF. Herbal Medicine. Hippocrates, Verlag Stuttgart; 1988.
2. Jehan B, Muhammad T, Huma A, Amjad I, Mohammad S. Effect of different solvent extracted sample of *Allium sativum* (Linn.) on bacteria and fungi. Afr J Biotechnol 2011;10:5910-5.
3. Onyeagba RA, Ugbogu OC, Okeke CU, Iroakasi O. Studies on the antimicrobial effects of garlic (*Allium sativum* Linn), ginger (Zingiberofficinale Roscoe) and lime (Citrus aurantifolia Linn) Afr J Biotechnol 2004;3:552-4.
4. Shaloo V, Sopreet K, Joginder S, Akshay G. Antibacterial effects of garlic (*Allium sativum L.*) extract on different pathogenic and non-pathogenic bacteria. RJPBCS 2015;6:1103.
5. Aviello G, Abenavoli L, Borrelli F, Capasso R, Izzo AA, Lembo F, *et al*. Garlic: Empiricism or science? Nat Prod Commun 2009;4:1785-96.
6. Dannesteter J. The origins of medicine. Translated from Sacred Books of the East, American Edition. New York: The Christian Literature Company; 2003.
7. Rivlrn RS. Patient with hyperlipidemia whoreceived garlic supplements Lipid management. Rep Lipid Educat Council 1998;3:6-7.
8. Colín-González AL, Santana RA, Silva-Islas CA, Chánez-Cárdenas ME, Santamaría A, Maldonado PD. The antioxidant mechanisms underlying the aged garlic extract- and S-allylcysteine-induced protection. Oxid Med Cell Longev 2012;2012:907162.
9. Dikasso D. Antiviral Effect of Garlic. Addis Ababa: Berhanena Selam Printing Press; 1999.
10. Abebe D, Ayehu A. Medicinal Plants and Health Practice in Ethiopia. Addis Ababa: Berhanena Selam Printing Press; 1993. p. 219-21.
11. Debella A. Procedures in Preparation of Medicine from Plants. Addis Ababa: Aartistic Printing Press; 2004.
12. Tatarintsev AV, Vrzhets PV, Ershov DE, Turgiev AS, Karamov EV, *et al*. The ajoene blockade of integrin dependent processes in an HIV-infected cell system. Vestn Ross Akad Med Nauk 1992;11:6-10.
13. World Health Organization. Antimicrobial resistance: Report of a Working Group. Bull WHO 1983;61:383-4.
14. Nkang AO, Okonko IO, Mejeha OK, Adewale OG, Udeze AO, Fowotade A, Fajobi EA, *et al*. Assessment of antibiotics susceptibility profiles of some selected clinical isolates from laboratories in Nigeria. J Microbiol Antimicrob 2009;1:19 26.
15. Deresse D. Antibacterial effect of garlic (*Allium sativum*) on *Staphylococcu aureus:* An *in vitro* study. Asian J Med Sci 2010;2:62-5.
16. Abebe D. Medicinal Plants. Vol. 17. Addis Ababa: Berhanena Selam Press; 2003. p. 1108-12.
17. Yadav S, Trivedi NA, Bhatt JD. Antimicrobial activity of fresh

garlic juice: An in vitro study. Ayu. 2015;36:203-7.

18. Aliy E. Asefaw berhe anti-bacterial effect of garlic (*Allium sativum*) against clinical isolates of *Staphylococcus aureus* and *Escherichia coli* from patients attending hawassa referral hospital, Ethiopia. J Infect Dis Treatment 2016;2:18.
19. Shokrzadeh M, Ebadi AG. Antibacterial effect of garlic (*Allium sativum* L.) on *Staphylococcus*. Pakistan J Biol Sci 2006;9:1755-579.

Original Article

Anaesthetic Efficacy of Lidocaine and Articaine in Inferior Alveolar Nerve Block Combined with Buccal Infiltration in Patients with Irreversible Pulpitis

Shrimanikandan Ayappa Gandhi[1], Sambarta Das[2], Abhisek Das[3], Yoshaskam Agnihotri[3], Rajanna Venkatraman Mohan[4], Venkata Ramanan Dasu Subramanian[5]

[1]Department of Craniofacial Surgery and Dentistry, Velammal Medical Hospital and Research Institute, Madurai, Tamil Nadu, India, [2]Department of Conservative Dentistry and Endodontics, Hi-Tech Dental College and Hospital, Bhubaneswar, Odisha, India, [3]Department of Conservative Dentistry and Endodontics, Hi-Tech Dental College, Bhubaneswar, Odisha, India, [4]Oral Pathology and Microbiology, Madurai, Tamil Nadu, [5]Conservative Dentistry and Endodontics, Best Dental Science College and Hospital, Madurai, Tamil Nadu, India

Submitted: 20-Nov-2020
Accepted: 24-Nov-2020
Published: 05-Jun-2021

ABSTRACT

Purpose: This prospective, randomized, double-blinded study was conducted to compare the anesthetic efficacy of 2% lidocaine with 1:200,000 epinephrine and 4% articaine with 1:200,000 epinephrine in inferior alveolar nerve block (IANB) combined with buccal infiltration in patients with irreversible pulpitis. **Methods:** Group I: Thirty patients received IANB of 2% lidocaine without buccal infiltration. Group II: Thirty patients received IANB of 2% lidocaine followed by buccal infiltration with 2% lidocaine. Group III: Thirty patients received IANB with 4% articaine followed by buccal infiltration with 4% articaine. Pain during the procedures was recorded by using a Heft Parker visual analog scale. No pain or mild pain on endodontic access was recorded as success and analyzed using Chi-square analysis. **Results:** Group I obtained 30% success rate. Fifty percent successful anesthesia was obtained for Group II. The success rate was increased to 70% for Group III with statistically significant difference among all the groups ($P < 0.05$). **Conclusion:** The use of 4% articaine as both IANB and buccal infiltration recorded the highest success rate (70%) when compared to either 2% lidocaine as IANB with buccal infiltration (50%) or 2% lidocaine as IANB alone (30%) in patients with irreversible pulpitis.

KEYWORDS: *Anesthetic efficacy, artcaine, irreversible pulpitis, lidocaine, local anesthesia*

INTRODUCTION

The fundamental goal of dentists while performing endodontic therapy is to obtain an adequate pulpal anesthesia.[1] Pulpal anesthesia during posterior mandibular endodontic procedures has been traditionally achieved by inferior alveolar nerve block (IANB).[2-4] In irreversible pulpitis, the success rate of IANB ranges only from 19% to 56%.[5] The possible reason for the failure of IANB could be due to the existing inflammatory activation of nociceptors,[6,7] anatomic variations like cross and accessory innervations,[8-11] and tachyphylaxis due to anesthetic solutions.[11] Therefore, it would be highly desirable to improve the success rate of IANB in endodontics.[12]

Various supporting techniques have been recommended to overcome this failure in IANB anesthesia like intra-osseous, periodontal ligament injections and these techniques require special equipment.[6] Previous studies have demonstrated that only buccal or buccal with lingual infiltrations provide successful anesthesia in 32%–67% of patients with lidocaine and 57%–92% with articaine, even without administration of standard IANB.[10,13,14]

Address for correspondence: Dr. Shrimanikandan Ayappa Gandhi, Assistant Professor, Department of Craniofacial Surgery and Dentistry, Velammal Medical Hospital and Research Institute, Madurai - 625 009, Tamil Nadu, India.
E-mail: shrimanikandan88@gmail.com

Access this article online

Quick Response Code:

Website: www.jpbsonline.org

DOI: 10.4103/jpbs.JPBS_747_20

How to cite this article: Gandhi SA, Das S, Das A, Agnihotri Y, Rajanna VR, Subramanian VR. Anaesthetic efficacy of lidocaine and articaine in inferior alveolar nerve block combined with buccal infiltration in patients with irreversible pulpitis. J Pharm Bioall Sci 2021;13:S731-4.

The introduction of articaine for dental anesthesia was introduced in the United States in 2000.[15] A study by Haas *et al*. found no statistical differences between 4% articaine and 4% prilocaine infiltrations in mandibular canines and second molars IN in asymptomatic patients.[8,9] Also, Kanaa *et al*. showed that 4% articaine (64.5%) produced more effective pulpal anesthesia than 2% lidocaine (38.7%) in mandibular molars after buccal infiltration in asymptomatic subjects.[10]

Several studies compared articaine either as primary IANB or as supplemental infiltration alone.[10,12,16-18] We hypothesize that articaine usage as both IANB and supplemental infiltration would increase the success rate. Thus the aim of this study was to compare the anesthetic efficacy of 4% articaine as IANB combined with buccal infiltration and 2% lidocaine as IANB combined with buccal infiltration in mandibular molars in patients with irreversible pulpitis.

Methods

Ninety three patients enrolled in this prospective, double blind, randomized, clinical trial. The sample size calculation was done by keeping Type I error α level at 0.05 for a two tailed test and Type II error β level at 0.20 with 80% power to detect 15% difference among the test groups. All of them were emergency patients with actively experiencing pain and were in good health without any co–morbid conditions as determined by detailed medical and dental history. An ethical clearance was sought from the institute ethical committee (REF: CSP/11/FEB/14/12) and all subjects were enrolled after a written informed consent was obtained.

Exclusion criteria included patients; below 18 years of age, with negative response to cold testing or peri–radicular pathosis (other than a widened periodontal ligament), known allergy to local anesthetics, pregnancy, significant co–morbid conditions, taking any premedication's that might interact with anesthetic assessment, active sites of pathosis in injection site and inability to sign informed consent. Inclusion criteria included vital mandibular molar tooth with moderate to severe active pain and a prolonged response to cold testing with an ice stick, and an electric pulp tester (Parkell, D624, Farmingdale, NY 11735, USA®) with vital coronal pulp tissue on access opening. The patients were asked to rate their pain on a Heft-Parker visual analog scale (HP VAS). Randomization was done by simple random sampling. A blinded dental hygienist randomly allocated the patients to the following groups:

- Group I: IANB with 1.8 ml (mL) of 2% lidocaine (control group)
- Group II: IANB with 1.8 mL of 2% lidocaine and 2% lidocaine as buccal infiltration
- Group III: IANB with 1.8 mL of 4% articaine and 4% articaine as buccal infiltration.

Standard IANB was performed by using either "2% lidocaine with 1:200,000 epinephrine" (Lignocaine; Neon laboratories limited, Mumbai, Maharashtra, India®) or "4% articaine with 1:200,000 epinephrine" (Septanest, France®). The solution was injected by using 27 gauge long needles. Upon reaching the target area, 1.8 mL of solution was deposited at a rate of 1 mL/min after aspiration.

For buccal infiltration, the needle, with its bevel towards the bone, was gently inserted into the buccal alveolar mucosa opposite to the furcation area until it approximately reached the apical end of the roots. Followed by which aspiration was done and 1.8 mL of solution was given. In control group, the normal saline was given as buccal infiltration (placebo) to double blind the experiment. The solutions were masked with a code number by the first author while the second author performed the injections with the solutions masked with code numbers. Blinding was done by entering only the code numbers in the data sheets. After 15 min of the IANB, subjective evaluation for the presence/absence of lip numbness was done. If lip numbness was not achieved within 15 min, the block was considered unsuccessful, and the patients were excluded from the study. Rubber dam isolation was done for patients with successful anesthetic outcome and access was initiated. The patients were asked to rate any discomfort during the treatment with HP VAS.

The HP VAS consists of 170 mm line marked with various pain ratings was used in the study. The millimeter (mm) readings were removed from the scale and the scale was divided in to 4 divisions. No pain: 0 mm, mild pain: >0 mm and ≤54 mm which includes the descriptors of weak and faint pain, moderate pain: >54 mm and <114 mm and including only the descriptor of moderate pain, and severe pain: ≥114 mm and includes the descriptors of strong, intense, and maximum possible. The anesthetic efficacy of the solution was considered successful when there was "no pain" or "weak/mild" pain during endodontic access preparation and instrumentation.[12] If the patient had moderate to severe pain (VAS rating >54 mm) during the procedures, the injection was considered a failure, and an intrapulpal injection was administered. Age and initial and post injection pain were analyzed using multiple comparison analysis of variance (Kruskal–Wallis) and *post hoc* tests at a significant difference level of $P < 0.05$. Comparisons of Articaine and lidocaine solutions for anesthetic success were analyzed using Chi-square test.

Results

Three patients; one from each group who did not have subjective lip numbness at 15 min were excluded from the study. There was no statistical significance comparing age (P = 0.23), sex (P = 0.87), initial (P = 0.52) and post injection pain (P = 0.17) and distribution of teeth (P = 0.86) between Groups I, II, and III [Tables 1 and 2].

The comparison of percentage of patients with successful anesthesia ("no pain" or "weak/mild" pain during endodontic access preparation and instrumentation) between Groups I, II, III (P = 0.001) showed statistical significance $P < 0.05$ [Table 3].

Control IANB with 2% lidocaine gave 30% success rate (9 out of 30 patients). Use of 2% Lidocaine IANB with 2% lidocaine buccal infiltration resulted in the success rate of 50% (15 out of 30 patients). But when using 4% articaine IANB with 4% articaine buccal infiltration, the success rate was increased to 70% (21 out of 30 patients) and was statistically significant with other groups; $P < 0.05$. 100% success rate was not achieved in any groups.

Discussion

Local anesthesia using an IANB may provide successful anesthesia in 70% of uninflamed pulp, but the success rate falls drastically to 30% in irreversible pulpitis.[2-4,11] In comparison to normal patients, patients with irreversible pulpitis have eight times more chances of local anesthestic failure.[6] The reason for failure in IANB in irreversible pulpitis may be due to local acidosis or activation of nociceptors by inflammation.[6,19,20]

It is reasonable to effectively block the activated nociceptors by locally depositing a supplemental dose of local anesthetic solution in the vicinity of the involved tooth.[16] Various supplemental injection techniques have been suggested such as infiltration, intraligamentary, and intraosseous injections, which can actively deliver the anesthetic solution near the apices of involved teeth.[4,7,21] In intraligamentary technique, the anesthetic solution actually diffuses along the outer surface of the cribriform plate and not through the periodontal space, with short duration of action and also with a significant incidence of postoperative pain.[16,22,23] While intraosseous injection involves perforation into the cortical bone along with the possible risks of postoperative hyperocclusion, and infection at the site of perforation.[6] These techniques require specialized delivery equipment. Successful supplemental infiltration anesthesia of the mandibular posterior teeth would be highly advantageous in irreversible pulpitis conditions.[16]

In our study, 4% articaine IANB along with 4% articaine buccal infiltration showed higher success rate (70%) when compared with either 2% lidocaine as a IANB along with 2% lidocaine buccal infiltration (50%) or with 2% lidocaine as a IANB (30%) alone. The use of 4% articaine as an IANB along with 4% articaine buccal infiltration has increased the success rate by 70%. This is in concurrence with previous studies by Kanaa *et al*. which showed that articaine had a higher success rate than lidocaine in achieving buccal infiltration anesthesia of first molar in asymptomatic subjects.[10] The reason could be articaine has better bone penetration efficacy in comparison with lidocaine, which has limited diffusion through compact cortical bone.[14,16] Articaine with increased liposolubility and increased degree of dissociation along with the presence of unique thiophene ring instead of benzene ring which is not possessed by other amide groups and it may facilitate better diffusion through soft and hard tissues more reliably than other local anesthetics.[8,14,24]

The results also showed that supplemental buccal infiltration had increased the success rate for lidocaine and articaine compared to lidocaine IANB alone. This is in concurrence with previous studies, which showed that addition of supplemental buccal infiltration to IANB resulted in increased success rate.[5,16,18] Jung *et al*. stated that buccal infiltration of 4% articaine with

Table 1: Comparison of age, sex, initial and postinjection pain in Group I, Group II and Group III

	Group I	Group II	Group III
Age	30±8	29±8	28±7
Sex			
Men	16	15	17
Women	14	15	13
Initial pain (HP VAS scale)	110±35	114±30	116±29
Post injection pain (after 15 min)	11±6	10±5	10±6

There was no significant difference between the groups (P>0.05).
HP VAS: Heft-parker visual analog scale

Table 2: Teeth distribution for Group I, Group II and Group III

Tooth	Group I	Group II	Group III
First molar (%)	19/30 (63.3)	20/30 (66.7)	21/30 (70)
Second molar (%)	11/30 (36.7)	10/30 (33.3)	9/30 (30)

There was no significant difference between the groups (P>0.05)

Table 3: Percentage of successful anesthesia between Group I, Group II and Group III

Group	Success (%)	Failure (%)
I	9 (30)	21 (70)
II	15 (50)	15 (50)
III	21 (70)	9 (30)

There was a significant difference between the groups (P=0.01)

1:100,000 adrenaline can provide a similar success rate as compared with standard IANB to anesthetize normal uninflamed mandibular first molars.[14] Thus the IANB alone will not be sufficient enough to produce adequate pulpal anesthesia in irreversible pulpitis condition. Supplemental injection techniques are often required to increase the success rate in such conditions.

The overall success rate of 70% for the 4% articaine IANB along with buccal infiltration in mandibular posterior teeth in this study is lower than the success rates of 82%–91% recorded with supplemental intraosseous anesthesia with lidocaine or articaine formulations in previous studies.[7,21] The reason for the higher success rates with the intraosseous injection may be attributed to the efficacy of injecting the local anesthetic solution directly into the medullary bone surrounding the apices of the teeth.[25]

Conclusion

The use of 4% articaine as both IANB and buccal infiltration had a significantly higher success rate (70%) when compared to either 2% lidocaine as IANB with buccal infiltration (50%) or 2% lidocaine as IANB alone (30%) in patients with irreversible pulpitis.

Financial support and sponsorship

Nil.

Conflicts of interest

There are no conflicts of interest.

References

1. Walton RE, Reader A, Nusstein JM. Local anesthesia. In: Torabinejad M, Walton RE, editors. Endodontics, Principles and Practice. 4th ed. St. Louis MO: Saunders Elsevier; 2008. p.129-47.
2. Goldberg S, Reader A, Drum M, Nusstein J, Beck M. Comparison of the anesthetic efficacy of the conventional inferior alveolar, Gow-Gates, and Vazirani-Akinosi techniques. J Endod 2008;34:1306-11.
3. Cohen HP, Cha BY, Spångberg LS. Endodontic anesthesia in mandibular molars: A clinical study. J Endod 1993;19:370-3.
4. Childers M, Reader A, Nist R, Beck M, Meyers WJ. Anesthetic efficacy of the periodontal ligament injection after an inferior alveolar nerve block. J Endod 1996;22:317-20.
5. Matthews R, Drum M, Reader A, Nusstein J, Beck M. Articaine for supplemental buccal mandibular infiltration anesthesia in patients with irreversible pulpitis when the inferior alveolar nerve block fails. J Endod 2009;35:343-6.
6. Hargreaves KM, Keiser K. Local anesthetic failure in endodontics: Mechanisms and Management. Endod Topics 2002;1:26-39.
7. Nusstein J, Reader A, Nist R, Beck M, Meyers WJ. Anesthetic efficacy of the supplemental intraosseous injection of 2% lidocaine with 1:100,000 epinephrine in irreversible pulpitis. J Endod 1998;24:487-91.
8. Haas DA, Harper DG, Saso MA, Young ER. Comparison of articaine and prilocaine anesthesia by infiltration in maxillary and mandibular arches. Anesth Prog 1990;37:230-7.
9. Haas DA, Harper DG, Saso MA, Young ER. Lack of differential effect by Ultracaine (articaine) and Citanest (prilocaine) in infiltration anaesthesia. J Can Dent Assoc 1991;57:217-23.
10. Kanaa MD, Whitworth JM, Corbett IP, Meechan JG. Articaine and lidocaine mandibular buccal infiltration anesthesia: A prospective randomized double-blind cross-over study. J Endod 2006;32:296-8.
11. Tortamano IP, Siviero M, Costa CG, Buscariolo IA, Armonia PL. A comparison of the anesthetic efficacy of articaine and lidocaine in patients with irreversible pulpitis. J Endod 2009;35:165-8.
12. Claffey E, Reader A, Nusstein J, Beck M, Weaver J. Anesthetic efficacy of articaine for inferior alveolar nerve blocks in patients with irreversible pulpitis. J Endod 2004;30:568-71.
13. Meechan JG, Kanaa MD, Corbett IP, Steen IN, Whitworth JM. Pulpal anaesthesia for mandibular permanent first molar teeth: A double-blind randomized cross-over trial comparing buccal and buccal plus lingual infiltration injections in volunteers. Int Endod J 2006;39:764-9.
14. Jung IY, Kim JH, Kim ES, Lee CY, Lee SJ. An evaluation of buccal infiltrations and inferior alveolar nerve blocks in pulpal anesthesia for mandibular first molars. J Endod 2008;34:11-3.
15. Malamed SF, Gagnon S, Leblanc D. Articaine hydrochloride: A study of the safety of a new amide local anesthetic. J Am Dent Assoc 2001;132:177-85.
16. Aggarwal V, Jain A, Kabi D. Anesthetic efficacy of supplemental buccal and lingual infiltrations of articaine and lidocaine after an inferior alveolar nerve block in patients with irreversible pulpitis. J Endod 2009;35:925-9.
17. Corbett IP, Kanaa MD, Whitworth JM, Meechan JG. Articaine infiltration for anesthesia of mandibular first molars. J Endod 2008;34:514-8.
18. Rosenberg PA, Amin KG, Zibari Y, Lin LM. Comparison of 4% articaine with 1:100,000 epinephrine and 2% lidocaine with 1:100,000 epinephrine when used as a supplemental anesthetic. J Endod 2007;33:403-5.
19. Chaudhary P, Martenson ME, Baumann TK. Vanilloid receptor expression and capsaicin excitation of rat dental primary afferent neurons. J Dent Res 2001;80:1518-23.
20. Goodis HE, Poon A, Hargreaves KM. Tissue pH and temperature regulate pulpal nociceptors. J Dent Res 2006;85:1046-9.
21. Parente SA, Anderson RW, Herman WW, Kimbrough WF, Weller RN. Anesthetic efficacy of the supplemental intraosseous injection for teeth with irreversible pulpitis. J Endod 1998;24:826-8.
22. Walton RE, Abbott BJ. Periodontal ligament injection: A clinical evaluation. J Am Dent Assoc 1981;103:571-5.
23. Tagger M, Tagger E, Sarnat H. Periodontal ligament injection: Spread of the solution in the dog. J Endod 1994;20:283-7.
24. Winther JE, Patirupanusara B. Evaluation of carticaine - a new local analgesic. Int J Oral Surg 1974;3:422-7.
25. Robertson D, Nusstein J, Reader A, Beck M, McCartney M. The anesthetic efficacy of articaine in buccal infiltration of mandibular posterior teeth. J Am Dent Assoc 2007;138:1104-12.

Conflict of interest: All authors declare they have no conflicts of interest related to the present study.

References

1. Jhala M, Menon R. Examining the impact of an asynchronous communication platform versus existing communication methods: an observational study. *BMJ Innov* 2021;**7**:68–74.
2. Ahmed OH, Carmody S, Walker LJ, Ahmad I. The need for speed! 10 ways that WhatsApp and instant messaging can enhance communication (and clinical care) in sport and exercise medicine. *Br J Sports Med* 2020;**54**:1128–9.
3. Linz D, Garcia R, Guerra F, Kommata V, Bollman A, Duncker D. Twitter for professional use in electrophysiology: practical guide for #EPeeps. *Europace* 2021;**23**:1192–9.
4. Regulation (EU) 2016/679 of the European Parliament and of the Council of 27 April 2016 on the protection of natural persons with regard to the processing of personal data and on the free movement of such data, and repealing Directive 95/46/EC (General Data Protection Regulation). https://eur-lex.europa.eu/eli/reg/2016/679/2016-05-04 (07 February 2021, date last accessed).
5. Pluymaekers NAHA, Hermans ANL, van der Velden RMJ, Gawałko M, den Uijl DW, Buskes S *et al.* Implementation of an on-demand app-based heart rate and rhythm monitoring infrastructure for the management of atrial fibrillation through teleconsultation: teleCheck-AF. *Europace* 2021;doi:10.1093/europace/euaa201.
6. Kochar A, Rymer J, Samad Z; Duke Cardiovascular Education Group. Disrupting fellow education through group texting: WhatsApp in fellow education? *J Am Coll Cardiol* 2018;**72**:3366–9.
7. Clavier T, Ramen J, Dureuil B, Veber B, Hanouz JL, Dupont H *et al.* Use of the Smartphone app WhatsApp as an E-learning method for medical residents: multicenter controlled randomized trial. *JMIR Mhealth Uhealth* 2019;**7**:e12825.

IMAGES IN ELECTROPHYSIOLOGY

doi:10.1093/europace/euaa380
Online publish-ahead-of-print 17 December 2020

Vanishing left bundle branch potential during physiological pacing

Shunmuga Sundaram Ponnusamy

Department of Cardiology, Velammal Village, Velammal Medical College Hospital and Research Institute, Madurai 625009, Tamil Nadu, India

Corresponding author. Tel: +919444712846. *E-mail address:* shunmuga.pgi@gmail.com

A 67-years-old gentleman had undergone left bundle branch pacing for symptomatic intra-Hisian block (*Panel A*). Left bundle branch potential (LBB-Po) was noted after six rapid rotations (*Panel B*). Additional rotations were given as the peak left ventricular activation time was not short and constant, which resulted in the disappearance of potential. As the unipolar pacing threshold was 0.3 V at 0.5 ms pulse-width and unipolar impedance 620 Ω with LBB current of injury (Type II LBB-COI), we decided to wait before considering lead repositioning for a probable septal perforation. Gradual re-appearance of LBB-Po was noted as the COI settled and final paced QRS confirmed LBB capture.

Conflict of interest: Consultant; Medtronic.

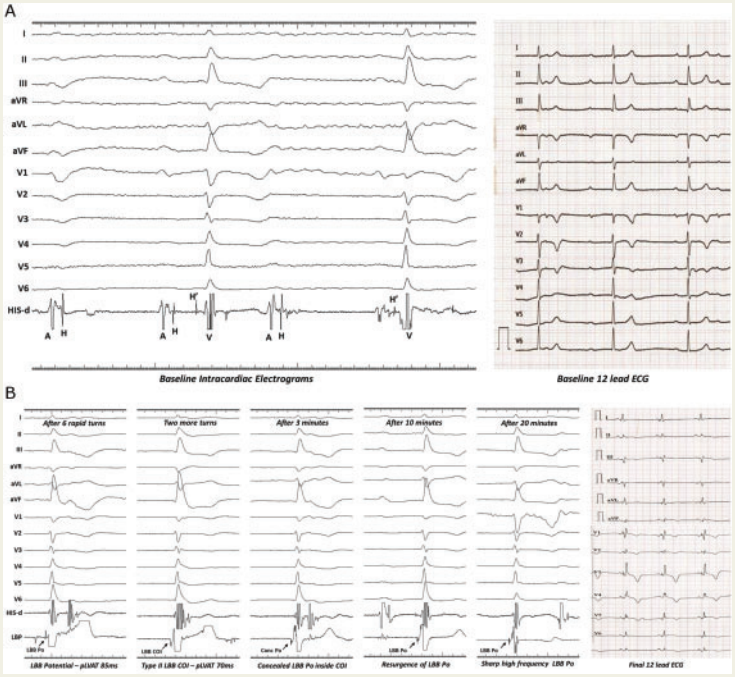

Type of manuscript: EP rounds
Title of the article:

Uncommon modes of initiation of 'A on V' narrow QRS tachycardia- What are the mechanisms?

Authors: Raghav Bansal, MD, DM[1], Ramalingam Vadivelu, MD, DM[2], Yash Lokhandwala, MD, DM, FACC[3]

Institution affiliation and address:

[1] Assistant Professor Cardiology, All India Institute of Medical Sciences, New Delhi, India-110029

[2] Assistant Professor Cardiology, Velammal Medical College Hospital and Research Institute, Madurai, India-625009

[3] Department of Cardiology, Bandra Holy Family Hospital and Research Centre, Mumbai, India-400050

Name and address of corresponding author:

Dr Ramalingam Vadivelu, Department of Cardiology, Velammal Medical College Hospital and Research Institute, Madurai, India-625009

Phone number: +91-8156843960 Email id: vvelu00@gmail.com

No financial support or grant was received

Conflict of interest statement

There are no conflicts of interest regarding this work from authors

Number of words: 701 (excluding references) **Number of figures**: 3

This article has been accepted for publication and undergone full peer review but has not been through the copyediting, typesetting, pagination and proofreading process, which may lead to differences between this version and the Version of Record. Please cite this article as doi: 10.1111/pace.14127.

Manuscript

A 55-year old man with a structurally normal heart underwent electrophysiology study for recurrent episodes of drug refractory paroxysmal palpitations, requiring multiple hospital admissions. The baseline intervals were normal with AH of 76 ms and HV of38 ms; there was no manifest or latent preexcitation. Ventricular extrastimuli (VES) repeatedly induced a narrow QRS tachycardia (Figure1, left and right panels). What is the tachycardia mechanism and what are the modes of initiation?

Discussion

The left panel of Figure 1 shows VES inducing tachycardia with a cycle length of 390ms. With S2 there is decremental ventriculoatrial conduction, but S3 is not conducted to the atrium. After S3, tachycardia is induced with a 'A on V' pattern. The right panel of Figure 1 shows the tachycardia to be induced by a less premature S2, followed by a V-A-V sequence.

The differential diagnoses include 1) Typical AVNRT, 2) Atrial tachycardia with a long PR interval, 3) Junctional tachycardia and 4) Orthodromic AVRT using a concealed nodofascicular accessory pathway. Tachycardia was noted to spontaneously terminate in the atrioventricular node, after an atrial complex making atrial tachycardia less likely. Multiple His-refractory VES failed to affect the atrial activation, making a concealed nodofascicular pathway unlikely. Early atrial extrastimuli did not advance the next QRS complex, making automatic junctional tachycardia less likely. It will be uncommon for tachycardias like junctional or atrial tachycardia to have onset with ventricular extrastimulation as described in this patient. Further, the tachycardia initiated with an AH jump upon atrial extrastimuli and

ventricular overdrive pacing during tachycardia demonstrated a difference between post-pacing interval and tachycardia cycle length of 134 ms. A diagnosis of typical AVNRT was suggested based on these findings.

Typical AVNRT is usually initiated by atrial extrastimuli. In this case, VES from the right ventricular outflow tract (Figure 1,right panel) also initiated typical AVNRT with a V-A-V sequence. The atrium is activated retrogradely via the fast pathway, reentering via the slow pathway to set up slow-fast AVNRT (Figure 2, right panel).This can happen when retrograde slow pathway conduction is poor or absent, which is unusual. The moot point is the initiation of typical AVNRT by VES delivered from the right ventricular apex, with a V-V/A initiation sequence (Figure 1, left panel). This can be explained by one of three mechanisms: i) The S3 complex is conducted into the AV node via the fast pathway but blocks onward to the atrium; it however reenters via the slow pathway and sets off AVNRT. This is however not tenable since the RR interval (425 ms) between S3 and the next QRS is much shorter than RR interval (600 ms) between S2 and the first QRS complex of AVNRT as seen in Figure 2, right panel. ii)The S3 initiates a junctional complex which travels up the fast pathway and reenters via the slow pathway, setting up typical AVNRT (Figure 2, left panel). iii) The more likely explanation is simpler (Figure 3). The right panel shows a typical AVNRT induced by retrograde fast and anterograde slow with an A to onset V interval of 470 ms from the A after S2 to the onset of QRS of the first tachycardia beat. In the left panel, the interval from the A after S2 to the QRS onset of the first tachycardia beat is the same, i.e. 470 ms. Thus, in the left panel, it is really S2 that started the tachycardia whileS3 merely blocked retrogradely without getting into the circuit and was just a ‘bystander’.

The slow pathway region was mapped in sinus rhythm. RF ablation was performed in the slow pathway region, just 1 cm anterosuperior to the coronary sinus ostium, resulting in

frequent junctional acceleration. After this, tachycardia could not be induced despite aggressive atrial and ventricular stimulation protocol even after isoprenaline and atropine challenge.

Conclusion

Typical AVNRT is usually inducible by atrial pacing maneuvers, and uncommonly by VES.[1] Rarely, typical AVNRT can be induced only by VES and can be explained by the two different mechanisms as explained in this case. Different electrophysiological parameters of dual AV nodal pathways have been described in patients with typical slow fast AVNRT where tachycardia could be induced only ventricular pacing or VES protocol.[2]

Bibliography

1. Cunha Guerra M, Lokhandwala Y, Oyarzun R, et al. When and how does a single ventricular premature beat initiate and terminate supraventricular tachycardia?. Ann Noninvasive Electrocardiol. 2019;24(5): e12650. doi:10.1111/anec.12650.
2. Lee PC, Tai CT, Hwang B et al. The Electrophysiologic Characteristics in Patients with Only Ventricular-Pacing Inducible Slow–Fast Form Atrioventricular Nodal Reentrant Tachycardia. Journal of interventional cardiac electrophysiology. 2005 Dec 1;14(3):153-7.

Figure legends

Figure 1: Left and right panels: Ventricular extrastimualtion (VES) inducing a narrow QRS tachycardia. Surface electrocardiogram (I, aVF,V1,V6) and intracardiac electrograms) - Coronary sinus (CS) 910 dipoles at CS ostium, CS 12 dipoles at distal CS and His bundle electrogram distal and proximal (HISD, HISP).

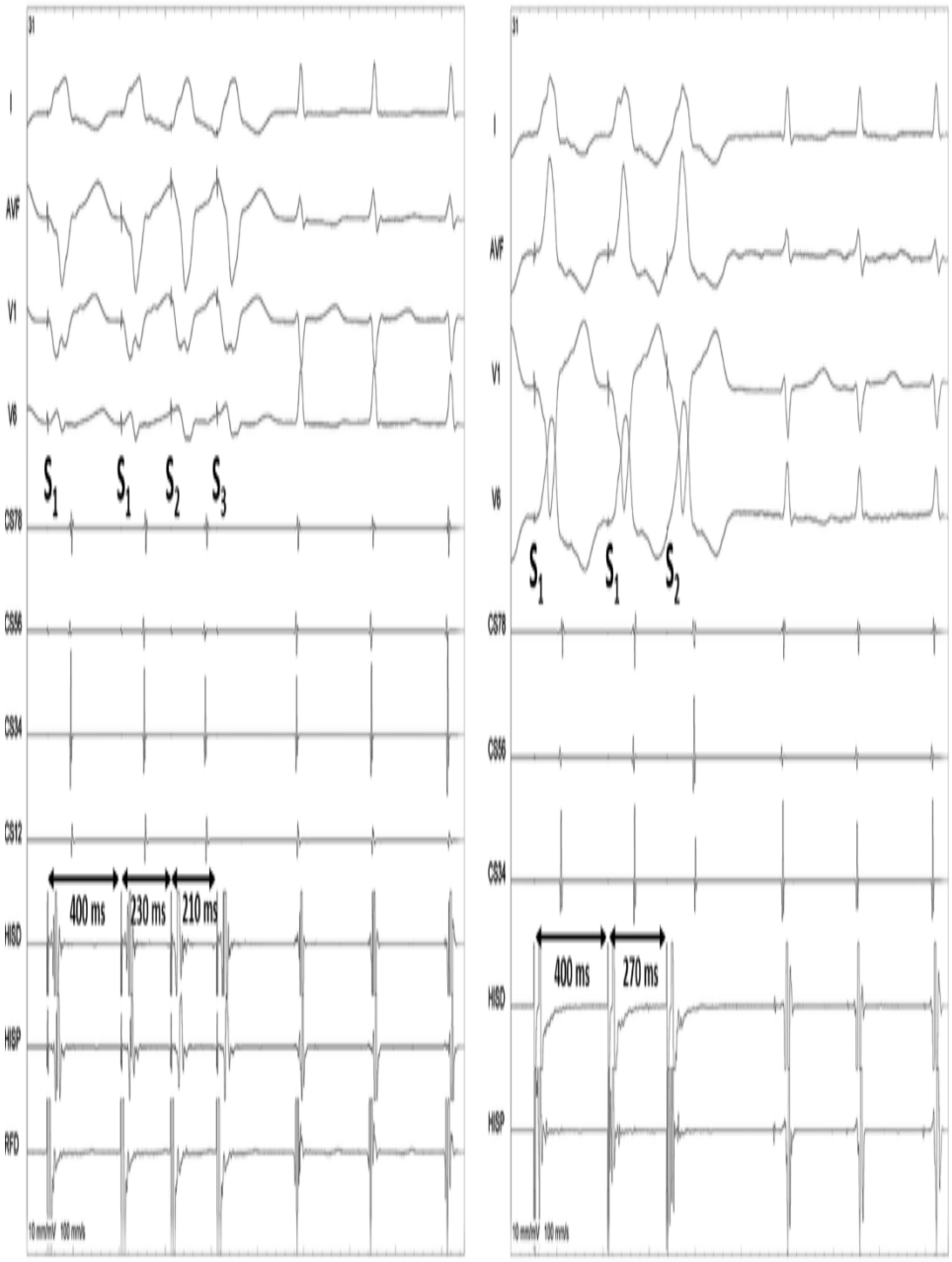

Figure 2: The **left panel** shows right ventricular apical pacing with retrograde concentric atrial activation. After the second extrastimulus (S2), there is decremental VA conduction. After S3, there is no atrial complex and typical AVNRT is induced with a 'V-V-A' initiation sequence. Ladder diagram: SA- Sinoatrial node; A-atrium; AVN-AV node; V-Ventricle; FP-fast pathway; SP-slow pathway; J- Junctional beat. The proposed mechanism is a spontaneous junctional complex which travels up the fast pathway and re-initiates AVNRT. The **right panel** shows right ventricular outflow pacing with retrograde concentric atrial activation. After the second extra stimulus (S2), there is retrograde VA conduction via the fast pathway and re-entrant antegrade conduction by the slow pathway, initiating typical slow fast AVNRT.

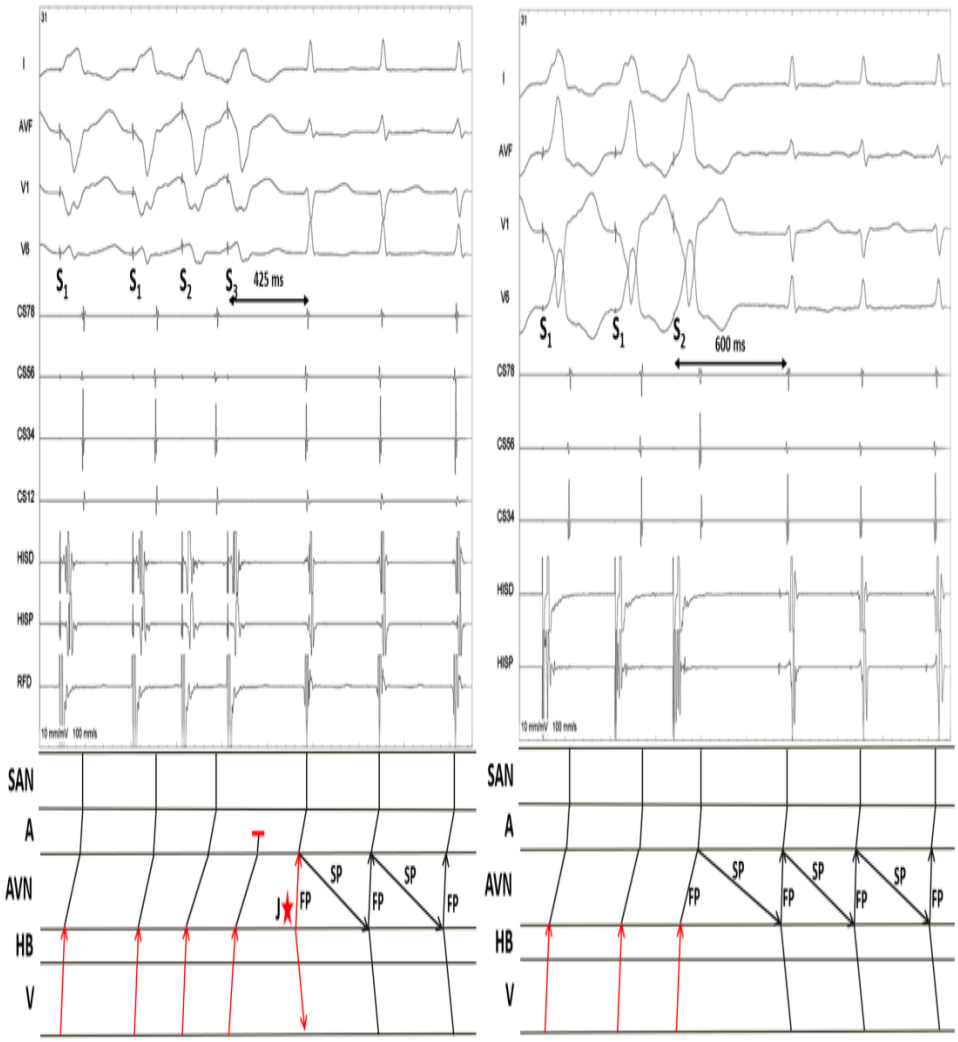

Figure 3: Left and right panels: Ventricular extrastimualtion (VES) inducing a narrow QRS tachycardia. Surface electrocardiogram (I, aVF,V1, V6) and intracardiac electrograms) - Coronary sinus (CS) 910 dipoles at CS ostium, CS 12 dipoles at distal CS and His bundle electrogram distal and proximal (HISD, HISP).The right panel shows a typical AVNRT induced by retrograde fast and anterograde slow with an 'A' to onset V interval of 470 ms. In the left panel, the interval from the 'A' after S2 to the QRS onset of the first tachycardia beat is the same, i.e. 470 ms.

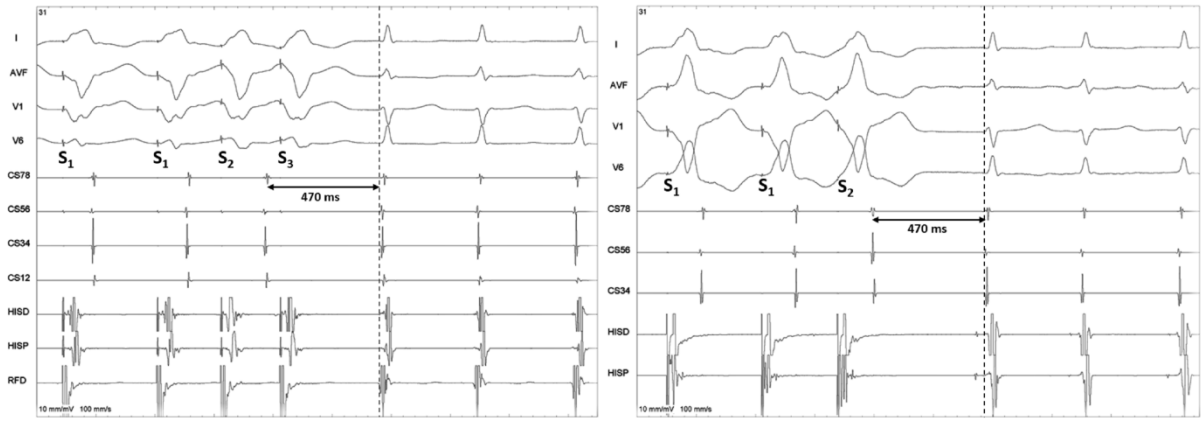

Acta Cardiologica

ISSN: 0001-5385 (Print) 0373-7934 (Online) Journal homepage: https://www.tandfonline.com/loi/tacd20

Impact of plaque burden and composition on coronary slow flow in ST-segment elevation myocardial infarction undergoing percutaneous coronary intervention: intravascular ultrasound and virtual histology analysis

Sreenivas Reddy, Raghavendra Rao K, Jeet Ram Kashyap, Vikas Kadiyala, Hithesh Reddy, Samir Malhotra, Ramesh Daggubati, Suraj Kumar, Hariom Soni, Naindeep Kaur, Jaspreet Kaur & Vadivelu Ramalingam

To cite this article: Sreenivas Reddy, Raghavendra Rao K, Jeet Ram Kashyap, Vikas Kadiyala, Hithesh Reddy, Samir Malhotra, Ramesh Daggubati, Suraj Kumar, Hariom Soni, Naindeep Kaur, Jaspreet Kaur & Vadivelu Ramalingam (2020): Impact of plaque burden and composition on coronary slow flow in ST-segment elevation myocardial infarction undergoing percutaneous coronary intervention: intravascular ultrasound and virtual histology analysis, Acta Cardiologica, DOI: 10.1080/00015385.2020.1767842

To link to this article: https://doi.org/10.1080/00015385.2020.1767842

Published online: 26 May 2020.

ACTA CARDIOLOGICA
https://doi.org/10.1080/00015385.2020.1767842

ORIGINAL SCIENTIFIC PAPER

Impact of plaque burden and composition on coronary slow flow in ST-segment elevation myocardial infarction undergoing percutaneous coronary intervention: intravascular ultrasound and virtual histology analysis

Sreenivas Reddy[a], Raghavendra Rao K[a], Jeet Ram Kashyap[a], Vikas Kadiyala[a], Hithesh Reddy[a], Samir Malhotra[b], Ramesh Daggubati[c], Suraj Kumar[a], Hariom Soni[b], Naindeep Kaur[a], Jaspreet Kaur[a] and Vadivelu Ramalingam[d]

[a]Department of Cardiology, Government Medical College and Hospital, Chandigarh, India; [b]Department of Pharmacology, Post Graduate Institute of Medical Education and Research (PGIMER), Chandigarh, India; [c]Cardiology, West Virginia University, Morgantown, WV, USA; [d]Department of Cardiology, Velammal Medical College Hospital and Research Institute, Madurai, India

ABSTRACT

Aim: Coronary slow flow (SF) is an important complication of percutaneous coronary intervention (PCI) associated with poor prognosis. The aim was to assess grey-scale intravascular ultrasound (IVUS) and virtual histology (VH-IVUS) characteristics of culprit lesion in ST-elevation myocardial infarction (STEMI).

Methods: A total of 295 consecutive patients with STEMI underwent coronary angiogram and IVUS. Following PCI, patients divided into two groups; SF (thrombolysis in myocardial infarction [TIMI] flow ≤ 2, $n = 74$) and normal flow (NF) (TIMI flow >2, $n = 221$). Coronary plaque burden and its composition in relation to SF were evaluated.

Results: On grey-scale IVUS, the plaque area (12.3 mm^2 *vs.* 11.5 mm^2, $p = .01$), plaque volume (110.7 mm^3 *vs.* 99.8 mm^3, $p < .001$), lesion external elastic membrane (EEM) cross-sectional area (14.9 mm^2 *vs.* 14.0 mm^2, $p = .011$) and remodelling index (1.3 *vs.* 1.2, $p = .043$) were significantly higher in SF group. On VH-IVUS, absolute fibrous volume (48.1 mm^3 *vs.* 41.5 mm^3, $p \leq .001$), fibrofatty volume (23.8 mm^3 *vs.* 18.6 mm^3, $p = .015$), necrotic core volume (8.3 mm^3 *vs.* 5.5 mm^3, $p < .001$), dense calcium volume (1.2 mm^3 *vs.* 0.6 mm^3, $p = .003$) and thin cap fibroatheroma either single (30.1% *vs.* 16.1%, $p < .001$) or multiple (9.6% *vs.* 1.8%, $p < .001$) were higher in SF arm. In multivariable analysis, absolute necrotic core volume (odds ratio = 1.159; 95% CI 1.030–1.305, $p = .015$) was the only independent predictor of SF.

Conclusions: Higher necrotic core volume as detected by VH-IVUS may be a potential risk factor for the development of coronary SF phenomenon in patients with STEMI after PCI.

ARTICLE HISTORY
Received 14 February 2020
Revised 6 April 2020
Accepted 5 May 2020

KEYWORDS
ST-elevation myocardial infarction; percutaneous coronary intervention; intravascular ultrasound; virtual histology-intravascular ultrasound; predictors; slow flow

1. Introduction

Percutaneous coronary intervention (PCI) has become the accepted standard of care in the management of acute ST-elevation myocardial infarction (STEMI) [1–3]. A varying number of patients fail to achieve thrombolysis in myocardial infarction (TIMI) III flow in STEMI mainly because of coronary slow flow (SF). The incidence of coronary SF in patients with STEMI undergoing PCI ranges widely from 11% to 45% [4–7]. The occurrence of SF increases not only the in-hospital mortality but also 6 months and long-term mortality [8–11]. The exact mechanism responsible for SF has not been identified but various mechanisms have been proposed like ischemic–reperfusion injury, atherothrombotic distal embolisation, and individual predisposition of coronary microcirculation, making it a multifactorial pathogenesis [12–14]. In view of the significant short-term and long-term morbidity as well as mortality associated with SF, it is of pivotal importance to identify its predictors in patients with STEMI planned for PCI to help the clinician to identify the high-risk patients and adopt aggressive therapeutic strategies so as to decrease the occurrence of SF and improve clinical outcomes [9].

Intravascular ultrasound (IVUS) has emerged as an essential modality for the quantitative and qualitative characterisation of the atherosclerotic plaque burden in the recent times. Different grey-scale IVUS

CONTACT Sreenivas Reddy reddycardio2911@gmail.com Department of Cardiology, Government Medical College and Hospital, Sector 32, Chandigarh 160030, India

parameters have been identified to predict SF in patients with acute coronary syndrome (ACS) [15–20]. However, the grey-scale IVUS has its own inherent limitations in the assessment of plaque composition hence, virtual histology (VH)-IVUS is utilised for better qualitative and quantitative information [21]. Different components of VH have been identified as the predictors of coronary SF in STEMI after PCI such as necrotic core volume and dense calcium volume [5,7,22,23]. We intended to study the grey-scale IVUS and VH-IVUS predictors of SF in patients with STEMI undergoing PCI, depicting the real-world situation, wherein presentation to the clinician with varied modes and timings to performance of PCI.

2. Materials and methods

This is a single-centre prospective observational study.

2.1. Objectives

1) Comparison of the quantitative and qualitative differences in the coronary plaque burden and its composition as determined by grey-scale IVUS and VH-IVUS in patients with SF *vs.* normal flow (NF) in STEMI patients undergoing PCI.

2) Identification of grey-scale IVUS and VH-IVUS predictors and discriminators of coronary SF in STEMI patients undergoing PCI.

2.2. Study population

This is a single-centre prospective observational study carried out in the Department of Cardiology of a tertiary care hospital in North India. From June 2017 to September 2019, a total of 416 patients with ACS presenting to our institute were screened as part of an ongoing study of IVUS in ACS. Patients with unstable angina and NSTEMI comprising 42 and 39 each, respectively, were excluded. In 40 patients with STEMI, IVUS analysis was not possible, hence excluded and the remaining 295 patients were enrolled of which 74 patients developed SF and 221 patients had NF. Patients with STEMI who underwent successful primary PCI within 12 h of symptom onset, patients with chest pain of >12 h duration but who underwent PCI within 24 h after the appearance of symptoms and rescue PCI in patients with failed thrombolytic therapy with ongoing ischaemia were all included in the study. STEMI was defined in accordance with the American College of Cardiology Foundation/American Heart Association Task Force on Practice Guidelines based on the criteria of clinical presentation, electrocardiogram findings, and cardiac enzyme [24]. Patients with deranged renal function, tortuous coronary vessels precluding IVUS examination, past history of PCI or coronary artery bypass graft (CABG) , and refusal of consent were also excluded. All participants provided a written informed consent and the study was approved by the Institutional Ethics Committee, GMCH, Chandigarh (reference number IEC/2017/12 dated 04.05.2017). All procedures were conducted in accordance with Good Clinical Practice (GCP) principles as outlined in the Declaration of Helsinki.

2.3. PCI procedure

Prior to the PCI procedure, all patients were given 325 mg aspirin and either clopidogrel 300–600 mg or prasugrel 60 mg or ticagrelor 180 mg and intravenous unfractionated heparin titrated to achieve therapeutic range activated clotting time. IVUS imaging was performed using a 20-MHz, 2.9 French, Eagle Eye® Platinum RX digital IVUS catheter (Eagle Eye, Philips Volcano, San Diego, CA). All patients were administered 200 mcg of intracoronary nitroglycerine and IVUS pull back was taken starting 15 mm distal to the lesion till the aorto-ostial junction using an automatic pull back at a speed of 0.5 mm/s prior to (before) any balloon dilatation. In completely occluded artery, a small 1.25 mm diameter balloon predilation was performed to ensure antegrade flow and facilitate IVUS catheter passage. The decision of using GPIIb/IIIa inhibitors, intracoronary nitroglycerine (100–200 mcg bolus), intracoronary adenosine (48–200 mcg bolus), and nicorandil (1–2 mg bolus) was taken by the primary operator.

2.4. Angiographic analysis

Coronary angiography and PCI were done for all patients at a frame rate of 15/s. Angiograms acquired at the baseline, immediately after the deployment of stent and at the end of PCI were evaluated by the coronary angiography software Medis Q Angio® XA 7.3 (Medis medical imaging systems, Leiden, the Netherlands) offline analysis by two independent observers (RK and HR). SF was defined as a TIMI flow grade ≤ 2 in the angiogram acquired immediately after the deployment of stent after excluding mechanical obstruction to the flow. Corrected thrombolysis in myocardial infarction frame count (CTFC) was calculated for the subjective assessment of SF and was measured immediately after stent deployment [25]. As

per the standard methods, the cine frame count obtained was multiplied by 30 and divided by 15 for reporting. A CTFC score of 100 was given if a TIMI flow grade 0 or 1 after PCI was noted [17]. Coronary collateral flow was graded as described by Rentrop and colleagues [26]. The grading of coronary thrombus on the baseline angiogram was done from 0 to 5 as suggested by Gibson et al. [25].

2.5. Grey-scale IVUS and virtual histology acquisition analysis

The IVUS images of all the patients enrolled in the study were recorded and stored on a DVD-ROM. The offline analysis was performed by two independent observers who had no prior knowledge of the patient details or angiograms (VK and SK). A consensus was obtained if there was discordance in the analyses by repeated off line readings. Quantitative and qualitative IVUS analysis was performed in accordance with the American College of Cardiology Clinical Expert Consensus Document on Standards for Acquisition, Measurement and Reporting of Intravascular Ultrasound Studies [27]. All the IVUS and VH analysis were done using a validated and computerised INDEC'S Echo plaque 4.3.12J software (INDEC Medical Systems, Inc., Santa Clara, CA). The culprit lesion was the smallest lumen site whereas the proximal and distal reference segments were near normal looking image slices within 10 mm distal and proximal to the lesion without any significant side branch. A vascular segment length of 10 mm, with tight stenosis as midpoint, was considered for analysis. After automatic border detection for the lumen and media-adventitia interface by the software, manually correction and confirmation done to obtain the results calculated to be displayed automatically.

External elastic membrane (EEM) and lumen cross-sectional areas (CSA) were measured first and plaque and media (P&M) CSA was calculated as EEM minus lumen CSA. Plaque burden was calculated as plaque and media CSA/EEM CSA $\times$ 100. Remodelling index was the ratio of lesion site EEM CSA divided by the average of the proximal and distal reference EEM CSA. VH analysis classified the colour-coded tissue into four major components: green (Fibrous, F); yellow-green (Fibrofatty, FF); white (Dense calcium, DC); and red (Necrotic core, NC) [28]. The reporting was done in terms of absolute values and as percentage of plaque area or volume. Thin-cap fibroatheroma (TCFA) was considered when necrotic core more than $\geq$10% of plaque area in three or more consecutive image slices abutting the lumen with no overlying fibrous tissue and subtending a plaque burden of $\geq$40% [29].

2.6. Statistical analysis

In the literature the prevalence of SF in patients with STEMI is approximately 11–45%, for sample size calculation, we assumed the prevalence to be about 25% in our setting with 5% level of significance and 5% margin of error, we calculated that 290 patients would be required for our study. All the statistical analysis was done using SPSS version 22.0 (SPSS Inc., Chicago, IL). Categorical data were presented as percentages (%) and frequencies, and Chi-square test or Fisher's exact test was used as appropriate. Distribution of the continuous variables was evaluated using Kolmogorov–Smirnov test and was presented as mean with standard deviation if normally distributed and median with 25th and 75th percentiles when skewed distributed. Univariate analysis was done to find out association of categorical variables between the two study groups using either Chi-square test or Fisher's exact test as appropriate. Similarly to compare normally distributed continuous variables between two study groups, independent t-test was applied and Mann–Whitney U test was utilised to compare skewed distributed variables. Variables showing significant difference ($p < .05$) were included in the enter method of logistic regression model to identify the independent predictors of SF. Receiver operating characteristic (ROC) curve analyses were performed to determine the best cut-off values (using the Youden index J) of the intravascular ultrasound parameters for differentiating coronary SF from NF along with area under the curve (AUC), sensitivity, specificity, positive, and negative predictive values. A p value $< .05$ was taken as statistically significant for the analyses.

3. Results

3.1. Baseline clinical characteristics

A total of 295 patients were included in the study of which 74 patients (25%) developed SF post PCI. The baseline clinical characteristics of the patients are outlined in Table 1. There was no appreciable difference in the age and gender between the groups. Coronary artery disease risk factors like hypertension, diabetes mellitus, smoking, and family history of premature CAD did not differ between the two groups. In addition, no significant difference was observed in the thrombolysis rate, usage of glycoprotein IIb/IIIa inhibitors, and symptom onset to PCI time among the two

Table 1. Baseline characteristics of the patients ($n = 295$).

Variables	Slow flow ($n = 74$)	Normal flow ($n = 221$)	p Value
Age (years)	55 (47–63)	54 (45–60)	.098
Male, *n* (%)	56 (75.7%)	184 (83.3%)	.147
Hypertension, *n* (%)	27 (36.5%)	72 (32.6%)	.538
Diabetes mellitus, *n* (%)	14 (18.9%)	61 (27.6%)	.138
Smoking, *n* (%)	27 (36.5%)	106 (48.0%)	.086
Family history of CAD, *n* (%)	13 (17.6%)	59 (26.7%)	.114
BMI (kg/m^2)	24.75 (22.3–27.3)	24.9 (22.7–27.4)	.433
BSA (m^2)	1.71 (1.61–1.83)	1.72 (1.63–1.82)	.945
Symptom onset to PCI time (hours)	8.85 (7.02–11.4)	8.20 (6.2–11.8)	.207
Haemoglobin (g/dL)	12.5 (11.2–13.9)	13.0 (11.8–14.2)	.197
Creatinine (mg/dL)	1.10 (1.00–1.20)	0.90 (1.10–1.30)	.423
Total cholesterol (mg/dL)	147.5 (125.5–177.5)	147 (118–170)	.404
Triglycerides (mg/dL)	111 (94.7–148.1)	120 (97–154)	.357
LDL-cholesterol (mg/dL)	92 (67.7–118)	81 (62–118)	.310
HDL-cholesterol (mg/dL)	40 (32.7–46.2)	38 (31–43)	.089
CK-MB (IU/l)	66 (37.6–160.5)	38 (29.5–75)	.081
Ejection fraction (%)	43.0 (41.12–48.0)	47.0 (42.5–52.5)	.229
Thrombolysis, *n* (%)	20 (27.0%)	41 (18.6%)	.119
Glycoprotein IIb-IIIa inhibitors use, *n* (%)	43 (58.1%)	109 (49.3%)	.191

CAD: coronary artery disease; BMI: body mass index; BSA: body surface area; PCI: percutaneous coronary intervention; LDL: low-density lipoprotein; HDL: high-density lipoprotein; CK-MB: creatine kinase-MB (IU/l). Data are presented as mean ± SD, median (interquartile range) or *n* (%).

groups. Investigations such as haemoglobin, creatinine, lipid profile, creatine kinase-MB, and LV ejection fraction were comparable among the groups.

3.2. Angiographic characteristics and procedure findings

Angiographic characteristics and procedure findings are shown in Table 2. Considering the angiographic findings, the culprit vessel, number of vessels diseased, ACC/AHA lesion type, baseline TIMI flow, collateral flow grade, and TIMI thrombus grading were comparable between the two groups. The TIMI thrombus grades >3 (12.2%) and <3 (5.9%) were compared between the two groups, respectively, however, there was no statistically significant difference between them ($p = .075$). The maximum inflation pressure of the stents was comparable between the two groups however the CTFC was markedly higher in the SF group (59.41 *vs.* 30; $p < .001$).

3.3. Grey-scale IVUS findings

The grey-scale IVUS findings are listed in Table 3. IVUS derived lesion length was comparable in both the groups. The measurements in the proximal and distal reference segments did not differ between the two groups except the proximal reference lumen CSA and EEM CSA which were higher in the SF group as compared to the NF group (proximal reference lumen CSA: 10.54 mm^2 *vs.* 9.6 mm^2, $p = .047$; proximal reference EEM CSA: 15.64 mm^2 *vs.* 14.29 mm^2, $p = .031$, respectively). The lesion EEM CSA, plaque area and plaque volume were significantly greater in the SF group as compared to the NF group (lesion EEM CSA: 14.91 mm^2 *vs.* 14.06 mm^2, $p = .011$; plaque area: 12.37 mm^2 *vs.* 11.5 mm^2, $p = .010$; plaque volume: 110.7 mm^3 *vs.* 99.8 mm^3, $p < .001$, respectively). Remodelling index was higher in the SF group in comparison to the NF group (1.3 *vs.* 1.2; $p = .043$).

3.4. Virtual Histology-IVUS findings

Culprit lesion site plaque composition comparing the SF and NF group by VH-IVUS is shown in Figure 1. The percentages of each plaque component did not differ across the groups. However, the absolute volumes of fibrous, fibrofatty, necrotic core and dense calcium were significantly higher in the SF arm in comparison to the NF arm (Fibrous volume: 48.1 mm^3 *vs.* 41.5 mm^3, $p < .001$; fibrofatty volume: 23.85 mm^3 *vs.* 18.65 mm^3, $p = .015$; NC volume: 8.3 mm^3 *vs.* 5.5 mm^3, $p < .001$; DC volume: 1.20 mm^3 *vs.* 0.6 mm^3, $p = .003$, respectively). The presence of TCFA either single or multiple was more common in the SF group as compared to the NF group (30.1% *vs.* 16.1%, $p < .001$; 9.6% *vs.* 1.8%; $p < .001$, respectively) (Figure 2).

3.5. Predictors of slow flow

Univariate analysis was performed in the first instance to identify the potential predictors of SF. Following which the variables with p value <.05, which include proximal reference EEM CSA, proximal reference lumen CSA, lesion EEM CSA, remodelling index, lesion plaque volume, absolute fibrous volume,

Table 2. Angiographic characteristics and procedure findings ($n = 295$).

Variables	Slow flow ($n = 74$)	Normal flow ($n = 221$)	p Value
Culprit vessel, *n* (%)			
LAD	55 (74.3%)	133 (60.2%)	.168
LCX	6 (8.1%)	24 (10.9%)	
RCA	13 (17.6%)	61 (27.6%)	
RAMUS	0 (0%)	3 (1.4%)	
Diseased vessels, *n* (%)			
SVD	49 (66.2%)	155 (70.1%)	.527
DVD	17 (23%)	49 (22.2%)	.886
TVD	8 (10.8%)	17 (7.7%)	.404
ACC/AHA lesion type, *n* (%)			
Type A	16 (21.6%)	76 (34.4%)	.146
Type B_1	16 (21.6%)	46 (20.8%)	
Type B_2	27 (36.5%)	56 (25.3%)	
Type C	15 (20.3%)	43 (19.5%)	
Baseline TIMI flow grade, *n* (%)			
0	14 (18.9%)	49 (22.2%)	.643
1	3 (4.1%)	4 (1.8%)	
2	15 (20.3%)	49 (22.2%)	
3	42 (56.8%)	119 (53.8%)	
Collateral flow grade (Rentrop), *n* (%)			.200
0	64 (86.5%)	202 (91.4%)	
1	2 (2.7%)	1 (0.5%)	
2	8 (10.8%)	16 (7.2%)	
3	0 (0%)	2 (0.9%)	
TIMI Thrombus grading, *n* (%)			.169
0	45 (60.8%)	164 (74.2%)	
1	18 (24.3%)	36 (16.3%)	
2	1 (1.4%)	5 (2.3%)	
3	1 (1.4%)	3 (1.4%)	
4	3 (4.1%)	6 (2.7%)	
5	6 (8.1%)	7 (3.2%)	
Maximum inflation pressure, atm	13.93 ± 0.30	13.97 ± 0.48	.501
CTFC after PCI	59.41(49.4–91.5)	30 (24.7–34.1)	<.001*

LAD: left anterior descending coronary artery; LCX: left circumflex coronary artery; RCA: right coronary artery; SVD: single-vessel disease; DVD: double vessel disease; TVD: triple vessel disease; TIMI: thrombolysis in myocardial infarction; CTFC: corrected thrombolysis in myocardial infarction frame count; PCI: percutaneous coronary intervention.
*Denotes significant value. Data are presented as mean ± SD, median (interquartile range) or *n* (%).

Table 3. Grey-scale IVUS findings ($n = 295$).

Variables	Slow flow ($n = 74$)	Normal flow ($n = 221$)	p Value
IVUS Lesion length (mm)	30.70 (18.5–42.2)	27.8 (19.6–37.2)	.412
Proximal reference			
Lumen CSA (mm^2)	10.54 (8.19–12.87)	9.6 (8.0–11.6)	.047*
EEM CSA (mm^2)	15.64 (12.66–18.68)	14.29 (11.72–16.5)	.031*
Plaque burden (%)	32.27 (25.6–37.14)	31 (24.25–36.63)	.433
Distal reference			
Lumen CSA (mm^2)	5.78 (4.22–7.53)	6.22 (4.86–7.59)	.255
EEM CSA (mm^2)	8.48 (5.94–11.98)	8.9 (6.68–11.19)	.488
Plaque burden	27.85 (22.94–34.04)	28.94 (23.17–35.54)	.660
Average/Mean Lumen CSA (mm^2)	8.44 (6.93–9.94)	7.90 (6.68–9.35)	.241
Average/Mean EEM CSA (mm^2)	12.23 (9.99–14.45)	11.50 (9.46–13.65)	.140
Lesion measurements			
Lesion minimum luminal diameter (mm)	1.57 (1.51–1.66)	1.58 (1.52–1.67)	.603
Lesion maximum luminal diameter (mm)	2.02 (1.84–2.26)	1.94 (1.80–2.16)	.083
Lesion Lumen CSA (mm^2)	2.51 (2.18–2.84)	2.40 (2.13–2.79)	.214
Lesion EEM CSA (mm^2)	14.91 (12.94–18.81)	14.06 (11.90–16.17)	.011*
Lesion lumen area stenosis (%)	68.04 (60.94–73.34)	68.45 (60.75–73.59)	.918
Lesion plaque area (mm^2)	12.37 (10.55–16)	11.50 (9.55–13.56)	.010*
Lesion plaque burden (%)	82.15 (80.30–85.80)	81.60 (79.45–84.60)	.084
Lesion plaque volume (mm^3)	110.7 (97.32–135.87)	99.8 (79.7–119.75)	<.001*
Remodelling index	1.3 (1.10–1.52)	1.2 (1.03–1.38)	.043*

IVUS: intravascular ultrasound; EEM CSA: external elastic membrane cross-sectional area. Data are presented as mean ± SD, median (interquartile range) or *n* (%).
*Denotes significant value.

absolute fibrofatty volume, absolute NC volume, and absolute DC volume were tested for multivariate analysis. The absolute NC volume over the lesion length was the only independent predictor of coronary SF in STEMI after PCI (odds ratio = 1.159; 95% CI 1.030–1.305, $p = .015$).

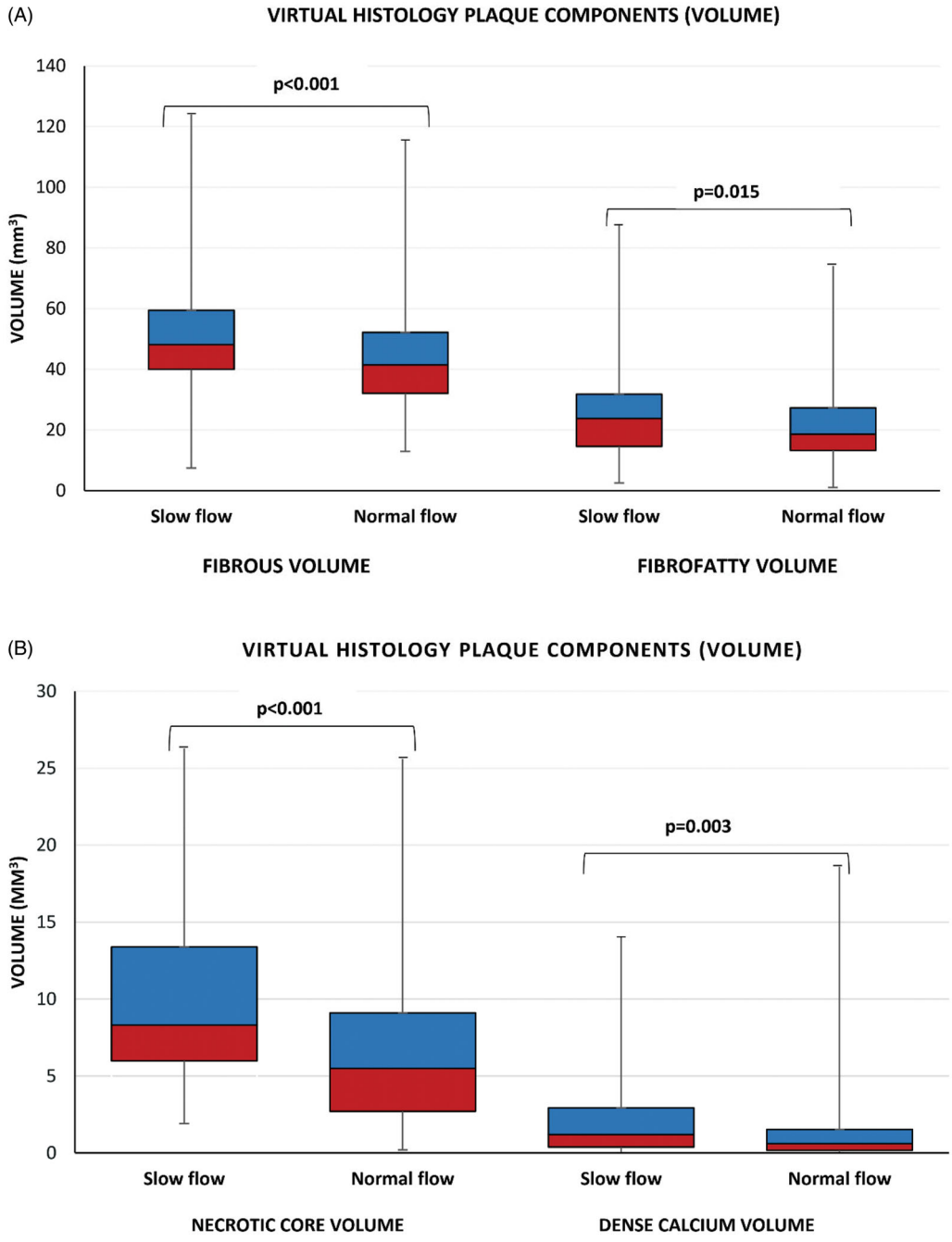

Figure 1. Comparison of the absolute plaque volumes derived by the virtual histology between the slow flow and normal flow groups. (A) Fibrous volume and fibrofatty volume (B) Necrotic core volume and dense calcium volume. Box and whisker plots, line within the box represent the median value, the upper and lower lines of the boxes represent the 75th and the 25th percentiles, respectively. The upper and the lower bars outside the boxes represent the highest and the lowest values, respectively.

3.6. Discriminators of slow flow

ROC curve analyses were performed to identify the grey-scale IVUS (proximal reference EEM CSA, proximal reference lumen CSA, lesion EEM CSA, plaque area, plaque volume, and remodelling index) and VH-IVUS parameters (absolute fibrous volume, absolute fibrofatty volume, absolute NC volume, and absolute DC volume) that could be helpful in differentiating cases of SF from NF as shown in Table 4 and Figure 3. The culprit lesion plaque volume (AUC = 0.644, $p < .001$) and the absolute necrotic core volume (AUC = 0.699, $p < .001$) were the best discriminators of SF from normal slow (Table 5).

4. Discussion

The salient findings of this study are as follows: (1) The grey-scale IVUS analysis revealed that the

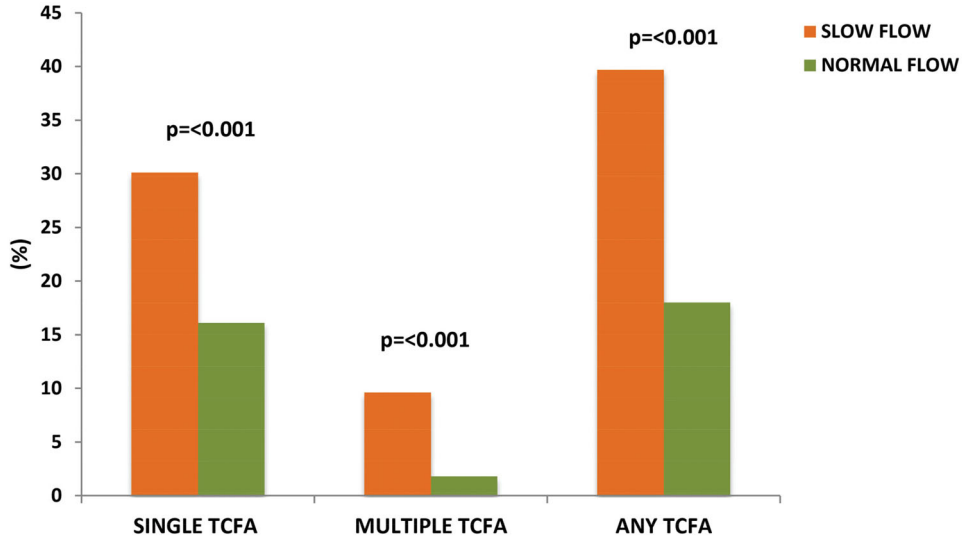

Figure 2. The incidence of thin cap fibroatheroma (TCFA). The single, multiple, or any TCFAs were more frequent in the slow flow arm.

Table 4. Intravascular ultrasound-virtual histology findings.

Variables	Slow flow	Normal flow	*p* Value
Patients, *n*	74	221	–
Each plaque component			
Percentages (%)			
VH Fibrous (%)	60 (56–64)	60 (56–65)	.584
VH Fibrofatty (%)	27 (22–34.25)	28 (23–35)	.433
VH Necrotic core (%)	8 (5–13.25)	8 (4–12)	.231
VH Dense calcium (%)	1 (0–3)	1 (0–2.25)	.116
Absolute volumes (mm^3)			
VH fibrous volume (mm^3)	48.1 (39.95–59.42)	41.5 (32.07–52.12)	<.001*
VH fibrofatty volume (mm^3)	23.85 (14.55–31.80)	18.65 (13.27–27.35)	.015*
VH necrotic core volume (mm^3)	8.30 (5.97–13.37)	5.50 (2.70–9.10)	<.001*
VH dense calcium volume (mm^3)	1.2 (0.37–2.92)	0.6 (0.17–1.52)	.003*
Single TCFA	22 (30.1%)	35 (16.1%)	<.001*
Multiple TCFAs	7 (9.6%)	4 (1.8%)	<.001*
Any TCFA	29 (39.7%)	39 (18.0%)	<.001*

VH: virtual histology; TCFA: thin cap fibroatheroma. Data are presented as mean ± SD, median (inter quartile range) or *n* (%).
*Denotes significant value.

pre-interventional parameters like; lesion EEM CSA, plaque area, plaque volume, and remodelling index were significantly higher in the SF group as compared to the NF group; (2) VH-IVUS analysis demonstrated that the absolute fibrous volume, fibrofatty volume, NC volume, DC volume, and TCFA were remarkably higher in the SF group in comparison to the NF group; (3) absolute NC volume was the only independent predictor of SF in STEMI patients undergoing PCI; (4) Grey-scale IVUS derived plaque volume and VH-IVUS derived absolute NC volume were the best discriminators of SF from NF.

SF is defined as the impedance to the normal myocardial perfusion despite opening up of the occluded coronary artery [13,30]. SF is multifactorial in its pathogenesis with one of the mechanisms being mechanical fragmentation of the vulnerable plaque during PCI leading to distal embolisation of thrombus, large amount of lipid content, and plaque debris which disturb the coronary microcirculation with an element of increased local thrombogenicity [6,31,32].

Positive remodelling has been noted in the coronary arteries with ACSs and is generally associated with vulnerable plaque, high thrombus burden leading to distal embolisation, and disturbance of distal coronary microcirculation [33–35]. In this study, the grey-scale IVUS parameters like, lesion EEM CSA, plaque area, plaque volume, and remodelling index were significantly higher in the SF group in comparison to the NF group. Our findings corroborated with the studies published in the literature, emphasising the role of plaque volume in the pathogenesis of SF [4,5,18,20,36,37].

Continuous efforts have been made in the past by various authors to identify the VH-IVUS predictors of coronary SF in patients with ACS undergoing PCI, yielding contradicting results. Our study showed that

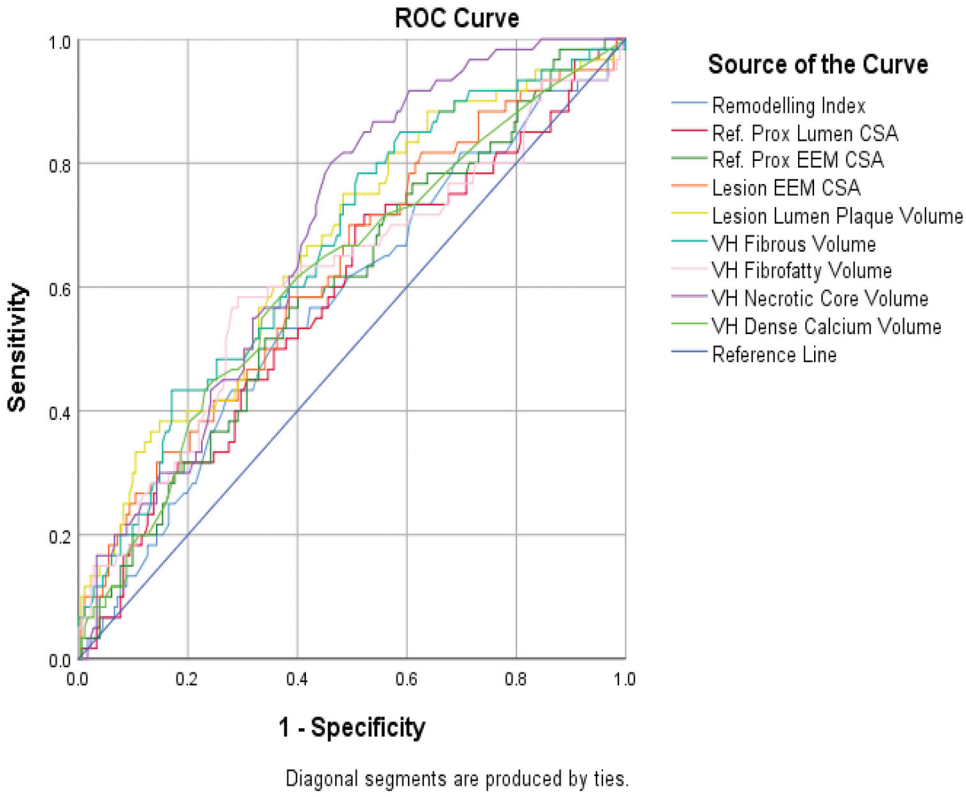

Figure 3. Receiver-operating characteristic (ROC) curves of grey-scale IVUS and VH-IVUS parameters for the discriminators of slow flow.

Table 5. Best cut-off values of the discriminators of slow flow and normal flow.

IVUS parameters	Cut off	Youden Index J	AUC (95% CI)	Sensitivity (95% CI)	Specificity (95% CI)	PPV (95% CI)	NPV (95% CI)
Lesion EEM CSA (mm^2)	>18.6	0.170	0.59 (0.54– 0.65)	27.03 (17.4–38.6)	90.05 (85.3–93.7)	47.6 (32–63.6)	78.7 (73.1–83.5)
Lesion plaque volume (mm^3)	>97.6	0.240	0.64 (0.58–0.69)	75.68 (64.3–84.9)	48.42 (41.7–55.2)	32.9 (25.9–40.6)	85.6 (78.2–91.2)
Remodelling index	>1.29	0.172	0.58 (0.522–0.648)	54.10 (40.8–66.9)	63.16 (55.9–70)	32.0 (23.2–42)	81.1 (73.8–87)
Absolute fibrofatty volume (mm^3)	>22.5	0.234	0.59 (0.53–0.65)	56.76 (44.7–68.2)	66.67 (59.9–73.0)	37.5 (28.5–47.1)	81.4 (74.8–86.9)
Absolute necrotic core volume (mm^3)	>5.6	0.348	0.69 (0.64–0.75)	82.43 (71.8–90.3)	52.38 (45.4–59.3)	37.9 (30.4–45.9)	89.4 (82.6–94.3)
Absolute dense calcium volume (mm^3)	>1	0.196	0.61 (0.55–0.67)	55.41 (43.4–67)	64.29 (57.4–70.8)	35.3 (26.7–44.8)	80.4 (73.5–86.1)

IVUS: Intravascular ultrasound; EEM CSA: external elastic membrane cross-sectional area; AUC: area under the curve; CI: confidence interval; PPV: positive predictive value; NPV: negative predictive value.

the VH-IVUS derived absolute fibrous volume, fibrofatty volume, NC volume, and the DC volumes were significantly higher in patients who developed SF as compared to those with NF indicating the importance of these plaque components. However, the absolute NC volume was the only independent predictor of SF in STEMI after PCI.

ACSs are in general caused by the rupture or erosion of the fibrous cap overlying the lipid rich-necrotic core of the vulnerable plaques [38]. The NC component of the VH consists of fragile tissues, such as cholesterol crystals, lipid deposition with foam cells, micro-calcifications, and intramural bleeding which undergo mechanical fragmentation during PCI and embolise to the distal coronary microcirculation contributing to SF [23,28,39]. The NC component has been associated with poor ST-segment resolution and ST-segment re-elevation in patients with STEMI after revascularisation [40,41]. The percentage of NC component and the percentage NC volume have been identified as predictors of SF in patients with ACS undergoing PCI [22,23]. Therefore, the NC component plays a crucial role in the pathogenesis of coronary SF in patients with STEMI undergoing PCI and was reiterated in this study. Thin cap fibroatheroma characterised by fibrous tissue thickness $< 65\,\mu m$ with an underlying necrotic core is considered to be the precursor lesion of plaque rupture [29,42]. This study showed that the VH-IVUS derived TCFA both single as well as multiple were remarkably higher in the SF group emphasising the findings described earlier [7,23].

Coronary calcium is a well-established marker of atherosclerotic plaque burden correlating with total atheroma volume and also predicts adverse cardiac events [43,44]. Spotty and superficial calcification has been linked to plaque vulnerability and mechanical instability whereas extensive calcification has been suggested to promote local biomechanical plaque stability [45–47]. Coronary artery calcium has also been described as a potential predictor of coronary SF in STEMI [7,48]. Our study demonstrated that the patients with SF had significantly higher absolute dense calcium volume suggesting the role of coronary calcification in SF.

The fibrofatty component of the VH-IVUS has been described previously as a predictor of SF in patients with STEMI undergoing PCI, similarly our study also demonstrated a significant difference in the absolute fibrofatty volume between the two groups [5,7]. The absolute fibrous volume was remarkably higher in the SF arm in comparison to NF arm which could be either due to the underlying predominant atherosclerotic plaque burden or inappropriate identification of intramural thrombus as fibrous tissue by the VH-IVUS analysis [49].

Despite maximum utilisation of dual antiplatelet therapy and glycoprotein IIb/IIIa inhibitors in STEMI in this study, coronary SF persists in a significant proportion. This supports the concept that the plaque components and atheroma burden are important contributors towards SF by the mechanical fragmentation during PCI and subsequent distal embolisation. Hibi et al. showed that in patients presenting with ACS and high-risk feature (attenuated plaque $\geq$5 mm) as identified on IVUS, the usage of distal embolic protection device was not only associated with decreased incidence of SF but also had lesser serious adverse cardiac events [50]. On the basis of our findings in this study, we also suggest that high-risk features as described on IVUS can identify patients who might benefit from embolic protection devices.

5. Limitations

First, the study was a single centre prospective observational study. Second, the major limitation of VH-IVUS is the misclassification of the thrombus as fibrous/fibro fatty and further, it also obscures the identification of TCFA. Third, a proportion of STEMI patients with high-risk features like cardiogenic shock, renal failure, and severe heart failure were excluded. Fourth, our study population may not reflect most of the STEMI cases in the western countries, as we had a mean symptom onset to PCI time of more than 8 h. Hence, this study might not be the true reflection of the entire spectrum of STEMI presentation. Long-term follow up for the assessment of clinical outcomes is warranted.

6. Conclusion

This study demonstrated that the IVUS derived plaque area and plaque volume along with high-risk features of VH-IVUS such as necrotic core volume, dense calcium volume, and TCFAs were significantly higher in STEMI patients with coronary SF as compared to those with NF during PCI. The only independent predictor of coronary SF was the absolute necrotic core volume. The pre-interventional identification of high-risk features of SF using IVUS and VH in patients with STEMI may benefit from distal protection devices.

Acknowledgements

We thank the secretarial assistance of Ashok Kumar (PhD scholar, Department of Neurology, PGIMER, Chandigarh, India) and Ms Damanpreet Kaur.

Compliance with ethical standards

- Research involving Human Participants and/or Animals: The study was approved by the institutional ethics committee. All procedures performed in the study involving human participants were in accordance with the ethical standards of the institutional and/or national research committee (Institutional Ethics Committee, GMCH, Chandigarh with reference number IEC/2017/12 dated 04.05.2017) and with the 1964 Helsinki declaration and its later amendments or comparable ethical standards.
- Informed consent: Informed consent was obtained from all individual participants prior to their inclusion in the study.

Disclosure statement

The authors declare that they have no conflicts of interest. All authors contributed to the study conception and design. Material preparation, data collection, and analysis were performed by all the authors. The first draft of the manuscript was written by Sreenivas Reddy and Raghavendra Rao and all authors commented on previous versions of the manuscript. All authors read and approved the final manuscript.

ORCID

Hariom Soni http://orcid.org/0000-0003-3579-4958

References

[1] Weaver WD, Simes RJ, Betriu A, et al. Comparison of primary coronary angioplasty and intravenous

thrombolytic therapy for acute myocardial infarction: a quantitative review. JAMA. 1997;278(23):2093–2098.
[2] Grines CL, Cox DA, Stone GW, et al. Coronary angioplasty with or without stent implantation for acute myocardial infarction. Stent primary angioplasty in myocardial infarction study group. N Engl J Med. 1999;341(26):1949–1956.
[3] Keeley EC, Boura JA, Grines CL. Primary angioplasty versus intravenous thrombolytic therapy for acute myocardial infarction: a quantitative review of 23 randomised trials. Lancet. 2003;361(9351):13–20.
[4] Li J, Wu L, Tian X, et al. Intravascular ultrasound observation of the mechanism of no-reflow phenomenon in acute myocardial infarction. PLoS One. 2015; 10(6):e0119223.
[5] Bae JH, Kwon TG, Hyun DW, et al. Predictors of slow flow during primary percutaneous coronary intervention: an intravascular ultrasound-virtual histology study. Heart. 2008;94(12):1559–1564.
[6] Soeda T, Higuma T, Abe N, et al. Morphological predictors for no reflow phenomenon after primary percutaneous coronary intervention in patients with ST-segment elevation myocardial infarction caused by plaque rupture. Eur Heart J Cardiovasc Imaging. 2017; 18(1):103–110.
[7] Ohshima K, Ikeda S, Watanabe K, et al. Relationship between plaque composition and no-reflow phenomenon following primary angioplasty in patients with ST-segment elevation myocardial infarction–analysis with virtual histology intravascular ultrasound. J Cardiol. 2009;54(2):205–213.
[8] Yip HK, Chen MC, Chang HW, et al. Angiographic morphologic features of infarct-related arteries and timely reperfusion in acute myocardial infarction: predictors of slow-flow and no-reflow phenomenon. Chest. 2002;122(4):1322–1332.
[9] Harrison RW, Aggarwal A, Ou FS, et al. Incidence and outcomes of no-reflow phenomenon during percutaneous coronary intervention among patients with acute myocardial infarction. Am J Cardiol. 2013;111(2): 178–184.
[10] Mehta RH, Harjai KJ, Boura J, et al. Prognostic significance of transient no-reflow during primary percutaneous coronary intervention for ST-elevation acute myocardial infarction. Am J Cardiol. 2003;92(12): 1445–1447.
[11] Morishima I, Sone T, Okumura K, et al. Angiographic no-reflow phenomenon as a predictor of adverse long-term outcome in patients treated with percutaneous transluminal coronary angioplasty for first acute myocardial infarction. J Am Coll Cardiol. 2000;36(4): 1202–1209.
[12] Niccoli G, Burzotta F, Galiuto L, et al. Myocardial no-reflow in humans. J Am Coll Cardiol. 2009;54(4): 281–292.
[13] Rezkalla SH, Kloner RA. No-reflow phenomenon. Circulation. 2002;105(5):656–662.
[14] Bouleti C, Mewton N, Germain S. The no-reflow phenomenon: state of the art. Arch Cardiovasc Dis. 2015; 108(12):661–674.
[15] Iijima R, Shinji H, Ikeda N, et al. Comparison of coronary arterial finding by intravascular ultrasound in patients with "transient no-reflow" versus "reflow" during percutaneous coronary intervention in acute coronary syndrome. Am J Cardiol. 2006;97(1):29–33.
[16] Katayama T, Kubo N, Takagi Y, et al. Relation of atherothrombosis burden and volume detected by intravascular ultrasound to angiographic no-reflow phenomenon during stent implantation in patients with acute myocardial infarction. Am J Cardiol. 2006; 97(3):301–304.
[17] Endo M, Hibi K, Shimizu T, et al. Impact of ultrasound attenuation and plaque rupture as detected by intravascular ultrasound on the incidence of no-reflow phenomenon after percutaneous coronary intervention in ST-segment elevation myocardial infarction. JACC Cardiovasc Interv. 2010;3(5):540–549.
[18] Tanaka A, Kawarabayashi T, Nishibori Y, et al. No-reflow phenomenon and lesion morphology in patients with acute myocardial infarction. Circulation. 2002;105(18):2148–2152.
[19] Amano H, Ikeda T, Toda M, et al. Plaque composition and no-reflow phenomenon during percutaneous coronary intervention of low-echoic structures in gray-scale intravascular ultrasound. Int Heart J. 2016;57(3): 285–291.
[20] Watanabe T, Nanto S, Uematsu M, et al. Prediction of no-reflow phenomenon after successful percutaneous coronary intervention in patients with acute myocardial infarction: intravascular ultrasound findings. Circ J. 2003;67(8):667–671.
[21] Hiro T, Leung CY, De Guzman S, et al. Are soft echoes really soft? Intravascular ultrasound assessment of mechanical properties in human atherosclerotic tissue. Am Heart J. 1997;133(1):1–7.
[22] Higashikuni Y, Tanabe K, Tanimoto S, et al. Impact of culprit plaque composition on the no-reflow phenomenon in patients with acute coronary syndrome: an intravascular ultrasound radiofrequency analysis. Circ J. 2008;72(8):1235–1241.
[23] Hong YJ, Jeong MH, Choi YH, et al. Impact of plaque components on no-reflow phenomenon after stent deployment in patients with acute coronary syndrome: a virtual histology-intravascular ultrasound analysis. Eur Heart J. 2011;32(16):2059–2066.
[24] O'Gara PT, Kushner FG, Ascheim DD, et al. ACCF/AHA guideline for the management of ST-elevation myocardial infarction: a report of the American College of Cardiology Foundation/American Heart Association Task Force on Practice Guidelines. J Am Coll Cardiol. 2013;61:e78–e140.
[25] Gibson CM, de Lemos JA, Murphy SA, et al. Combination therapy with abciximab reduces angiographically evident thrombus in acute myocardial infarction: a TIMI 14 substudy. Circulation. 2001; 103(21):2550–2554.
[26] Rentrop KP, Cohen M, Blanke H, et al. Changes in collateral channel filling immediately after controlled coronary artery occlusion by an angioplasty balloon in human subjects. J Am Coll Cardiol. 1985;5(3): 587–592.
[27] Mintz GS, Nissen SE, Anderson WD, et al. American college of cardiology clinical expert consensus document on standards for acquisition, measurement and

reporting of intravascular ultrasound studies (IVUS). A report of the American college of cardiology task force on clinical expert consensus documents. J Am Coll Cardiol. 2001;37(5):1478–1492.

[28] Nair A, Kuban BD, Tuzcu EM, et al. Coronary plaque classification with intravascular ultrasound radiofrequency data analysis. Circulation. 2002;106(17): 2200–2206.

[29] Rodriguez-Granillo GA, Garcia-Garcia HM, Mc Fadden EP, et al. In vivo intravascular ultrasound-derived thin-cap fibroatheroma detection using ultrasound radiofrequency data analysis. J Am Coll Cardiol. 2005; 46(11):2038–2042.

[30] Kloner RA, Ganote CE, Jennings RB. The "no-reflow" phenomenon after temporary coronary occlusion in the dog. J Clin Invest. 1974;54(6):1496–1508.

[31] Hong YJ, Ahn Y, Jeong MH. Role of intravascular ultrasound in patients with acute myocardial infarction. Korean Circ J. 2015;45(4):259–265.

[32] Fernandez-Ortiz A, Badimon JJ, Falk E, et al. Characterization of the relative thrombogenicity of atherosclerotic plaque components: implications for consequences of plaque rupture. J Am Coll Cardiol. 1994;23(7):1562–1569.

[33] Varnava AM, Mills PG, Davies MJ. Relationship between coronary artery remodeling and plaque vulnerability. Circulation. 2002;105(8):939–943.

[34] Schoenhagen P, Ziada KM, Kapadia SR, et al. Extent and direction of arterial remodeling in stable versus unstable coronary syndromes: an intravascular ultrasound study. Circulation. 2000;101(6):598–603.

[35] Hong YJ, Jeong MH, Choi YH, et al. Positive remodeling is associated with more plaque vulnerability and higher frequency of plaque prolapse accompanied with post-procedural cardiac enzyme elevation compared with intermediate/negative remodeling in patients with acute myocardial infarction. J Cardiol. 2009;53(2):278–287.

[36] Nakamura T, Kubo N, Ako J, et al. Angiographic no-reflow phenomenon and plaque characteristics by virtual histology intravascular ultrasound in patients with acute myocardial infarction. J Interv Cardiol. 2007;20(5):335–339.

[37] Kotani J, Mintz GS, Castagna MT, et al. Relation of plaque morphology to thrombolysis in myocardial infarction flow in acute myocardial infarction determined by intravascular ultrasound. Am J Cardiol. 2003;91(9): 1096–1099.

[38] Falk E, Shah PK, Fuster V. Coronary plaque disruption. Circulation. 1995;92(3):657–671.

[39] Kawamoto T, Okura H, Koyama Y, et al. The relationship between coronary plaque characteristics and small embolic particles during coronary stent implantation. J Am Coll Cardiol. 2007;50(17):1635–1640.

[40] Ohshima K, Ikeda S, Kadota H, et al. Impact of culprit plaque volume and composition on myocardial microcirculation following primary angioplasty in patients with ST-segment elevation myocardial infarction: virtual histology intravascular ultrasound analysis. Int J Cardiol. 2013;167(3):1000–1005.

[41] Kawaguchi R, Oshima S, Jingu M, et al. Usefulness of virtual histology intravascular ultrasound to predict distal embolization for ST-segment elevation myocardial infarction. J Am Coll Cardiol. 2007;50(17): 1641–1646.

[42] Virmani R, Burke AP, Farb A, et al. Pathology of the vulnerable plaque. J Am Coll Cardiol. 2006;47(8): C13–8.

[43] Nicholls SJ, Tuzcu EM, Wolski K, et al. Coronary artery calcification and changes in atheroma burden in response to established medical therapies. J Am Coll Cardiol. 2007;49(2):263–270.

[44] Arad Y, Spadaro LA, Goodman K, et al. Prediction of coronary events with electron beam computed tomography. J Am Coll Cardiol. 2000;36(4):1253–1260.

[45] Ehara S, Kobayashi Y, Yoshiyama M, et al. Spotty calcification typifies the culprit plaque in patients with acute myocardial infarction: an intravascular ultrasound study. Circulation. 2004;110(22):3424–3429.

[46] Mizukoshi M, Kubo T, Takarada S, et al. Coronary superficial and spotty calcium deposits in culprit coronary lesions of acute coronary syndrome as determined by optical coherence tomography. Am J Cardiol. 2013;112(1):34–40.

[47] Abedin M, Tintut Y, Demer LL. Vascular calcification: mechanisms and clinical ramifications. Arterioscler Thromb Vasc Biol. 2004;24(7):1161–1170.

[48] Modolo R, Figueiredo VN, Moura FA, et al. Coronary artery calcification score is an independent predictor of the no-reflow phenomenon after reperfusion therapy in acute myocardial infarction. Coron Artery Dis. 2015;26:562–566.

[49] Nasu K, Tsuchikane E, Katoh O, et al. Impact of intramural thrombus in coronary arteries on the accuracy of tissue characterization by in vivo intravascular ultrasound radiofrequency data analysis. Am J Cardiol. 2008;101(8):1079–1083.

[50] Hibi K, Kozuma K, Sonoda S, et al. A randomized study of distal filter protection versus conventional treatment during percutaneous coronary intervention in patients with attenuated plaque identified by intravascular ultrasound. JACC Cardiovasc Interv. 2018; 11(16):1545–1555.

Indian Pacing and Electrophysiology Journal 21 (2021) 62–64

Contents lists available at ScienceDirect

Indian Pacing and Electrophysiology Journal

journal homepage: www.elsevier.com/locate/IPEJ

Ventricular tachycardia as the presenting feature in two patients with cardiac lipoma and cardiac fibroma

Ramalingam Vadivelu [a, *], Shomu Bohora [b], Neeta Bachani [c], Rajeev Sharma [c], Gopi Panicker [d], Yash Lokhandwala [c]

[a] Department of Cardiology, Velammal Medical College Hospital, Madurai, 625009, India
[b] Department of Cardiology, UN Mehta Institute of Cardiology and Research Centre, Ahmedabad, India
[c] Department of Cardiology, Holy Family Hospital, Bandra, Mumbai, India
[d] Cardiac Safety Services, Quintiles Research India Pvt. Ltd, IQVIA, Mumbai, India

ARTICLE INFO

Article history:
Received 25 August 2020
Accepted 12 October 2020
Available online 15 October 2020

Keywords:
Cardiac tumours
Sudden death
Cardiac imaging

ABSTRACT

We hereby present two patients with benign cardiac tumours presenting as ventricular tachycardia (VT). Most such tumours have a favorable prognosis, unless complicated by arrhythmias. Intracavitary tumours are easily diagnosed by echocardiography. Intramural tumours as in our patients may be missed at times by echocardiography. Multimodality imaging helped confirm the diagnosis and etiology, since biopsy was not safe. Surgical removal was not feasible due to extensive infiltration. The patients are so far doing well on medical therapy.

1. Introduction

Primary cardiac tumours are more common in children and more than half of such tumours are diagnosed in infancy [1,2]. Most of them are benign in nature and usually regress over a period of time. But some of them eventually grow and produce obstruction of the cardiac chambers, valves and outflow tracts producing heart failure symptoms. Rarely, they manifest as ventricular arrhythmia, atrial arrhythmia or atrioventricular block.

1.1. Case 1

A 21-year old man presented with hemodynamically unstable monomorphic VT @ 180/min, which was cardioverted. The VT (Fig. 1) showed a QRS of 160 ms with RBBB-like morphology and northwest QRS axis. The sinus rhythm after cardioversion was normal. The echocardiogram showed a disruption of the lateral wall of the left ventricle (LV), possibly because of an infiltrating mass (Fig. 2, Panel A). There was also an area of increased echogenicity in the LV lateral wall (Fig. 2, Panel B). A cardiac CT scan was performed, which showed a 4.8 × 7.2 × 1.4 cm sized fat density lesion suggestive of cardiac lipoma, in the LV lateral wall, apex and inferior wall (Fig. 2, Panels C, D) with insinuation within the underlying subendocardium and overlying epicardium.

The final diagnosis was VT due to lipomatous invasion. Due to extensive infiltration within the myocardium surgical excision was not feasible. He was advised an implantable defibrillator but refused the same. He was started on amiodarone and metoprolol. Except for one VT recurrence when he had stopped the medicines, he remains asymptomatic at three years of follow up.

1.2. Case 2

A 47-year old man presented with unstable VT at 200 bpm which was DC Cardioverted. The ECG (Fig. 3, Panel A) showed a QRS of 160 ms duration with a RBBB-like morphology and a QRS axis of +40°. In the reconstructed CT image (Fig. 3, Panels B), the left anterior descending coronary artery was seen coursing superior to the tumor but no evidence of coronary compression was seen. The cardiac MRI showed a 4.6 × 3.5 cm homogenously enhancing mass in the basolateral region which was hypointense on the T2 weighted sequence (Fig. 3, Panels C). The contrast study showed intense homogenous delayed enhancement of the tumor on late gadolinium enhancement sequences, characteristic of fibroma (Fig. 3, Panel D).

* Corresponding author. Department of Cardiology, Velammal Medical College Hospital and Research Institute, Madurai, Tamilnadu, India.
E-mail address: vvelu00@gmail.com (R. Vadivelu).
Peer review under responsibility of Indian Heart Rhythm Society.

https://doi.org/10.1016/j.ipej.2020.10.001

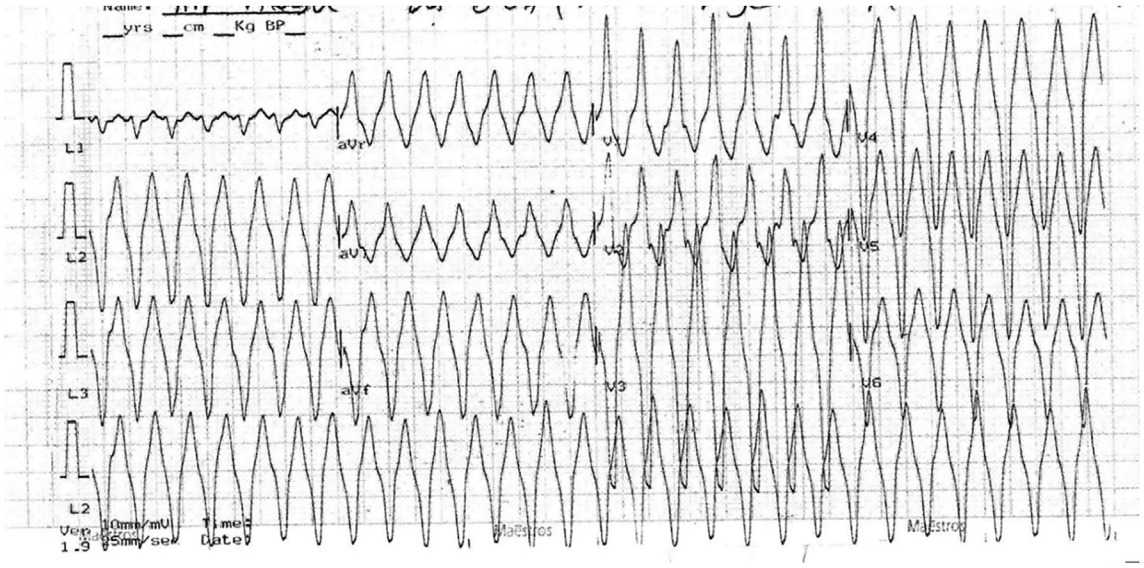

Fig. 1. ECG shows wide QRS tachycardia, RBBB, northwest axis, rate 180/min s/o Ventricular tachycardia.

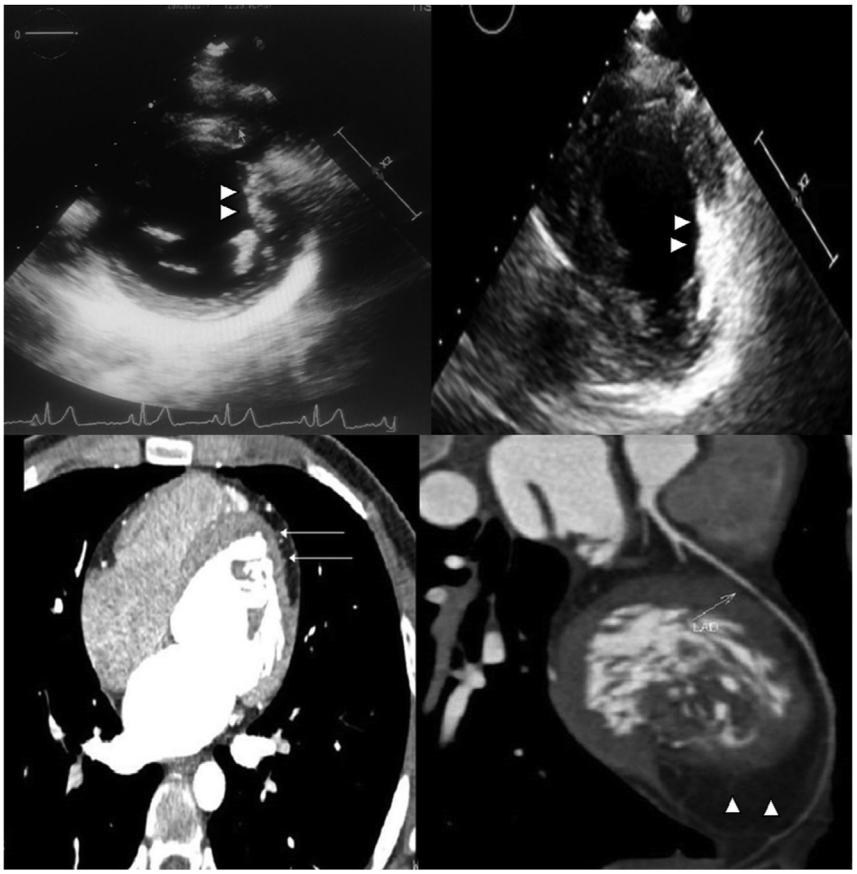

Fig. 2. Panel A: Transthoracic 2D Echocardiogram in parasternal short axis view showing a disruption of the lateral wall of the left ventricle (LV), possibly because of an infiltrating mass (white arrow heads). Panel B: 2D Echocardiogram in parasternal short axis view showing an area of increased echogenicity in the LV lateral wall secondary to intramural tumor (white arrow heads). Panel C and Panel D: Cardiac CT scan in horizontal long axis view showing a 4.8 × 7.2 × 1.4 cm sized fat density lesion suggestive of cardiac lipoma, in the LV lateral wall, apex and inferior wall (white arrows in Panel C and white arrow heads in Panel D).

The final diagnosis was VT due to a large LV intramural fibroma. He was advised an implantable defibrillator but refused the same. On conservative management with amiodarone and metoprolol, there has been no recurrence of VT at five years of follow up.

2. Discussion

Secondary cardiac tumours due to metastasis from systemic malignancies are much more common than primary cardiac

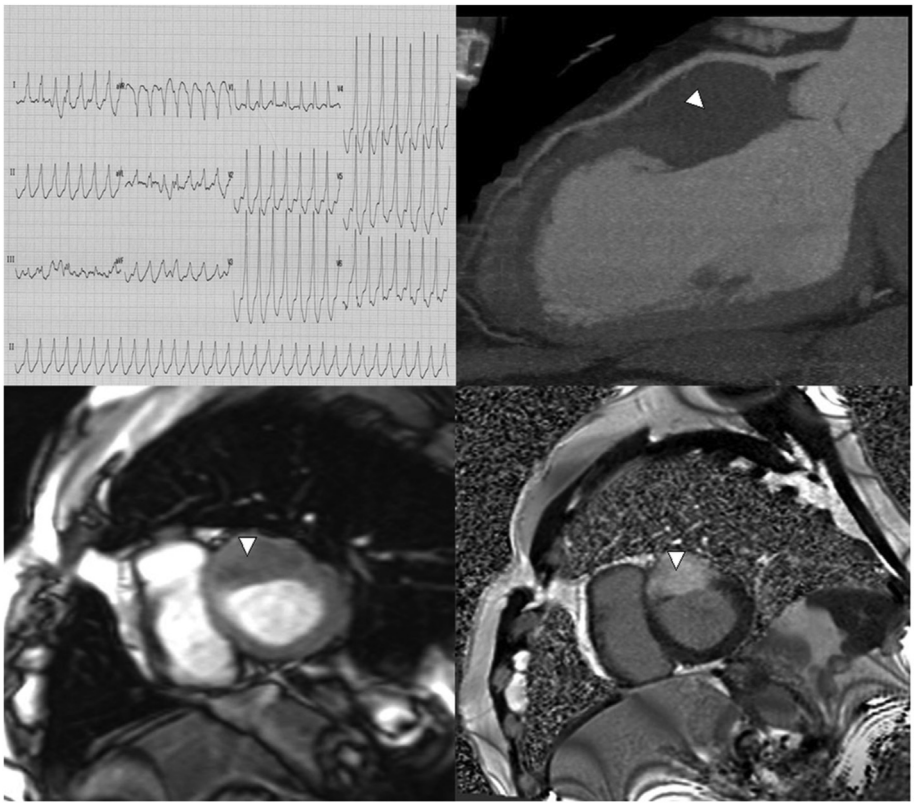

Fig. 3. Panel A: ECG showing VT at 200 bpm and QRS duration of 160 ms duration with a RBBB-like morphology and a QRS axis of +40°. Panel B: Reconstructed CT image in vertical long axis view demonstrating the tumor (white arrow head) and left anterior descending coronary artery coursing superior to the tumor without any evidence of coronary compression. Panel C: Cardiac MRI, short axis view, in T2 weighted sequence showing a 4.6 × 3.5 cm hypointense mass in the basolateral region of LV (white arrow head). Panel D: Cardiac MRI, short axis view, in the contrast films demonstrating a characteristic delayed homogenous contrast enhancement suggestive of LV fibroma (arrow head).

tumours. Majority of the primary cardiac tumours are benign, among which the most common in children is rhabdomyoma, while in adults it is myxoma. The others benign tumours include fibromas, papillary fibroelastoma, lipoma, teratoma, hemangioma and mesothelioma. The presentation can be secondary to mass effect, obstruction, valvulopathy, tachyarrhythmias or conduction disturbances. The mechanism of arrhythmias include: i) differing refractory periods within the tumor mass resulting in asynchronous activation, ii) local re-entry circuit areas where the normal myocardium is interspersed within the infiltrating tumor and iii) compression of His bundle or bundle branches.

Both our patients presented with hemodynamically unstable VT. The first case was lipoma with invasion into subendocardium and epicardium. This accounts for one-tenth of benign cardiac tumours, the mean age of presentation being 50 years [3]. Lipomas are homogenous encapsulated fatty tumours and usually detected on imaging or autopsy due to their benign nature and are rarely infiltrating tumours. They primarily arise from the subendocardium but can also arise from myocardium or subepicardium. Myocardial location is a risk factor for VT or conduction disturbance. Sudden death is a rare manifestation of cardiac lipoma [4,5]. Echocardiographically, a lipoma is usually hyperechoic. On CT imaging, cardiac lipomas are visualised as homogeneous, low-attenuation masses. On T1 weighted MRI imaging, lipomas show homogeneously increased signal intensity which characteristically reduces in fat-saturated sequences.Our second case was fibroma in the basolateral LV wall. Fibromas are solitary tumours composed of fibroblasts and connective tissue. While a presentation with arrhythmias is seen in only 10–15% of cases, sudden death is not rare [2,6,7]. They are typically intramural in location, exhibiting slow growth and infiltrating around coronary arteries and conduction tissue, making surgical resection difficult.

Conflicts of interest

No potential conflicts of interest.

References

[1] Freedom RM, Lee KJ, MacDonald C, Taylor G. Selected aspects of cardiac tumors in infancy and childhood. Pediatr Cardiol 2000 Jul 1;21(4):299–316.
[2] Stratemann S, Dzurik Y, Fish F, Parra D. Left ventricular cardiac fibroma in a child presenting with ventricular tachycardia. Pediatr Cardiol 2008 Jan 1;29(1):223–6.
[3] Burke A, Jeudy J, Virmani R. Cardiac tumours: an update. Heart 2008;94:117–23.
[4] Shenthar J, Sharma R, Rai MK, Simha P. Infiltrating cardiac lipoma presenting as ventricular tachycardia in a young adult. Indian Heart J 2015;67:359–61.
[5] Friedberg MK, Chang IL, Silverman NH, Ramamoorthy C, Chan FP. Near sudden death from cardiac lipoma in an adolescent. Circulation 2006;113:778–80.
[6] Sharma K, Rohlicek C, Cecere R, Tchervenkov CI. Malignant arrhythmias secondary to a cardiac fibroma requiring transplantation in a teenager. J Heart Lung Transplant 2007;26:639–41.
[7] Ottaviani G, Rossi L, Ramos SG, Matturri L. Pathology of the heart and conduction system in a case of sudden death due to a cardiac fibroma in a 6-month-old child. Cardiovasc Pathol 1999;8:109–12.

Review Article OPEN ACCESS

How to Implant His Bundle and Left Bundle Pacing Leads: Tips and Pearls

Shunmuga Sundaram Ponnusamy, Pugazhendhi Vijayaraman

Abstract

Cardiac pacing is the treatment of choice for the management of patients with bradycardia. Although right ventricular apical pacing is the standard therapy, it is associated with an increased risk of pacing-induced cardiomyopathy and heart failure. Physiological pacing using His bundle pacing and left bundle branch pacing has recently evolved as the preferred alternative pacing option. Both His bundle pacing and left bundle branch pacing have also demonstrated significant efficacy in correcting left bundle branch block and achieving cardiac resynchronisation therapy. In this article, the authors review the implantation tools and techniques to perform conduction system pacing.

Related content

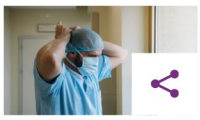

Article

Standards & Guidelines

A Nurse's Perspective from the COVID-19 Front Line

Katie Caldwell, Alan Moore, Taylor Rali

Read time: 9 Mins

Article

Heart Failure

Polypharmacy in Older People With Heart Failure

Maria Stefil, Matthew Dixon, Jameela Bahar, et al

Read time: 21 Mins

Keywords

His bundle pacing, left bundle branch pacing, cardiac resynchronisation therapy, atrioventricular block, left bundle branch block, heart failure; pacemaker

Disclosure: SSP has worked as a consultant for Medtronic. PV has received speaker fees and fellowship support from Medtronic, has acted as a consultant for Medtronic and has conducted research for Medtronic, has acted as a consultant for Abbott, Biotronik, and Boston Scientific, and has a patent (US 10,737,097 B2) for a His bundle pacing delivery tool.

Received: 30 March 2021

Accepted: 04 May 2021

Published online: 06 August 2021

Citation:
Cardiac Failure Review 2021;7:e13.

DOI: https://doi.org/10.15420/cfr.2021.04

Correspondence Details: Pugazhendhi Vijayaraman, Director, Cardiac Electrophysiology, Geisinger Heart Institute, MC 36–10, 1000 E Mountain Blvd, Wilkes-Barre, PA 18711, US. E: pvijayaraman1@geisinger.edu

Cardiac pacing is the treatment of choice for the management of patients with symptomatic bradyarrhythmia. For nearly six decades, right ventricular (RV) apical (A) pacing has been the standard approach because it is a safe procedure with proven long-term efficacy. However, RVA pacing is fraught with limitations due to associated electrical and mechanical dyssynchrony.[1] Pre-excitation of the septum coupled with delayed activation of the left ventricular (LV) free wall produces dyssynchronous activation and less effective contraction.[2] Clinically, this can translate into pacing-induced cardiomyopathy in up to 20% of patients and increased risk for heart failure hospitalisation during long-term follow-up.[3]

The quest for alternative pacing sites has met with limited success because using the RV septum or RV outflow tract failed to demonstrate clinical pacing.[4] ›opting biventricular pacing for all patients ¡uiring ventricular pacing is not a cost-effective strategy. An ideal pacing site should provide

Article

Heart Failure

Ventricular Assist Devices: Challenges of the One-device Era

Gassan Moady, Shaul Atar, Binyamin Ben-Avraham, et al

Read time: 10 Mins

Article

Heart Failure

Breaking the Cycle of HFpEF and AF

Otilia Țica, Waseem Khamboo, Dipak Kotecha

Read time: 18 Mins

Article

Imaging & Diagnostics, Heart Failure

Multimodality Imaging in Valvular Structural Interventions

Karine Grigoryan, Camelia Demetrescu, Ioannis Kasouridis, et al

Read time: 24 Mins

synchronised ventricular activation by engaging the conduction system of the heart. The concept of conduction system pacing is not new, because temporary capture of the His bundle (HB) was demonstrated more than five decades ago by Scherlag et al.[5] The feasibility of permanent HB pacing (HBP) was demonstrated only 30 years later by Deshmukh et al.[6] This review provides insights into the procedural technique and clinical implications of HBP and left bundle branch pacing (LBBP).

Anatomy of the Cardiac Conduction System

The electrical impulse of the heart arises from the sinus node at the superior vena cava–right atrial junction and reaches the atrioventricular (AV) node via three internodal pathways. The AV node at the apex of Koch's triangle continues as the HB overlying the membranous septum.[7] The membranous septum is divided by the septal tricuspid leaflet into an atrioventricular component and a ventriculoventricular component. The penetrating portion of the HB arises from the anterior end of the AV node with loosely arranged fibres in an interweaving pattern. It reaches the ventricle by penetrating the central fibrous body of the heart, where the fibres of left bundle branch (LBB) are given off after it emerges from the fibrous body at the level of the non-coronary aortic cusp. The branching portion of the HB starts from the point where the posterior-most fibres of the LBB arise (posterior fascicles), to the point where the HB continues as the right bundle branch (RBB) after giving rise to the anterior fascicles of the LBB (*Figure 1*). The LBB, after its origin, runs inferiorly and anteriorly for 10–15 mm, reaching its maximum width before dividing into anterior and posterior fascicles that head towards the corresponding papillary muscles of the LV.[8]

Anatomical studies have shown three common variations of HB relative to the ventricular aspect of the membranous septum.[9] In the Type I variation (47%), the HB courses along the inferior border of the membranous septum with a thin layer of myocardial fibres spanning from the muscular septum. In the Type II variation (32%), the HB is separate to below the membranous septum and courses within the interventricular muscle. In the Type III variation (21%), the HB is exposed superficially, lying immediately below the endocardium (naked HB). Both atrial and ventricular components of the HB can be accessed for permanent HBP.

His Bundle Pacing: Implantation Technique

Deshmukh et al. first demonstrated the clinical sibility of HBP in patients with AF and LV function using standard pacing leads by reshaping the stylet.[6] The lead placement was done

by targeting the site with largest His deflection recorded from the electrophysiology mapping catheter. This technique was fraught with high pacing thresholds and frequent lead dislodgements. The development of specialised sheaths (C304, C315His and C304His, Selectsite; Medtronic) and a pacing lead (3830 Selectsecure; Medtronic) has made HBP technically feasible with high implant success rates.[10]

Anatomy of the Conduction System

Figure 1: Anatomy of the Conduction System

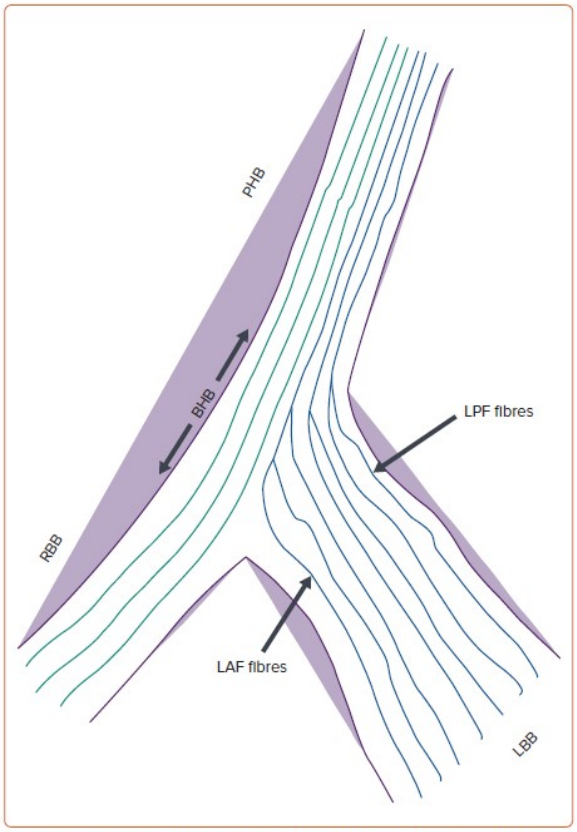

The His bundle (HB) has two components: the PHB portion and the BHB portion. The LBB branches out of the HB before the true bifurcation point and the RBB is considered as a direct continuation of the HB. Note the longitudinal dissociation as fibres are predestined inside the HB to reach the RBB or LBB. BHB = branching His bundle; LAF = left anterior fascicle; LBB = left bundle branch; LPF = left posterior fascicle; PHB = penetrating His bundle; RBB = right bundle branch.

Download

HBP is performed using continuous recording of intracardiac electrograms and 12-lead ECG in an electrophysiology (EP) recording system.[10] His signals are recorded directly from the pacing lead tip in a unipolar connection, and are simultaneously recorded in the EP system and in the pacing system analyser (PSA). After obtaining venous access, the C315 sheath is introduced over the guidewire and placed across the tricuspid valve. The sheath has a proximal curve to point towards the tricuspid annulus and a septal curve to direct the lead towards the His region. A 3830 Selectsecure lead is then advanced just exposing the helix outside the sheath, and the signals mapped in unipolar fashion. Both the atrial and ventricular parts of the membranous

septum can be targeted for HBP. If a predominant atrial signal is recorded, the sheath is moved gently forward with clockwise rotation aiming for a larger His signal with a small or no atrial component.

Gu et al. showed that visualisation of the tricuspid valve annulus by performing contrast angiography before lead implantation resulted in a shorter fluoroscopic time (7.1 versus 10.1 minutes) with similar capture thresholds.[11] There was no significant difference in procedural success rates. Zanon et al. demonstrated that HBP can be performed primarily using an electrogram with zero or minimal fluoroscopy with high success rates.[12] In that study, the sheath, along with the lead, was advanced gently with counterclockwise and clockwise rotation into the right atrium through a standard 7 Fr introducer. The pacing lead was then connected to the alligator cable in a unipolar fashion. After confirming the position of the sheath in the atrium by a sharp atrial signal in the recording system, the system was advanced gently to get both atrial and ventricular signals. Further anticlockwise rotation helped reach the HB area.[12] Gentle manipulation of the system helped record a clear near-field His potential from the pacing lead. Unipolar threshold measurement was performed at a pulse width of 1 ms before fixing the lead in the membranous septum. Transient fluoroscopy was used in all patients to confirm lead stability before removing the C315 sheath. Both selective and non-selective HB capture was accepted as procedural success. HBP could be performed safely in 95% of patients (39/41) in that study using electrograms with minimal or zero fluoroscopy.[12]

Alternatively, HBP can be performed using 3D electroanatomical mapping (EAM), especially in patients with complex heart disease.[13] Sharma et al. created EAM of the RA before lead placement using a conventional 3D mapping system.[13] His bundle potentials were tagged. The approach to mapping was axillary or cephalic unless the patient was undergoing an AV junction ablation, in which case a femoral approach was used. Pacing was done at the sites with His potentials to note the response to pacing. The 3830 lead was implanted using a C315 or C304 sheath with continuous tracking of the lead course using the 3D system. Transient fluoroscopy was used to confirm full helix deployment and lead slack. Sharma et al. concluded that EAM-guided HBP could significantly reduce fluoroscopy duration and exposure.[13]

Once a sharp near-field His signal is identified, unipolar pacing is done to confirm the capture of the HB. Intracardiac electrograms and 12-lead ECG will help assess conduction system capture. In patients with underlying bundle branch block or His–ventricle (HV) block, mapping of the distal HB must be done to achieve complete correction of bundle branch block or to overcome HV block. If an optimal site is

identified, the fluoroscopic image may be saved as a reference in orthogonal oblique views (left anterior oblique [LAO] 30° and right anterior oblique [RAO] 30°). The sheath is held firmly with a gentle counterclockwise torque to oppose it towards the septum and five to six clockwise rotations are given to the pacing lead without releasing it between rotations. Lead rotations can be best visualised in the LAO 30° fluoroscopic view. Rebound of the lead after the rotation will confirm its penetration into the membranous septum. If lead rebound is not observed, the sheath position is optimised to provide adequate support before giving further rotations. Care must be taken to avoid pinning the tricuspid leaflet into the septum when the ventricular component is targeted by using contrast angiography or echocardiography if there is difficulty in deploying the lead. Alternatively, the sheath can be moved into the RV apex and pulled back gradually to the target site.

After confirming lead fixation, the sheath is gently withdrawn into the high right atrium, providing adequate slack for the lead. The lead parameters are checked in both the unipolar and bipolar configuration. Optimal parameters include a unipolar pacing threshold of <1.5 V at a pulse width of 1 ms and a sensed R-wave of >1.5–2 mV without atrial oversensing. An HB current of injury (COI) recorded from the pacing lead electrogram indicates lead fixation in the HB and predicts excellent pacing thresholds.

Defining Selective and Non-selective Capture of the His Bundle

Based on the paced QRS morphology, two forms of HB capture can be observed: selective (S) and non-selective (NS) HBP.[14] During selective capture, pacing will result in direct activation of the HB alone and the ventricular activation occurs completely through the His–Purkinje system (HPS). Because the impulse takes 35–55 ms to reach the ventricular myocardium, there will be an isoelectric interval before the onset of QRS, and the interval from the pacing spike to the onset of QRS (S-QRS) will be equal to the native HV interval. However, in patients with significant HPS disease, the S-QRS would be less than the native HV interval. The lead electrogram will show the ventricular electrogram discrete from the pacing artefact, and the paced QRS morphology is same as the native QRS.

During NS-HBP, there will be simultaneous activation of both the HB and the surrounding myocardium (*Figure 2*). Because ventricular activation starts simultaneously with the pacing artefact due to local myocardial capture, NS-HB capture is characterised by an absent isoelectric interval and slurred QRS upstroke (pseudo-delta wave) and the absence of a discrete local electrogram. The paced QRS duration be longer than the native QRS duration. There be two distinct capture thresholds: RV and His capture. In patients with HPS disease, three distinct

thresholds may be observed: RV, His capture with correction of bundle branch block and His capture without correction. Various characteristics of S- and NS-HBP in normal and diseased HPS are presented in *Table 1*. Although S-HBP results in ideal QRS morphology, studies using myocardial perfusion imaging have shown preserved LV electromechanical synchrony even in patients with NS-HBP.[15,16] In patients with HV block, NS-HBP provides the advantage of myocardial safety pacing. A recent observational study showed no significant difference in clinical outcomes between S- and NS-HBP.[17]

Clinical Implications of His Bundle Pacing

HBP is considered as an effective alternative to RVA pacing because it avoids many of the limitations of RVA. HBP can be considered in any patient with symptomatic bradycardia requiring ventricular pacing. Vijayaraman et al. reported an 84% success rate in 100 consecutive patients with AV block.[18] The procedural success was higher in patients with AV nodal block (93%) than in patients with infranodal block (76%).[18] The three proposed mechanisms for the correction of infranodal block are pacing the HB distal to the site of block, a virtual electrode polarisation effect and a differential source–sink relationship. The role of the HBP as an alternative to biventricular pacing for cardiac resynchronisation therapy (CRT) has been explored with good success.

In a retrospective study, Sharma et al. reported 90% procedural success for HBP in 106 CRT-eligible patients.[19] On-treatment comparison analysis of the His-Sync Pilot trial showed that patients receiving His CRT had superior electrical resynchronisation and a non-significantly higher echocardiographic response than those receiving biventricular CRT.[20] In patients with dilated cardiomyopathy and left bundle branch block (LBBB), Huang et al. achieved a 76% success rate for permanent HBP to achieve CRT and demonstrated very high rates (>85%) of echocardiographic super-response (*Figure 3*).[21]

Vijayaraman et al. reported a 95% success rate for HBP in patients with AF and uncontrolled ventricular rates undergoing AV node ablation.[22] LV ejection fraction improved from 43% to 50%, with a significant improvement in functional class.[22] In another study of 94 patients undergoing AV node ablation, HBP was successful in 86% of patients with an improvement in LV ejection fraction (from 44.9 ± 14.9% [mean ± standard deviation] at baseline to 57.6 ± 12.5% after a median follow-up of 3.0 years).[23] The efficacy of HBP may be uncertain in patients with intraventricular conduction delay, ⁻nificant LV scar and in 10–30% of LBBB patients ₩hom the site of block may be distal to the HB.

Non-selective to Selective His Bundle Pacing

Figure 2: Non-selective to Selective His Bundle Pacing

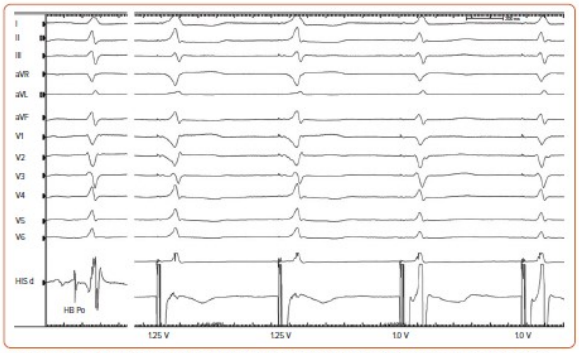

As the pacing output is reduced, note the change in QRS morphology and the local ventricular electrogram during non-selective to selective His bundle capture transition. HB Po = His potential.

Download

Left Bundle Branch Block Correction by His Bundle Pacing

Figure 3: Left Bundle Branch Block Correction by His Bundle Pacing

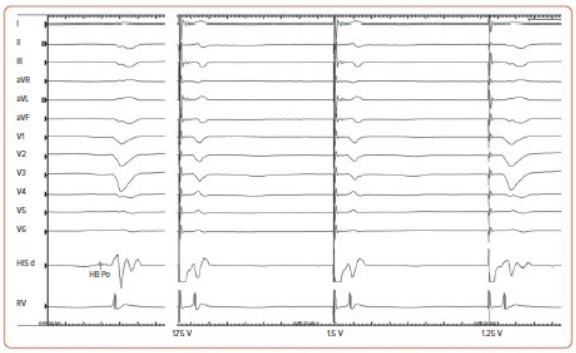

Complete correction of left bundle branch block could be achieved at a pacing output of 1.5 V at a pulse width of 1 ms (bundle branch block correction threshold). HB Po = His potential.

Download

Limitations of His Bundle Pacing

Although considered an acceptable alternative to RV pacing, HBP has some inherent limitations. Because the fibres are electrically insulated from the surrounding myocardium in the membranous septum, the capture threshold for HBP can be higher than that of RV pacing in 10–20% of patients. In our experience, HBP can be successfully achieved in >95% of patients with normal His–Purkinje conduction. In patients with a deeply seated HB, the helix may not be long enough to provide an acceptable pacing threshold. A capture threshold of >2 V at a pulse width of 1 ms may be seen in approximately 10% of patients and, before the advent of left bundle pacing, these values were accepted if NS-HB capture could be demonstrated with a significantly lower RV capture threshold.

Approximately 12% of patients were noted to have an increase in pacing threshold of >1 V in our cohort

of patients followed up for 5 years.[24] Lead revisions may be required during follow-up for an unacceptable increase in threshold in 5–7% of patients.[10] During the early phase of the learning curve, RV back-up pacing with an additional lead can be considered. However, if the unipolar pacing threshold is <1.5 V at a pulse width of 1 ms with COI at the time of implantation, back-up pacing may not be required. Other limitations include atrial oversensing, ventricular undersensing, premature battery depletion due to high output pacing and an inability to correct distal conduction system disease.

Criteria for His Bundle Pacing

Table 1: Criteria for His Bundle Pacing

Baseline	Normal QRS	His–Purkinje Conduction Disease	
		With Correction	Without Correction
S-HBP	S-QRS = H-QRS with isoelectric interval	S-QRS ≤ H-QRS with isoelectric interval	S-QRS ≤ or > H-QRS with isoelectric interval
	Discrete local ventricular electrogram in HBP lead with S-V = H-V	Discrete local ventricular electrogram in HBP lead	Discrete local ventricular electrogram in HBP lead
	Paced QRS = native QRS	Paced QRS < native QRS	Paced QRS = native QRS
	Single capture threshold (His bundle)	Two distinct capture thresholds (HBP with BBB correction, HBP without BBB correction)	Single capture threshold (HBP with BBB)
NS-HBP	S-QRS < H-QRS (S-QRS usually 0, $S\text{-}QRS_{nar}$ = $H\text{-}QRS_{nar}$) with or without isoelectric interval (pseudo-delta wave +/–)	S-QRS < H-QRS (S-QRS usually 0, $S\text{-}QRS_{nar}$ < $H\text{-}QRS_{nar}$) with or without isoelectric interval (pseudo-delta wave +/–)	S-QRS < H-QRS (S-QRS usually 0) with or without isoelectric interval (pseudo-delta wave +/–)
	Direct capture of local ventricular electrogram in HBP lead by stimulus artefact (local myocardial capture)	Direct capture of local ventricular electrogram in HBP lead by stimulus artefact	Direct capture of local ventricular electrogram in HBP lead by stimulus artefact
	Paced QRS > native QRS with normalisation of precordial and limb lead axes with respect to rapid dV/dt components of the QRS	Paced QRS ≤ native QRS	Paced QRS > native QRS
	Two distinct capture thresholds (His bundle capture, RV capture)	Three distinct capture thresholds possible (HBP with BBB correction, HBP without BBB correction, RV capture)	Two distinct capture thresholds (HBP with BBB, RV capture)

BBB = bundle branch block; dV/dt = rate of change in voltage; HBP = His bundle pacing; H-V = His–ventricular; H-QRS = His–QRS; NS-HBP = His bundle pacing; RV = right ventricle; S-HBP = selective His bundle pacing; S-QRS = stimulus–QRS; S-V = stimulus–ventricular. Source: Vijayaraman et al.[18] Adapted with permission from Elsevier.

Download

Left Bundle Branch Pacing

In an attempt to overcome the limitations of HBP, distal conduction system capture was first demonstrated by Huang et al. by deep septal placement of the lead.[25] LBBP is defined as the capture of either the proximal left bundle or one of its fascicles along with the septal myocardium at a low threshold.[26,27] Anatomically, the left bundle branch is a wide target, with fibres fanning on the left subendocardial aspect of the proximal interventricular septum, compared with the narrow band of the HB. Criteria for confirming LBB capture have been proposed but not validated in large trials. LBB capture is confirmed by paced QRS morphology of RBB delay pattern (qR or rSR in lead V1) along with any one of the following criteria:[26,27]

- Demonstration of non-selective to selective capture or non-selective to septal capture transition during threshold testing.
- Abrupt shortening of R-wave peak times (RWPT), as measured in leads V5 or V6 during lead implantation at the mid-septum and subsequent short and constant RWPT at the final site.
- Demonstration of LBB potential.
- Programmed deep septal stimulation from the pacing lead to demonstrate conduction system capture, especially selective capture.[27]
- Meeting physiology-based electrocardiographic criteria, namely paced RWPT in V6 (measured from QRS onset) equals the native RWPT and paced RWPT (measured from the stimulus)

equals the LBBP potential to V6.[29]

Left Bundle Branch Pacing Implantation Techniques

The LBBP implantation tools are the same as those for HBP. Pre-implantation echocardiography should be performed to assess the thickness of the interventricular septum in multiple views, the presence of septal scar, dilatation of cardiac chambers and valvular regurgitation. Careful assessment of the proximal septum is important because it determines procedural success.

Intracardiac electrograms and 12-lead ECG are continuously recorded using an EP recording system. Placing a quadripolar mapping catheter across the HB is optional to delineate the distal extent of His electrograms. Alternatively, the pacing lead can be used to map the HB to mark its distal extent. After obtaining venous access, the C315 sheath, along with the 3830 lead (*Figure 4*), is placed in the proximal interventricular septum 1–1.5 cm below the distal HB along an imaginary line connecting the distal HB to the RVA in the RAO 30° fluoroscopic view. Pace mapping of the septum is done by gentle counterclockwise rotation of the sheath to obtain a paced QRS morphology of a 'W' pattern in lead V1 with the notch on the nadir of QRS, tall R in lead II, RS in lead III and discordant QRS complexes in leads aVR and aVL. Although classically described, the W pattern is not mandatory, and, in our experience, this is not seen in 20% of patients. The sheath should be held firmly with counterclockwise torque, with the hub of the sheath pointing towards the right hand of the implanter (3 o'clock to 4 o'clock position) to orient it perpendicular to the septum.

Once the optimal site is identified on the right side of the septum, lead deployment can be done by one of two techniques:

- conventional (gradual deployment with monitoring of paced QRS morphology and unipolar pacing impedance); or
- premature ventricular complex (PVC) guided (rapid deployment with monitoring of PVC morphology).

In the conventional technique, the lead is deployed gradually with a few rapid rotations at a time and monitoring of three important parameters: paced QRS morphology (the notch on the nadir of lead V1 will gradually ascend to form an R wave), unipolar pacing impedance (increases gradually before it drops by 100–200 Ω as the lead reaches the LV subendocardium) and myocardial COI on the lead electrogram.[26] A drop in pacing impedance of >200 Ω, unipolar impedance <400 Ω and a reduction in sensed R wave amplitude with loss of COI in the unipolar electrogram may suggest lead perforation the LV cavity.

Left Bundle Branch Pacing Implantation

Technique

Figure 4: Left Bundle Branch Pacing Implantation Technique

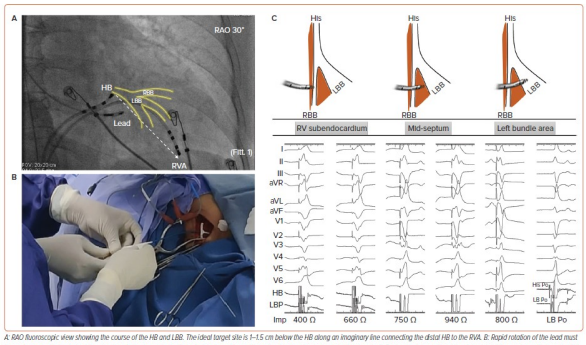

A: RAO fluoroscopic view showing the course of the HB and LBB. The ideal target site is 1–1.5 cm below the HB along an imaginary line connecting the distal HB to the RVA. B: Rapid rotation of the lead must be performed with the hub of the sheath pointing towards the 3- to 4-o'clock position, with preferably dry gloves closer to the sheath. C: Pacing the target site at the right side of the septum will show the 'W' pattern in lead V1, tall R in lead II and discordant QRS complexes in aVR and aVL. As the lead reaches the LBB area, paced QRS will show a qR pattern in lead V1 along with LB Po preceding the local ventricular electrogram. HB = His bundle; LBB = left bundle branch; LB Po = left bundle potential; RAO = Right anterior oblique; RBB = right bundle branch; RV = right ventricle; RVA = right ventricle apex.

Download

In the PVC-guided lead deployment technique, rapid turns are given to deploy the lead.[30] Lead movement during rapid deployment can be appreciated in the LAO 30° view. PVCs are commonly noted during rapid penetration of the lead into the septum (*Figure 5*). The morphology of PVCs changes from wide QRS with QS morphology in lead V1 to narrow QRS with an RBB delay pattern (qR/rSR) as the lead traverses from the right to left side of the septum. Template or fixation beat is defined as a PVC with an RBB delay pattern and a duration of <130 ms.[29–31] Rotations should be stopped immediately on observing a template beat. LBB capture can be confirmed at this site by the aforementioned criteria. Template beat-guided LBBP is associated with less fluoroscopic time and minimal myocardial injury, and avoids septal perforation during lead deployment.[29,31]

In patients with narrow QRS or RBBB morphology at baseline, a sharp high-frequency LBB potential should be seen preceding the local ventricular electrogram by 20–35 ms. In patients with LBBB, antegrade activation of LBB will not occur due to complete block of conduction in the distal HB/proximal LBB. LBB potential may be demonstrated by His-corrective pacing in patients with LBBB. In some patients the LBB potential may be masked due to significant COI. Concealed LBB potential must be considered before repositioning the lead if other parameters confirm LBB capture.[32] Non-selective left bundle (NS-LB) to selective left bundle (S-LB) branch capture transition can be demonstrated during threshold testing at near-threshold output (*Figure 6*). S-LB capture is characterised by a distinct local ventricular electrogram on the pacing lead separate from the pacing artefact, along with a change in paced QRS morphology. NS-LB is characterised by a pacing artefact immediately followed by a local ventricular electrogram with a pseudo-delta wave on the surface ECG. However, in many patients, demonstration of isoelectric interval or discrete local electrogram may be difficult due to short stimulus to QRS

intervals. RWPT is measured in leads V5 or V6 from the onset of the pacing spike to the peak of the R wave. Differential pacing at 10 and 2 V must produce short and constant RWPT (preferably <80 ms) to confirm the capture of the LBB. If peak LV activation time is prolonged at 2 V compared with pacing at 10 V, additional turns are given to get the shortest RWPT. In patients with cardiomyopathy, LV hypertrophy and distal conduction system disease, RWPT is generally <90 ms, but occasionally may be longer.[33]

Template or Fixation Beats During Lead Deployment

Figure 5: Template or Fixation Beats During Lead Deployment

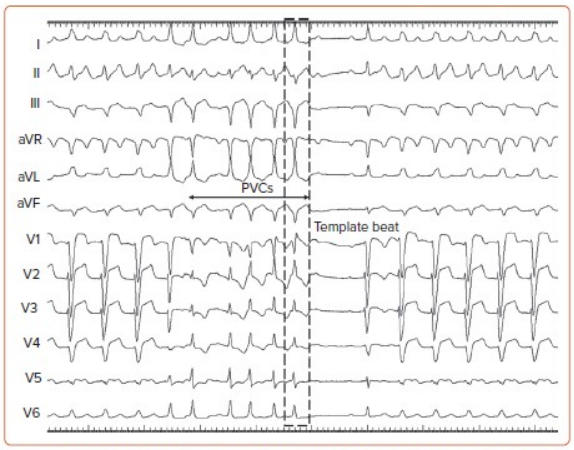

PVCs are generated during lead deployment with morphology changing from QS to qR (template beat) in lead V1 as it reaches the left bundle branch area. PVC = premature ventricular complex.

Download

Non-selective to Selective Left Bundle Branch Capture

Figure 6: Non-selective to Selective Left Bundle Branch Capture

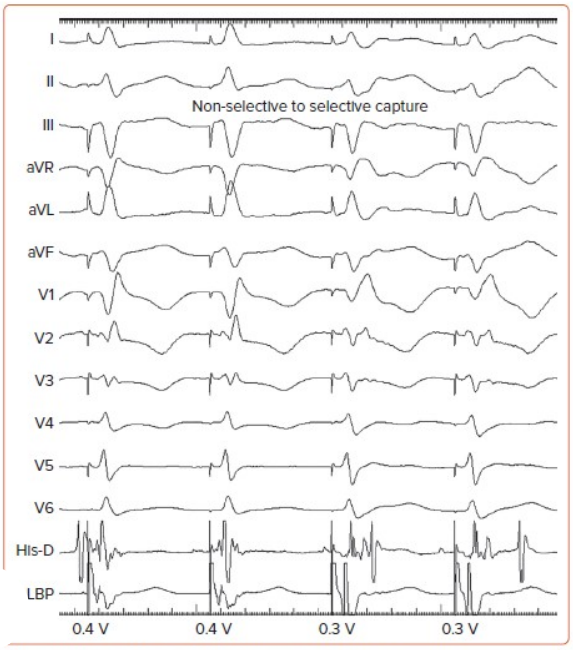

As the output is reduced from 0.4 to 0.3 V at a pulse width of 0.5 ms, non-selective to selective left

bundle branch (LBB) capture is seen. Note the discrete local ventricular electrogram from the pacing artefact during selective capture of the LBB along with subtle changes in QRS morphology. LBP = left bundle pacing lead.

Download

The novel physiology-based ECG criteria for LBB capture proposed by Jastrzebski et al., namely paced RWPT in V6 (measured from QRS onset) equal to native V6 RWPT and paced RWPT (measured from stimulus) equal to the LBB potential to V6 RWPT (*Figure 7*), had sensitivity and specificity of 98–88% and 85–95% respectively.[29] When measured from stimulus, the optimal and 100% specific V6 RWPT values for differentiating LBB capture from LV septal capture in patients with narrow QRS/RBBB were 83 and 74 ms, respectively. In patients with LBBB/ventricular escape rhythm, the optimal and 100% specific values were 101 and 80 ms, respectively.[29]

After confirming LBB capture, the sheath is gently pulled back into the right atrium with adequate lead slack. There is a tendency for the formation of an alpha loop in the lead while removing the sheath. The alpha loop can be undone in the RAO view by gently retracting the lead back with a counterclockwise rotation. Pacing parameters must be checked again in both the unipolar and bipolar configurations. Because part of the anode is often inside the septum, the anodal capture threshold must be checked by gradually reducing the pacing output in the bipolar configuration. Lead V1 will show changes in QRS morphology from the QS pattern (as the anode captures the right side of the septum) to the qR/rSR pattern once the anode loses it capture. Electroanatomical mapping with creation of 3D geometry of the atrium and ventricle, along with delineation of His signals to facilitate lead deployment, can minimise radiation exposure.[34]

Physiology-based ECG Criteria for Left Bundle Branch Capture

Figure 7: Physiology-based ECG Criteria for Left Bundle Branch Capture

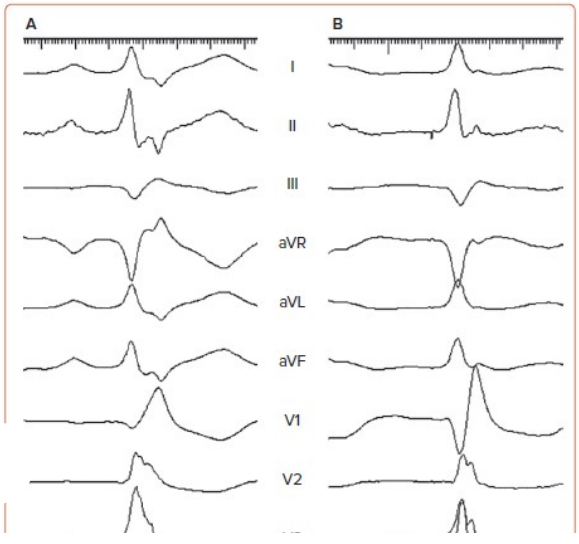

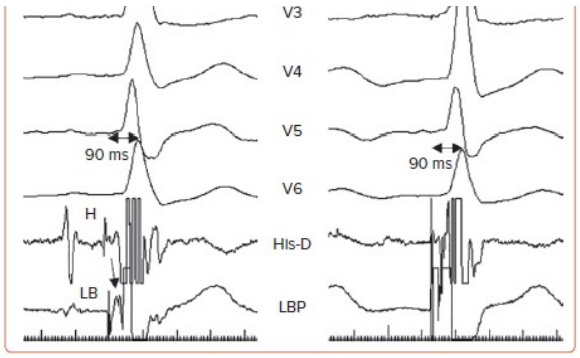

R-Wave peak time in lead V6 during native rhythm (A), as measured from the onset of LBP, will be equal to the R-wave peak time during left bundle branch pacing (B), as measured from the onset of pacing artefact. Also note the LB current of injury immediately after the LBP (black arrow). H = His; LB = left bundle; LBP = left bundle branch potential.

Download

Troubleshooting Difficult Cases

The reported success rate for LBBP is between 80.5% and 97%.[35–37] The reasons for failure include inability of the lead to penetrate deep into the septum, inadequate sheath support and improper sheath–septal orientation. Both the gloves and the lead must be dry while performing rapid rotations. If the basal septum is scarred, the left posterior fascicle can be targeted by placing the lead in mid-septum posteriorly.[38] Entanglement of the septal tricuspid leaflet may prevent deep septal penetration of the lead. To overcome this issue, the sheath is advanced towards the RV apex before bringing it back to the target site. RBB conduction delay created by pacing the LBB can be corrected by optimising the AV delay to allow native fusion, by programming pacing output to allow the anodal capture or by placing additional lead in the RV septum. In patients with cardiomyopathy and a diseased distal conduction system, LBBP may not result in ideal electrical resynchronisation. In these patients, LBBP may be combined with a coronary venous lead to achieve maximum electrical resynchronisation.

Clinical Implications

LBBP has the potential to overcome the limitations of HBP because it provides a low and stable threshold, excellent lead stability and the ability to correct conduction disease in the distal HB/proximal LB. In patients with AV block after transcatheter aortic valve replacement, Vijayaraman et al. reported success rates of 63% and 93% for HBP and LBBP, respectively.[39] Huang et al. reported a 97% success rate in patients with non-ischaemic cardiomyopathy and LBBB, with significant improvement in LV function.[40]

Atrioventricular Junction Ablation and Left Bundle Branch Pacing

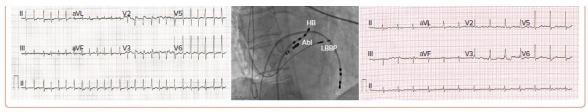

A: Baseline ECG showing AF with a fast ventricular rate. B: Note the distance between the Abl and the LBBP. C: Final paced QRS duration of 90 ms with a qR pattern in V1. Abl = ablation catheter; HB = His bundle; LBBP = left bundle branch pacing lead; RAO = right anterior oblique.

Download

A retrospective multicentre study by Vijayaraman et al. reported an 85% acute procedural success rate for LBBP in 325 CRT-eligible patients.[33] LBBP resulted in a reduction in QRS duration from 152 to 137 ms, along with an improvement in LV ejection fraction from 33% to 44%.[33] In patients undergoing AV junction ablation, LBBP provides additional safety because the lead is away from the site of ablation compared with HBP (*Figure 8*).

Limitations of Left Bundle Branch Pacing

Although LBBP provides a low capture threshold, excellent lead stability and a shorter learning curve, long-term safety data are lacking. In a recent report of 632 patients, Su et al. reported a 97.8% success rate for LBBP.[41] The mean follow-up time in that study was 18.6 months and the LBBP capture threshold remained stable at the 2-year follow-up. RBB injury was noted in 8.9% of patients and 1% of patients had either loss of capture or an increase in the threshold to >3 V with successful LBBP.[41] Lead perforation into the LV cavity, RBB injury, myocardial trauma with troponin release, septal arterial injury and coronary cameral fistula are potential complications to be monitored.[42–44] The implications of extraction of an LBBP lead implanted deep in the septum are unknown. Large-scale randomised multicentre studies are required to establish the long-term safety and efficacy of LBBP before it can be adopted as the main pacing strategy.

Conclusion

Conduction system pacing has gained significant interest over the past decade with the development of specially designed tools. HBP and LBBP are acceptable alternatives to RV pacing. The limitations of HBP are well addressed by LBBP, which provides a remarkably low and stable threshold. Early data suggest that HBP and LBBP may also be reasonable alternatives to biventricular pacing to achieve CRT.

References

1. Tops LF, Schalij MJ, Bax JJ. The effects of right ventricular apical pacing on ventricular function and dyssynchrony implications for therapy. J Am Coll Cardiol 2009;54:764–76.
Crossref | PubMed
2. Poole JE, Singh JP, Birgersdotter-Green U. QRS duration or QRS morphology: what really matters in cardiac resynchronization therapy? J Am Coll Cardiol

2016;67:1104–17.
Crossref | PubMed

3. Kurshid S, Epstein AE, Verdino RJ, et al. Incidence and predictors of right ventricular pacing-induced cardiomyopathy. Heart Rhythm 2014;11:1619–25.
Crossref | PubMed
4. Kaye GC, Linker NJ, Marwick TH, et al. Effect of right ventricular pacing lead site on left ventricular function in patients with high-grade atrioventricular block: results of the Protect-Pace study. Eur Heart J 2015;36:856–62.
Crossref | PubMed
5. Scherlag BJ, Lau SH, Helfant RH, et al. Catheter technique for recording His bundle activity in man. Circulation 1969;39:13–8.
Crossref | PubMed
6. Deshmukh P, Casavant DA, Romanyshyn M, et al. Permanent, direct His-bundle pacing: a novel approach to cardiac pacing in patients with normal His–Purkinje activation. Circulation 2000;101:869–77.
Crossref | PubMed
7. Tawara S. Das Reizleitungssystem des Saügetierherzens. Jena: GustavFischer, 1906;135–8.
8. Hudson REB. Surgical pathology of the conducting system of the heart. Br Heart J 1967;29:646–70.
Crossref | PubMed
9. Kawashima T, Sasaki H. A macroscopic anatomical investigation of atrioventricular bundle locational variation relative to the membranous part of the ventricular septum in elderly human hearts. Surg Radiol Anat 2005;27:206–13.
Crossref | PubMed
10. Vijayaraman P, Chung MK, Dandamudi G, et al. His bundle pacing. J Am Coll Cardiol 2018;72:927–47.
Crossref | PubMed
11. Gu M, Niu H, Hu Y, et al. Permanent His bundle pacing implantation facility by visualization of the tricuspid valve annulus. Circ Arrhythm Electrophysiol. 2020;13:e008370.
Crossref | PubMed
12. Zanon F, Marcantoni L, Zuin M, et al. Electrogram-only guided approach to His bundle pacing with minimal fluoroscopy: a single-center experience. J Cardiovasc Electrophysiol 2020;31:805–12.
Crossref | PubMed
13. Sharma PS, Huang HD, Trohman RG, et al. Low fluoroscopy permanent His bundle pacing using electroanatomic mapping: a feasibility study. Circ Arrhythm Electrophysiol. 2019;12:e006967.
Crossref | PubMed
14. Vijayaraman P, Dandamudi G, Zanon F, et al. Permanent His bundle pacing (HBP): recommendations from International HBP Collaborative Group for standardization of definitions, implant measurements and follow-up. Heart Rhythm 2018;15:460–8.
Crossref | PubMed
15. Zhang J, Guo J, Hou X, et al. Comparison of the effects of selective and non-selective His bundle pacing on cardiac electrical and mechanical synchrony. Europace 2018;20:1010–7.
Crossref | PubMed
16. Upadhyay GA, Tung R. Selective versus nonselective

His bundle pacing for cardiac resynchronization therapy. J Electrocardiol 2017;50:191–4.
Crossref | PubMed

17. Beer D, Sharma PS, Subzposh FA, et al. Clinical outcomes of selective versus nonselective His bundle pacing. JACC Clin Electrophysiol 2019;5:766–74.
Crossref | PubMed
18. Vijayaraman P, Naperkowski A, Ellenbogen KA, Dandamudi G. Electrophysiologic insights into site of atrioventricular block: lessons from permanent His bundle pacing. JACC Clin Electrophysiol 2015;1:571–81.
Crossref | PubMed
19. Sharma PS, Dandamudi G, Herweg B, et al. Permanent His bundle pacing as an alternative to biventricular pacing for cardiac resynchronization therapy: a multicenter experience. Heart Rhythm 2018;15:413–20.
Crossref | PubMed
20. Upadhyay GA, Vijayaraman P, Nayak HM, et al. On-treatment comparison between corrective His bundle pacing and biventricular pacing for cardiac resynchronization: a secondary analysis of His-SYNC pilot trial. Heart Rhythm 2019;16:1797–807.
Crossref | PubMed
21. Huang W, Su L, Wu S, et al. Long-term outcomes of His bundle pacing in patients with heart failure with left bundle branch block. Heart 2019;105:137–43.
Crossref | PubMed
22. Vijayaraman P, Subzposh FA, Naperkowski A. Atrioventricular node ablation and His bundle pacing. Europace 2017;19(Suppl 4):iv10–6.
Crossref | PubMed
23. Su L, Cai M, Wu S, et al. Long-term performance and risk factors analysis after permanent His-bundle pacing and atrioventricular node ablation in patients with atrial fibrillation and heart failure. Europace 2020;22(Suppl 2):ii19–26.
Crossref | PubMed
24. Vijayaraman P, Naperkowski A, Subzposh FA, et al. Permanent His-bundle pacing: Long-term lead performance and clinical outcomes. Heart Rhythm 2018;15:696–702.
Crossref | PubMed
25. Huang W, Su L, Wu S, et al. A novel pacing strategy with low and stable output: pacing the left bundle branch immediately beyond the conduction block. Can J Cardiol 2017;33:1736.e1–3.
Crossref | PubMed
26. Huang W, Chen X, Su L, et al. A beginner's guide to permanent left bundle branch pacing. Heart Rhythm 2019;16;1791–6.
Crossref | PubMed
27. Ponnusamy SS, Arora V, Namboodiri N, et al. Left bundle branch pacing: a comprehensive review. J Cardiovasc Electrophysiol 2020;31:2462–73
Crossref | PubMed
28. Jastrzebski M, Moskal P, Bednarek A, et al. Programmed deep septal stimulation – a novel maneuver for the diagnosis of left bundle branch capture during permanent pacing. J Cardiovasc Electrophysiol 2020;31:485–93.
Crossref | PubMed

29. Jastrzebski M, Keilbasa G, Curila K, et al. Physiology-based electrocardiographic criteria for left bundle branch capture. Heart Rhythm 2021;18:935–43.
Crossref | PubMed
30. Ponnusamy SS, Vijayaraman P. Left bundle branch pacing guided by premature ventricular complexes during implant. HeartRhythm Case Rep 2020;6:850–3
Crossref | PubMed
31. Ponnusamy SS, Ganesan V, Syed T, et al. Template beat: a novel marker for left bundle branch capture during physiological pacing. Circ Arrhythm Electrophysiol 2021;14:e009677.
Crossref | PubMed
32. Ponnusamy SS, Vijayaraman P. Concealed left bundle branch potential during physiological pacing. J Interv Card Electrophysiol 2021;61:213–4.
Crossref | PubMed
33. Vijayaraman P, Ponnusamy SS, Cano O, et al. Left bundle branch area pacing for cardiac resynchronization therapy: results from international LBBAP collaborative study group. JACC Clin Electrophysiol 2021;7:135–47.
Crossref | PubMed
34. Ponnusamy SS, Bopanna D, Kumar S. Electro-anatomical mapping guided low fluoroscopy left bundle branch pacing. JACC Clin Electrophysiol 2020;6:1045–7.
Crossref | PubMed
35. Vijayaraman P, Subzposh FA, Naperkowski A, et al. Prospective evaluation of feasibility, electrophysiologic and echocardiographic characteristics of left bundle branch area pacing. Heart Rhythm 2019;16:1774–82.
Crossref | PubMed
36. Ponnusamy SS, Muthu G, Kumar M, et al. Mid-term feasibility, safety and outcomes of left bundle branch pacing – single center experience. J Interv Card Electrophysiol 2021;60:337–46.
Crossref | PubMed
37. Li Y, Chen K, Dai Y, et al. Left bundle branch pacing for symptomatic bradycardia: implant success rate, safety, and pacing characteristics. Heart Rhythm 2019;16:1758–65.
Crossref | PubMed
38. Ponnusamy SS, Syed T, Kumar S. Left posterior fascicular pacing. J Innov Card Rhythm Manag 2021;12:4493–6.
Crossref | PubMed
39. Vijayaraman P, Cano O, Koruth JS, et al. His–Purikinje conduction system pacing following transcatheter aortic valve replacement – feasibility and safety. JACC Clin Electrophysio. 2020;6:649–57.
Crossref | PubMed
40. Huang W, Wu S, Vijayaraman P, et al. Cardiac resynchronization therapy in patients with non-ischemic cardiomyopathy utilizing left bundle branch pacing. JACC Clin Electrophysiol 2020;6:849–58
Crossref | PubMed
41. Su L, Wang S, Wu S, et al. Long-term safety and feasibility of left bundle branch pacing in a large single-enter study. Circ Arrhythm Electrophysiol 021;14:e009261.
Crossref | PubMed

42. Ravi V, Larsen T, Ooms S, et al. Late-onset interventricular septal perforation from left bundle branch pacing. HeartRhythm Case Rep 2020;6:627–31.
Crossref | PubMed
43. Ponnusamy SS, Patel NR, Naperkowski A, et al. Cardiac troponin release following left bundle branch pacing. J Cardiovasc Electrophysiol 2021;32:851–5.
Crossref | PubMed
44. Ponnusamy SS, Vijayaraman P. Aborted ST-elevation myocardial infarction – an unusual complication of left bundle branch pacing. HeartRhythm Case Rep

Indian Heart Journal 73 (2021) 221–222

Contents lists available at ScienceDirect

Indian Heart Journal

journal homepage: www.elsevier.com/locate/ihj

How significant is the radiation exposure during electrophysiology study and ablation procedures for supraventricular tachycardia?

Avishek Bagchi*, Ramalingam Vadivelu, Chetan Rathi, Bhavesh Gunaji Chavan, Yash Lokhandwala

Department of Cardiology, Holy Family Hospital, Bandra West, Mumbai, India

ARTICLE INFO

Article history:
Received 24 July 2020
Received in revised form
11 February 2021
Accepted 8 March 2021
Available online 17 March 2021

Keywords:
Radiofrequency ablation
Fluoroscopy

ABSTRACT

Radiation exposure during electrophysiology procedures has been a point of discussion. We measured the ionising radiation dosage during ablation procedures for supraventricular tachycardia. This was compared with coronary angiographies performed via the radial route to put it in perspective. We found that the radiation dosage during the ablation procedure was far lower, less than forty percent of that during coronary angiography (Air Kerma 249.1 mGy ± 266.95 mGy v/s 671.9 mGy ± 328.6 mGy; $p < 0.001$).

1. Introduction

Radiation exposure during conventional electrophysiology and radiofrequency (EP/RFA) procedures has been a reason cited for the increasing use of newer expensive electroanatomic mapping systems. To put this in perspective, we compared the Ionizing Radiation (IR) exposure in conventional EP/RFA procedures for supraventricular tachycardia (SVT), with coronary angiography (CAG) performed via the radial route.

2. Method

We prospectively analyzed the two-month data (January and February 2020) of IR exposure in all successful SVT ablation procedures and radial CAG. Patients with atrioventricular nodal reentrant tachycardia, accessory pathways and atrial tachycardia were included. Patients with more than one tachycardia mechanism were excluded. In the CAG arm, we excluded patients with i) acute coronary syndrome taken for primary intervention, ii) anomalous coronary origins and iii) prior coronary artery bypass surgery. During CAG, fluoroscopy was at 15 frames per second (FPS) of pulse rate (PR), while EP/RFA was done mostly with 7.5 FPS of PR (during transseptal puncture, it was increased to 15 FPS). All the procedures were done in a floor mounted catheterisation laboratory (Artis Zee, Siemens).

We collected the data regarding air kinetic energy release in matter (Kerma), measured in milli-gray (mGy), dose area product (DAP) measured in cGy.cm,^{2} total cine exposures and the fluoroscopy time, measured in minutes. These we compared among the two groups using the independent '*t*' test.

3. Results

Altogether 55 patients with CAG and 45 patients with EP/RFA were found eligible for the study. All procedures were performed with conventional mapping. The age of the CAG group was 57.8 ± 11 years, with male/female distribution of 37/18; in the EP/RFA group the age was 42 years ± 15.2 years, with male/female distribution of 22/23. The diagnoses were atrioventricular nodal re-entrant tachycardia (23, 51.1%) [amongst which 2 were atypical and rest typical], accessory pathways (18, 40.0%) [amongst which 9 were right sided pathways, 7 left sided pathways, 1 of coronary sinus diverticulum and 1 of anteroseptal pathway], and atrial tachycardia (4, 8.9%) [amongst which 2 were left atrial tachycardias, 1 was ablated from non-coronary sinus of aorta and 1 was ablated from upper septum]. Two left atrial tachycardias and 3 left-sided pathways required septal punctures. No jugular puncture was needed. All procedures were successful.

The details of IR exposure are detailed in Table 1. As evident, the Air Kerma was much less in EP/RFA as compared to CAG

* Corresponding author.
E-mail address: avi25986@gmail.com (A. Bagchi).

https://doi.org/10.1016/j.ihj.2021.03.003

Table 1
Radiation dosage in coronary angiogram and electrophysiology study/radiofrequency ablation procedures.

Parameters	Coronary Angiogram (n = 55)	EP/RF ablation (n = 45)	p value
Air Kerma (mGy)	671.9 ± 328.6	249.1 ± 267.0	**<0.001**
Dose area product (cGy.cm^2)	3373.3 ± 1800.4	1747.7 ± 2309.0	**<0.001**
Fluoroscopy time (minutes)	3.6 ± 2.8	13.4 ± 10.6	**<0.001**
Cine exposures	9.6 ± 2.4	3.7 ± 4.1	**<0.001**

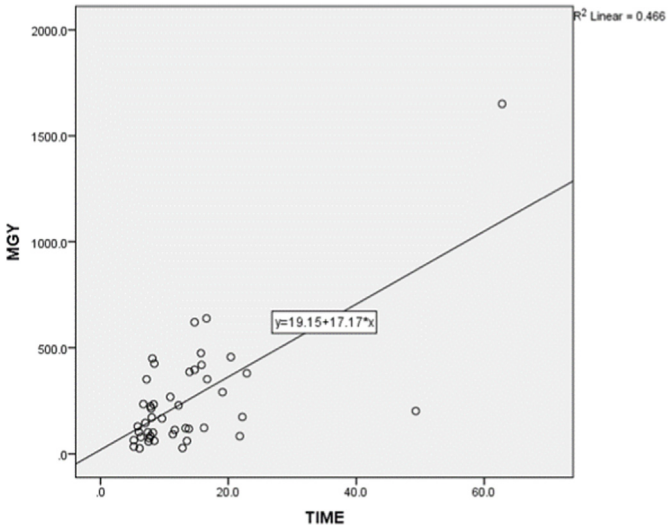

Fig. 1. Scatter diagram showing the relation between fluoroscopy time and Air Kerma of EP/RFA cases.

(249.1 ± 267 mGy v/s 671.9 ± 328.6 mGy, p < 0.001); as was DAP (1747.7 ± 2309 cGy cm^2 v/s 3373.3 ± 1800.4 cGy cm^2 p < 0.001). The total number of cine exposures were also much less in EP/RFA as compared to CAG (3.71 ± 4.1 v/s 9.55 ± 2.44, p < 0.001). The fluoroscopy time was higher in EP/RFA as compared to CAG (13.4 ± 10.6 min v/s 3.6 ± 2.8 min, p < 0.001). A Pearson product–moment correlation was run to determine the relationship between fluoroscopy time and Air Kerma in the EP/RFA group. There was a strong, positive correlation between fluoroscopy time and Air Kerma, which was statistically significant ($r = .682$, n = 45, p < .001). A linear regression established that fluoroscopy time statistically significantly predict Air Kerma, F (1, 43) = 37.47, p = .0001 and fluoroscopy time accounted for 46.6% of the explained variability in Air Kerma. The regression equation was predicted Air Kerma = 19.15 + 17.17 x (fluoroscopy time) (Fig. 1). According to this equation around 38 min (which is three times the mean fluoroscopy time of an EP/RFA case) of fluoroscopy time would be required in an EP/RFA case to equalize the mean radiation exposure of a CAG.

4. Discussion

Standard studies post 2010 show an average Air Kerma in the range of 500–600 mGy, average DAP around 3000–4000 cGy cm^2 and average fluoroscopy time in the range 3–8 min for CAG.[1,2] Studies on EP/RFA of SVT show Air Kerma in the range of 200–300 mGy, an average DAP of around 2000 cGy cm^2 and average fluoroscopy time of 12–15 min.[3,4] Our study gives us similar findings in the two categories, and is unique in comparing the IR between CAG and EP/RFA in the same center. We found that a conventional EP/RFA procedure for an SVT can be done in much lesser IR exposure than a CAG procedure. The major factors for this are i) the requirement for a higher digital PR during CAG and ii) The negligible need for cine-imaging during EP/RFA procedures. Hence, despite a three-fold longer fluoroscopy time, the total IR for EP/RFA was just around 40% of that during CAG procedures. Next-generation operators may use low/zero-fluoroscopy techniques for the standard procedures included in this study. However, in addition to the financial burden, this has to match or better the excellent long-term safety record of AVNRT ablation using conventional mapping.

5. Conclusion

The radiation exposure during conventional EP/RFA procedures for SVT was modest, far less than that for a diagnostic CAG done via the radial route.

Funding

None.

Declaration of competing interest

None.

References

1. Crowhurst JA, Whitby M, Thiele D, et al. Radiation dose in coronary angiography and intervention: initial results from the establishment of a multi-centre diagnostic reference level in Queensland public hospitals. *J Med Radiat Sci*. 2014 Sep;61(3):135–141.
2. Agarwal S, Parashar A, Ellis SG, et al. Measures to reduce radiation in a modern cardiac catheterization laboratory. *Circ Cardiovasc Interv*. 2014;7(4):447–455. Aug.
3. Jiang X, Dekker LR. Observations and considerations on patient X-ray exposure in the electrophysiology lab. *Arrhythmia Electrophysiol Rev*. 2013;2(2):141–144. Nov.
4. Casella M, Dello Russo A, Russo E, et al. X-Ray exposure in cardiac electrophysiology: a retrospective analysis in 8150 patients over 7 Years of activity in a modern, large-volume laboratory. *J Am Heart Assoc*. 2018;7(11), e008233. May 22.

Indian Pacing and Electrophysiology Journal 21 (2021) 324–326

Contents lists available at ScienceDirect

Indian Pacing and Electrophysiology Journal

journal homepage: www.elsevier.com/locate/IPEJ

EP / Device Rounds

QRS alternans during right ventricular pacing while ablating a concealed left sided accessory pathway

Raghav Bansal [a], Ramalingam Vadivelu [b, *], Eduardo Back Sternick [c], Yash Lokhandwala [d]

[a] Assistant Professor Cardiology, All India Institute of Medical Sciences, New Delhi, India
[b] Assistant Professor Cardiology, Velammal Medical College Hospital and Research Institute, Madurai, India
[c] Department of Arrhythmia and Electrophysiology, Biocor Institute, NovaLima, Brazil
[d] Department of Cardiology, Holy Family Hospital and Research Centre, Bandra West, Mumbai, India

ARTICLE INFO

Article history:
Received 1 April 2021
Received in revised form
16 May 2021
Accepted 24 May 2021
Available online 23 June 2021

Keywords:
QRS alternans
Catheter induced bigeminy
Radiofrequency ablation
Left free wall accessory pathway

ABSTRACT

A 16-year-old boy was referred for an electrophysiological study for documented regular narrow complex tachycardia. A diagnosis of a concealed left lateral accessory pathway was made with an eccentric atrial activation sequence both during tachycardia and right ventricular (RV) pacing. The pathway was mapped at the left posterior mitral vestibule during RV pacing, performed through the distal tip of the His bundle catheter pushed into right ventricular outflow tract. An unusual response to ventricular stimulation with alternation of QRS complex width and morphology was noted. The possible mechanisms are hereby discussed.

1. Case presentation

A 16-year-old boy was referred for an electrophysiology study in view of rapid episodic palpitations with documented regular narrow complex tachycardia. He had no manifest pre-excitation. Clinical tachycardia with cycle length of 360 ms was easily inducible by prematureatrial complexes. A diagnosis of a concealed left lateral accessory pathway was made with an eccentric atrial activation sequence both during tachycardia and right ventricular (RV) pacing. The pathway was mapped at the left posterior mitral vestibule during RV pacing (Fig. 1, left-hand panel), performed through the distal tip of the His bundle catheter, which was pushed deeper into the right ventricle (Fig. 1, right-hand panel). Intracardiac electrograms at the start of radiofrequency (RF) energy are depicted in the left-hand panel of Fig. 2. As the energy continues, as shown in the right-hand panel of Fig. 2, there is an alternation of QRS complex width and morphology. How is this explained?

2. Discussion

The right-hand panel in Fig. 1 depicts the site of ablation of a concealed left free-wall accessory pathway (red arrow) via a retrograde transaortic approach. Ablation during ventricular pacing is preferable compared to during sustained tachycardia in view of the advantage of catheter stability, especially after elimination of the pathway during ablation. Notably, pacing was performed just below the RV basal outflow tract with the His bundle catheter pushed distally (white arrowhead, right-hand panels of Fig. 1). The ablation signal inthe left panel of Fig. 2 marks the 'A' with an arrow, the small potential just after the ventricular electrogram in the RF distal channel. The early atrial activation along with the absence of isoelectric interval between V and A suggest that it is likely to be a successful ablation site.

With initiation of RF energy, there was an increase in the ventriculo-atrial (VA) interval in the distal coronary sinus (CS12) and RF distal channels with a change in atrial activation sequence (Fig. 2, left panel). During continuation of ablation,the alternate wide and narrow QRS beats have the same retrograde concentric atrial activation pattern with a constant VA interval, as depicted in Fig. 3. The narrower QRS complexes are associated with a reversal of the ventricular activation sequence in the coronary sinus channels. This may occur due to one of the following mechanisms: i)

* Corresponding author. Department of Cardiology, Velammal Medical College Hospital and Research Institute Madurai, India.
E-mail address: vvelu00@gmail.com (R. Vadivelu).
Peer review under responsibility of Indian Heart Rhythm Society.

https://doi.org/10.1016/j.ipej.2021.05.010

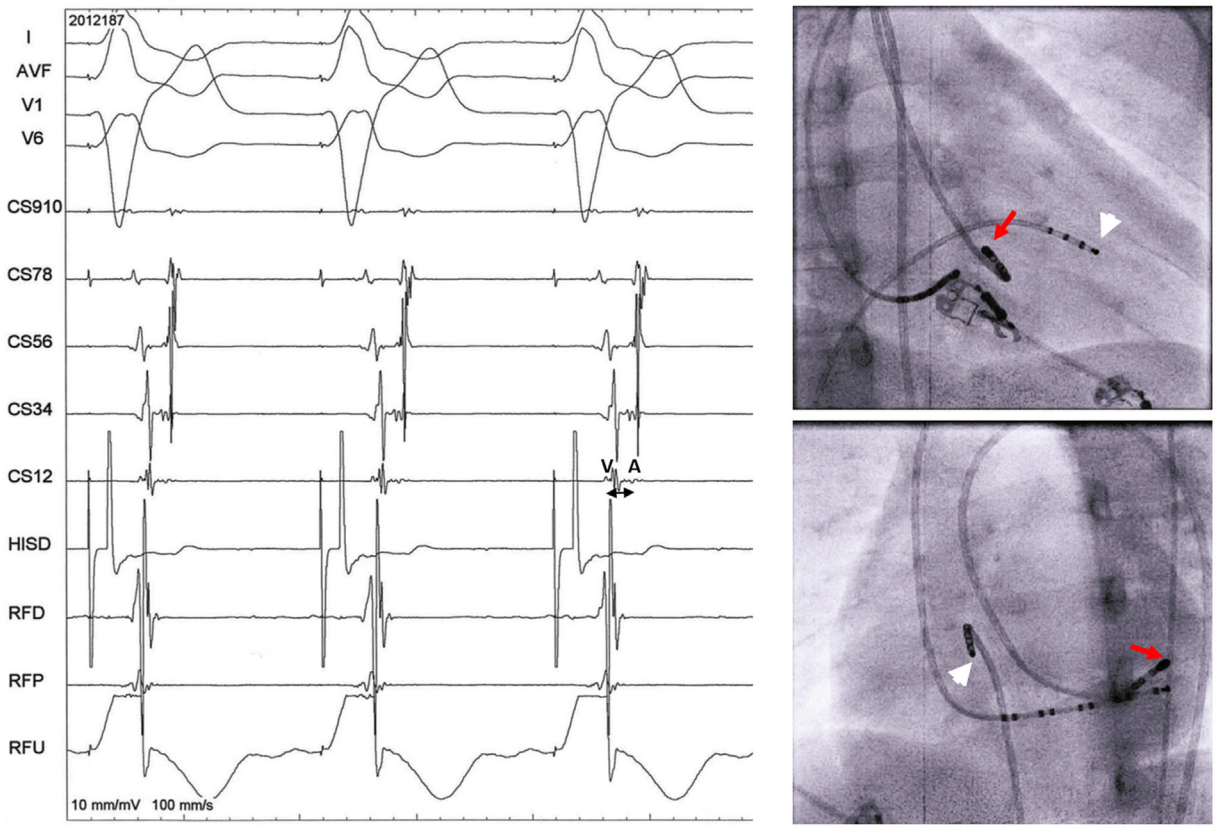

Fig. 1. Left hand panel. Mapping during right ventricular pacing revealing left lateral accessory pathway with eccentric atrial activation noted in the CS channels. **Right hand panel.** Fluoroscopic view demonstrating position of catheters in RAO 30° view (upper figure) and LAO 40° view (lower figure). The red arrow marks the tip of radiofrequency ablation catheter and the white arrow marks the position of the pacing catheter inside the right ventricle.

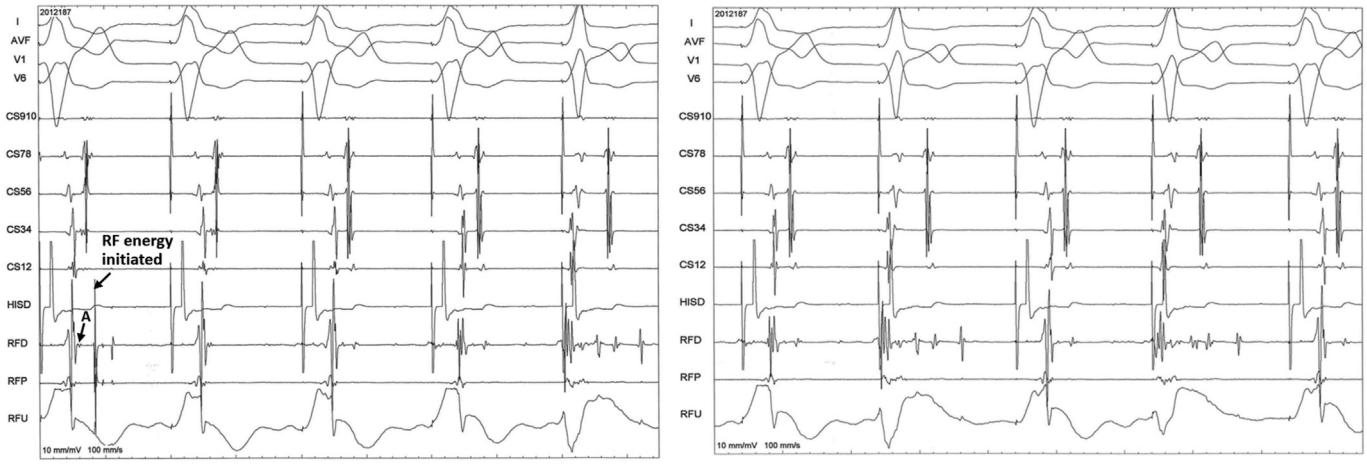

Fig. 2. Left hand panel. Intracardiac electrograms at the start of radiofrequency energy application. Note that the atrial activation pattern changes on the 2nd beat after initiation of energy, suggesting a successful ablation. Also note, the last QRS complex is narrower. **Right hand panel.** Note the alternating wide and narrow QRS morphology.

alternate His bundle capture and non-capture; ii) capture of the antero-basal left ventricle (which might occur with *trans*-septal activation due to its close proximity to the right ventricular outflow tract) along with the RV on alternate beats; this possibility is remote; iii) RF catheter induced premature ventricular complexes (PVCs), causing fusion and narrowing of the alternate beats. His bundle capture is unlikely in this case as the catheter was placed deeper in the RV base and there was no His signal in the His distal channel at baseline. Furthermore, the relatively long VA intervals during concentric atrial activation and the early left free wall activation during narrow QRS complexes (Fig. 2, right panel) are points against His bundle capture. Capture of the antero-basal left ventricle on alternate beats resulting in narrow QRS is a possibility; however, the ventricular electrogram in the RF catheter would not

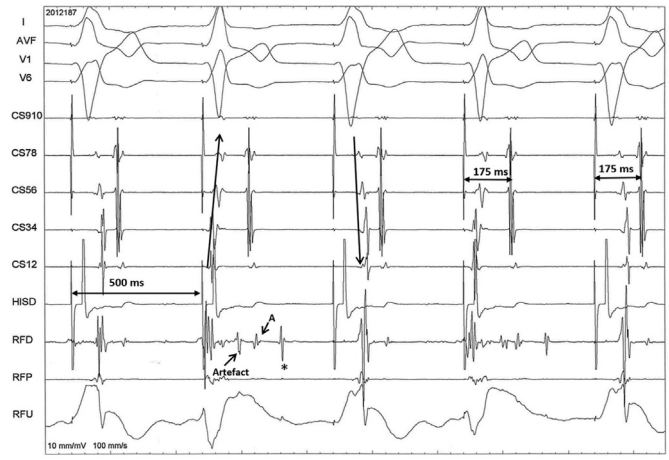

Fig. 3. Intracardiac electrograms during radiofrequency energy application, the same as the right-hand panel of Fig. 2. Note that ventricular activation in the CS channels changes along with alternating wide and narrow QRS morphology, being earliest in the left lateral region (CS12) during the narrow QRS complexes. Also note that after the narrow QRS complexes, multiple electrograms follow the ventricular electrogram in the RF distal channel. The first one is likely to be an artefact, the second and third ones being split atrial potentials.

be coincident with the pacing stimulus, seeing the large distance between the RF catheter and the His catheter (Fig. 1, right-hand panel). Catheter induced PVCshave been reported to occur in a bigeminal pattern [1]due to cardiac motion during tachycardia or ventricular pacing and then fuse with the paced beat, resulting in a narrower QRScomplex. The earliest ventricular activation in the RF distal channel followed by ventricular activation wave front from distal to proximal in the CS suggests catheter induced PVCs as a putative mechanism in this case.

The change in the atrial activation pattern from eccentric to concentric is consistent with elimination of accessory pathway conduction. However, residual accessory pathway conduction may be missed by RV pacing. Interestingly, the phenomenon of alternating narrow and wide QRS complexes allows insight into the assessment of the success of RF ablation in this case. The atrial activation pattern and the stimulus to atrial activation interval remains exactly the samedespite early left ventricular free wall capture. Note in the RF distal signal in Fig. 3, the presence of four different potentials: the first immediately following the pacing spike is the local ventricular potential (V), follow by a likely artefact, followed by an atrial potential (A) and another potential (*). This additional electrogram marked by an asterisk is possibly a split atrial electrogram. Rarely, radiofrequency energy application might convert a rapidly conducting accessory pathway into a decremental accessory pathway [2]. This might uncover a second pathway with variable fusion between the conduction from two pathways and the conduction system, and thus lead to multiple potentials. This may also be seen in case of electrical disconnection of the coronary sinus from the left atrium.

The present case highlights that while focusing on atrial activation for retrograde conduction during pacing, one should not lose sight of variations in QRS width and ventricular activation patterns, especially in the coronary sinus. An early ventricular activation in the RF catheter during pacing from a remote site may suggest catheter induced PVCs.

Declaration of competing interest

There are no conflicts of interest to state.

References

[1] Bhargava K, Jindal R, Kler TS. Narrow QRS tachycardia with alternate wide QRS beats: what is the mechanism? Indian Pacing Electrophysiol J 2008;8(3):234–7.
[2] Sternick EB, Correa FS, Rego S, Santos DM, Damascena F, Scarpelli R, Gerken LM, Wellens HJ. Postablation-acquired short atrioventricular Mahaim-type fibers: observations on their clinical, electrocardiographic, and electrophysiologic profile. Heart Rhythm 2012;9(6):850–8.

Journal of Electrocardiology 68 (2021) 11–13

Contents lists available at ScienceDirect

Journal of Electrocardiology

journal homepage: www.jecgonline.com

Review

Electrocardiography guided left bundle branch pacing

Shunmuga Sundaram Ponnusamy, MD., DM., PDF (EP) [a,*], Pugazhendhi Vijayaraman, MD., FHRS [b]

[a] Associate Professor, Department of Cardiology, Velammal Medical College Hospital and Research Institute, Madurai, Tamilnadu, India
[b] Professor of Medicine, Geisinger Commonwealth School of Medicine, Geisinger Heart Institute, MC 36-10, 1000 E Mountain Blvd, Wilkes-Barre, PA 18711, United States of America

ARTICLE INFO

Available online xxxx

Keywords:
Left bundle branch pacing
Electrocardiography
Template beat
Right bundle branch delay
Anodal capture

ABSTRACT

Left bundle branch pacing is a novel technique where LBB is directly captured by placing the lead deep inside the proximal septum. Electrocardiology plays a major role in identifying the target site on the right side of the septum, monitoring the lead deployment and confirming the LBB-capture. The lead is deployed 1–1.5 cm below the His bundle along an imaginary line connecting distal His signals to right ventricular apex. Rapid deployment of the lead will generate premature ventricular complexes which will guide in reaching the left bundle branch area. Several ECG based criteria will assist in confirming the conduction system capture. Further randomized trials will help in establishing the long-term safety of this novel pacing modality.

Introduction

Conduction system pacing ensures physiological activation of the left ventricle by capture of His-Purkinje system. Left bundle branch pacing(LBBP) is defined as direct capture of proximal left-bundle or one of its fascicles along with septal myocardium [1]. Huang et al [2] first demonstrated the procedure by placing the lead deep inside the septum below the His bundle(HB) with careful monitoring of paced-QRS morphology and unipolar pacing impedance. Intracardiac electrograms are continuously recorded during the procedure. Careful monitoring of the 12-lead electrocardiography(ECG) is important for successful lead deployment in the left bundle branch area. This review will focus on the role of ECG in assisting the procedure and confirming the capture of the conduction system.

Electrocardiography during left bundle branch pacing

Identifying the target-site

Since the lead has to be placed in the left sub-endocardium from the right side of the septum, appropriate target-site must be identified. The pacing lead and the sheath is placed 1–1.5 cm below the HB along an imaginary line connecting the distal His signals to right ventricular (RV) apex (Fig. 1B) [1]. Pacing there will usually show 'W'-pattern with notch on the nadir of the QS in lead-V1, tall-R in lead-II and biphasic-QRS in lead-III. QRS-complexes will be discordant in lead-aVR and aVL. The notch in lead-V1 will gradually ascend up to form a R-wave as the lead reaches the left bundle branch area (Fig. 1A). The 'W'-pattern in lead-V1 may not be seen in 20% of the patients and hence it is not mandatory prior to lead advancement [1]. A tall R-wave in lead-II is essential to capture the main left-bundle as opposed to a predominantly negative QRS which result in the capture of posterior fascicular branches.

Lead deployment

During rapid deployment of the lead inside the septum, premature-ventricular-complexes (PVC) are generated [3,4]. As the lead traverses from the right to the left-side of the septum, the PVC morphology changes from wide-QRS with QS-morphology to narrow-QRS with right bundle branch(RBB) delay pattern(qR/rSR) in lead-V1. A PVC with RBB-delay pattern with QRS duration of <130 ms is labelled as template-beat or fixation-beat [3,4]. In PVC-guided approach for LBBP, lead rotations should be stopped immediately on observing a template beat. Final LBB paced QRS-morphology will mimic the template beat (Fig. 2A & 2B). LBB capture can be confirmed by the standard criteria and subsequent rotations may be given based on pacing impedance and peak-left ventricular activation time (pLVAT). Excessive rotations after observing a template beat may result in septal perforation. If lead rotations are interrupted before getting a PVC with RBB-delay pattern, further turns are given till a template beat is generated. Template beat guided-LBBP is associated with short procedural time, minimal myocardial injury and avoids septal perforation during lead deployment [3]. Similar change in QRS-morphology can also be observed by continuously pacing the lead during deployment [5].

* Corresponding author.
E-mail address: shunmuga.pgi@gmail.com (S.S. Ponnusamy).

https://doi.org/10.1016/j.jelectrocard.2021.07.001
0022-0736/

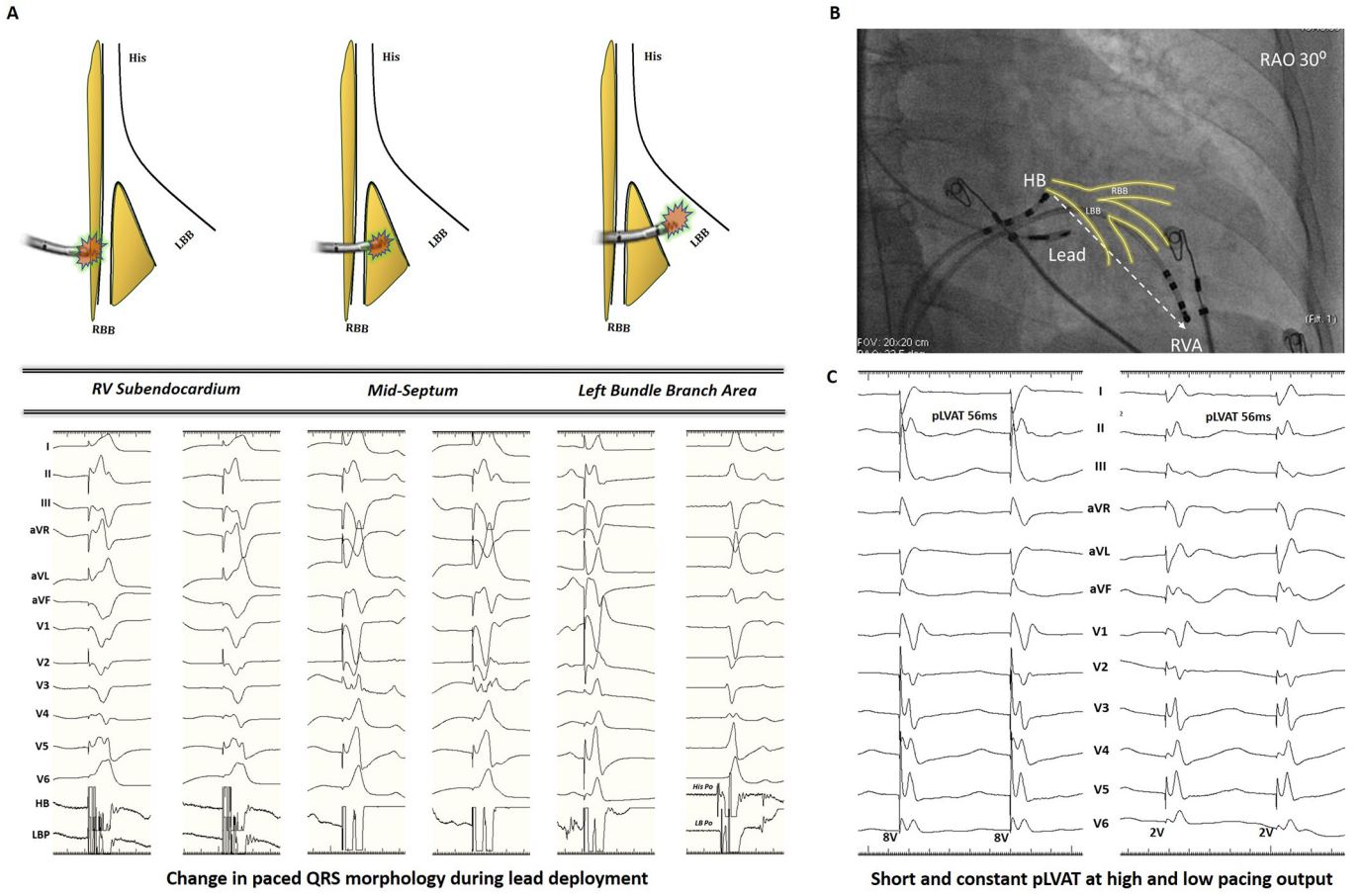

Fig. 1. A – Change in paced QRS morphology from the right side of the septum to left bundle branch area. Note the notch on the nadir of QS in lead V1 gradually ascend up to form a R-wave as the lead reach the LBB. B – Fluoroscopic right anterior oblique 30^0 view showing the target site for lead deployment. C – Short and constant pLVAT at 8 V and 2 V (56 ms) confirming LBB capture. RBB- right bundle branch, LBB- left bundle branch, LBP – left bundle pacing lead, HB- His bundle, RVA – right ventricular apex.

Confirming LBB capture

Paced QRS duration alone cannot predict conduction system capture as there is a significant overlap of QRS duration between LBBP and LV septal pacing [9]. As the left bundle is directly captured, pre-excitation of LV results in RBB-delay pattern in the ECG. A qR/rSR pattern in lead-V1 is a sensitive but not a specific marker for LBBP as it is also seen in 23–44% of patients with LV-septal capture [6]. The pLVAT is measured from the onset of pacing-artefact to the peak of R-wave in lead-V5. An abrupt shortening of pLVAT may be observed as the lead

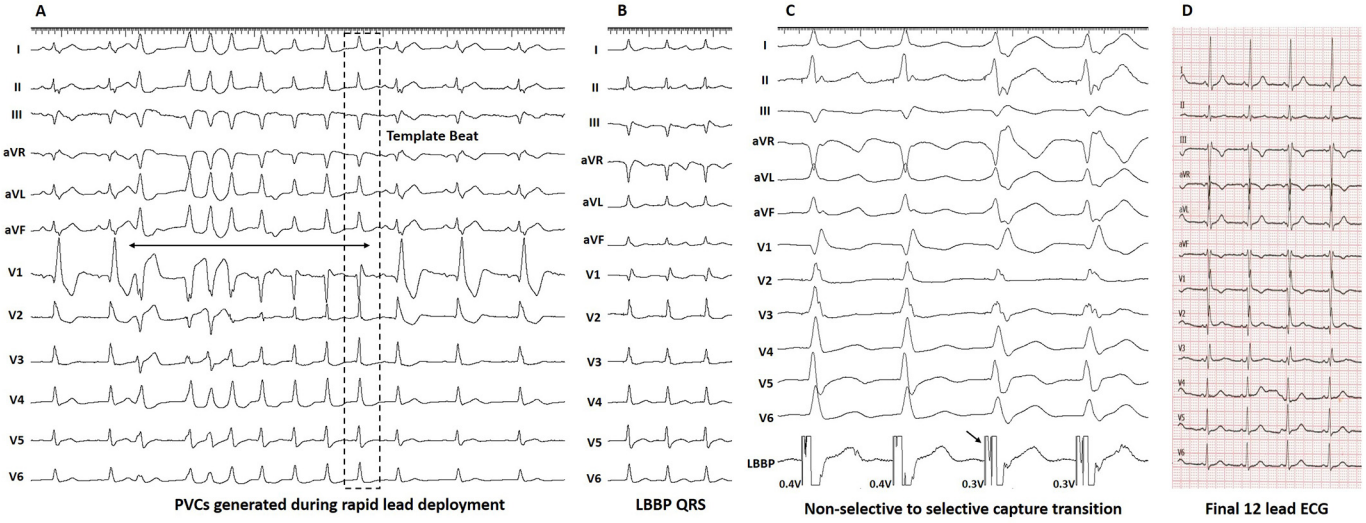

Fig. 2. A- PVCs generated by lead movement inside the septum. Note the change in morphology as the lead reach the LBB. Last generated PVC with RBB delay pattern labelled as template beat. B- LBBP QRS mimicked the template beat. C – Non-selective to selective capture transition during threshold testing. Note the change in QRS morphology (qR to rsR in lead-V1 and increase in S-wave duration in lead V6) and pacing lead electrogram (ventricular electrogram distinct from the pacing artefact). D- Final LBB paced 12 lead ECG

reaches the left bundle and it remains short and constant irrespective of the pacing-output (Fig. 1C). Further rotations are required for LBB capture only if the pLVAT is prolonged by >10 ms as the pacing output is decreased below 2 V. Huang et al [6] showed pLVAT of <75 ms in patients with baseline non-LBBB morphology and <85 ms for LBBB morphology has good sensitivity and specificity(82% and 95%; 76% and 93% respectively). Jastrzebski et al [9] showed lead-V6 R-wave peak time(RWPT) of <83 ms confirmed LBB capture in patients with non-LBBB morphology(sensitivity-84.7%;specificity-96.3%) and <101 ms for LBBB morphology(sensitivity-90.4%;specificity-78.9%). Paced QRS-axis depends on the baseline-axis, location of lead in the septum and site of the conduction system capture. A left-axis deviation usually indicates capture of the posterior-fascicle rather than the left main bundle. Programmed-deep-septal stimulation can be done to differentiate LBB capture from LV-septal capture by demonstrating change in QRS-morphology, rightward-shift in axis and delay in pLVAT in lateral-leads [7]. Another important criterion to confirm LBB-capture is to observe transition from non-selective to selective or non-selective to LV-septal capture at near-threshold output (Fig. 2C).

Selective vs non-selective LBB pacing

Based on the paced-QRS morphology, 2 forms of LBB capture can be observed – selective and non-selective LBBP. Non-selective LBBP is characterized by capture of LBB along with septal myocardium. ECG will show RBB delay pattern, short and constant pLVAT in lateral-leads, slurred-QRS upstroke immediately after the pacing artefact and Qr/qR-pattern in lead-V1 (Fig. 2C). Selective capture is characterized by capture of LBB alone with ECG showing rSR'/M-pattern in lead-V1, increase in S-wave duration in lead-V6, minimal prolongation of QRS duration and distinct isoelectric interval of 15-35 ms from the pacing-artefact to the onset of QRS (Fig. 2C) [4]. Intracardiac electrograms from the pacing lead may also show discrete isoelectric interval during selective capture of LB. The proportion of patients showing selective-LBB capture varies between 40% to 90% [6].

ECG optimization after LBBP

RBB delay due to LBBP can be corrected by two ways (a) anodal capture and (b) optimization of atrioventricular(AV)-delay to allow native fusion. As the pacing lead is deep inside, part of the anode ring will be in contact with the RV-septum. Anodal capture during bipolar-pacing results in simultaneous activation of right and left- side of the septum thereby minimizing the RBB-delay pattern. In patients with preserved AV-nodal conduction, AV-delay optimization can correct the RBB-delay by allowing fusion *via* right bundle branch activation (Fig. S1). With restoration of native conduction system activation during physiological pacing it is not uncommon to see unmasking of pathological-Q waves after correction of wide-QRS with ischemic cardiomyopathy [8].

Conclusion

Electrocardiography plays an important role in identifying the target-site for lead deployment, monitoring the lead-movement and confirming the LBB-capture. Physiology-based criteria [9] combining intracardiac-electrograms with ECG increase the procedural success, ensure electrical and mechanical synchrony and avoid chronic right-ventricular pacing related complications. Further randomized multicenter-trials to assess clinical outcomes and long-term safety of LBBP will help in establishing this novel-modality as the pacing mode of choice.

Disclosures

SSP: Consultant: Medtronic.

PV: Honoraria, consultant, research, fellowship support: Medtronic, consultant: Boston Scientific, Abbott, Biotronik, Eaglepoint LLC.

Financial source

No funding or financial sources received for this study.

The study was conducted after getting the ethical committee approval.

Declaration of Competing Interest

We have no conflicts of interest to disclose.

The Paper is not under consideration elsewhere. None of the paper's contents have been previously published. All authors have read and approved the manuscript.

Appendix A. Supplementary data

Supplementary data to this article can be found online at https://doi.org/10.1016/j.jelectrocard.2021.07.001.

References

[1] Ponnusamy SS, Arora V, Namboodiri N, et al. Left bundle branch pacing: a comprehensive review. J Cardiovasc Electrophysiol. 2020;31(9):2462–73.

[2] Huang W, Su L, Wu S, et al. A novel pacing strategy with low and stable output: pacing the left bundle branch immediately beyond the conduction block. Can J Cardiol. 1736; 2017(33):e1–3.

[3] Ponnusamy SS, Ganesan V, Syed T, et al. Template beat: a novel marker for left bundle branch capture during physiological pacing. Circ Arrhythm Electrophysiol. 2021;14 (4):e009677. https://doi.org/10.1161/CIRCEP.120.009677.

[4] Jastrzebski M, Keilbasa G, Moskal P, et al. Fixation beats: a novel marker for reaching the left bundle branch area during deep septal lead implantation. Heart Rhythm. 2021;18(4):562–9.

[5] Jastrzebski M, Moskal P. Reaching the left bundle branch pacing area within 36 heartbeats. Kardiol Pol. 2021;79(5):587–8. https://doi.org/10.33963/KP.15914.

[6] Wu S, Chen X, Wang S, et al. Evaluation of the criteria to distinguish left bundle branch pacing from left ventricular septal pacing. J Am Coll Cardiol EP. 2021;22. https://doi.org/10.1016/j.jacep.2021.02.018 S2405-500X(21)00202-4.

[7] Jastrzebski M, Moskal P, Bednarek A, et al. Programmed deep septal stimulation - a novel maneuver for the diagnosis of left bundle branch capture during permanent pacing. J Cardiovasc Electrophysiol. 2020;31:485–93.

[8] Ponnusamy SS, Vijayaraman P. Unmasking of pathological Q waves by left bundle branch pacing. J Interv Card Electrophysiol. 2021;60:555–6.

[9] Jastrzebski M, Keilbasa G, Curila K, et al. Physiology-based electrocardiographic criteria for left bundle branch capture. Heart Rhythm. 2021;18(6):935–43.

JACC: CLINICAL ELECTROPHYSIOLOGY VOL. 7, NO. 9, 2021

PUBLISHED BY ELSEVIER

CIED - PHYSIOLOGICAL PACING

Left Bundle Branch Block–Induced Cardiomyopathy

Insights From Left Bundle Branch Pacing

Shunmuga Sundaram Ponnusamy, MD,[a] Pugazhendhi Vijayaraman, MD[b]

ABSTRACT

OBJECTIVES The aim of the study was to report the efficacy of left bundle branch pacing (LBBP) in the management of left bundle branch block (LBBB)-induced cardiomyopathy (LIC).

BACKGROUND Chronic LBBB is known to cause mechanical dyssynchrony and cardiomyopathy. Hyperresponse to cardiac resynchronization therapy (CRT) with biventricular pacing (BVP) is a hallmark of LIC. LBBP has recently shown promise as an alternative to BVP.

METHODS Patients undergoing CRT between 2018 and 2020 were retrospectively screened, and those who met the criteria for LIC were included in the study. Duration of LBBB, CRT type, and response were documented. Pacing parameters, and electrocardiographic and echocardiographic data were collected.

RESULTS Possible LIC was identified in 17 of 159 patients undergoing CRT and LBBP was successfully performed in 13 patients. Duration of LBBB before left ventricular dysfunction was 4.2 ± 3.9 years. Temporary His bundle pacing corrected underlying LBBB in all patients. During LBBP, there was significant reduction in QRS duration (167.8 ± 11.6 ms to 110.4 ± 13.1 ms; $p < 0.0001$) and repolarization parameters of QTc, Tpeak-Tend, and Tpeak-Tend/QTc ratio. LBBP threshold and R waves at implant were 0.53 ± 0.21 V/0.5 ms and 11.7 ± 7.1 mV and remained stable. Cardiac magnetic resonance imaging showed no evidence of scar ($n = 8$). During follow-up, left ventricular ejection fraction improved from 30.4 ± 6.6% to 57.4 ± 4.7% ($p < 0.0001$) and New York Heart Association functional class improved from 3.1 ± 0.3 to 1.2 ± 0.4 ($p < 0.0001$) compared with baseline.

CONCLUSIONS LBBP is a reasonable option for CRT in patients with LIC, as it provides low and stable capture threshold with complete correction of underlying electrical and mechanical abnormalities associated with LBBB.
(J Am Coll Cardiol EP 2021;7:1155–1165) © 2021 by the American College of Cardiology Foundation.

Dilated cardiomyopathy is defined as left ventricular (LV) or biventricular dilatation with systolic dysfunction in the absence of coronary artery disease or abnormal loading condition (1). The relationship between left bundle branch block (LBBB) and dilated cardiomyopathy is well known. The prevalence of LBBB in the general population is between 0.2% and 1.1% (2–4). Isolated LBBB can also be seen in individuals with a structurally normal heart. Although LBBB confers increased

From the [a]Velammal Medical College, Madurai, India; and the [b]Geisinger Heart Institute, Geisinger Commonwealth School of Medicine, Wilkes-Barre, Pennsylvania, USA.
The authors attest they are in compliance with human studies committees and animal welfare regulations of the authors' institutions and Food and Drug Administration guidelines, including patient consent where appropriate. For more information, visit the Author Center.

Manuscript received December 29, 2020; revised manuscript received February 1, 2021, accepted February 3, 2021.

ISSN 2405-500X/$36.00 https://doi.org/10.1016/j.jacep.2021.02.004

ABBREVIATIONS AND ACRONYMS

BVP = biventricular pacing

CRT = cardiac resynchronization therapy

ECG = electrocardiography

HBP = His bundle pacing

LBBB = left bundle branch block

LIC = LBBB-induced cardiomyopathy

LBBP = left bundle branch pacing

LV = left ventricular

LVEF = left ventricular ejection fraction

mortality risk in elderly patients and those with underlying structural heart disease, it has minimal effects on younger healthy individuals (5–7). However, chronic LBBB has been known to result in asynchronous LV contraction and subsequent impairment in LV function. Several studies have suggested a causative link between LBBB and chronic LV dilation, dysfunction, and heart failure (8–10).

The relationship between LBBB and LV dysfunction is complex and poorly understood. It may appear during the course of the disease indicating the severity and poor prognosis or it may play a causative role in the development of dyssynchronous contraction and worsening of LV function. Blanc et al (8) demonstrated normalization of ejection fraction (EF) in patients with LV dyssynchrony-mediated cardiomyopathy. Subsequently, Vaillant et al (10) defined the term LBBB-induced cardiomyopathy (LIC) in a retrospective review of patients with baseline LBBB and normal LV function and who subsequently developed dysfunction (10). This group of patients demonstrated hyperresponse to cardiac resynchronization therapy (CRT). NEOLITH (New-Onset LBBB-Associated Idiopathic Cardiomyopathy) and NEOLITH II studies showed earlier CRT implantation (before 3 months of guideline-directed medical therapy) was associated with favorable outcome in patients with new-onset nonischemic cardiomyopathy and LBBB (11,12).

CRT is the treatment of choice for patients with LBBB and refractory heart failure, and several studies have established the role of biventricular pacing (BVP) as a standard therapy. Nearly one-third of the patients do not respond favorably to BVP (13). Recently, Singh et al (14) in a retrospective study demonstrated normalization of LVEF after His bundle pacing (HBP) in 7 patients with LIC. HBP is often associated with higher LBBB correction thresholds and lower implant success rates (15). Recently, several studies have demonstrated the feasibility of left bundle branch pacing (LBBP) to achieve CRT (16,17). The aim of our study was to assess the role of LBBP as an alternative strategy for LIC.

METHODS

STUDY POPULATION. This was a retrospective, nonrandomized, observational study performed at 2 centers. The data collection was approved by each institutional review board. Chart review of patients who had undergone CRT between 2018 and 2020 was performed. Patients who met the criteria for LIC (10) were included in the study. All patients provided written informed consent for His-Purkinje conduction system pacing as a nonstandard approach for CRT.

DEFINITION OF LBBB AND LIC. LIC (10) was defined in our study by the presence of: 1) history of LBBB for more than 1 year; 2) LVEF >50% at the time of diagnosis of LBBB; 3) progressive decline in LVEF to <40% and development of New York Heart Association functional class II to IV; 4) no other identifiable cause for cardiomyopathy; and 5) echocardiographic evidence of dyssynchrony (interventricular mechanical delay >40 ms; aortic pre-ejection delay of >140 ms; septal to lateral wall delay of >65 ms) (18–21). LBBB on the 12-lead electrocardiography (ECG) was defined as QRS duration of >130 ms in women and >140 ms in men and presence of mid-QRS notching/slurring in at least 2 consecutive leads I, aVL,V_1,V_2,V_5, or V_6 (13).

PROCEDURAL TECHNIQUE. Intracardiac electrograms and 12-lead ECG were continuously monitored in the electrophysiology recording system. LBBP was performed as previously described (16,17,22,23). Temporary pacing at the His bundle was performed (by using electrophysiology catheter or HBP lead) at high outputs to assess correction of underlying LBBB and documented. Briefly, 4.1-F sized 3830 SelectSecure lead was deployed 1.5 cm apical to the His bundle along an imaginary line joining the distal His site to the right ventricular apex using C315His or C304His sheath (Medtronic Inc.). The paced QRS morphology and unipolar pacing impedance were monitored. Left bundle branch (LBB) capture was confirmed by the published criteria (22,23) to obtain a short and constant peak LV activation time in leads V_5 to V_6 and right bundle branch conduction delay pattern in lead V_1, demonstration of transition from nonselective LBBP to selective LBBP (**Figure 1**) or LV septal capture during threshold testing, and/or demonstration of LBB potential during corrective HBP. If optimal LBBP could not be achieved, conventional BVP was performed. All patients received guideline-directed medical therapy including beta-blockers, angiotensin-converting enzyme inhibitors/angiotensin receptor blockers, and diuretics for at least 3 months before the implantation.

DATA COLLECTION. Baseline characteristics of the study population were collected. ECG parameters were analyzed at baseline, immediate post procedure, and after 6 weeks, which included QRS duration, QT

FIGURE 1 **LBBP for LBBB**

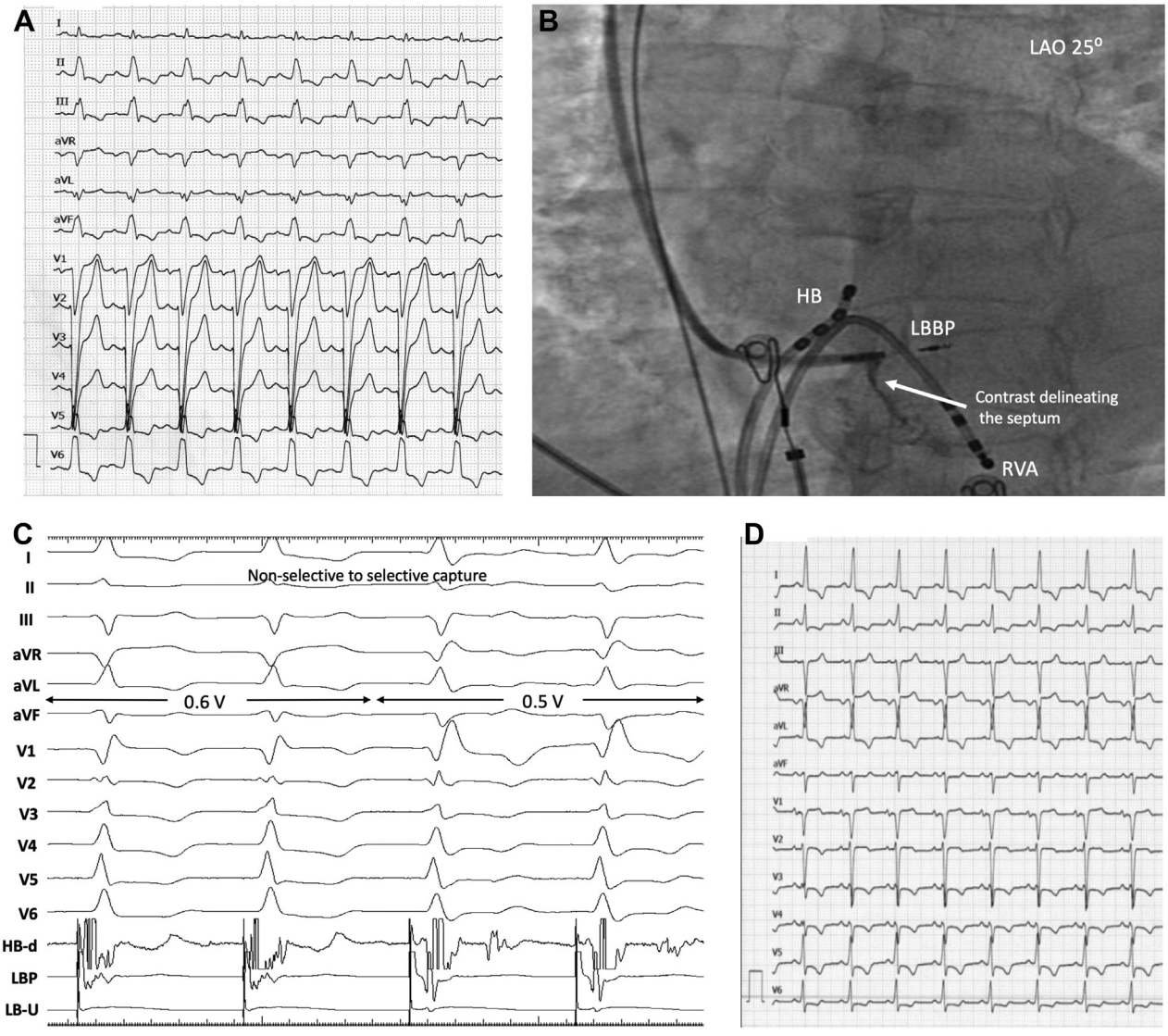

Baseline ECG showing complete LBBB with QRS duration of 156 ms. **(B)** Left anterior oblique fluoroscopy view showing the depth of the LBBP lead inside the septum. **(C)** Nonselective to selective LBB capture transition at near threshold outputs. **(D)** Final ECG after correction of right bundle branch delay by optimizing the atrioventricular interval. ECG = electrocardiogram; HB = His bundle; LBB = left bundle branch; LBBB = left bundle branch block; LBBP = left bundle branch pacing lead; RVA = right ventricular apex.

interval, T peak to T end (Tp-Te) duration (interval between the peak of positive or nadir of negative T-wave to the end of the T wave in the mid-precordial lead showing the longest value). QT interval was calculated from the Q-wave onset to the end of T-wave in precordial lead showing the longest value, and rate correction (QTc) was done by Bazett's formula (24). Tpeak-Tend/QTc ratio was also calculated. Echocardiography was done before implantation and during follow-up to document the interventricular septal thickness, LVEF by modified Simpson's method, LV diastolic dimensions, and valvular regurgitation. Cardiac magnetic resonance imaging (MRI) was done when feasible to assess the LV wall thickness, LVEF, and for the presence of late gadolinium enhancement. In patients undergoing conduction system pacing, LBBB correction by pacing at the His bundle was documented. HV intervals, LBBB

FIGURE 2 Patient Flow Diagram of the Study Population

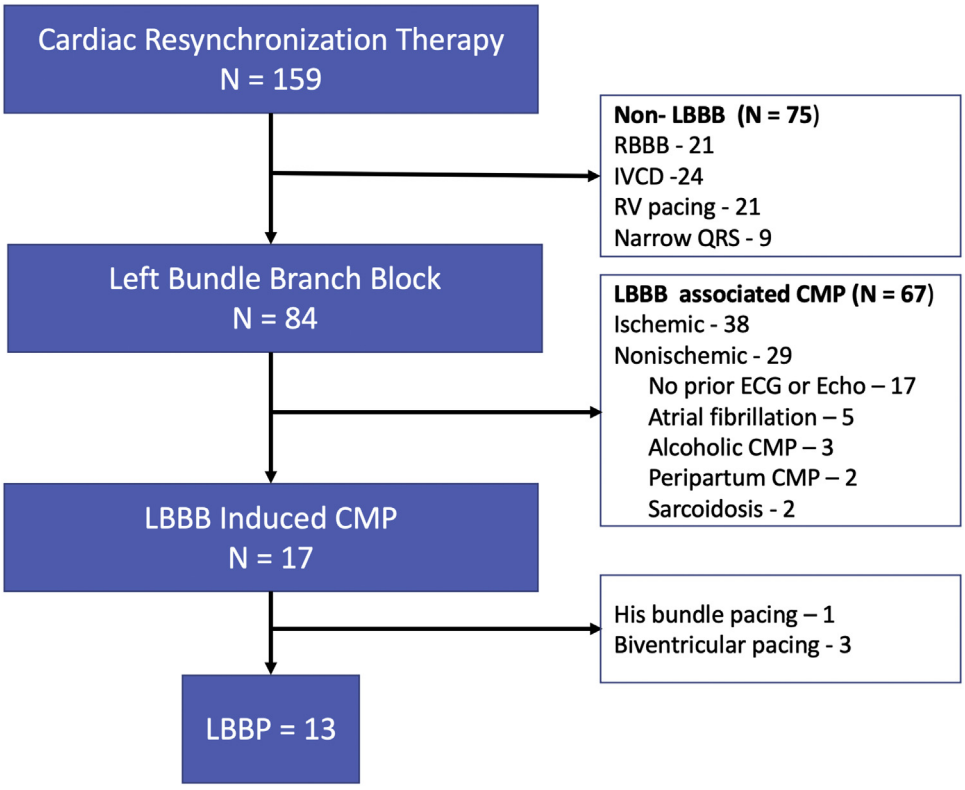

CMP = cardiomyopathy; ECG = electrocardiogram; IVCD = intraventricular conduction defect; LBBB = left bundle branch block; LBBP = left bundle branch pacing; RBBB = right bundle branch block; RV = right ventricle.

correction by selective or nonselective HBP, and QRS duration with corrective HBP were documented. In patients with nonselective HBP with correction, QRS duration was measured from stimulus to QRS end at sweep speed of 100 mm/s. Pacing parameters were collected at the time of implantation, 2 weeks, and during follow-up in the device clinic in person or remote check every 3 months. Any ventricular arrhythmias detected or treated by the device were documented. New York Heart Association functional class at baseline and during follow-up, heart failure hospitalizations, or death were documented.

STATISTICAL ANALYSIS. Continuous variables were reported as mean ± SD and compared with paired *t*-test. Categorical variables were reported as percentages. All statistical tests were 2-tailed. A p value of <0.05 was considered to indicate statistical significance.

RESULTS

BASELINE CHARACTERISTICS. A total of 159 patients had undergone CRT during the study period in the 2 centers (Figure 2). Complete LBBB with heart failure as indication for CRT was observed in 84 patients (52.8%). Retrospective analysis of the available data showed 17 (20%) of the 84 patients had possible LIC as defined by the inclusion criteria (Central Illustration). In the remaining 67 patients, 38 had ischemic cardiomyopathy. Nonischemic cardiomyopathy was present in 29 patients: no prior echo or ECG was available in 17, atrial fibrillation with LBBB in 5, alcoholic cardiomyopathy in 3, peripartum cardiomyopathy in 2, and sarcoidosis in 2. Among patients with LIC, LBBP was performed in 13 patients, HBP in 1 patient, and BVP with coronary sinus lead in 3 patients. The patients with LIC and successful LBBP comprised the study population. The mean duration between first diagnosis of LBBB and onset of LV

CENTRAL ILLUSTRATION **Left Bundle Branch Pacing for LBBB-Induced Cardiomyopathy**

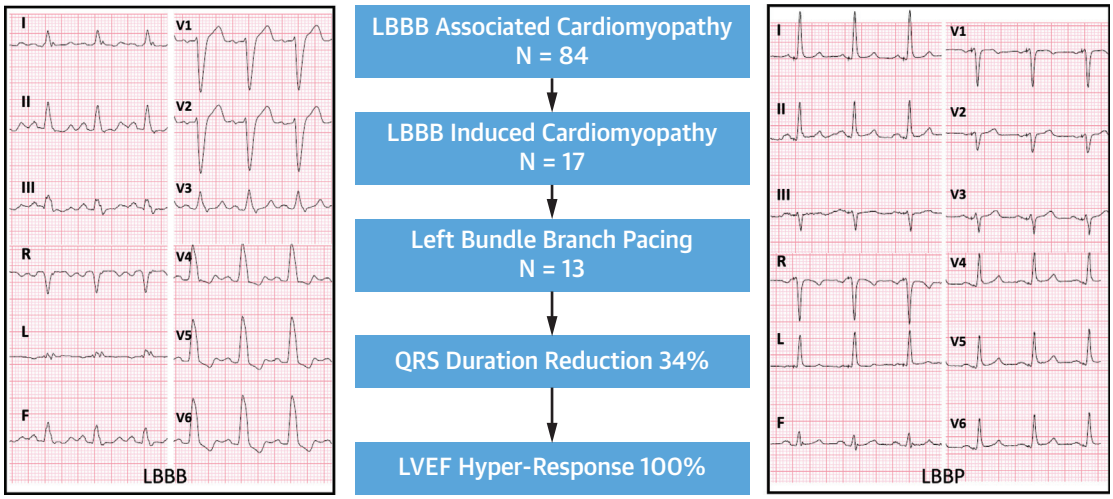

Ponnusamy, S.S. et al. J Am Coll Cardiol EP. 2021;7(9):1155–1165.

LBBB = left bundle branch block; LVEF = left ventricular ejection fraction.

dysfunction with heart failure was 4.1 ± 3.9 years. The mean LVEF when LBBB was first diagnosed in this group was 53.6 ± 2.4%. Individual patient characteristics, timeline of diagnosis of LBBB and LBBP are shown in Table 1. The mean age of the study population was 63.2 ± 16.4 years (Table 2). Three patients had associated obstructive coronary artery disease without a history of myocardial infarction for which percutaneous coronary intervention was done. Baseline QRS morphology fulfilled Strauss criteria for complete LBBB in all patients. The mean QRS duration at baseline was 167.2 ± 12.7 ms and the mean baseline LVEF before LBBP was 30.5 ± 6.7%. Cardiac MRI at baseline was available in 8 patients and showed preserved wall thickness with no evidence of scar, as demonstrated by absent late gadolinium enhancement in the LV (Figure 3).

ELECTROPHYSIOLOGIC CHARACTERISTICS. Pacing from the His bundle region resulted in correction of underlying LBBB in all 13 patients (Figure 4). Nonselective and selective HBP with correction of LBBB was observed in 8 and 5 patients, respectively. Mean HV intervals at baseline were 60.8 ± 9.2 ms (range 45 to 76 ms). During corrective HBP, QRS duration decreased from 167.8 ± 11.7 ms at baseline to 119.5 ± 19.1 ms ($p < 0.0001$).

LBBP was performed using 3830 SelectSecure lead (Medtronic Inc.) in 13 patients. The unipolar pacing threshold at the time of implantation was 0.53 ± 0.21 V at 0.5 ms pulse-width and the sensed R wave amplitude was 11.7 ± 7.1 mV (Table 3). The unipolar pacing impedance was 715.7 ± 124.7 ohms. QRS duration reduced from 167.2 ± 12.7 ms at baseline to 110.4 ± 13.1 with LBBP. The peak LV activation time as measured in lead V_6 was 68.7 ± 8.2 ms. LBB capture could be demonstrated in all patients as per the defined criteria. The mean duration of follow-up after LBBP was 12.7 ± 5.2 months (range 3-22 months). The pacing threshold remained stable at 0.61 ± 0.14 V at 0.5 ms pulse-width ($p = 0.26$). The R-wave amplitude was 13.9 ± 7.5 mV (range 3.5 to 27 mV; $p = 0.44$). There was a drop in unipolar pacing impedance from 715.7 ± 124.7 ohms at implantation to 530.6 ± 90.9 ohms during follow-up ($p < 0.0001$). LBB capture was evident in all patients during follow-up.

Among the study group, 5 patients received CRT-defibrillator (LBBP lead connected to LV port) and the remaining 8 patients received dual chamber pulse generator with LBBP lead connected to ventricular port.

Analysis of ECG at baseline, immediately after LBBP, and after 6 weeks showed significant improvement in depolarization-repolarization parameters (Table 3). In addition to reduction in QRS duration, the QTc interval reduced from baseline of 508.1 ± 48.6 ms to 441.1 ± 35.4 ms ($p < 0.0001$). Tpeak to Tend (Tp-Te) duration was reduced from 115.3 ±

JACC: CLINICAL ELECTROPHYSIOLOGY VOL. 7, NO. 9, 2021
SEPTEMBER 2021:1155–1165

TABLE 1 Individual Characteristics of Patients With LBBB-Induced Cardiomyopathy and LBBP

Patient #	Age (yrs)	Sex	LBBB Discovery	Time to LV Dysfunction	Time to LBBP	QRS Duration (ms)		LV Ejection Fraction (%)		
						LBBB	LBBP	Baseline	Pre-LBBP	Follow-Up
1	59	F	2016	2019	2020	183	110	55	29	60
2	41	F	2016	2018	2019	146	94	53	33	65
3	67	F	2015	2018	2019	165	110	55	35	60
4	50	F	2015	2019	2020	163	106	57	30	66
5	64	F	2017	2019	2020	163	108	52	34	57
6	55	F	2016	2018	2019	166	106	58	35	62
7	38	F	2018	2020	2020	174	98	54	38	54
8	46	F	2015	2018	2019	161	120	54	26	50
9	79	M	2000	2016	2019	175	126	50	40	60
10	79	M	2015	2017	2019	170	122	50	20	54
11	76	F	2008	2010	2018	176	86	52	20	54
12	87	M	2012	2018	2019	152	132	55	34	55
13	81	M	2012	2019	2019	188	118	52	22	54

LBBB = left bundle branch block; LBBP = left bundle branch pacing; LV = left ventricle.

5.1 ms to 74.7 ± 8.4 ms ($p < 0.0001$). Tp-Te/QTc ratio, a predictor of arrhythmic risk was significantly reduced from 0.22 ± 0.02 to 0.16 ± 0.01 ($p < 0.0001$). Significant T wave memory changes were noted post-LBBP, which resolved at approximately 6 weeks in all patients (Figure 5).

ECHOCARDIOGRAPHIC CHARACTERISTICS. In the study group, LVEF improved from 30.4 ± 6.6% at baseline to 57.4 ± 4.7% ($p < 0.0001$) with reduction in LV diastolic diameter from 55.7 ± 2.7 mm to 47.3 ± 3.4 mm ($p < 0.0001$). Serial echocardiography showed the natural history of response to resynchronization therapy by LBBP. LVEF improved from 30.4 ± 6.6% at baseline (n = 13) to 47.8 ± 6.8% at 1 month (n = 7), 57.4% ± 4% at 3 to 6 months (n = 13), and 62.3 ± 2.5% at 12 months (n = 8). All patients with LBBP had normalization of LV function between 3 and 6 months after implantation.

New York Heart Association functional class improved from baseline of 3.1 ± 0.3 to 1.2 ± 0.4 ($p < 0.0001$). The lead was deployed at a depth of 9.7 ± 0.4 mm inside the proximal septum. Worsening of tricuspid regurgitation was not observed in any of these patients during follow-up. There were no acute procedure-related complications. Diuretic medications were tapered during follow-up with the improvement in LV function. There were no episodes of lead-related complications, such as increase in pacing threshold, lead dislodgement, or thromboembolic complications noted during follow-up. No ventricular arrhythmias, deaths, or heart failure hospitalizations were observed during follow-up.

TABLE 2 Baseline Characteristics

Left bundle branch pacing	13
Age (yrs)	63.2 ± 16.4
Male: Female	4:9
Mean follow-up (months)	17.1 ± 10.9
Hypertension	8 (62)
Diabetes mellitus	5 (38)
Atrial fibrillation	0
Coronary artery disease	3 (23)
Baseline LV ejection fraction (%)	30.4 ± 6.6
Baseline QRS duration (ms)	167.2 ± 12.7
Medications (%)	
Beta-blocker	100
ACE inhibitor/ARB	100
Diuretics	77
Aldosterone antagonist	62

Values are n, mean ± SD, or n (%).
ACE = angiotensin-converting enzyme; ARB = angiotensin receptor blocker; LV = left ventricular.

DISCUSSION

The main findings of this study are as follows: 1) possible LIC was prevalent in 20% of the patients with cardiomyopathy and LBBB referred for CRT; 2) complete correction of LBBB by HBP may be a hallmark of proximal conduction disease in this group; 3) LBBP was associated with high degree of success in reversing LIC; 4) Lack of myocardial scarring/delayed gadolinium enhancement on cardiac MRI may be a clinical feature of LIC; and 5) LBBP was associated with significant improvement in both depolarization and repolarization parameters compared with baseline.

FIGURE 3 Cardiac MRI

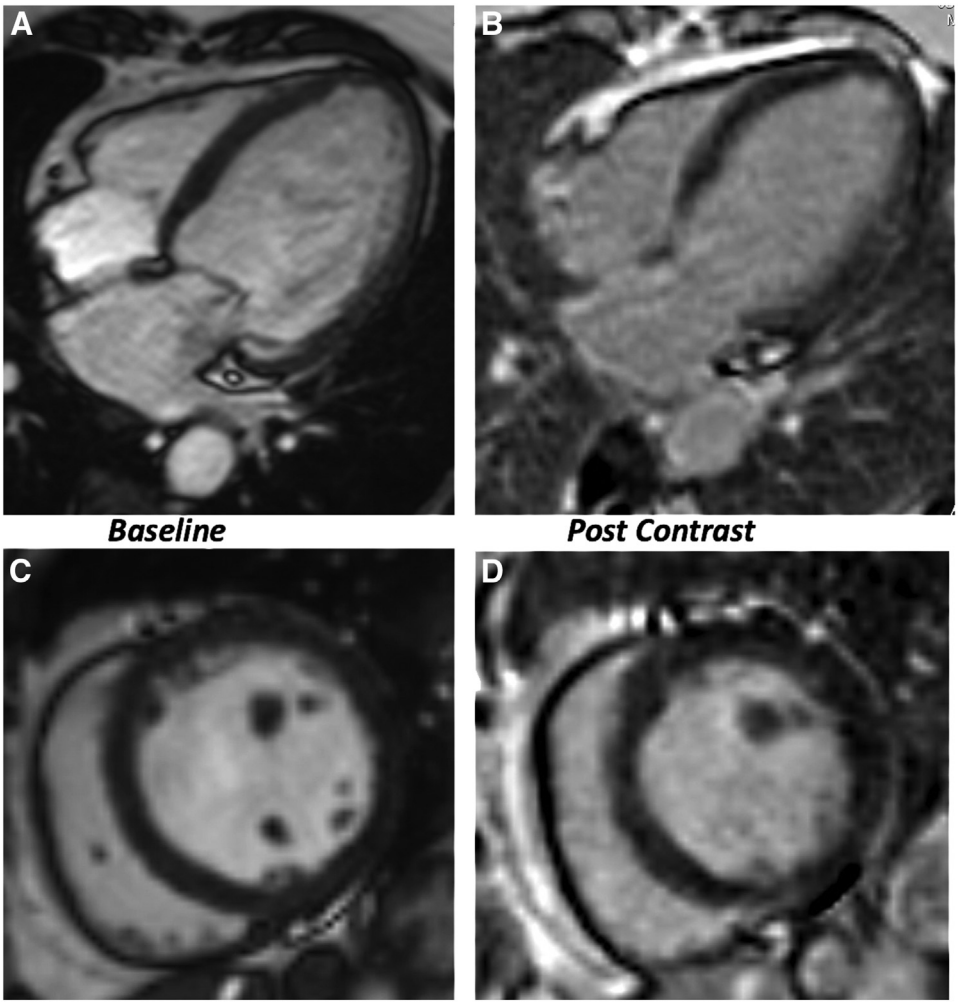

(A, B) Horizontal long and short axis views showing dilated left ventricle with preserved wall thickness. **(C, D)** Images taken after 20 minutes of contrast showing no evidence of scar, as demonstrated by lack of late gadolinium enhancement. MRI = magnetic resonance imaging.

In LBBB, the electrical activation of the LV is altered leading to delay and inhomogeneity in depolarization and repolarization. The resultant dyssynchronous contraction and relaxation may lead to LV dilatation and dysfunction and ultimately LIC and heart failure. Because the bundle branch block is the primary etiology, correction of LBBB by physiological pacing would result in electrical and mechanical synchrony and normalization of LV function. Vaillant et al (10), defined LIC as: 1) normal sinus rhythm and >5 years typical history of LBBB; 2) LVEF >50% at the time of diagnosis of LBBB; 3) Progressive decrease in EF to <40%; 4) LV end-diastolic diameter >55 mm; 5) presence of LV mechanical dyssynchrony; and 6) no other identifiable cause for cardiomyopathy. With these criteria they identified 8 patients (2%) from more than 375 CRT-eligible patients. Six of these 8 patients demonstrated hyperresponse to BVP. It is unclear why the 2 patients did not respond to BVP. It is possible that these patients presented late in the course of the disease wherein irreversible changes had occurred or cardiac resynchronization was incomplete in these patients. Singh et al (14) recently showed that HBP was effective in reversing LIC in 7 patients. LVEF improved from 25% to 50% during a mean follow-up of 14.5 months. HBP resulted in reduction in QRS duration from 152 ms to 115 ms. In our series, all patients demonstrated hyperresponse to LBBP with normalization of LV function. By pacing the proximal left bundle or its branches, LV

FIGURE 4 LBBB Correction During HBP

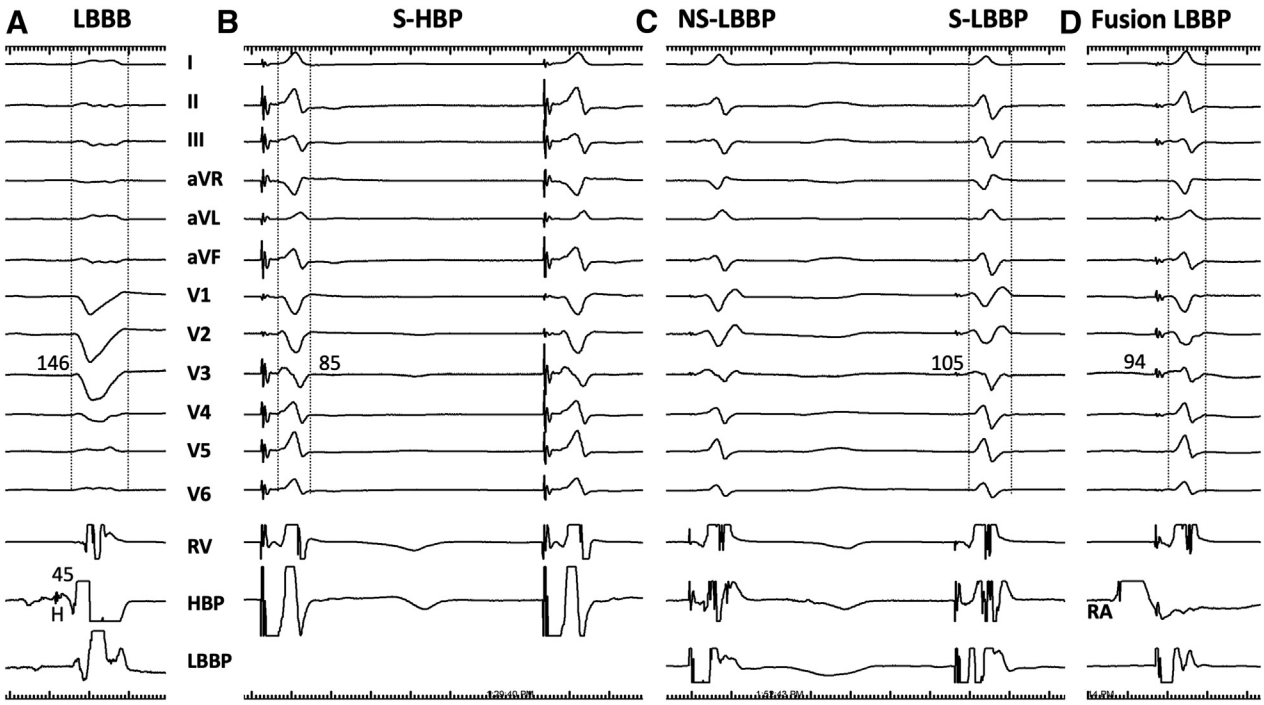

12-lead ECG and electrograms from right ventricle (RV), HBP, and left bundle branch pacing (LBBP) leads are shown at a sweep speed of 100 mm/s. **(A)** Baseline LBBB with QRS duration of 146 ms and HV interval of 45 ms is shown. **(B)** Pacing from the HBP lead results in selective (S) His capture with correction of LBBB and QRS narrowing to 86 ms. **(C)** During threshold testing from LBBP lead, transition from nonselective to selective capture is seen. During selective (S) LBBP, QRS duration is 106 ms. **(D)** During LBBP at optimized AV delay, QRS duration is further narrowed to 94 ms. LBBB = left bundle branch block; HBP = His bundle pacing.

dyssynchrony could be completely reversed, thus targeting the root cause of the underlying problem.

The NEOLITH study (11) showed that guideline-directed medical therapy did not significantly improve LVEF in new-onset LBBB-associated cardiomyopathy at 3 months. Most of these patients at the end of 3 months of medical therapy remained CRT candidates, and a high percentage (35%) were super-responders. Similar results were observed in the NEOLITH II study (12), in which patients who had undergone BVP within 9 months from the time of diagnosis of LBBB-associated cardiomyopathy had more favorable cardiac remodeling as compared with those who received it after 9 months. Delay in device implantation may miss a critical period to halt disease progression and reverse the progressive myocardial damage. It is likely that early intervention with conduction system pacing (HBP or LBBP) and normalization of conduction patterns may reverse the disease process.

In our study, among those patients who required CRT, 52.8% (84 of 159 patients) had complete LBBB with heart failure. LIC was the possible etiology of LV dilatation and LV dysfunction in 17 (20%) of 84 patients. LV dysfunction with heart failure was diagnosed at a mean duration of 4.2 years after the first diagnosis of LBBB. The incidence of LBBB in dilated cardiomyopathy is as high as 31% (25); however, the true incidence of LIC is unknown, as LBBB and

TABLE 3 Pacing, Echocardiographic, and ECG Characteristics

	Baseline	Follow-Up	p Value
Unipolar pacing threshold (V)	0.5 ± 0.2	0.6 ± 0.1	0.11
R-wave amplitude (mV)	11.7 ± 7.1	13.9 ± 7.5	0.44
Unipolar pacing impedance (ohms)	715.7 ± 124.7	530.6 ± 90.9	0.001
LV end diastolic (mm)	55.7 ± 2.7	47.3 ± 3.4	<0.0001
LV ejection fraction (%)	30.4 ± 6.6	57.4 ± 4.7	<0.0001
NYHA functional class	3.1 ± 0.3	1.2 ± 0.4	<0.0001
	Baseline	**Immediate**	**6 Weeks**	
QRS duration (ms)	167.2 ± 12.7	119.5 ± 8.6	110.4 ± 13.1	<0.0001
Tpeak-Tend duration (ms)	115.3 ± 5.1	81.5 ± 8	74.7 ± 8.4	<0.0001
QTc duration (ms)	508.1 ± 48.6	465.7 ± 27.8	441.1 ± 35.4	<0.0001
Tp-Te/QTc ratio	0.22 ± 0.02	0.17 ± 0.01	0.16 ± 0.01	<0.0001

Values are mean ± SD.
LV = left ventricle; NYHA = New York Heart Association.

FIGURE 5 T-Wave Memory After LBBP

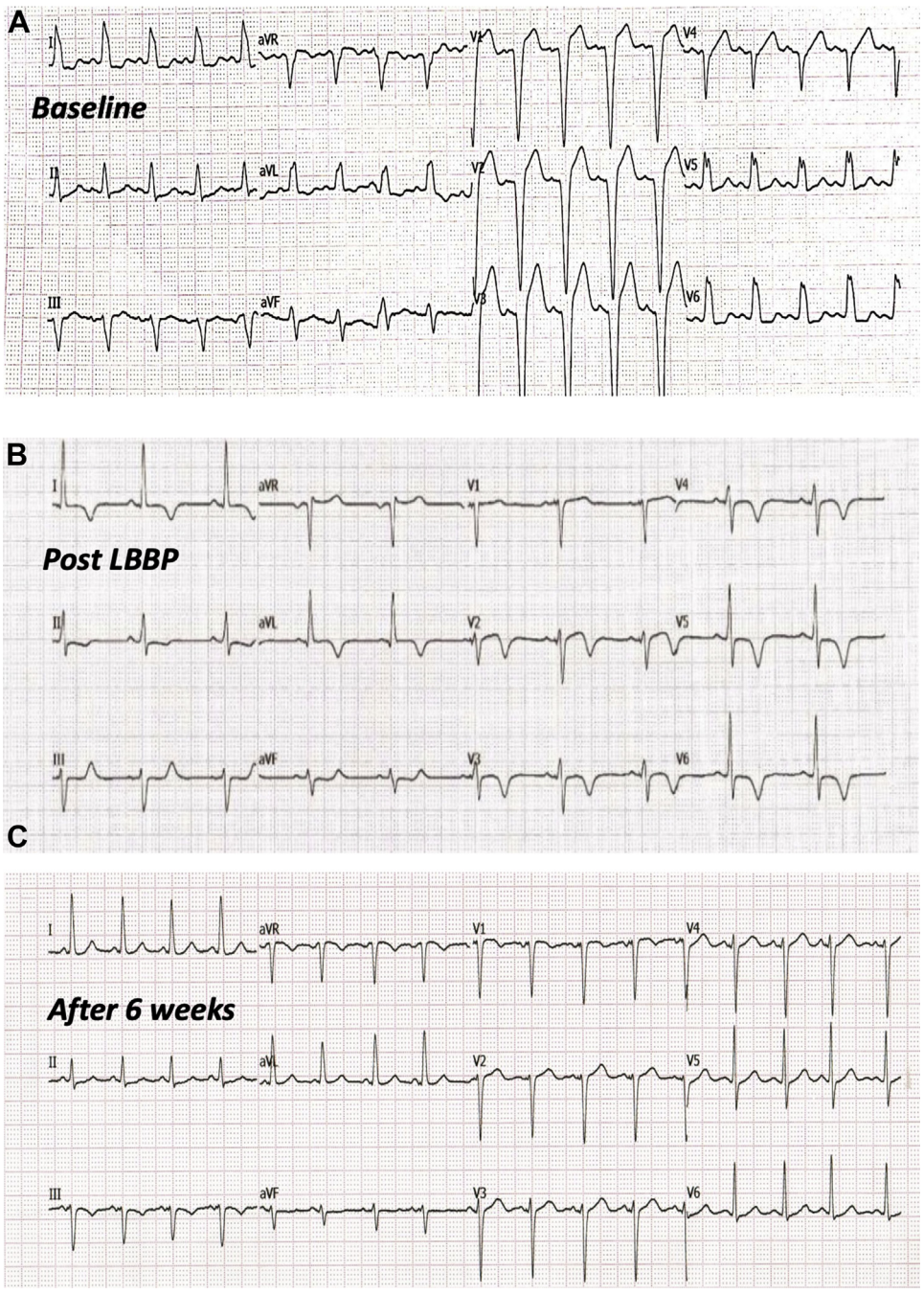

Baseline LBBB, T-wave memory changes during immediate post-LBBP, and T-wave normalization at 6 weeks is shown. Abbreviations as in Figure 1.

cardiomyopathy are identified for the first time during their initial presentation in many patients. Similarly, the true rate of development of cardiomyopathy in patients with LBBB and preserved LV function is also not clear. A recent retrospective review of 1,000 patients with LBBB identified 17% of patients (37 of 216 patients with preserved LV function and absence of coronary artery disease) who developed

JACC: CLINICAL ELECTROPHYSIOLOGY VOL. 7, NO. 9, 2021
SEPTEMBER 2021:1155–1165

dyssynchrony-induced cardiomyopathy during a mean follow-up of 55 ± 31 months (26).

Findings from our study provide additional characteristics defining LIC. Cardiac MRI demonstrated no evidence for myocardial scarring and/or delayed gadolinium enhancement in those studied. It is possible that even in patients with LIC, myocardial scarring may be identified late in the course of this disease. In addition, we demonstrated in this series that the conduction disease is primarily in the proximal conduction system and correction of LBBB by HBP may be a necessary criterion for LIC.

Pacing parameters remained stable with consistent LBB capture during follow-up. In addition to reduction in QRS duration and normalized ventricular depolarization, LBBP was associated with immediate reduction in Tp-Te duration and corrected QT interval compared with baseline followed by further reduction after resolution of memory T-waves. Tp-Te/QTc ratio, a better marker of arrhythmogenesis was reduced from 0.22 ± 0.02 to 0.17 ± 0.01 immediately after LBBP and to 0.16 ± 0.01 after 6 weeks conferring potential additional benefit of reduction in arrhythmic risk. T-wave memory changes were observed in all patients immediately following LBBP, which resolved at 6 weeks.

Complete normalization of LV function with significant reduction in LV end-diastolic dimensions was observed in all patients, between 3 and 6 months after implantation. Eight patients received dual chamber pacemaker only without a defibrillator. In the absence of myocardial scarring and normalization of repolarization abnormalities, His-Purkinje conduction system pacing may obviate the need for defibrillator therapy. No ventricular arrhythmias, sudden death, or heart failure hospitalizations were observed in this entire cohort of patients during a mean follow-up of 12 months. Prospective, randomized studies with longer term follow-up are necessary to confirm the above hypothesis in this select group of patients who meet the extended criteria.

LBBP provides a wider target compared with HBP to correct LBBB with low and stable capture thresholds and has emerged as an attractive alternative to achieve CRT. Vijayaraman et al (16) showed the feasibility, safety, and efficacy of LBBP as an alternative form of CRT in 325 patients with 85% procedural success rate. LBBP resulted in significant reduction in QRS duration from 152 ± 32 ms to 137 ± 22 ms ($p < 0.01$) with improvement in LVEF from 33 ± 10% to 44 ± 11% ($p < 0.01$). LBBB was a strong predictor of clinical and echocardiographic response to LBBP. Huang et al (17) in a prospective, multicenter study showed 97% success rate (61 of 63 patients) for LBBP in patients with LBBB and nonischemic cardiomyopathy requiring CRT. LVEF significantly improved from 33 ± 8% to 55 ± 10%. LVEF had normalized in 75% of patients at 1 year.

It is important to recognize LBBB as the main contributing factor for cardiomyopathy. Progressive decline in LV function since the time of diagnosis of LBBB, preserved LV myocardial thickness with dyssynchronous contraction, absence of significant coronary artery stenosis, absence of late gadolinium enhancement in cardiac MRI and correction of LBBB by HBP would help in diagnosing LIC. With the advent of physiological pacing wherein complete correction of LBBB is possible, earlier device implantation for symptomatic patients with even mild LV dysfunction may prevent development of severe cardiomyopathy.

STUDY LIMITATIONS. This was a retrospective observational study from 2 centers with significant experience in conduction system pacing. Although the number of patients with LIC in our cohort was small, this represents the largest such series of patients. The long-term safety and extractability of LBBP leads are still not known and need to be carefully studied before widespread adoption of this approach. Last, the overall incidence of LIC may be underestimated in our series due to lack of ECG data in preceding years in patients presenting with LBBB and cardiomyopathy.

CONCLUSIONS

LBBP is a reasonable strategy of conduction system pacing in patients with LIC, as it provides low and stable capture thresholds with complete correction of underlying conduction system disease. LBBP is associated with normalization of LV function and improvement in depolarization/repolarization abnormalities related to LBBB.

FUNDING SUPPORT AND AUTHOR DISCLOSURES

Dr Ponnusamy has been a consultant for Medtronic. Dr Vijayaraman has been a speaker and consultant, and has received research and fellowship support from Medtronic; has been a consultant for Abbott, Biotronik, and Boston Scientific; and has received a patent for the HBP delivery tool.

ADDRESS FOR CORRESPONDENCE: Dr Pugazhendhi Vijayaraman, Cardiac Electrophysiology, Geisinger Heart Institute, MC 36-10, 1000 East Mountain Boulevard, Wilkes-Barre, Pennsylvania 18711, USA. E-mail: pvijayaraman1@geisinger.edu OR pvijayaraman@gmail.com.

PERSPECTIVES

COMPETENCY IN MEDICAL KNOWLEDGE: LIC is associated with hyperresponse to CRT. Permanent LBBP is a novel approach to CRT. LBBP can reverse electrical and mechanical dyssynchrony induced by LBBB.

TRANSLATIONAL OUTLOOK: LBBP may provide a reasonable alternative to traditional biventricular pacing in patients with LIC. Randomized controlled clinical trials are necessary to confirm the clinical benefits of permanent LBBP compared with biventricular pacing in patients with LIC.

REFERENCES

1. Elliott P, Andersson B, Arbustini E, et al. Classification of the cardiomyopathies: a position statement from the European Society Of Cardiology Working Group on Myocardial and Pericardial Diseases. *Eur Heart J*. 2008;29:270–276.

2. Hiss RG, Lamb LE. Electrocardiographic findings in 122,043 individuals. *Circulation*. 1962;25:947–961.

3. Ostrander LD Jr., Brandt RL, Kjelsberg MO, Epstein FH. Electrocardiographic findings among the adult population of a Total natural community, Tecumseh, Michigan. *Circulation*. 1965;31:888–898.

4. Siegman-Igra Y, Yahini JH, Goldbourt U, Neufeld HN. Intraventricular conduction disturbances: a review of prevalence, etiology, and progression for ten years within a stable population of Israeli adult males. *Am Heart J*. 1978;96:669–679.

5. Rotman M, Triebwasser JH. A clinical and follow-up study of right and left bundle branch block. *Circulation*. 1975;51:477–484.

6. Zhang ZM, Rautaharju PM, Soliman EZ, et al. Mortality risk associated with bundle branch blocks and related repolarization abnormalities (from the Women's Health Initiative [WHI]). *Am J Cardiol*. 2012;110:1489–1495.

7. Eriksson P, Wilhelmsen L, Rosengren A. Bundle-branch block in middle-aged men: risk of complications and death over 28 years. The primary prevention study in Goteborg, Sweden. *Eur Heart J*. 2005;26:2300–2306.

8. Blanc JJ, Fatemi M, Bertault V, Baraket F, Etienne Y. Evaluation of left bundle branch block as a reversible cause of non-ischaemic dilated cardiomyopathy with severe heart failure. A new concept of left ventricular dyssynchrony-induced cardiomyopathy. *Europace*. 2005;7:604–610.

9. Castellant P, Fatemi M, Orhan E, Etienne Y, Blanc JJ. Patients with non-ischaemic dilated cardiomyopathy and hyper-responders to cardiac resynchronization therapy: characteristics and long-term evolution. *Europace*. 2009;11:350–355.

10. Vaillant C, Martins RP, Donal E, et al. Resolution of left bundle branch block induced cardiomyopathy by cardiac resynchronization therapy. *J Am Coll Cardiol*. 2013;61:1089–1095.

11. Wang NC, Singh M, Adelstein EC, et al. New-onset left bundle branch block associated idiopathic nonischemic cardiomyopathy and left ventricular ejection fraction response to guideline-directed therapies: the NEOLITH study. *Heart Rhythm*. 2016;13:933–942.

12. Wang NC, Li JZ, Adelstein EC, et al. New-onset left bundle branch block associated idiopathic nonischemic cardiomyopathy and time from diagnosis to cardiac resynchronization therapy: the NEOLITH II study. *Pacing Clin Electrophysiol*. 2018;41:143–154.

13. Strauss DG, Selvester RH, Wagner GS. Defining left bundle branch block in the era of cardiac resynchronization therapy. *Am J Cardiol*. 2011;107:927–934.

14. Singh R, Devabhatkuni S, Ezzeddine F, Simon J, Khaira K, Dandamudi G. His bundle pacing: a novel treatment for left bundle branch block mediated cardiomyopathy. *J Cardiovasc Electrophysiol*. 2020;31:2730–2736.

15. Upadhyay GA, Vijayaraman P, Nayak HM, et al. On-treatment comparison between corrective His bundle pacing and biventricular pacing for cardiac resynchronization: a secondary analysis of the His-SYNC pilot trial. *Heart Rhythm*. 2019;16:1797–1807.

16. Vijayaraman P, Ponnusamy SS, Cano O, et al. Left bundle branch area pacing for cardiac resynchronization therapy: results from international LBBAP collaborative study group. *J Am Coll Cardiol EP*. 2021;7:135–147.

17. Huang W, Wu S, Vijayaraman P, et al. Cardiac resynchronization therapy in patients with non-ischemic cardiomyopathy utilizing left bundle branch pacing. *J Am Coll Cardiol EP*. 2020;6:849–858.

18. Cleland JG, Daubert JC, Erdmann E, et al. The effect of cardiac resynchronization on morbidity and mortality in heart failure. *N Engl J Med*. 2005;352:1539–1549.

19. Pitzalis MV, Iacoviello M, Romito R, et al. Cardiac resynchronization therapy tailored by echocardiographic evaluation of ventricular asynchrony. *J Am Coll Cardiol*. 2002;40:1615–1622.

20. Pitzalis MV, Iacoviello M, Romito R, et al. Ventricular asynchrony predicts a better outcome in patients with chronic heart failure receiving cardiac resynchronization therapy. *J Am Coll Cardiol*. 2005;45:65–69.

21. Richardson M, Freemantle N, Calvert MJ, Cleland JGF, Tavazzi L. Predictors and treatment response with cardiac resynchronization therapy in patients with heart failure characterized by dyssynchrony: a pre-defined analysis from the CARE-HF trial. *Eur Heart J*. 2007;28:1827–1834.

22. Huang W, Chen X, Su L, Wu S, Xia X, Vijayaraman P. A beginner's guide to permanent left bundle branch pacing. *Heart Rhythm*. 2019;16:1791–1796.

23. Ponnusamy SS, Arora V, Namboodiri N, Kumar V, Kapoor A, Vijayaraman P. Left bundle branch pacing: a comprehensive review. *J Cardiovasc Electrophysiol*. 2020;31:2462–2473.

24. Bazett HC. Analysis of the time relations of electrocardiograms. *Heart*. 1920;7:353–370.

25. Aleksova A, Carriere C, Zecchin M, et al. New-onset left bundle branch block independently predicts long-term mortality in patients with idiopathic dilated cardiomyopathy: data from the Trieste Heart Muscle Disease Registry. *Europace*. 2014;16:1450–1459.

26. Sharma S, Barot HV, Schwartzman AD, et al. Risk and predictors of dyssynchrony cardiomyopathy in left bundle branch block with preserved left ventricular ejection fraction. *Clin Cardiol*. 2020;43:1494–1500.

KEY WORDS cardiac resynchronization therapy, heart failure, LBBB-induced cardiomyopathy, left bundle branch block, left bundle branch pacing

Circulation: Arrhythmia and Electrophysiology

RESEARCH LETTER

Template Beat

A Novel Marker for Left Bundle Branch Capture During Physiological Pacing

Shunmuga Sundaram Ponnusamy, MD; Vithiya Ganesan, MD; Thabish Syed, MD; Suryakumar Balasubramanian, MBBS; Pugazhendhi Vijayaraman, MD

Physiological pacing has witnessed a revolutionary growth in the last decade. Left bundle branch (LBB) pacing (LBBP), where direct capture of the proximal main left bundle could be achieved at low capture threshold, has overcome the limitations of His bundle pacing.[1,2] The criteria for confirming the capture of the LBB had been defined but never validated.[3] We had recently proposed a novel method of performing LBBP by observing the premature ventricular complexes (PVCs) generated during lead deployment.[4] A PVC with right bundle branch delay morphology (qR/rSR in lead V_1) with a QRS duration of <130 ms would be generated as the lead reaches the LBB area. We labeled this PVC as template beat as it mimicked the LBB paced QRS morphology (Figure [A]). Further rotations would be avoided if a template beat was noted during rapid lead deployment. We aimed at analyzing the incidence of template beat as a marker of LBB capture during LBBP and its clinical significance.

This was a prospective observational study that included 90 consecutive patients who had undergone successful LBBP using C315-sheath and 3830 Selectsecure lead (Medtronic, Minneapolis). The study was approved by the institutional review board, and patients gave informed consent. Continuous rapid rotations were given to deploy the lead in the proximal septum until a template beat was obtained. If there were no PVCs during lead deployment, the final placement was decided on paced QRS morphology, unipolar pacing impedance, and peak left ventricular activation time. The data that support the findings of the study are available from the corresponding author upon reasonable request.

The study population was divided into 2 groups based on the occurrence of template beat during lead deployment: group I with template beat (n=53; 59%) and group II without template beat (n=37; 41%). Female patients had higher incidence (67%) of template beat. There was no difference in septal thickness, basal QRS duration, and ejection fraction in both groups. The lead depth inside the septum was 10.3±2.1 mm in group I and 10.5±2.1 mm in group II (*P*=0.67). Both the groups demonstrated capture of LBB. No patients in group I developed septal perforation during implantation, but 8 patients in group II had perforation (0% versus 21.6%; *P*=0.004). The final LBB paced QRS morphology mimicked the template beat in group I (Figure [A–C]).

The fluoroscopy time for LBBP lead deployment and total fluoroscopy time were significantly less in group I as compared with group II (14.5±7.8 versus 20.4±14.2 minutes, *P*=0.04, and 19.7±9.9 versus 26.3±16.6 minutes, *P*=0.02). Only rapid lead deployment generated template beat as opposed to slow gradual deployment with impedance and paced QRS morphology monitoring after each set of rotations. Cardiac magnetic resonance imaging was not done in all patients, which could have documented late gadolinium enhancement as one of the reasons for slow progression of lead movement inside the septum. Template beats showed right bundle branch delay pattern with a mean QRS duration of 121.1±3.7 ms. If the rotations were interrupted for some reason with narrow QS pattern as last generated PVC, additional turns were given till template beat was observed (Figure [C]).

Paced QRS duration after correction of right bundle branch delay by atrioventricular interval optimization was significantly less in group I as compared with group II (108.9±8.3 versus 116.1±13.3 ms; *P*=0.002).

Key Words: bundle of His ■ heart conduction system ■ incidence ■ physiology ■ ventricular premature complexes

Correspondence to: Shunmuga Sundaram Ponnusamy, MD, DM, PDF, CEPS, Department of Cardiology, Velammal Village, Velammal Medical College Hospital and Research Institute, Madurai 625009, Tamilnadu, India. Email shunmuga.pgi@gmail.com

For Sources of Funding and Disclosures, see page 450.

Circulation: Arrhythmia and Electrophysiology is available at www.ahajournals.org/journal/circep

There was a trend toward better Tpeak-Tend/QTc ratio (0.18±0.03 versus 0.19±0.02; *P*=0.08) and peak left ventricular activation time (68.3±13.8 versus 73.6±13.1 ms; *P*=0.07) in group I. Peak cTnI (cardiac troponin-I) measured after the procedure was significantly higher in group II as compared with group I (232.9±373.5 versus 123.1±106.1 pg/mL; *P*=0.04 [independent samples *t* test]), indicating less myocardial injury in patients who had undergone PVC-guided lead deployment.

The main findings of our study were (1) template beat with right bundle branch delay pattern was observed in 58% of patients and can be considered as marker of LBB capture; (2) predicts less fluoroscopy time, narrow paced QRS duration, and shorter peak left ventricular activation time; (3) template beat–guided lead deployment would confer minimal myocardial injury and avoid septal perforation during lead deployment.

It may be difficult to confirm conduction system capture based on the published criteria in some patients. PVC (template beat)-guided lead deployment can help as it confirms the capture of LBB. Template beats are generated from the Purkinje fibers due to mechanical trauma induced by the pacing lead as it moves rapidly into the LBB area.[4] In the presence of scar, rapid penetration of the septum may not be possible and template beats would not be seen. This might result in repeated attempts in lead positioning and increase in cTnI release from myocardium. Avoiding further rotations once the template beats are observed would prevent further progression of lead into the septum, resulting in perforation.

LBBP is emerging as an alternative to His bundle pacing. Template beat–guided lead placement would help in safe positioning of the lead in the LBB area, avoiding septal perforation, and minimizing the myocardial damage. Further studies are required to validate this novel technique as a criterion for LBB capture.

ARTICLE INFORMATION

Affiliations

Departments of Cardiology (S.S.P., T.S., S.B.) and Microbiology (V.G.), Velammal Medical College, Madurai, Tamil Nadu, India. Department of Cardiology, Geisinger Heart Institute, Wilkes Barre, PA (P.V.).

Sources of Funding

None.

Disclosures

Dr Ponnusamy has received honoraria from Medtronic. Dr Vijayaraman has received honoraria, consulting fees, and research support form Medtronic and consulting fees from Boston Scientific, Abbott, Biotronik, and Eaglepoint. The other authors report no conflicts.

REFERENCES

1. Huang W, Chen X, Su L, Wu S, Xia X, Vijayaraman P. A beginner's guide to permanent left bundle branch pacing. *Heart Rhythm*. 2019;16:1791–1796. doi: 10.1016/j.hrthm.2019.06.016
2. Ponnusamy SS, Arora V, Namboodiri N, Kumar V, Kapoor A, Vijayaraman P. Left bundle branch pacing: a comprehensive review. *J Cardiovasc Electrophysiol*. 2020;31:2462–2473. doi: 10.1111/jce.14681
3. Vijayaraman P, Ponnusamy S, Cano Ó, Sharma PS, Naperkowski A, Subsposh FA, Moskal P, Bednarek A, Dal Forno AR, Young W, et al. Left bundle branch area pacing for cardiac resynchronization therapy: results from the International LBBAP Collaborative Study Group. *JACC Clin Electrophysiol*. 2021;7:135–147. doi: 10.1016/j.jacep.2020.08.015
4. Ponnusamy SS, Vijayaraman P. Left bundle branch pacing guided by premature ventricular complexes during implant. *HeartRhythm Case Rep*. 2020;6:850–853. doi: 10.1016/j.hrcr.2020.08.010

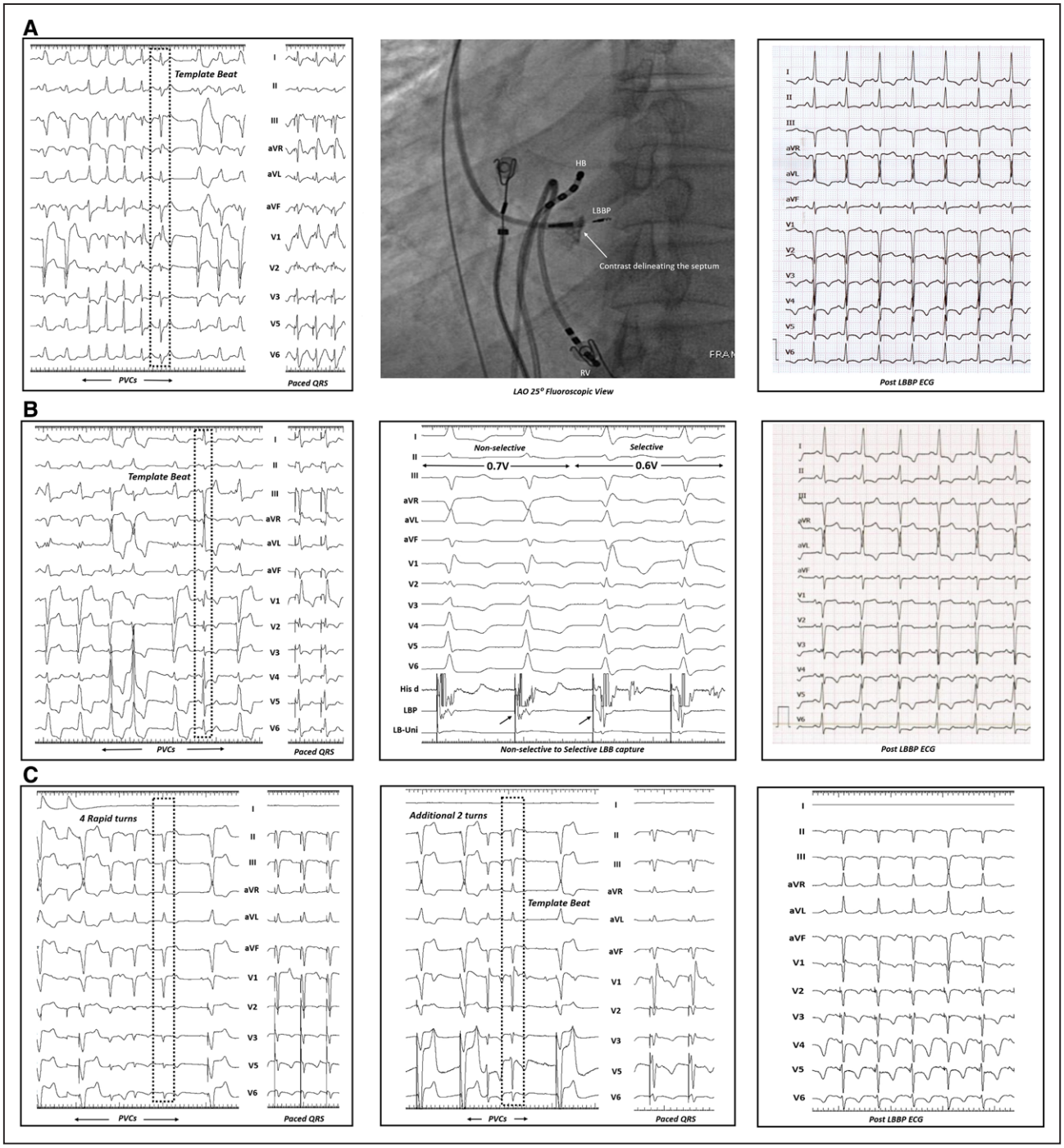

Figure. Template beat–guided left bundle branch pacing (LBBP).
A, Left bundle branch block (LBBB) correction by LBBP. Rapid deployment resulted in premature ventricular complexes (PVCs) with changing morphology until a template beat is obtained. Final paced QRS duration was 98 ms after right bundle branch delay correction by atrioventricular delay optimization. **B**, Template beat–guided LBBP in a patient with LBBB with left ventricular dysfunction. Nonselective to selective capture transition could be demonstrated at near threshold output, and final paced QRS duration was 100 ms. **C**, Template beat–guided LBBP in a patient with complete heart block. Initial 4 rapid turns resulted in QS pattern PVCs, which mimicked the paced QRS morphology at the site. Few more turns were given till the appearance of template beat, which matched the final paced QRS morphology. Final paced QRS duration was 110 ms with T-wave memory. HB indicates His bundle; LAO, left anterior-oblique; LBB, left bundle branch; and RV, right ventricle.

Journal of Interventional Cardiac Electrophysiology
https://doi.org/10.1007/s10840-020-00807-w

Mid-term feasibility, safety and outcomes of left bundle branch pacing–single center experience

Shunmuga Sundaram Ponnusamy[1] · Giridhar Muthu[1] · Mahesh Kumar[1] · Dasarath Bopanna[1] · Vijesh Anand[1] · Surya Kumar[1]

Received: 28 April 2020 / Accepted: 22 June 2020

Abstract

Background His bundle pacing (HBP) has evolved as the most physiological form of pacing but associated with limitations. Recently, left bundle branch pacing (LBBP) is emerging as an effective alternative strategy for HBP.

Objectives Our study was designed to assess the feasibility, efficacy, electrophysiological parameters, and mid-term outcomes of LBBP in Indian population.

Methods All patients requiring permanent pacemaker implantation for symptomatic bradycardia and heart failure were prospectively enrolled. Echocardiography, QRS duration, pacing parameters, left bundle (LB) potentials, paced QRS duration, and peak left ventricular activation time (pLVAT) were recorded.

Results LBBP was successful in 93 out of 99 patients (94% acute success). Mean age was 62.6 ± 13 years, male 59%, diabetes 69%, and coronary artery disease 65%. Follow-up duration was 4.8 months (range1–12 months). Indication for pacing included atrioventricular (AV) block 43%, cardiac resynchronization therapy 44%, and AV node ablation 4%. LB potential was noted in 37 patients (40%). QRS duration reduced from 144.38 ± 34.6 at baseline to 110.8 ± 12.4 ms after LBBP ($p < 0.0001$). Pacing threshold was 0.59 ± 0.22 V and sensed R wave 14.14 ± 7.19 mV, and it remained stable during follow-up. Lead depth in the septum was 9.62 mm. LV ejection fraction increased from 44.96 to 53.3% after LBBP ($p < 0.0001$). One died due to respiratory tract infection on follow up.

Conclusion LBBP is a safe and effective strategy (94% acute success) of physiological pacing. The pacing parameters remained stable over a period of 12 months follow-up. LBBP can effectively overcome the limitations of HBP.

Keywords Physiological pacing · Left bundle pacing · AV block · Heart failure · Left ventricular activation time

Highlights of the study

1. Data for left bundle branch pacing for south Asian population is unknown.
2. LBB pacing was successful in 94% of pacing indicated Indian population (93 out of 99 patients).
3. Low and stable threshold remained constant throughout the study period.
4. AV block was the indication in 43% ($n = 40$) and Sinus node dysfunction in 9% ($n = 8$). LBBP was successful in 91% of patients with AV block (40 out of 44 attempted patients).
5. Effective reduction in QRS duration from 144 before pacing to 110 ms after LBB pacing though QRS reduction alone may not confer clinical benefit.
6. Significant improvement in LV ejection fraction from 44 to 53% along with non-significant reduction in LV end-diastolic diameter (53.1 to 51.1 mm).
7. Cardiac resynchronization therapy could be achieved in 41 out of 43 attempted patients resulting in significant reduction in QRS duration and improvement in LV ejection fraction.

✉ Shunmuga Sundaram Ponnusamy
shunmuga.pgi@gmail.com

[1] Department of Cardiology, Velammal Medical College Hospital and Research Institute, Velammal Village, Airport ring road, Madurai, Tamilnadu 625009, India

1 Introduction

For decades, right ventricle (RV) is considered the standard pacing site for the management of symptomatic bradyarrhythmias. But long-term right ventricular apical pacing is associated with increased risk of electrical and mechanical dyssynchrony resulting in atrial fibrillation and heart failure [1–4]. His bundle pacing (HBP) is considered the most physiological form of pacing [5]. Since normal cardiac conduction system is captured, incidence of heart failure, atrial arrhythmias, and pacing induced cardiomyopathy will be significantly reduced [6]. In 2000, Deshmukh et al. showed clinical improvement in a series of 12 patients with heart failure by permanent HBP [7]. The American College of Cardiology/American Heart Association (ACC/AHA) guidelines recommend HBP as class IIa indication for AV block with ejection fraction between 35 and 50% and class IIb indication in patients with AV block at the level of AV node [8].

Published online: 04 July 2020

His bundle pacing can be considered for patients with symptomatic bradycardia due to sinus node dysfunction, AV node, or His bundle disease [9–13]. Recent studies have shown HBP as an effective alternative to cardiac resynchronization therapy for correcting bundle branch blocks in patients with left ventricular (LV) dysfunction and heart failure [14–17]. But there are several factors which limit its widespread adoption [18]. These include longer learning curve, higher capture thresholds, and risk of lead dislodgement. [19–21] Huang et al. demonstrated the feasibility of pacing the left bundle branch by right ventricular approach in patients with LBBB and heart failure [22, 23]. Subsequently, many studies demonstrated the safety and efficacy of left bundle branch pacing [24–28].

Though many studies are available on left bundle branch pacing, there is paucity of data from India. The aim of our study is to assess the feasibility, efficacy, electrophysiological parameters, and mid-term outcomes of left bundle branch pacing (LBBP).

2 Material and methods

This is a prospective, single-center, observational study, conducted in our center from March 2019 to March 2020. The study was conducted after getting approval from our institutional ethical committee. All patients provided written informed consent. Pregnant patients, age less than 10 years and those who were not willing for the study, were excluded from the study.

2.1 Inclusion criteria

All consecutive patients requiring permanent pacemaker implantation for symptomatic bradyarrhythmias were included in the study. An option of physiological pacing was discussed for patients with dilated cardiomyopathy with wide QRS (duration more than 150 ms) and LV ejection fraction ≤ 35%. Patients with pacing induced cardiomyopathy, and those patients who had refractory atrial fibrillation with fast ventricular rate planned for AV node ablation with pacing were also included. Informed consent was obtained before the procedure from the patients who required cardiac resynchronization therapy and had undergone left bundle pacing, regarding the safety, benefits, and long-term concerns of left bundle pacing.

2.2 Procedural techniques

After obtaining informed consent, the procedure was done under local anesthesia. Twelve lead electrocardiography and intracardiac electrograms were continuously recorded in an electrophysiology recording (EP) system (Workmate Claris, Abbott, MN). Right ventricular (RV) back up pacing was used for patients with complete heart block (CHB) and left bundle branch block (LBBB). After obtaining extrathoracic left subclavian venous puncture, C315 HIS sheath and lumen less 3830 SelectSecure^{tm} lead (Medtronic, Minneapolis, MN) were used for LBBP. Deep septal placement of the lead was done 1–1.5 cm below the His bundle along an imaginary line connecting distal His signals to RV apex where pacing would show "W" pattern (Fig. 1A, Video 1). The paced QRS morphology, unipolar lead impedance, and unipolar electrograms were continuously monitored during lead placement. The impedance would rise gradually as the lead moves deep into the septum followed by a small drop as it reaches the left ventricular sub-endocardium (Fig. 2). In patients without LBBB or CHB, left bundle (LB) potential could be demonstrated. (Fig. 4). Sheath angiography was done in LAO 30^0 fluoroscopic view to show the depth of lead into the septum (Fig. 1b, Video 2). The criteria for confirming LB capture have not been validated so far. We have defined the capture of LB [29] as (a) paced QRS morphology of right bundle branch delay (qR in lead V1), (b) abrupt shortening of LVAT (as measured in lead V5 from the onset of pacing spike to peak of R wave), by increasing voltage output or short and constant LVAT at high- and low-output pacing, (c) presence of LB potential, (d) demonstration of non-selective to selective LB capture, and (e) programmed stimulation from the pacing lead to demonstrate change in QRS morphology and duration [30]. We confirmed LB capture as presence of qR pattern in lead V1 along with any one of above-mentioned parameters [24,34].

2.3 Programming

PG programming was done based on the native AV nodal conduction and duration between LB potential—surface QRS. In patients with sinus node dysfunction, long AV delay was kept to allow the native conduction. In patients with complete heart block, sensed AV delay of 80-100 ms was kept. In patients with bundle branch block and LV dysfunction, the AV delay was adjusted based on surface ECG and echocardiography to get native fusion.

2.4 Data collection

Patients' baseline parameters and pacing indications were documented. Electrocardiographic parameters like QRS duration, morphology, and type of bundle branch block were recorded. Pacing thresholds, impedance, R wave amplitude, paced QRS duration (from onset to end, Fig. 3c), presence of LB potentials (Fig. 3a), and LB potential to surface QRS interval were measured. The peak LV activation time (pLVAT) (pacing artifact to peak of R wave) duration was measured in lead V5 (Fig. 3b). Similarly, lead parameters and echocardiographic parameters were obtained during follow-up.

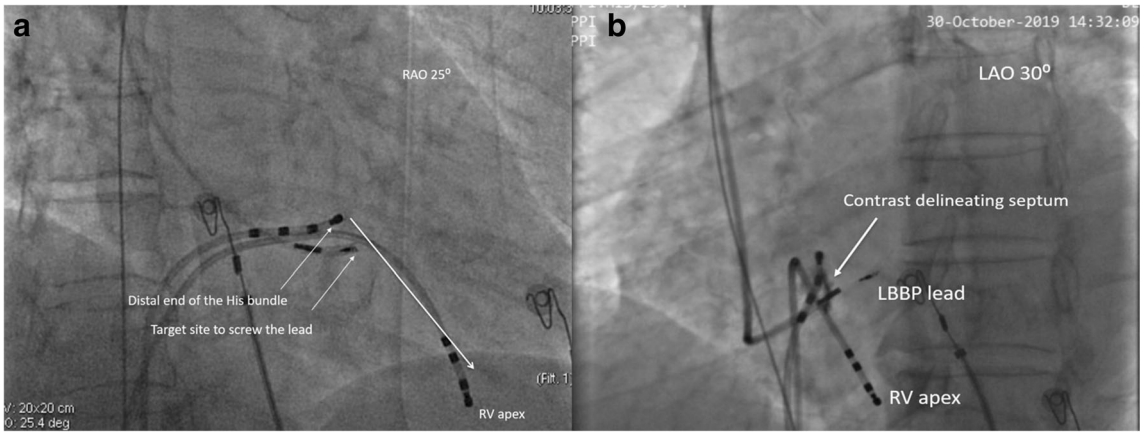

Fig. 1 Fluoroscopic view during left bundle branch pacing. **a** RAO 25^0 view showing the position of the lead before screwing. The pacing lead is kept 1 cm below the distal end of the His bundle signals along the imaginary line drawn toward RV apex (white arrow). **b** LAO 30^0 view showing the final lead position with almost half of the anodal ring inside the septum. Note the contrast delineating the septum (white arrow)

2.5 Echocardiographic parameters

Baseline echocardiographic parameters were documented. Septal thickness was measured in both parasternal short axis and apical four chamber view as it determines the depth of lead penetration for LBBP (Fig. 4). LV ejection fraction was measured by modified Simpson's method. The severity of tricuspid regurgitation post lead implantation was compared with the baseline. Serial echocardiography was done during follow-up of patients for whom pacing was done for bundle branch block correction.

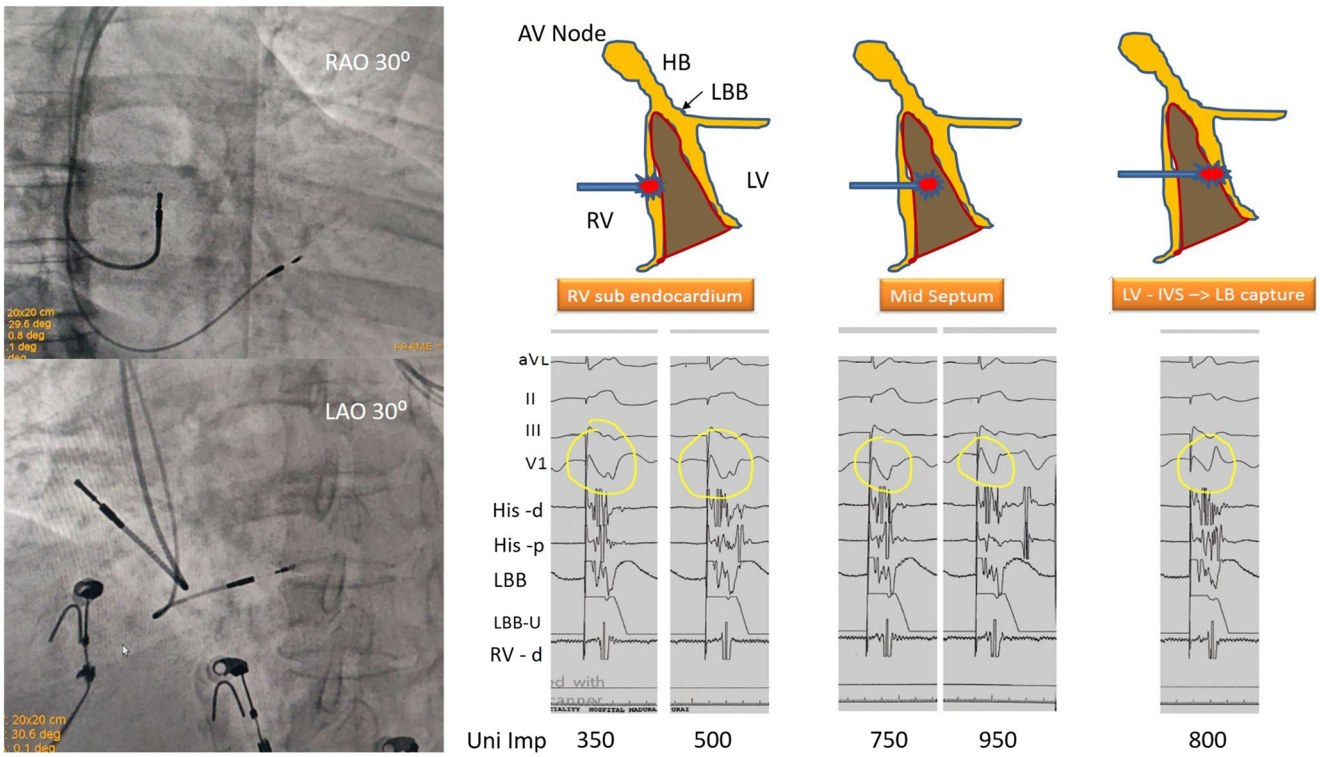

Fig. 2 Fluoroscopic view and characteristic change in QRS morphology and unipolar pacing impedance during left bundle branch pacing. On the left, final fluoroscopic position of the pacing lead in Right anterior oblique (RAO) 30^0 and LAO 30^0 view. On the right, progressive change in paced QRS morphology and duration during deep septal placement of the lead. Note in lead V1, the notch gradually ascended up to form an R wave as the lead reaches the left bundle branch area. His d, distal His electrogram from the quadripolar catheter; His p, proximal His electrogram; LBB, 3830 pacing lead electrogram. LBB-U, unipolar electrogram of 3830 pacing lead; RV d, distal RV electrogram from the quadripolar catheter; Uni Imp, unipolar lead impedance in Ohms

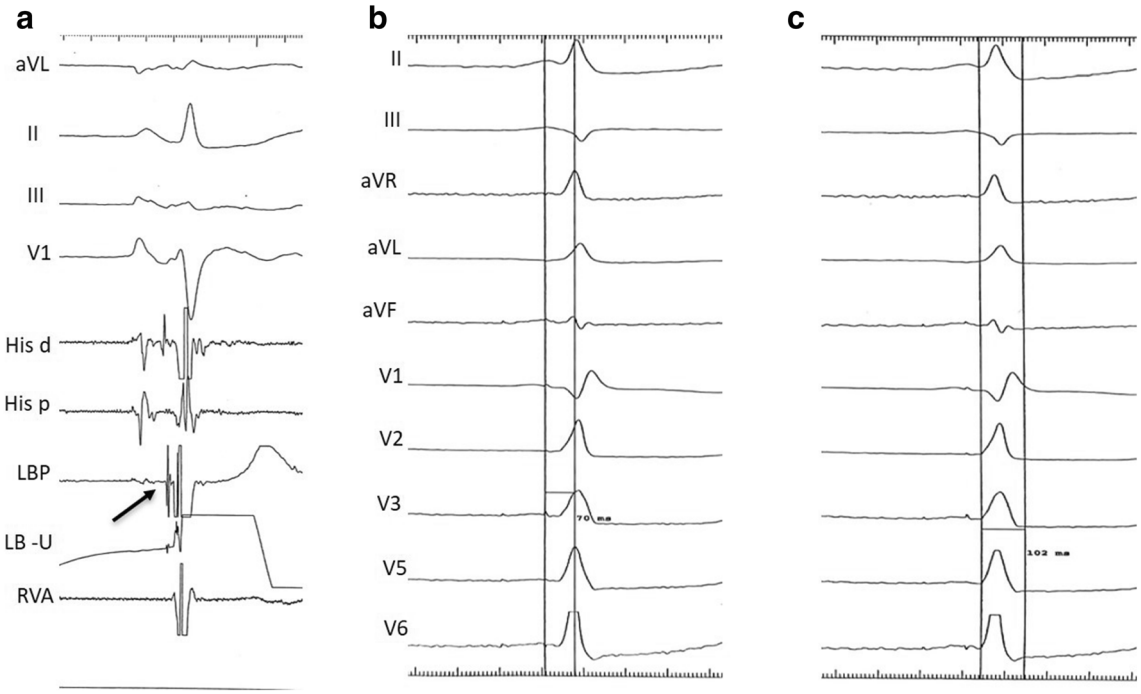

Fig. 3 **a** Intracardiac electrogram showing His bundle potential on His distal quadripolar electrodes and sharp left bundle potential (black arrow) preceding local ventricular electrogram. **b** and **c** 12 lead ECG showing the measurement of peak left ventricular activation time (70 ms) and paced QRS duration (102 ms). His p, proximal His electrogram; LBB, 3830 pacing lead electrogram. LBB-U, unipolar electrogram of 3830 pacing lead; RV d, distal RV electrogram from the quadripolar catheter

2.6 Statistical analysis

Continuous variables are reported as mean ± SD (standard deviation) and compared with two-tailed Student's *t* tests, and categorical variables were compared using Chi-Square test. All statistical tests were two-tailed; $P < 0.05$ was considered to indicate statistical significance.

3 Results

3.1 Baseline characteristics

Overall, 99 patients underwent an attempt for left bundle pacing during the study period. Out of these 99 attempts, 93 were successful (acute procedural success 94%). Table 1 shows the

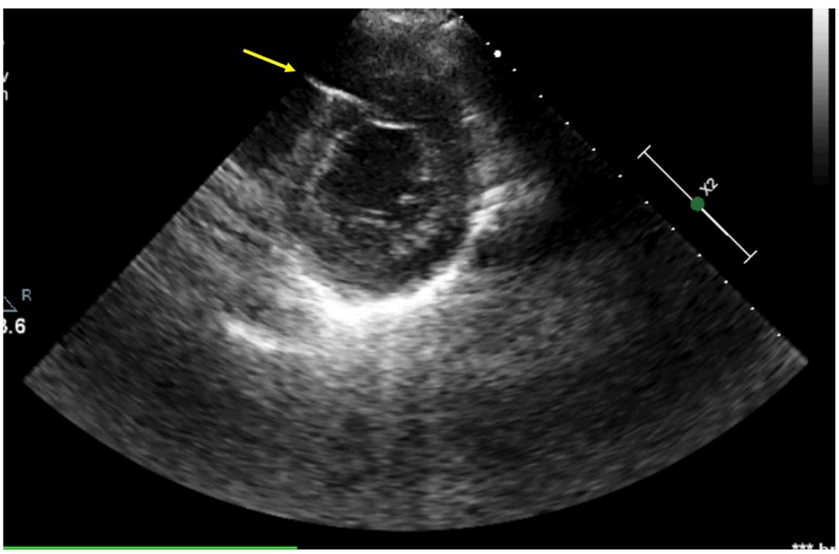

Fig. 4 Parasternal short axis view showing the pacing lead tip reaching up to left ventricular sub-endocardium (yellow arrow)

Table 1 Baseline and procedural characteristics

Total number of patients	99 patients
Successful LBB pacing	93 patients (94%)
Follow-up	4.8 months (range 1–12 months)
Age	62.6 ± 13.1 years
Men	55 (59%)
Women	38 (41%)
Hypertension	61%
Diabetes Mellitus	69%
Coronary artery disease	65%
Atrial fibrillation	6%
Left ventricular function	
Ejection Fraction < 50%	59.1% ($n = 55$)
Ejection Fraction > 50%	40.9% ($n = 38$)
Pacing Indication	
Sick sinus Syndrome	8 (9%)
AV block	40 (43%)
Cardiac resynchronisation therapy	41 (44%)
Atrial fibrillation with FVR/AVJ ablation	4 (4%)
Procedure characteristics	
LBBP fluoroscopy time	22.94 ± 11.7 min
Total fluoroscopy time	28.59 ± 13.3 min
Sheath Angiography	56 patients
Baseline ECG	
QRS duration	144.38 ± 34.6 ms
LBBB morphology	38
RBBB morphology	12
IVCD	7

baseline characteristics of the study population. Mean age of the study population was 62 ± 13 years. Sixty-nine percent were diabetics, 59% were men, and coronary artery disease was seen in 65%. Six patients had atrial fibrillation. The indication for permanent pacemaker implantation was sinus node dysfunction in 9% ($n = 8$), AV block in 43% ($n = 40$), CRT in 44% ($n = 41$; 32 with LBBB and 5 with RBBB, 4 with pacing-induced cardiomyopathy), and AV node ablation with pacing for refractory atrial fibrillation in 4% ($n = 4$). The baseline LV ejection fraction (EF) was 44.9 ± 14.6% as measured by modified Simpson's method. LV dysfunction (EF < 50%) was seen in 58.1% of the study population. Mean baseline QRS duration as analyzed on EP system was 144.38 ± 34.6 ms (from onset to the end). In patients with dilated cardiomyopathy and bundle branch block, LBBP with dual chamber pacemaker was done after obtaining informed consent regarding the current guidelines, risks, and benefits of LBBP (Fig. 5). The mean duration of follow-up was 4.8 months (range 1–12 months).

3.2 Procedural details

The target site was 1–1.5 cm apical to the imaginary line joining distal end of his bundle to right ventricular apex (Fig. 1a). Lead fixation was always done in LAO 30^0 fluoroscopic view. The average fluoroscopic time for left bundle branch lead implantation was 22.94 ± 11.7 min. Permanent left bundle branch pacing was successful in 93 out of 99 patients. LB capture could not be confirmed in 6 patients. In four of them who had AV block the lead could not penetrate the septum, hence conventional RV lead was placed. The remaining two of them had significant scar due to prior myocardial infarction and received cardiac resynchronization therapy using coronary sinus leads. Contrast sheath angiography was performed in 56 patients to confirm the lead depth in LAO 30^0 view (Fig. 1b). Septal perforations during implantation were recognized immediately during the procedure by fall in unipolar impedance below 500 Ω with loss of capture and lead repositioning was done. Four patients underwent AV nodal ablation during the procedure for managing permanent atrial fibrillation with fast ventricular rate. Ablation was done from right femoral venous access immediately after securing the pacing lead in position. Patients undergoing AV node ablation were paced at 80 beats per minute for 2 months after the procedure.

3.3 Electrophysiological parameters

The lead parameters were checked in unipolar and bipolar pacing mode. Non-selective to selective capture of LB could be demonstrated during unipolar threshold measurements at low output (Fig. 6). Left bundle (LB) potentials could be demonstrated in all patients except infra-Hisian complete heart block and left bundle branch block ($n = 37$, 40%) (Table 2). The interval between the onset of LB potential to surface QRS was 24.9 ± 0.49 ms. In those patients whom LB potential could not be recorded, other criteria as mentioned above were used to confirm LB capture. The mean QRS duration after implantation was 110.8 ± 12.4 ms. The peak left ventricular activation time was 72.5 ± 10.8 ms. Programmed stimulation protocol from the pacing lead was done when the final deep septal position was reached. After a basic drive (S1) of 8 beats at 600 ms, premature beats (S2) were delivered at progressively shorter interval starting from 400 ms. The responses were categorized as myocardial capture (broader, slurred QRS with change in amplitude, and axis), selective LB capture (RBB delay morphology with a latency interval), or non-diagnostic (progressive QRS prolongation with only minor amplitude changes). Programmed stimulation would differentiate non-selective LB capture from left septal myocardial capture by change in QRS morphology (qR to QS pattern in V1), prolongation of QRS duration, rightward shift of axis, and delayed R wave peak as shown in Fig. 7. Programmed deep septal

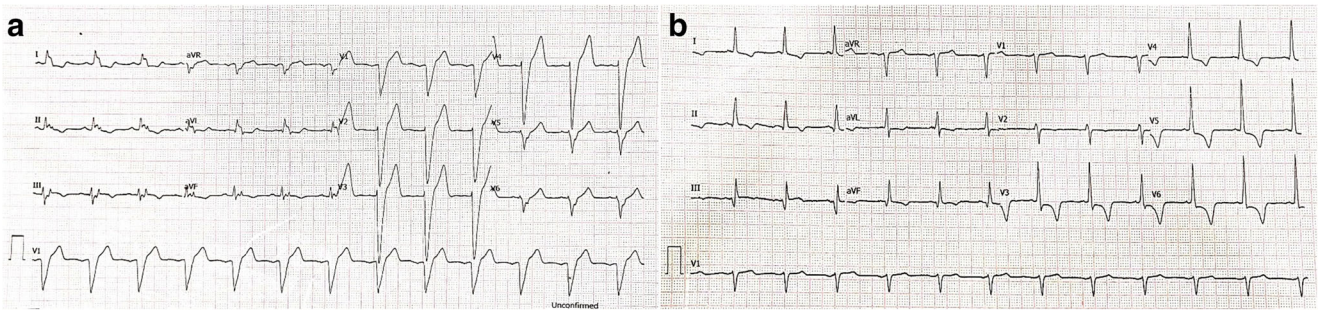

Fig. 5 LBBP for LBBB with LV dysfunction. **a** Baseline ECG showing complete LBBB with QRS duration of 150 ms. **d** Post procedure ECG showing QRS duration of 98 ms with T-wave memory (RBB delay due to LBBP was corrected by adjusting AV delay and pacing output)

stimulation was done in the last 8 patients enrolled where myocardial response was noted in 4 patients and non-diagnostic in the remaining 4 patients. This protocol would be useful to confirm LB capture when other criteria were inconclusive [29].

In patients with bundle branch block (LBBB and RBBB), if LB capture could not be demonstrated by the above-mentioned criteria, coronary sinus leads were placed to achieve resynchronization.

3.4 Echocardiographic parameters

Baseline echocardiography before procedure showed mean left ventricular ejection fraction of 44.9 ± 14.6%. Of patients, 58.1% had ejection fraction of less than 50% at the time of implantation. Baseline left ventricular end-diastolic diameter was 53.1 ± 9.6 mm. The average septal thickness was 10.73 ± 1.56 mm. The left ventricular ejection fraction improved from a mean value 44.9 ± 14.6 at baseline to 53.3 ± 10.9% on follow-up over a period of 12 months (p value < 0.0001). There was non-significant reduction in LV end-diastolic diameter to 51.1 ± 9.4 mm on follow-up (p value = 0.14). The length of the lead inside the septum as measured in parasternal short axis was 9.62 ± 1.01 mm. None of the patient developed lead dislodgement into the LV cavity. There was no worsening of tricuspid regurgitation on follow-up.

3.5 Cardiac resynchronization therapy

LBBP was successful in 41 out of 43 patients who required cardiac resynchronization therapy (LBBB 32, RBBB 5, pacing-induced cardiomyopathy 4). Coronary sinus leads were placed in the remaining two patients for whom LB could not be captured. The QRS duration was reduced from the baseline of 158.09 ms ± 31.69 ms to 113.32 ± 12.61 ms (p value < 0.0001). The left ventricular ejection fraction improved from 34.18 ± 7.96 at baseline to 48.43 ± 9.96% (p value < 0.0001).

3.6 Pacing parameters

Unipolar pacing threshold was 0.59 ± 0.22 V at 0.6 ms pulse width. Anodal capture threshold was 2.02 V at 0.6 ms pulse width. The mean sensed R wave during implantation was 14.14 ± 7.19 mV. The unipolar pacing impedance was 679.4 ± 123.7 Ω. Any impedance of less than 500 Ω was not accepted. Perforations were recognized on table by drop in impedance of more than 200 Ω, unipolar impedance of less than 500 Ω, raise in threshold, or loss of capture. On follow-up, the pacing threshold remained stable at 0.57 ± 0.12 V at 0.6 ms and pacing impedance at 607.7 ± 83.5 Ω (Table 3). There was no significant reduction in sensed R wave amplitude (13.68 ± 5.2 mV) (p value 0.199).

3.7 Safety parameters

Patients were followed-up in the device clinic at the end of 15 days, 1 month, and every 2 months thereafter. At least 6 months follow-up was available for 40 patients, 3 months follow-up for 80 patients, and the remaining patients had minimum of 1 month follow-up.

There was no acute or late lead dislodgement and no late raise in threshold on follow-up. No patient developed device or lead infection. There was no evidence of thromboembolic complication during the follow-up. One patient died after 1 month due to lower respiratory tract infection with sepsis and bi-cytopenia. Follow-up echocardiography showed significant increase in ejection fraction from a mean value of 44.96 to 53.3% (p value < 0.0001) with no worsening of tricuspid regurgitation.

4 Discussion

The search for alternate pacing site has resulted in physiological pacing wherein the His-Purkinje System is targeted [31]. The limitations of His bundle pacing include narrow target zone, lead stability, raise in threshold on follow-up, and need for lead revision. Huang

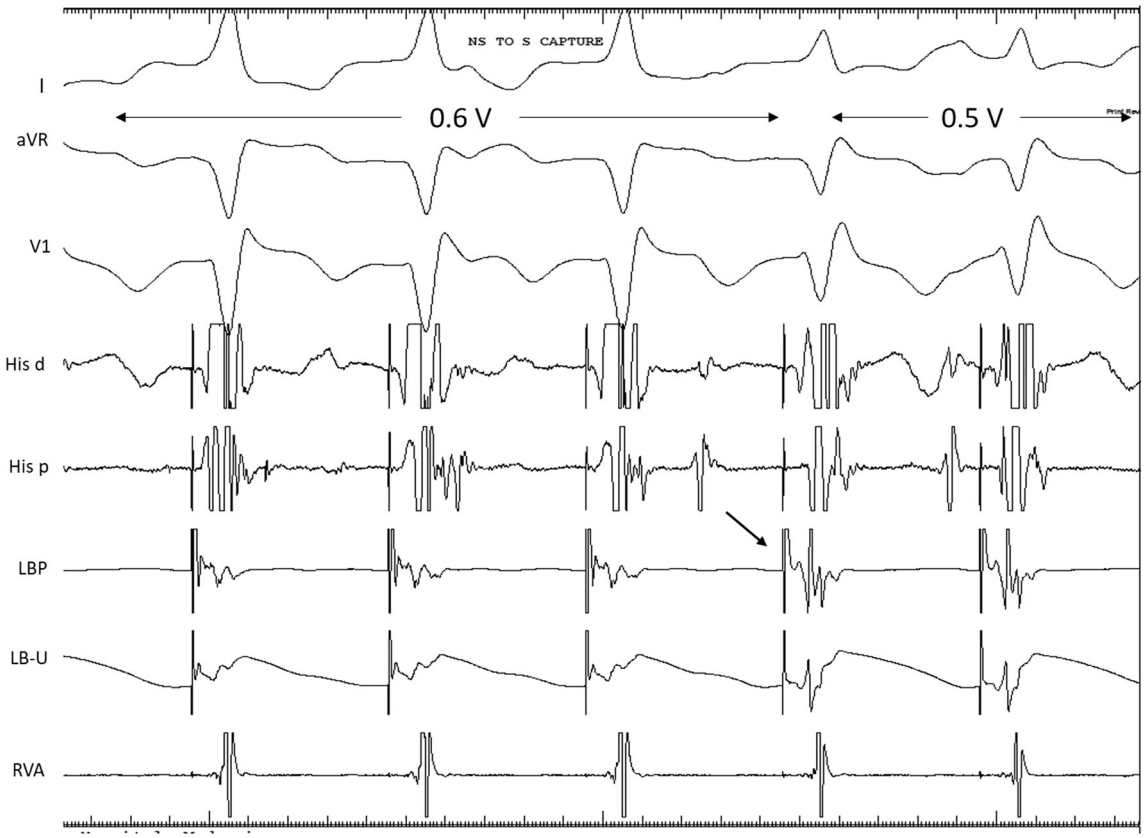

Fig. 6 Demonstration of non-selective to selective left bundle branch capture during unipolar pacing. Note the distinct local electrogram after the pacing spike (arrow head) and change in QRS morphology from qR to rSR during selective capture

Table 2 Electrophysiological and safety parameters

Left bundle potential	37 patients (40%)
LB potential-QRS duration	24.9 ± 0.49 ms
LB paced QRS duration	110.8 ± 12.4 ms
pLVAT	72.5 ± 10.8 ms
Pacing parameters	
Threshold (unipolar) @0.6 ms PW	0.59 ± 0.22 V
Anodal threshold @0.6 ms PW	2.02 ± 0.3 V
Sensed R wave (mV)	14.14 ± 7.19 mV
Unipolar pacing impedance (ohms)	679.4 ± 123.7 Ω
Echocardiographic parameters	
Baseline LVEF (%)	44.96 ± 14.6%
Septal thickness	10.73 ± 1.56 mm
Lead depth	9.62 ± 1.01 mm
Worsening of LVEF	Nil
Safety parameters	
Acute lead dislodgement	Nil
Late lead dislodgement	Nil
Late raise in threshold by > 1 V	Nil
Thromboembolic complication	Nil
Mortality	1 (noncardiac)

et al. demonstrated a strategy to directly capture the left bundle branch by deep septal pacing which overcomes many of the limitations of His bundle pacing [10]. Subsequently, many studies have shown the safety and efficacy of left bundle branch pacing [29, 32–34]. Vijayaraman et al. demonstrated the feasibility, electrophysiological, and echocardiographic parameters of successful left bundle pacing in 93 of 100 patients which include AV nodal block, left bundle branch block, right bundle branch block, and intraventricular conduction defect [18]. The average paced QRS duration was 136 ± 17 ms and the average pLVAT was 75 ± 16 ms. Pacing lead threshold was 0.6 V ± 0.4 V at 0.5 ms and R wave 10 ± 6 mV and remained stable during follow-up.

In our study, we have demonstrated the feasibility of left bundle branch pacing in Indian population. The important findings of our study are as follows:

1. LBB pacing is feasible in 94% of the patients irrespective of the indications for pacing.
2. The lead parameters are better than His bundle pacing—low and stable threshold, good lead stability, and better R wave sensing. The lead parameters remained stable during the follow-up of 12 months.

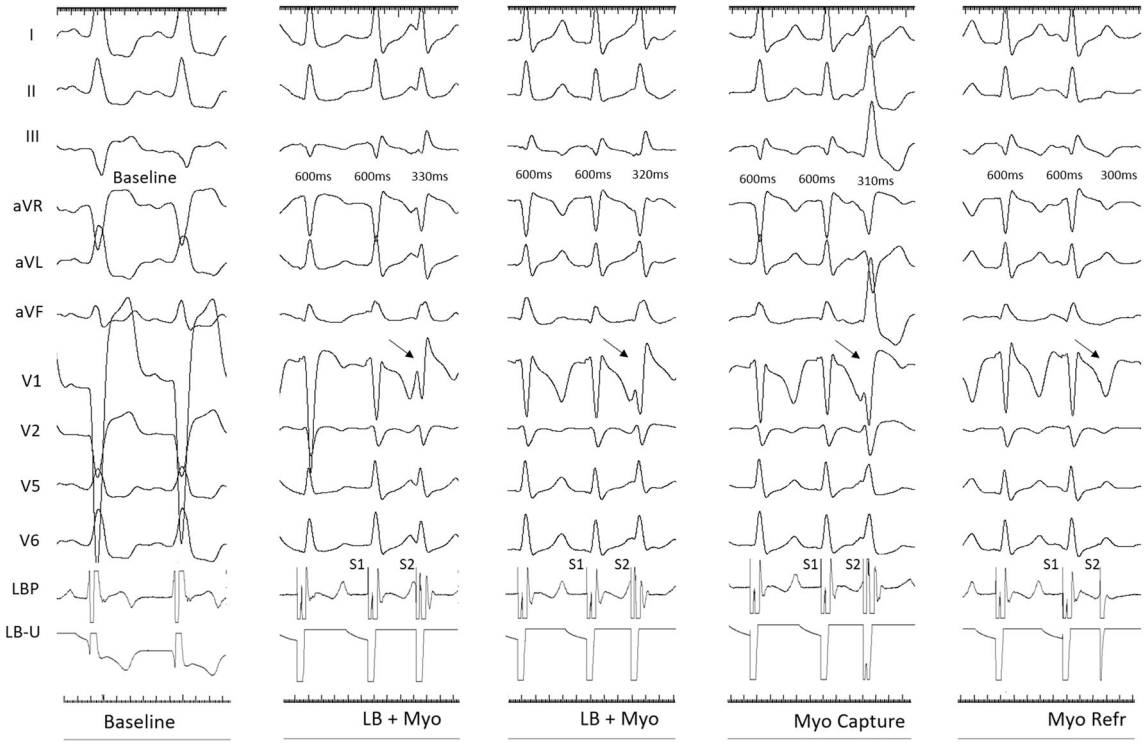

Fig. 7 Programmed stimulation from LB lead in patient who had undergone LBBP for LV dysfunction, heart failure. and LBBB. Non-selective LB with septal myocardium was captured until 320 ms. At 310 ms extra stimulus, only septal myocardial capture with change in QRS morphology, duration, axis, and delayed R wave peak was noted

3. Left bundle branch potential could be demonstrated in all patients except infra-Hisian complete heart block and complete left bundle branch block ($n = 37$, 40%). Rapid activation of left ventricle could be demonstrated by short peak left ventricular activation time (72.5 ± 10.8 ms).
4. Echocardiography showed the average lead depth of 9.62 mm inside the interventricular septum and also confirmed that no part of the lead is exposed to the left ventricular cavity. The left ventricular ejection fraction improved from a mean value 44.9 ± 14.6% at baseline to 53.3 ± 10.9% (p value < 0.0001) along with non-significant reduction in LV end-diastolic diameter from 53.1 ± 9.6 to 51.1 ± 9.4 mm (p value = 0.14).
5. In patients with standard bradycardia pacing indications (sinus node dysfunction and AV block), LBBP could be done successfully. We could achieve a success rate of 91% (40 out of 44 patients) in patients with AV block undergoing LBBP. Conduction system pacing maintains synchronized ventricular contraction thereby avoiding RV pacing-related complications.
6. LBB pacing could be effectively used as an alternative for cardiac resynchronization therapy. LB capture could be confirmed in 41 out of 43 attempted patients who required CRT (Fig. 5). The QRS duration was reduced from the baseline of 158.09 ms ± 31.69 to 113.32 ± 12.61 ms (p value < 0.0001). The left ventricular ejection fraction

Table 3 Pacing and echocardiographic parameters before implantation and during follow-up

	At implantation	Follow up (1–12 months)	p value
Pacing parameters			
Threshold (unipolar)	0.59 ± 0.22 V	0.57 ± 0.12 V	0.245
R wave	14.14 ± 7.19 mV	13.68 ± 5.2 mV	0.199
Pacing impedance	679.4 ± 123.7 Ω	607.7 ± 83.5 Ω	0.0012
ECG-QRS duration (pre and post)	144.38 ± 34.6 ms	110.8 ± 12.4 ms	< 0.0001
Echocardiographic parameters			
LV ejection fraction	44.96 ± 14.6%	53.3 ± 10.9%	< 0.0001
LV end diastolic diameter	53.1 ± 9.6 mm	51.1 ± 9.4 mm0.14	
Worsening of tricuspid regurgitation	-	Nil	

improved from 34.18 ± 7.96 at baseline to 48.43 ± 9.96% (p value < 0.0001).

7. Left bundle pacing can be an effective strategy for patients with permanent atrial fibrillation with fast ventricular rate planned for AV node ablation.
8. The average fluoroscopic time for the implantation of the left bundle lead (22.94 ± 11.7 min) was higher than the reported data due to initial learning curve.
9. Safety endpoints—no significant acute procedural complication noted. During follow-up, none of our patients developed migration of lead into LV cavity, thromboembolism, or significant reduction in LV ejection fraction.

Since conduction system capture will result in synchronized ventricular contraction, the risk of pacing-induced cardiomyopathy will not occur in patients with LBBP and HBP [32]. However, in patients undergoing LBBP, there is a theoretical risk of interventricular dyssynchrony due to RBB delay pattern on surface ECG. This could be minimized by adjusting the AV delay to get native fusion from AV nodal conduction (Fig. 5b), pacing output by allowing anodal capture or by placing additional leads at RV septum [29]. Radiation dose reduction during the procedure can be achieved by using electroanatomic mapping for creating geometry of cardiac chambers and tagging His bundle potentials [35]. Qian Z et al. recently published their pilot study on LVAT cut-off where they have shown that < 76 ms might be a practical parameter based on LV mechanical synchrony [36]. In our study, three-fourths of the patients had LVAT < 80 ms (n = 72) and remaining one-fourth had > 80 ms (n = 21). Prolonged LVAT was noted in patients with dilated left ventricle. The cut-off value for LVAT has to be validated in future trials below which clinical response can be predicted.

Left bundle branch pacing can be considered an alternative strategy for cardiac resynchronization therapy (CRT) in patients with dilated cardiomyopathy with left ventricular dysfunction [27]. In our study, we could show significant reduction of QRS duration from 144.3 ± 34.6 ms at baseline to 110.8 ± 12.4 ms after the procedure with significant improvement in ejection fraction. QRS duration remained stable on follow-up of these patients. In a study by Zhang et al [37], eleven patients with heart failure and LBBB were included. They have demonstrated not only reduction in QRS duration but also resynchronization of ventricular contraction with LV reverse remodeling and improvement in clinical symptoms. Vijayaraman et al. [38] showed CRT could be successfully achieved in 277 out of 325 patients (85% success rate) which included 44% of ischemic cardiomyopathy patients. LBBP resulted in significant reduction in QRS duration from 152 ± 32 to 137 ± 22 ms (p value < 0.01). LVEF improved from 33 ± 10 to 44 ± 11% (p value < 0.01). In our study, we could demonstrate significant reduction in QRS duration along with improvement in LV ejection fraction on follow-up.

4.1 Limitation

This is a single-center, prospective observational study done in patients undergoing left bundle branch pacing for symptomatic bradyarrhythmias and bundle branch correction therapy. Though we could provide safety data, the lead 3830 is not meant for deep septal pacing. The impact of myocardial contraction on the pacing lead tip is yet to be evaluated. Dual lead technique for lead placement as suggested by Huang et al.[34] was not performed because of financial issues in having additional 3830 lead with C315 sheath. Only limited patients had undergone programmed deep septal stimulation (n = 8). Since the lead is placed deep into the septum, the safety of lead extraction has to be studied in future. Further multicenter, randomized controlled trials are necessary to confirm the potential benefits of LBBP for patients undergoing pacemaker and CRT implantation.

5 Conclusion

LBBP is a safe and effective strategy of physiological pacing for patients requiring pacemaker implantation. It is feasible in high percentage of patients (94%) as shown in our study. The pacing parameters remained stable over a period of 12 months follow-up. LBBP can effectively overcome the limitations of HBP in terms of getting a low and stable threshold, battery longevity, and bypassing the diseased conduction system. Future randomized studies will help to establish the role of LBBP as an effective alternative to cardiac resynchronization therapy.

Compliance with ethical standards The study was conducted after getting the ethical committee approval. The paper is not under consideration elsewhere. None of the paper's contents have been previously published. All authors have read and approved the manuscript.

Conflict of interest We have no conflicts of interest to disclose.

References

1. Nielsen JC, Kristensen L, Andersen HR, Mortensen PT, Pedersen OL, Pedersen AK. A randomized comparison of atrial and dual chamber pacing in 177 consecutive patients with sick sinus syndrome: echocardiographic and clinical outcome. J Am Coll Cardiol. 2003;42:614–23.
2. Sweeney MO, Hellkamp AS, Ellenbogen KA, Greenspon AJ, Freedman RA, Lee KL, et al. Adverse effect of ventricular pacing on heart failure and atrial fibrillation among patients with normal baseline QRS duration in a clinical trial of pacemaker therapy for sinus node dysfunction. Circulation. 2003;107:2932–7.
3. Wilkoff BL, Cook JR, Epstein AE, Greene HL, Hallstrom AP, Hsia H, et al. Dualchamber pacing or ventricular backup pacing in patients with an implantable defibrillator—the dual chamber and VVI implantable defibrillator (DAVID) trial. J Am Med Assoc. 2002;288:3115–23.

4. Olshansky B, Day JD, Lerew DR, Brown S, Stolen KQ. Eliminating right ventricular pacing may not be best for patients requiring implantable cardioverter-defibrillators. Heart Rhythm. 2007;4:886–91.
5. Vijayaraman P, Chung MK, Dandamudi G, Upadhyay GA, Krishnan K, Crossley G, et al. His bundle pacing. J Am Coll Cardiol. 2018;72:927–47.
6. Vijayaraman P, Naperkowski A, Ellenbogen KA, Dandamudi G. Electrophysiologic insights into site of atrioventricular block: lessons from permanent His bundle pacing. JACC Clin Electrophysiol. 2015;1:571–81.
7. Deshmukh P, Casavant DA, Romanyshyn M, Anderson K. Permanent, direct His-bundle pacing: a novel approach to cardiac pacing in patients with normal His-Purkinje activation. Circulation. 2000;101:869–77.
8. 2018 ACC/AHA/HRS Guideline on the evaluation and management of patients with bradycardia and cardiac conduction delay: a report of the American College of Cardiology/American Heart Association Task Force on Clinical Practice Guidelines, and the Heart Rhythm Society. *J Am Coll Cardiol* 2018;Oct 28.
9. Occhetta E, Bortnik M, Marino P. Permanent parahisian pacing. Indian Pacing Electrophysiol J. 2006;7:110–25.
10. Barba-Pichardo R, Moriña-Vázquez P, Venegas-Gamero J, Maroto-Monserrat F, Cid-Cumplido M, Herrera-Carranzaa M. Permanent His-bundle pacing in patients with infra-Hisian atrioventricular block. Rev Esp Cardiol. 2006;59:553–8.
11. Kronborg MB, Mortensen PT, Gerdes JC, Jensen HK, Nielsen JC. His and para-His pacing in AV block: feasibility and electrocardiographic findings. J Interv Card Electrophysiol. 2011;31:255–62.
12. Alberti L, Pieragnoli P, Ricciardi G, Padeletti L. Hemodynamics of His bundle pacing. J Electrocardiol. 2017;50:161–5.
13. Patel B, Garg J, Chaudhary R, Sablani N, Gupta R, Shah M, et al. His bundle pacing: hemodynamics and clinical outcomes. Cardiol Rev. 2018;26:201–6.
14. Abdelrahman M, Subzposh FA, Beer D, Durr B, Naperkowski A, Sun H, et al. Clinical outcomes of His bundle pacing compared to right ventricular pacing. J Am Coll Cardiol. 2018;71:2319–30.
15. Huang W, Su L, Wu S, et al. Benefits of permanent His bundle pacing combined with atrioventricular node ablation in atrial fibrillation patients with heart failure with both preserved and reduced left ventricular ejection fraction. J Am Heart Assoc. 2017;6:e005309.
16. Huang W, Su L, Wu S, Xu L, Xiao F, Zhou X, et al. Long-term outcomes of His bundle pacing in patients with heart failure with left bundle branch block. Heart. 2019;105:137–43.
17. Lustgarten DL, Crespo EM, Arkhipova-Jenkins I, et al. His-bundle pacing versus biventricular pacing in cardiac resynchronization patients: a crossover design comparison. Heart Rhythm. 2015;12(7):1548–57.
18. Sharma PS, Dandamudi G, Herweg B, Wilson D, Singh R, Naperkowski A, et al. Permanent His-bundle pacing as an alternative to biventricular pacing for cardiac resynchronization therapy: a multicenter experience. Heart Rhythm. 2018;15:413–20.
19. Subzposh FA, Vijayaraman P. Long-term results of His bundle pacing. Card Electrophysiol Clin. 2018;10:537–42.
20. Barba-Pichardo R, Morina-Vazquez P, Fermandez-Gomes JM, et al. Permanent His-bundle pacing: seeking physiological ventricular pacing. Europace. 2010;12:527–33.
21. Zanon F, Ellenbogen KA, Dandamudi G, Sharma PS, Huang W, Lustgarten DL, et al. Permanent His-bundle pacing: a systematic literature review and meta-analysis. Europace. 2018;20:1819–26.
22. Huang W, Su L, Wu S, et al. A novel pacing strategy with low and stable output: pacing the left bundle branch immediately beyond the conduction block. Can J Cardiol. 1736;2017(33):e1–3.
23. Wu S, Su L, Wang S, Vijayaraman P, Ellenbogen KA, Huang W. Peri-left bundlebranch pacing in a patient with right ventricular pacing-induced cardiomyopathyand atrioventricular infra-Hisian block. Europace. 2019;21(7):1038.
24. Vijayaraman P, Subzposh FA, Naperkowski A, Panikkath R, John K, Mascarenhas V, et al. Prospective evaluation of feasibility, electrophysiologic and echocardiographic characteristics of left bundle branch area pacing. Heart Rhythm. 2019;16:1774–82.
25. Li X, Li H, Ma W, Ning X, Liang E, Pang K, et al. Permanent left bundle branch area pacing for atrioventricular block: feasibility, safety, and acute effect. Heart Rhythm. 2019;16:1766–73.
26. Zhang J, Wang Z, Cheng L, et al. Immediate clinical outcomes of left bundle branch area pacing vs conventional right ventricular pacing. Clin Cardiol. 2019;42:768–73.
27. Hou X, Qian Z, Wang Y, Qiu Y, Chen X, Jiang H, et al. Feasibility and cardiac synchrony of permanent left bundle branch pacing through the interventricular septum. Europace. 2019;21(11):1694–702.
28. Li Y, Chen K, et al. Left bundle branch pacing for symptomatic bradycardia: implant success rate, safety, and pacing characteristics. Heart Rhythm. 2019;16:1758–65.
29. Huang W, Chen X, Su L, Wu S, Xia X, Vijayaraman P. A beginner's guide to permanent left bundle branch pacing. Heart Rhythm. 2019;16:1791–6.
30. Jastrzebski M, Moskal P, Bednarek A, et al. Programmed deep septal stimulation - a novel maneuver for the diagnosis of left bundle branch capture during permanent pacing. J Cardiovasc Electrophysiol. 2020;31(2):485–93.
31. Su L, Wu SJ, Wang SJ, et al. Pacing parameters and success rates of permanent hisbundle pacing in patients with narrow QRS: a single-centre experience. Europace. 2019;21:763–70.
32. Chen K, Li Y, Dai Y, et al. Comparison of electrocardiogram characteristics and pacing parameters between left bundle branch pacing and right ventricular pacing in patients receiving pacemaker therapy. Europace. 2019;24:673–80.
33. Wang S, Wu S, Xu L, et al. Feasibility and efficacy of His bundle pacing or left bundle pacing combined with AV node ablation in patients with persistent atrial fibrillation and implantable cardioverter-defebrillator therapy. J Am Heart Assoc. 2019;8:e014253.
34. Chen K, Li Y. How to implant left bundle branch pacing lead in route clinical practice. J Cardiovasc Electrophysiol. 2019;30:2569–77.
35. Ponnusamy SS, Bopanna D, Kumar S. Electro-anatomic mapping guided low fluoroscopy left bundle branch pacing. J Am Coll Cardiol EP. 2020; (article in press).
36. Qian Z, Wang Y, Hou X, et al. A pilot study to determine if left ventricular activation time is a useful parameter for left bundle branch capture: validated by ventricular mechanical synchrony with SPECT imaging. J Nucl Cardiol. 2020. https://doi.org/10.1007/s12350-020-02111-6 (online ahead of print).
37. Zhang W, Huang J, Qi Y, Wang F, Guo L, Shi X, et al. Cardiac resynchronization therapy by left bundle branch area pacing in patients with heart failure and left bundle branch block. Heart Rhythm. 2019;16:1783–90.
38. Vijayaraman P, Sundaram S, Cano O, et al. Left bundle branch pacing for cardiac resynchronization therapy: results from international LBBP collaborative study group. HRS 2020 – Late breaking clinical trial.

Received: 29 September 2020 | Revised: 20 December 2020 | Accepted: 2 January 2021

DOI: 10.1111/jce.14905

BRIEF COMMUNICATION

WILEY

Cardiac troponin release following left bundle branch pacing

Shunumuga S. Ponnusamy MD, DM[1] | Neil R. Patel MD[2] | Angela Naperkowski RN, CEPS, CCDS, FHRS[3] | Faiz A. Subzposh MD[3] | Pugazhendhi Vijayaraman MD, FACC[3]

[1]Division of Cardiology, Velammal Medical College, Madurai, Tamil Nadu, India

[2]Division of Cardiology, The Wright Center, Scranton, Pennsylvania, USA

[3]Division of Cardiology, Geisinger Heart Institute, Wilkes-Barre, Pennsylvania, USA

Correspondence
Pugazhendhi Vijayaraman, MD, FACC, Division of Cardiology, Geisinger Heart Institute, MC 36-10, 1000 E Mountain Blvd, Wilkes-Barre, PA 18711, USA.
Email: pvijayaraman1@geisinger.edu and pvijayaraman@gmail.com

Abstract

Left bundle branch pacing (LBBP) has emerged as an alternative to His bundle pacing (HBP) to achieve physiologic ventricular stimulation. The extent of myocardial injury during permanent LBBP implantation is currently not known. The aim of the study was to prospectively assess the extent of myocardial injury during LBBP implantation. Cardiac troponin (cTn) levels were measured at baseline and 6–12 h following permanent LBBP. The number of attempts to achieve LBBP was documented. Troponin levels were measured in a control population undergoing other electrophysiology procedures including HBP, other devices involving right ventricular (RV) pacing, radiofrequency ablation for atrial fibrillation (AF) and supraventricular tachycardia (SVT). Significant elevation of troponin (SET) was defined as threefold increase above the upper reference limit (URL) for cTn. Between December 2019 and April 2020, 204 were prospectively enrolled: LBBP in 98 and Control group 106 (SVT, 55; AF, 20; HBP, 17; other devices, 14). SET (>3× URL) was seen in 49.4% of patients in the LBBP group compared to 58.4% in the control group ($p = .23$). Peak troponin levels were greater in the control group compared to the LBBP group (230.3 ± 320.1 vs. 87.4 ± 71.3 pg/ml; $p = .0001$). Compared to LBBP (49.4%), SET was observed less frequently following HBP (17.5%; $p = .01$), and other device implantation (29%; $p = .15$). Patients requiring >2 attempts ($n = 33$) had significantly higher incidence of SET compared to <2 attempts ($n = 56$; 66.7% vs. 39.3%; $p = .01$). LBBP implantation is associated with myocardial injury. Asymptomatic troponin release following LBBP is less than or comparable to other interventional electrophysiology procedures.

KEYWORDS

ablation, cardiac troponin, His bundle pacing, left bundle branch pacing

1 | INTRODUCTION

Physiological pacing has witnessed a revolutionary growth in the last decade. Though His bundle pacing (HBP) provides the most physiological form of pacing it is fraught with limitations including higher threshold, premature battery depletion, technical difficulty, and lead dislodgement. Left bundle branch pacing (LBBP) is emerging as an effective alternative to HBP as it overcomes many of its limitations.[1–3] While several studies have demonstrated LBBP to be safe in the short term, long-term safety data is yet to be available.

Disclosures: Faiz A. Subzposh serves as a speaker for Medtronic. Pugazhendhi Vijayaraman serves as a speaker, consultant, research, fellowship support for Medtronic; consultant for Biotronik, Boston Scientific, Abbott, and Eaglepoint LLC; and patent for His delivery tool. Other authors: No disclosures.

Injury to myocardium and coronary artery branches[4] are some of the concerns as the lead is placed deep in the proximal interventricular septum to capture the left bundle (LB) and often requires multiple attempts. Myocardial injury during LBBP implantation has not been studied so far. We aimed to analyze the extent of myocardial injury due to LBBP implantation by cardiac troponin (cTn) measurement in comparison to other interventional electrophysiology procedures.

2 | METHODS

This was a prospective observational study conducted at two centers between December 2019 and April 2020 after obtaining institutional review board approval. Informed written consent was obtained after explaining LBBP as a nonstandard approach. The data that support the findings of this study are available from the corresponding author upon reasonable request. All patients who had undergone successful LBBP implantation were included in the study group. The control group was constituted by other interventional electrophysiology procedures including pacemaker implantation other than LBBP and radiofrequency (RF) ablation of tachyarrhythmias. Patients with preprocedural positive cardiac markers were excluded from the study.

Procedural technique of LBBP implantation was described in our previous paper.[2] Briefly C315 His sheath was used to deploy 4.1F 3830 Selectsecure™ lead (Medtronic Inc.) deep inside the proximal interventricular septum to capture the LB. RF ablation for supraventricular arrhythmias were done as per standard protocol with electroanatomic mapping system in selected patients.

Quantitative troponin measurement was done at baseline and 6–12 h after the procedure in all patients. High sensitivity cardiac troponin T (cTnT) analysis was done in center A (upper reference limit [URL] 22 pg/ml) and high sensitivity cardiac troponin I (cTnI) in center B (URL 23 pg/ml). Significant elevation of troponin (SET) was defined as threefold increase above the URL for both cTnT and cTnI.

3 | RESULTS

Two hundred four patients were prospectively included in the study. Ninety-eight patients had undergone successful LBBP implantation with a single 3830 Selectsecure lead during the study period. Nine of them required additional atrioventricular junction (AVJ) ablation and hence they were excluded and analyzed separately. The indications for pacing were sick sinus syndrome ($n = 17$), atrioventricular (AV) block ($n = 46$), and cardiac resynchronization therapy ($n = 26$). RF ablation for supraventricular tachycardia (SVT, $n = 55$), atrial fibrillation (AF; $n = 20$), HBP ($n = 17$), and other device therapies ($n = 14$; implantable cardioverter-defibrillator [ICD] 8, cardiac resynchronization therapy defibrillator [CRT-D] 3, RV pacing 3) constituted the control group ($n = 106$).

LBBP group were older (68.7 ± 13.6 vs. 56.6 ± 17.4 years; $p < .0001$), with more hypertension and coronary artery disease (59% vs. 42%; $p = .01$ and 37% vs. 24%; $p = .02$, respectively) compared to the control group. The mean QRS duration decreased from 142.1 ± 32.3 ms at baseline to 124.9 ± 24.1 ms ($p = .001$) after LBBP. The mean peak left ventricular activation time (pLVAT) was 76.1 ± 12.8 ms.

Asymptomatic elevation of cTn was observed in both LBBP and control groups (Figure 1). SET (>3× URL) was seen in 49.4% of patients in the LBBP group compared to 58.4% in the control group ($p = .23$). Peak troponin levels were greater in the control

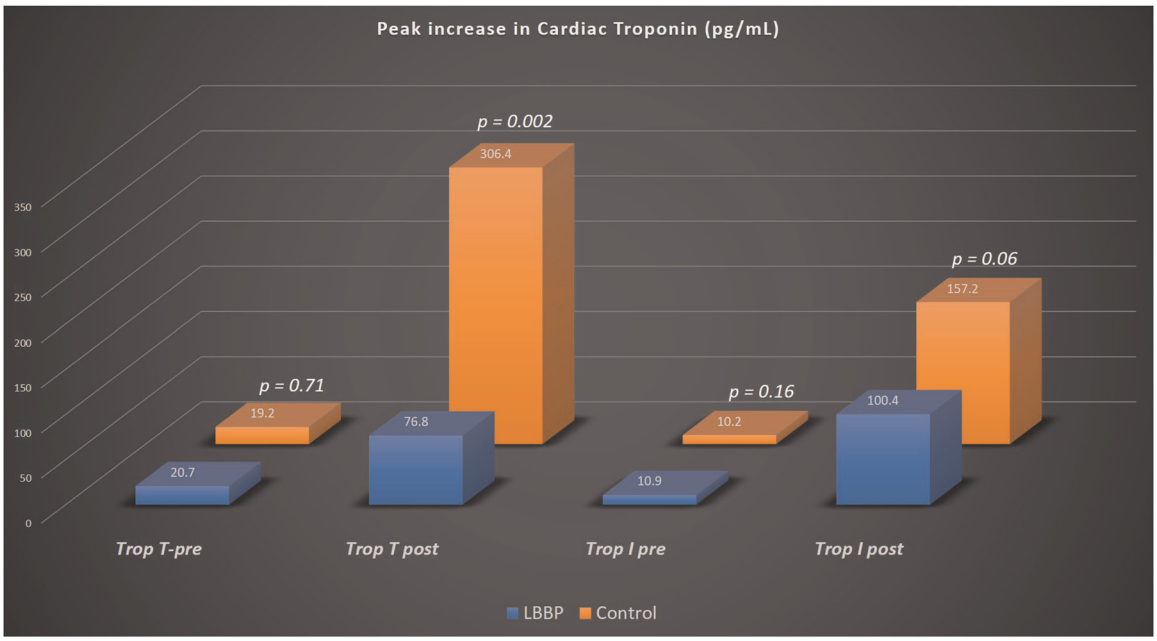

FIGURE 1 Cardiac troponin I and T levels before and after the procedure in the study population. LBBP, left bundle branch pacing

group compared to the LBBP group (230.3 ± 320.1 pg/ml; range 13–1385 vs. 87.4 ± 71.3 pg/ml; range 12–266; $p = .0001$). The subgroup analysis of the control group showed SET was noted in 54% of patients who had undergone RF ablation for SVT and AF. Peak troponin levels were significantly greater in this subgroup as compared to the study group (298.6 ± 354.6 vs. 87.4 ± 71.3 pg/ml; $p = .0001$). Compared to LBBP (49.4%), SET was observed less frequently following HBP (17.5%; $p = .01$), and other device implantation (29%; $p = .15$) while SVT ablation resulted in more frequent SET (69.1%, $p = .02$; Figure 2). AF ablation produced ninefold greater rise in peak cTn levels as compared to LBBP (903.1 ± 316.9 pg/ml; $p < .0001$). SET was observed in all nine patients (358 ± 112.9 pg/ml, 100%) with combined LBBP and AVJ ablation. The mean number of attempts for placing the lead deep into the septum during LBBP was 2.5 ± 1.9. Patients requiring >2 attempts ($n = 33$) had significantly higher incidence of SET compared to ≤2 attempts ($n = 56$; 66.7% vs. 39.3%; $p = .01$; 71.2 ± 56.1 vs. 115.1 ± 85.8 pg/ml; $p = .004$; Figure 3). There was no difference in the incidence of SET among patients who received active fixation ($n = 42$) as compared to passive fixation lead ($n = 47$) for atrium in the LBBP group (48% vs. 51%; p value, .78). There were no acute procedural complications including hypotension or need for cardioversion noted in either group. Post-procedure echocardiography did not show any new wall motion abnormalities.

4 | DISCUSSION

Though LBBP provides excellent results in terms of pacing parameters and QRS morphology, the long-term safety data is yet to be available. There is a concern of myocardial damage as the lead is buried deep inside the septum. The extent of myocardial damage and quantity of cardiac marker release were not previously studied in patients undergoing LBBP implantation. Martignani et al.[5] showed pacemaker implantation by conventional RV lead placement was associated with significant increase in cTnI in up to 37% of patients. Nikolaou et al.[6] showed elevation of cTnI in 59% of patients ($n = 167$ out of 283) after pacemaker implantation using passive fixation leads in the right ventricle. Pacemaker implantation may provoke a release of cardiac markers due to direct trauma to the myocardial cells by the endocardial leads. In a prospective controlled study[7] which included 118 patients planned for RF ablation for variety of arrhythmias, cTnI was increased in 68% of the patients. The degree of myocardial injury was more accurately assessed by cTnI levels rather than creatine kinase-MB levels. Similarly, RF ablation for AF resulted in troponin elevation in 100% of patients.[8] Diagnosis of acute coronary syndrome can be difficult in the post-procedural period as the increase may be related to direct myocardial injury during the procedure.

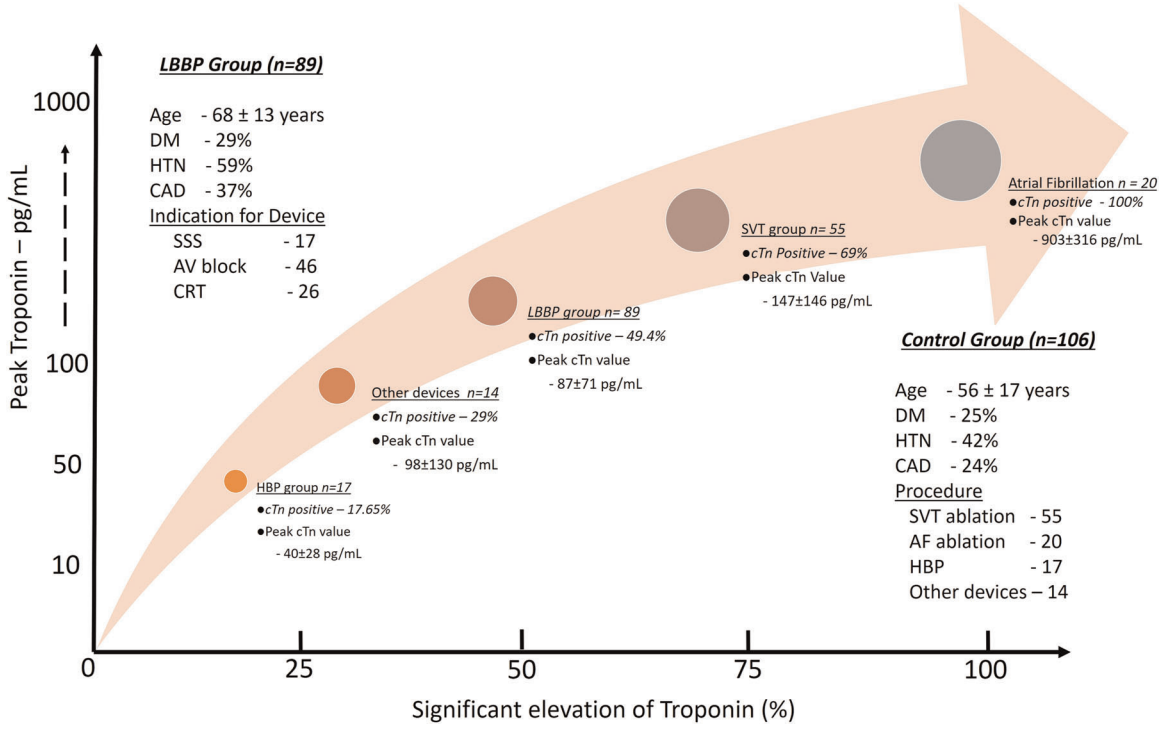

FIGURE 2 Cardiac troponin release during LBBP and other electrophysiology procedures. AF, atrial fibrillation; AV, atrioventricular; CAD, coronary artery disease; CRT, cardiac resynchronization therapy; DM, diabetes mellitus; HBP, His bundle pacing; HTN, hypertension; LBBP, left bundle branch pacing; SSS, sick sinus syndrome; SVT, supraventricular tachycardia

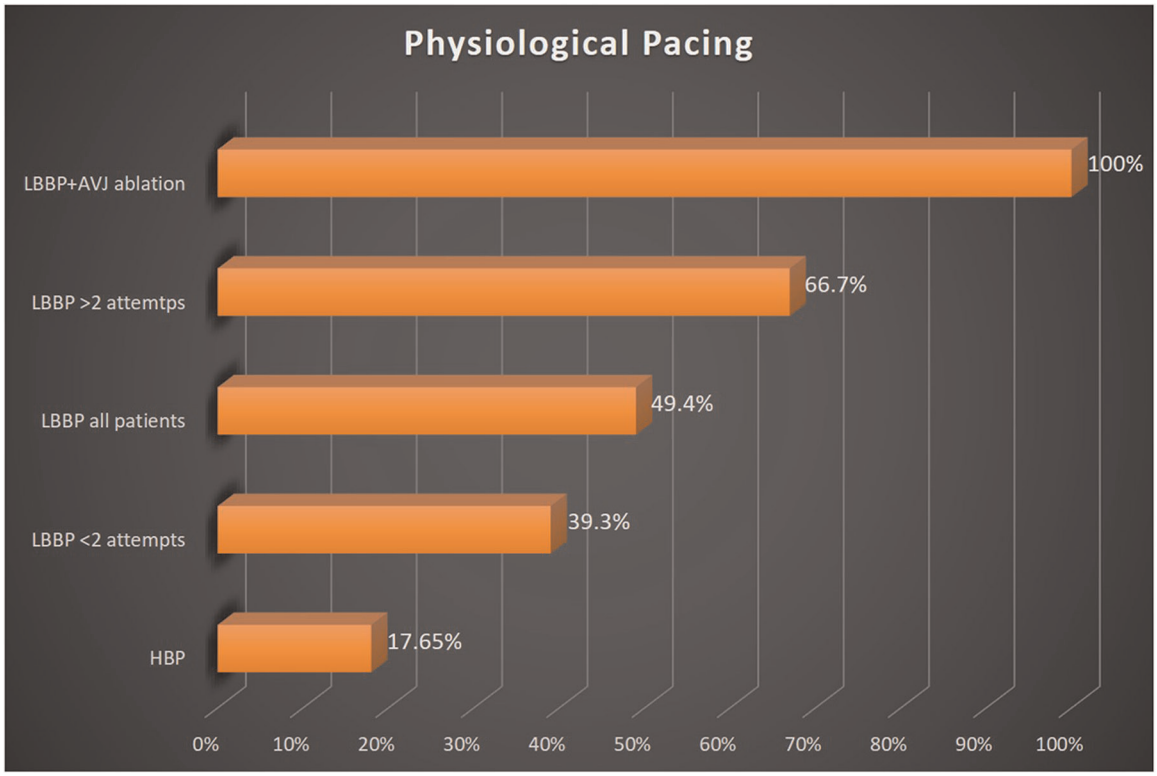

FIGURE 3 Troponin release (SET) in Physiological pacing. HBP, His bundle pacing; LBBP, left bundle branch pacing; SET, significant elevation of troponin

In our study, we have shown that asymptomatic increase in cTn levels are seen in both LBBP implantation and control group. But RF ablation resulted in greater troponin release as compared to LBBP. Myocyte injury associated with deep septal placement of the lead was less than RF ablation for SVTs. AF ablation resulted in ninefold greater increase in troponin levels as compared to LBBP implantation. This finding is important in establishing the safety of LBBP implantation and the extent of associated myocardial injury, which is less than other interventional electrophysiology procedures. HBP wherein the lead is placed in the membranous septum resulted in less troponin release as compared to LBBP thereby establishing it as better modality of physiological pacing in terms of myocardial damage (Figure 3). Among all the groups analyzed in our study, SET was observed the least in HBP than other groups. Though the myocyte injury is minimal, high threshold and lead dislodgements are the major concerns that limit widespread adoption of HBP.

LBBP is technically less challenging as compared to HBP and lead is placed by rapid turns into the proximal septum. Repeated attempts may be required in some patients to capture the LB. In our study patients requiring >2 attempts ($n = 33$) showed higher incidence of SET as compared to ≤2 attempts ($n = 56$). Better delineation of distal His signals, pace mapping to obtain 'W' pattern, and perpendicular sheath-septum orientation would increase the chance of successful LBBP with less attempts. Though SET was more frequently observed in LBBP > 2 attempts, SVT group had higher level, which was statistically not significant (66.7% vs. 69.1%; p value, .81). Coronary angiography was not done[9] immediately after the procedure in both study and control groups and could be considered as a limitation of our study.

5 | CONCLUSION

LBBP implantation is a safe way of capturing the cardiac conduction system. The minimal myocardial injury and associated asymptomatic troponin release are less than that occur during other interventional electrophysiology procedures.

DATA AVAILABILITY STATEMENT

The data that support the findings of this study are available from the corresponding author upon reasonable request.

ORCID

Shunumuga S. Ponnusamy https://orcid.org/0000-0002-7059-425X
Pugazhendhi Vijayaraman http://orcid.org/0000-0003-2230-100X

REFERENCES

1. Vijayaraman P, Subzposh FA, Naperkowski A, et al. Prospective evaluation of feasibility and electrophysiologic and echocardiographic characteristics of left bundle branch area pacing. *Heart Rhythm*. 2019; 16:1774-1782.

2. Ponnusamy SS, Arora V, Namboodiri N, Kumar V, Kapoor A, Vijayaraman P. Left bundle branch pacing: a comprehensive review. *J Cardiovasc Electrophysiol*. 2020;31(9):2462-2473. https://doi.org/10.1111/jce.14681
3. Huang W, Chen X, Su L, Wu S, Xia X, Vijayaraman P. A beginner's guide to permanent left bundle branch pacing. *Heart Rhythm*. 2019;16:1791-1796.
4. Ponnusamy SS, Vijayaraman P. Aborted ST-elevation myocardial infarction—an unusual complication of left bundle branch pacing. *Heart Rhythm Case Reports*. 2020;6(8):520-522. https://doi.org/10.1016/j.hrcr.2020.05.010
5. Martignani C, Diemberger I, Biffi M, et al. Troponin I rise after pacemaker implantation at the time of "universal definition of myocardial infarction". *Am J Cardiol*. 2009;103:1061-1065.
6. Nikolaou NI, Christou AH, Spanodimos SG, et al. Marked troponin elevation after implantation of a permanent antibradycardia pacemaker. *Hellenic J Cardiol*. 2011;52:489-492.
7. Manolis AS, Vassilikos V, Maounis T, et al. Detection of myocardial injury during radiofrequency catheter ablation by measuring serum cardiac troponin I levels: procedural correlates. *J Am Coll Cardiol*. 1999;34:1099-1105.
8. Haegeli LM, Kotschet E, Byrne J, et al. Cardiac injury after percutaneous catheter ablation for atrial fibrillation. *Europace*. 2008;10:273-275.
9. Huang W, Wu S, Vijayaraman P, et al. Cardiac resynchronization therapy in patients with nonischemic cardiomyopathy using left bundle branch pacing. *JACC Clin Electrophysiol*. 2020;6:849-858.

How to cite this article: Ponnusamy SS, Patel NR, Naperkowski A, Subzposh FA, Vijayaraman P. Cardiac troponin release following left bundle branch pacing. *J Cardiovasc Electrophysiol*. 2021;32:851-855. https://doi.org/10.1111/jce.14905

Indian Heart Journal 73 (2021) 117–120

Contents lists available at ScienceDirect

Indian Heart Journal

journal homepage: www.elsevier.com/locate/ihj

Research Brief

Feasibility, safety and outcomes of left bundle branch pacing in octogenarians

Shunmuga Sundaram Ponnusamy*, Dasarath Bopanna, Thabish Syed, Giridhar Muthu, Surya Kumar

Department of Cardiology, Velammal Medical College Hospital and Research Institute, Madurai, Tamilnadu, India

ARTICLE INFO

Article history:
Received 21 July 2020
Received in revised form
27 December 2020
Accepted 31 December 2020
Available online 6 January 2021

Keywords:
Physiological pacing
Octogenarians
Heart failure

ABSTRACT

Objectives: Left bundle branch pacing (LBBP) provides physiological pacing at low and stable threshold. The safety and efficacy of LBBP in elderly population is unknown. Our study was designed to assess the safety, efficacy and electrophysiological parameters of LBBP in octogenarian (≥80 years) population.
Results: LBBP was successful in 10 out of 11 patients. Mean age 82.1 ± 2.5 yrs. Follow up duration 7.7 months(range4–10). Indication for pacing included atrioventricular (AV) block 5 patients, Left bundle branch block (LBBB) with low ejection fraction (EF) 4 patients, sinus node dysfunction in 1. QRS duration reduced from 145.9 ± 27.7ms to 107.1 ± 9.5ms (*p* value0.00001) LV ejection fraction increased from 47.6% to 58.4% after LBBP (*p* value0.017). Pacing threshold was 0.58 ± 0.22 V and sensed R wave 17.35 ± 6.5 mV and it remained stable during follow up. LBBB with low EF patients also showed similar reduction in QRS duration along with improvement in LVEF.
Conclusion: LBBP is a safe and effective strategy (91% acute success) of physiological pacing in elderly patients. LBBP also provided effective resynchronization therapy in our small group of elderly patients. The pacing parameters remained stable over a period of 10 months follow up.

1. Introduction

Physiological pacing offers the advantage of capturing His-purikinje system directly thereby achieving synchronized ventricular contraction.[1] Although His bundle pacing (HBP) offers the most physiological form of pacing, it has some inherent limitations. Huang et al[2] reported direct capture of left bundle (LB) by deep septal pacing as an alternative to overcome the limitations of HBP. Though the safety of left bundle branch pacing (LBBP) has been established by several studies, the data for elderly population is lacking. This paper describes the feasibility, safety and electrophysiological properties of LBBP in octogenarians.

2. Methods

This is a retrospective, observational study conducted in our institute from march 2019 to march 2020 after getting institutional ethical committee approval. Patients provided written informed consent regarding LBBP as a non-standard approach. All patients aged between 80 and 89 years who were planned for permanent pacemaker implantation and those requiring cardiac resynchronization therapy (CRT) were included in the study. Patients who refused for the therapy were excluded.

The procedure was done as described by Huang et al[3] using C315 sheath and 3830 SelectSecure^{tm} lead (Medtronic, Minneapolis, MN). In brief, the pacing lead was placed deep inside the septum at a site 1–1.5 cm below the His bundle (Fig. 1A). LB capture was confirmed by presence of right bundle branch delay pattern (qR in lead V1) along with any one of the following criteria[4] (a) presence of LB potential (b) non-selective to selective LB capture during unipolar threshold measurement (Fig. 1B) (c) short and constant peak left ventricular activation time (pLVAT) < 80ms. (d) programmed stimulation from the pacing lead to show change in QRS morphology, duration and axis. Patients baseline characteristics and indications for pacing were documented. LVEF was measured by modified simpson's method.

* Corresponding author. Department of Cardiology, Velammal Village, Airport ring road, Velammal Medical college hospital and research institute, Madurai, 625009, India.
E-mail address: shunmuga.pgi@gmail.com (S.S. Ponnusamy).

https://doi.org/10.1016/j.ihj.2020.12.017

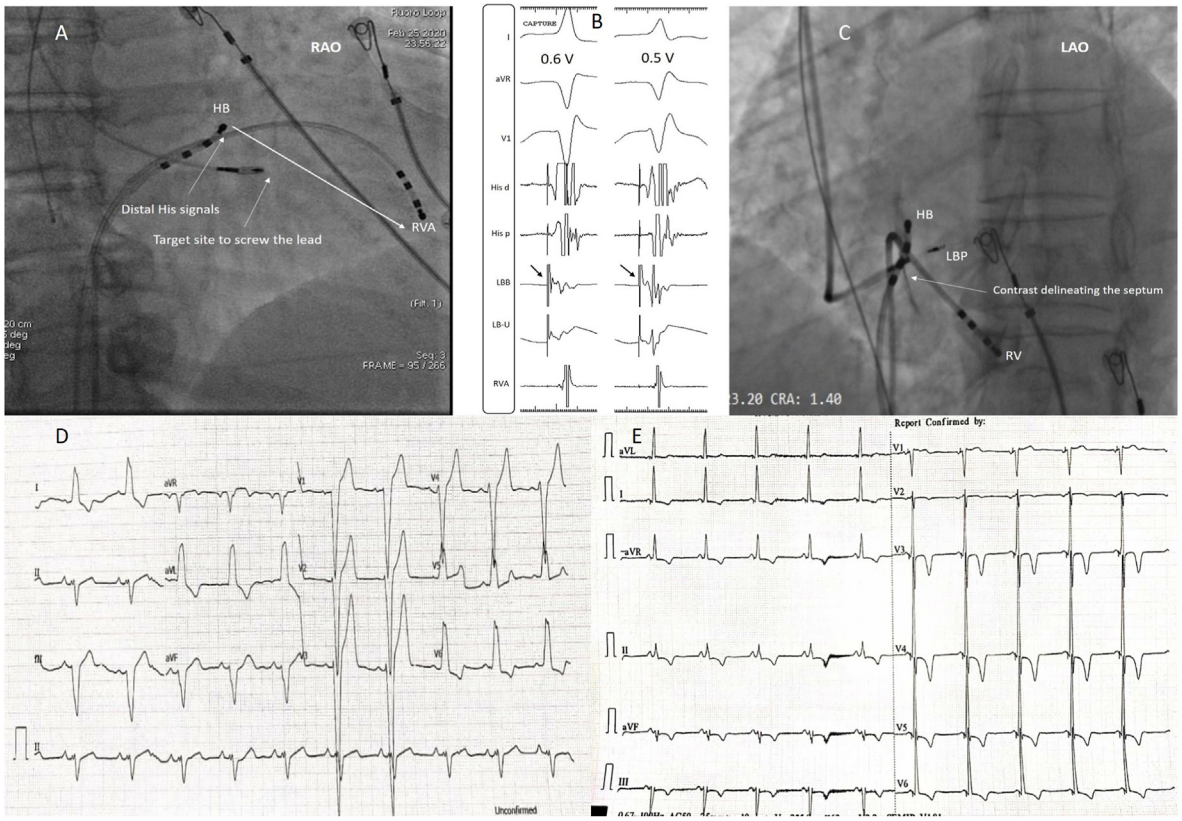

Fig. 1. LBBP for LBBB with low LVEF. A- RAO view showing the target site for the lead placement – 1.5 cm below distal His bundle (HB) along an imaginary line to RV apex (RVA). B – Non selective to selective LB capture as output reduced from 0.6 V to 0.5 V. Note the distinct LB lead electrogram after the pacing spike while selective capture along with change in QRS morphology from Qr to rSR in V1. C – Sheath angiography in LAO view showing the depth of the lead (LBP) inside the septum. D – Baseline ECG showing complete LBBB with QRS duration of 160ms. E– ECG after LBBP showing narrow QRS with T wave memory.

3. Results

11 patients satisfied the inclusion criteria. Successful LBBP could be performed in 10 out of 11 patients (91% acute success rate). In one patient with AV block, lead could not be penetrated deep and conventional RV lead was placed. Baseline and procedural characteristics are shown in Table 1. Mean age of the study population was 82.1 ± 2.5 years. The indication for pacemaker implantation was AV block in 5 patients, LBBB with low EF in 4 patients and sinus node dysfunction in one patient. The baseline QRS duration was 145.9 ± 27.7ms. Pre-procedural echocardiography showed mean EF of 47.6 ± 11.2% and septal thickness of 11.1 ± 0.7 mm.

The fluoroscopic time for LB lead placement was 17.9 ± 8.2 min. Non-selective to selective LB capture could be demonstrated in all patients (Fig. 1B). LB potential was noted in one patient. QRS duration was reduced to 107.1 ± 9.5ms (measured from the onset to the end;*p* value 0.00001). The pLVAT as measured in lead V5 (from pacing spike to peak of R wave) was 72.2 ± 5.3ms. The unipolar pacing threshold was 0.58 ± 0.22 V at 0.5ms pulse-width. The mean R wave amplitude was 17.35 ± 6.6 mV. The unipolar pacing impedance was 773.6 ± 112.9 Ω. All 4 patients with LBBB and low EF had complete correction of LBBB at low and stable threshold (Fig. 1C and D). No acute procedural complications noted.

3.1. Follow-up

The mean follow-up duration was 7.7 ± 1.9 months (range 4–10 months). The pacing threshold remained stable at 0.525 ± 0.07 V at 0.5ms pulse width and sensed R wave amplitude 15.6 ± 7.3 mV during follow up (Table 1B). The unipolar pacing impedance decreased to 663.1 ± 57.9 Ω (*p* value 0.002). Echocardiography showed significant improvement in LV ejection fraction from 47.6 ± 11.2% to 58.4 ± 3.7% (*p* value 0.017). The length of the lead inside the septum was 10.3 ± 0.82 mm. There was no acute or late lead dislodgement. There were no episodes of thrombo-embolism, pocket infection or mortality.

The findings are comparable to the general data on LBBP in Indian patients by our group where we showed 94% acute success rate with threshold of 0.59 ± 0.22 V and R wave of 14 ± 7 mV which remained stable over 12 months follow-up.[7] QRS duration was reduced from 144 ± 34ms to 110 ± 12ms along with improvement in LVEF from 44% to 53%.

3.2. Cardiac re-synchronization therapy

Four patients had undergone LBBP done for LBBB with low LVEF and normal epicardial coronaries. Three patients were symptomatic for the last four years and one had heart failure symptoms for two years. The age of onset of LBBB in these four patients were not known as serial ECGs were not available. The QRS duration was reduced from 169.7 ± 13.3ms to 111.5 ± 13.4ms and LVEF improved form 37.5 ± 8.8% to 57.7 ± 3.8% along with improvement in the NYHA functional class.

4. Discussion

Though multiple studies are available on feasibility and efficacy of LBBP,[5,6] there is no published data on safety of LBBP in elderly

Table 1
A- Baseline and procedural characteristics of the study population. B- Follow up data.

A	
Baseline and procedural Characteristics	
Total number of patients	11
Successful LB pacing	10 (91%)
Male	6
Female	4
Follow up (months)	7.7 (range 4–10 months)
Age in years	82.1 ± 2.5 years
Coronary artery disease	5 patients (50%)
Left ventricular function	
Ejection fraction <50%	7 patients
Ejection fraction >50%	3 patients
Pacing indications	
AV block	5 patients
LBBB with Low EF	4 patients
Sinus node dysfunction	1 patient
Procedural parameters	
LBBP fluoroscopy time (minutes)	17.9 ± 8.2 min
pLVAT (ms)	72.2 ± 5.3 ms

B	At implantation	Follow up (4–10 months)	*p* Value
Pacing Parameters			
Threshold (Unipolar)	0.58 ± 0.22 V	0.525 ± 0.07 V	0.23
R wave (mV)	17.35 ± 6.5 mV	15.65 ± 7.3 mV	0.26
Pacing Impedance (ohms)	773.6 ± 112.9 Ω	663.1 ± 57.9 Ω	0.002
ECG – QRS duration (Pre and Post)	145.9 ± 27.7ms (Pre)	107.1 ± 9.5 ms (post)	0.00001
LV ejection Fraction	47.6 ± 11.2%	58.4 ± 3.7%	0.017
Safety Parameters			
Lead dislodgement		Nil	
Late rise in Threshold by > 1 V		Nil	
Thrombo-embolic episodes		Nil	
Mortality		Nil	

patients. In this paper we have shown that LBBP could be successfully done in 10 out of 11 patients without any procedural complication. LBBP could reduce the QRS duration from 145.9 ± 27.7ms to 107.1 ± 9.5ms (*p* value 0.00001). LV ejection fraction improved from 47.6 ± 11.2% to 58.4 ± 3.7% (*p* value 0.017) during follow up. The lead parameters remained stable during follow up (Table 1B). All these findings are comparable to the published studies by other authors on LBBP[5,7,8]

Generally, CRT trials have excluded very old patients (>80 years old) and little data exist on outcomes of CRT in elderly.[9] Rigot et al,[10] in a retrospective study showed that the response to CRT was not compromised in patients aged >75 years with 14% mortality at the end of one year. Achilli et al[11] showed 2.4% LV lead dislodgement in patients aged >80 years undergoing CRT. Though similar clinical efficacy was noted as compared to those under 80 years, 17.3% mortality occurred during follow up of 12 months. LBBP could be safely done as an alternative for cardiac re-synchronization therapy in our small cohort aged ≥80 years. We could also show significant reduction in QRS duration along with improvement in LVEF in these patients. With the stable lead parameters and less procedural complication rate, LBBP has the potential to be an excellent alternative to CRT in elderly patients.

5. Conclusion

Left bundle branch pacing is a safe strategy of physiological pacing in octogenarians and we could show significant reduction in QRS duration and improvement in LV ejection fraction. Since it is a single center, retrospective observational study involving small numbers data cannot be extrapolated to general population. Further prospective, multicenter, randomized controlled trials will be required to assess the long safety of LBBP.

Key messages

1. Left bundle branch pacing is a novel strategy of physiological pacing with promising results
2. Safety and efficacy of LBBP in octogenarians are not well studied
3. This is the first study showing the feasibility and safety of LBBP with excellent mid-term outcomes
4. Cardiac resynchronization therapy by LBBP is feasible with promising results

Financial source

No funding or financial sources received for this study.

Declaration of competing interest

We have no conflicts of interest to disclose.

References

1. Vijayaraman P, Chung MK, Dandamudi G, et al. His bundle pacing. *J Am Coll Cardiol*. 2018;72:927–947.
2. Huang W, Su L, Wu S, et al. A novel pacing strategy with low and stable output: pacing the left bundle branch immediately beyond the conduction block. *Can J Cardiol*. 2017;33, 1736. e1–3.
3. Huang W, Chen X, Su L, et al. A beginner's guide to permanent left bundle branch pacing. *Heart Rhythm*. 2019;16:1791–1796.

4. Ponnusamy SS, Arora V, Namboodiri N, et al. Left bundle branch pacing: a comprehensive review. *J Cardiovasc Electrophysiol*. 2020 (article in press).
5. Vijayaraman P, Subzposh FA, Naperkowski A, et al. Prospective evaluation of feasibility, electrophysiologic and echocardiographic characteristics of left bundle branch area pacing. *Heart Rhythm*. 2019;16:1774–1782.
6. Zhang J, Wang Z, Cheng L, et al. Immediate clinical outcomes of left bundle branch area pacing vs conventional right ventricular pacing. *Clin Cardiol*. 2019;42:768–773.
7. Ponnusamy SS, Muthu G, Kumar M, et al. Mid-term feasibility, safety and outcomes of left bundle branch pacing – single center experience. *J Intervent Card Electrophysiol*. 2020. https://doi.org/10.1007/s10840-020-00807-w.
8. Li Y, Chen k, Dai Y, et al. Left bundle branch pacing for symptomatic bradycardia: implant success rate, safety, and pacing characteristics. *Heart Rhythm*. 2019;16:1758–1765.
9. Senni M, Tribouilloy CM, Rodeheffer RJ, et al. Congestive heart failure in the community. A study of all incident cases in Olmsted County, Minnesota, in 1991. *Circulation*. 1998;98:2282–2289.
10. Champ-Rigot L, Cornille AL, Ollitrault P, et al. Predictors of clinical outcomes after cardiac resynchronization therapy in patients ≥75 years of age: a retrospective cohort study. *BMC Geriatr*. 2019;19:325.
11. Achilli A, Turreni F, Gasparini M, et al. Efficacy of cardiac resynchronization therapy in very old patients: the Insync/Insync ICD Italian Registry. *Europace*. 2007;9:732–738.

JACC: CLINICAL ELECTROPHYSIOLOGY VOL. 7, NO. 2, 2021

PUBLISHED BY ELSEVIER

NEW RESEARCH PAPERS

CIED: PHYSIOLOGICAL PACING

Left Bundle Branch Area Pacing for Cardiac Resynchronization Therapy

Results From the International LBBAP Collaborative Study Group

Pugazhendhi Vijayaraman, MD,[a] ShunmugaSundaram Ponnusamy, MD, DM,[b] Óscar Cano, MD, PhD,[c] Parikshit S. Sharma, MD, MPH,[d] Angela Naperkowski, RN, CEPS, CCDS,[a] Faiz A. Subsposh, MD,[a] Pawel Moskal, MD, PhD,[a] Agnieszka Bednarek, MD, PhD,[e] Alexander R. Dal Forno, MD,[f] Wilson Young, MD, PhD,[a] Sudip Nanda, MD,[g] Dominik Beer, DO,[a] Bengt Herweg, MD,[h] Marek Jastrzebski, MD, PhD[e]

ABSTRACT

OBJECTIVES The aim of this study was to assess the feasibility and outcomes of left bundle branch area pacing (LBBAP) in patients eligible for cardiac resynchronization therapy (CRT) in an international, multicenter, collaborative study.

BACKGROUND CRT using biventricular pacing is effective in patients with heart failure and left bundle branch block (LBBB). LBBAP has been reported as an alternative option for CRT.

METHODS LBBAP was attempted in patients with left ventricular ejection fraction (LVEF) <50% and indications for CRT or pacing. Procedural outcomes, left bundle branch capture, New York Heart Association functional class, heart failure hospitalization, echocardiographic data, and lead complications were recorded. Clinical (no heart failure hospitalization and improvement in New York Heart Association functional class) and echocardiographic responses (≥5% improvement in LVEF) were assessed.

RESULTS LBBAP was attempted in 325 patients, and CRT was successfully achieved in 277 (85%) (mean age 71 ± 12 years, 35% women, ischemic cardiomyopathy in 44%). QRS configuration at baseline was LBBB in 39% and non-LBBB in 46%. Procedure and fluoroscopy duration were 105 ± 54 and 19 ± 15 min, respectively. LBBAP threshold and R-wave amplitudes were 0.6 ± 0.3 V at 0.5 ms and 10.6 ± 6 mV at implantation and remained stable during mean follow-up of 6 ± 5 months. LBBAP resulted in significant QRS narrowing from 152 ± 32 to 137 ± 22 ms ($p < 0.01$). LVEF improved from 33 ± 10% to 44 ± 11% ($p < 0.01$). Clinical and echocardiographic responses were observed in 72% and 73% of patients, respectively. Baseline LBBB (odds ratio: 3.96; 95% confidence interval: 1.64 to 9.26; $p < 0.01$) and left ventricular end-diastolic diameter (odds ratio: 0.62; 95% confidence interval: 0.49 to 0.79; $p < 0.01$) were independent predictors of echocardiographic response.

CONCLUSIONS LBBAP is feasible and safe and provides an alternative option for CRT. LBBAP provides remarkably low and stable pacing thresholds and was associated with improved clinical and echocardiographic outcomes.
(J Am Coll Cardiol EP 2021;7:135–47) © 2021 by the American College of Cardiology Foundation.

From the [a]Geisinger Heart Institute, Wilkes-Barre, Pennsylvania, USA; [b]Division of Cardiology, Velammal Medical College, Madurai, India; [c]Division of Cardiology, Hospital Universitari i Politècnic La Fe, Valencia, Spain; [d]Rush University Medical Center, Chicago, Illinois, USA; [e]First Department of Cardiology, Interventional Electrocardiology and Hypertension, Jagiellonian University, Medical College, Krakow, Poland; [f]SOS Cardio Hospital, Florinapolis, Brazil; [g]Division of Cardiology, St. Luke's University Health System, Bethlehem, Pennsylvania, USA; and the [h]Division of Cardiology, University of South Florida, Tampa, Florida, USA.
The authors attest they are in compliance with human studies committees and animal welfare regulations of the authors' institutions and Food and Drug Administration guidelines, including patient consent where appropriate. For more information, visit the Author Center.

Manuscript received June 9, 2020; revised manuscript received August 6, 2020, accepted August 6, 2020.

ISSN 2405-500X/$36.00 https://doi.org/10.1016/j.jacep.2020.08.015

ABBREVIATIONS AND ACRONYMS

BVP = biventricular pacing

CRT = cardiac resynchronization therapy

HBP = His bundle pacing

ICM = ischemic cardiomyopathy

LBBAP = left bundle branch area pacing

LBB = left bundle branch

LBBB = left bundle branch block

LV = left ventricular

LVEDD = left ventricular end-diastolic diameter

LVEF = left ventricular ejection fraction

NICM = nonischemic cardiomyopathy

NYHA = New York Heart Association

Cardiac resynchronization therapy (CRT) using biventricular pacing (BVP) is a well-established therapy for patients with cardiomyopathy, reduced left ventricular ejection fractions (LVEFs), heart failure, and left bundle branch block (LBBB). Several prospective randomized studies have shown that BVP improves quality of life, increases exercise capacity, reduces heart failure hospitalization, and decreases all-cause mortality (1–5). BVP is

SEE PAGE 148

also an accepted therapy for patients undergoing atrioventricular node ablation and those requiring >40% right ventricular pacing (6). However, up to one-third of patients treated with BVP may not derive clinical or echocardiographic benefit, and some may worsen (1,3,7). Recently, permanent His bundle pacing (HBP) has emerged as an acceptable alternative to deliver physiological ventricular pacing and is a Class IIa recommendation in patients with atrioventricular block and LVEFs of 35% to 50% (8) and a Class I recommendation for patients with tachycardiomyopathy undergoing atrioventricular node ablation (9). Several observational studies using HBP have demonstrated improved clinical and echocardiographic outcomes in patients with LBBB and left ventricular (LV) dysfunction (10–12). However, HBP may be associated with higher pacing thresholds to correct LBBB and lower success rates in addition to increased incidence of lead revisions (10–12). Intraseptal left bundle branch area pacing (LBBAP) is a novel technique to pace the conduction system beyond the site of block and is associated with low and stable capture thresholds (13–15). Recently LBBAP has been shown to restore LV synchrony in patients with LBBB (16). LBBAP has the potential advantage of backup LV septal capture in addition to left bundle branch (LBB) capture in these patients. The

FIGURE 1 LBBAP in a Patient With LBBB

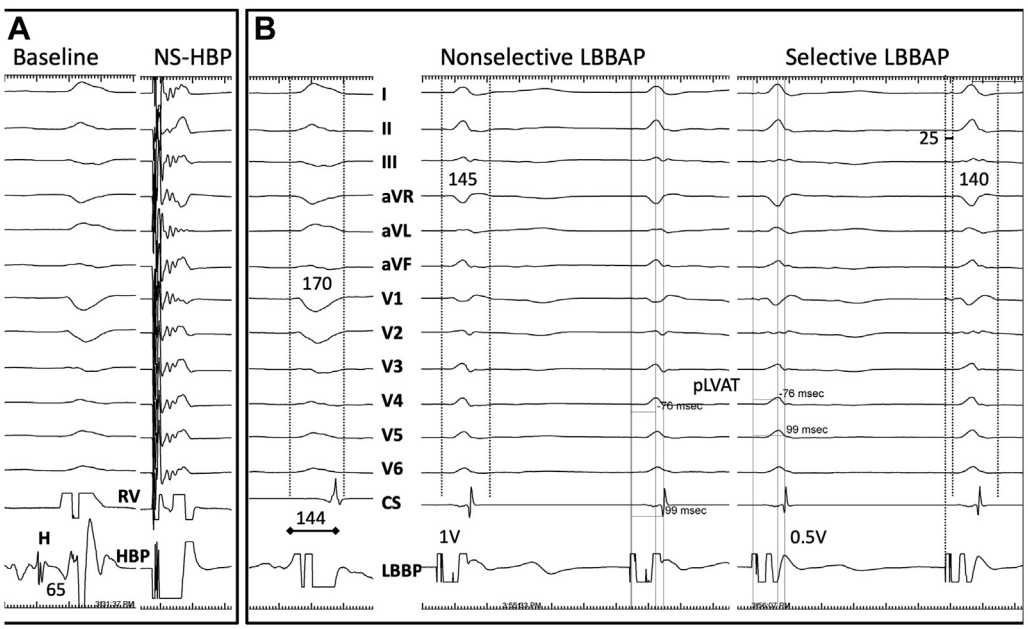

Twelve-lead electrocardiogram and intracardiac electrograms are shown at a sweep speed of 100 mm/s. **(A)** Left bundle branch block (LBBB) is corrected by nonselective His bundle pacing (NS-HBP) at high output. **(B)** At baseline, the surface QRS onset to left ventricular activation (Q-LV) in the coronary sinus (CS) lead was 144 ms. During decremental, asynchronous left bundle branch area pacing (LBBAP) from 1 to 0.5 V, transition from nonselective LBBAP (left ventricular [LV] septal + left bundle branch [LBB] capture) to selective LBBAP (LBB-only capture) is seen. Note that the stimulus to LV activation time in the CS lead and peak LV activation time (pLVAT) in leads V_4 to V_6 remain unchanged at 99 and 76 ms, respectively. QRS duration decreased from 170 ms at baseline to 145 ms with nonselective LBBAP and 140 ms during selective LBBAP with stimulus to QRS onset of 25 ms. RV = right ventricle.

FIGURE 2 Echocardiographic and Fluoroscopic Visualization of LBBAP Lead

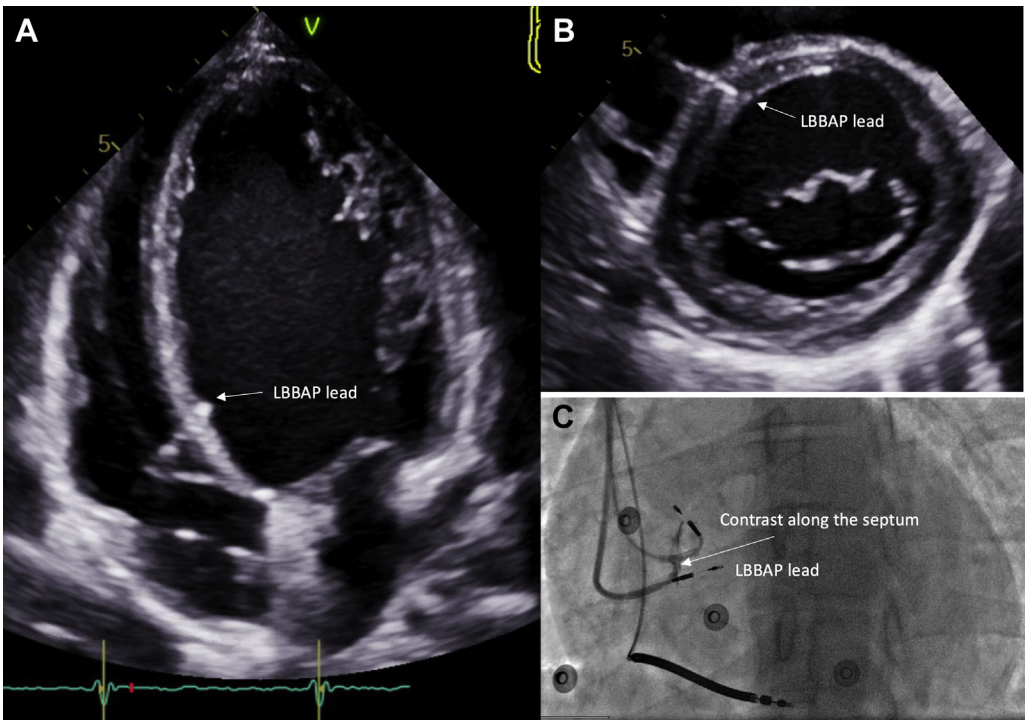

(A) Apical 4-chamber echocardiographic view shows the location of the left bundle branch area pacing (LBBAP) lead in the proximal interventricular septum. **(B)** Short-axis view demonstrating the lead tip in the basal septum. **(C)** Fluoroscopic view in left anterior oblique projection at 30° shows contrast delineating the right ventricular septum and the depth of the LBBAP lead.

aim of this multicenter study was to assess the feasibility and outcomes of LBBAP in CRT-eligible patients or those who had CRT was unsuccessful.

METHODS

STUDY POPULATION. This was a retrospective, multicenter, observational cohort study designed to evaluate the real-world experience of LBBAP. The study population included all patients who had LBBAP was attempted to achieve CRT at 8 centers (4 in the United States, 1 in Spain, 1 in India, 1 in Brazil, and 1 in Poland). All patients had New York Heart Association (NYHA) functional class II to IV heart failure symptoms, baseline LVEFs ≤50%, and indications for ventricular pacing and/or CRT. Patients provided informed consent and demonstrated an understanding of LBBAP as a nonstandard approach to achieve cardiac resynchronization. Baseline patient demographics together with relevant clinical information (QRS configuration and QRS duration, presence of coronary artery disease, hypertension, diabetes, etc.) were recorded. LBBB was defined as QRS duration >140 ms in men (>130 ms in women) and the presence of at least 2 mid-QRS notches or slurs in leads I, aVL, V_1, V_2, V_5, and V_6. Data collection was approved by the Institutional Review Board at each site.

PROCEDURAL DETAILS. At centers with extensive experience, HBP was attempted first, and if satisfactory electric outcomes (acceptable His capture or bundle branch block correction thresholds) were not achieved, LBBAP was attempted (**Figure 1**). At other centers, LBBAP was chosen as the first-line therapy without attempting HBP. LBBAP was also attempted when coronary sinus lead placement was unsuccessful. LBBAP was performed using the SelectSecure pacing lead (model 3830, 69 cm, Medtronic, Minneapolis, Minnesota) as previously described (17). The lead was delivered through a fixed curve sheath (C315His, Medtronic) or a deflectable sheath (C304His, Medtronic). Briefly, the His bundle region was mapped with the lead and marked as a reference image, and the sheath and lead were advanced about 1 to 2 cm apical (right anterior oblique projection) in the right ventricular septum. The lead was then rapidly rotated

FIGURE 3 Demonstration of LBB Potential in a Patient With LBBB

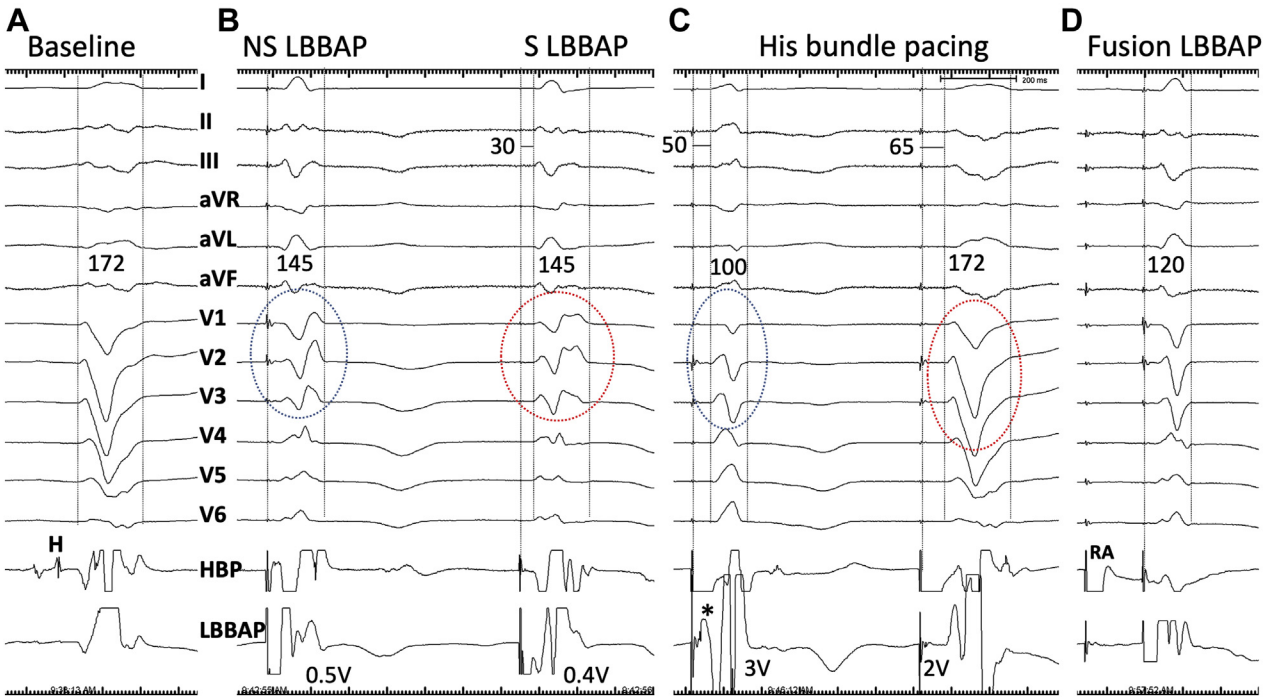

(A) Baseline LBBB with QRS duration (QRSd) of 170 ms and HV interval of 45 ms is shown. Note the absence of potentials in the LBBAP lead due to proximal conduction block. **(B)** During threshold testing from LBBAP lead, nonselective (NS) **(blue circle)** to selective (S) LBB capture **(red circle)** is seen. **(C)** Selective HBP with **(blue circle)** and without **(red circle)** LBBB correction is shown. During corrective HBP, LBB potentials with injury current **(asterisk)** is clearly seen. **(D)** Sequential DDD pacing with right atrial (RA) to LBBAP at 150-ms delay shows normalization of QRS configuration due to fusion with native conduction via right bundle branch. QRSd and stimulus to QRS onset intervals during pacing are shown. Abbreviations as in Figure 1.

until it penetrated deep into the interventricular septum. Unipolar-tip paced QRS configuration and pacing impedance were monitored along with measurement of peak LV activation times in leads V_4 to V_6 (Figure 1B). The depth of the lead in the interventricular septum was assessed by contrast injection via the sheath in the left anterior oblique projection (Figure 2). Presence of Purkinje potentials recorded from the LBBAP lead and the potential to QRS onset intervals (LBB-V) were documented. Pacing thresholds were assessed by evaluating the transition from nonselective to selective LBB capture (Figure 3) or nonselective LBB capture to LV septal myocardial capture. These phenomena were usually observed at near threshold pacing outputs. If primary LBBAP was unsuccessful, an LV lead was implanted via the traditional coronary venous approach in patients who had conduction system pacing was chosen as the initial approach.

DETERMINATION OF LBB CAPTURE. During unipolar-tip pacing, right bundle branch configuration was observed in addition to 1 or more of the following findings: 1) LBB potentials (LBB-V intervals of 15 to 35 ms); 2) transition from nonselective to selective LBB capture; 3) transition from nonselective LBB capture to left septal capture at near threshold outputs (Figure 4); 4) short and constant peak LV activation time (stimulus to peak of the R wave in leads V_4 to V_6 [peak LV activation time]) of <90 ms at high- and low-output pacing; and 5) programmed (extra-stimulus testing) deep septal stimulation to differentiate LV septal versus nonselective LBB capture (Supplemental Figure S1) (14,17,18). If LBB capture could not be confirmed, only LV septal capture was considered to be present.

FOLLOW-UP. Patients were followed in the device clinic at 2 weeks, 3 months, and 1 year and by remote monitoring every 3 months. R-wave amplitudes, capture thresholds, lead impedance, and percentage of ventricular pacing were recorded at each visit. All capture thresholds were defined using a pulse width of 0.5 ms. QRS duration during pacing was measured from stimulus to the end of the QRS complex. In patients with LBBB and normal PR intervals, further QRS narrowing was achieved by fusing with native

FIGURE 4 Nonselective to LV Septal Capture During LBBAP

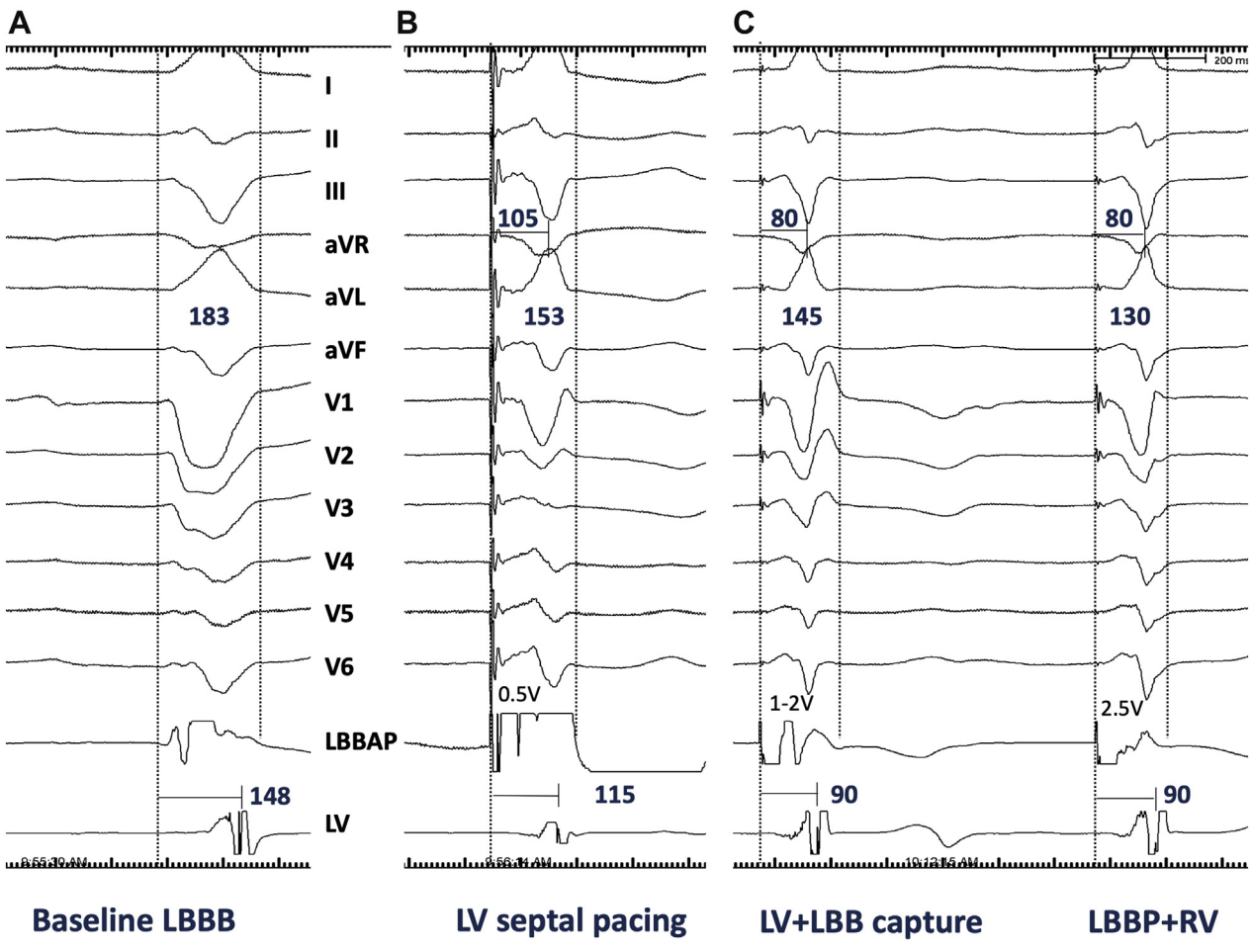

(A) Baseline LBBB with QRSd of 183 ms and Q-LV of 148 ms is shown. **(B)** Unipolar LBBAP at threshold shows LV septal capture only with QRSd of 153 ms, pLVAT of 105 ms, and stimulus to LV activation time of 115 ms. **(C)** Bipolar pacing at 1 to 2 V resulted in nonselective LBB capture with QRSd of 145 ms and at 2.5 V resulted in anodal right ventricular septal capture in addition to nonselective LBBAP, resulting in further narrowing of QRSd to 130 ms. Note the pLVAT and stimulus to LV activation time are further reduced to 80 and 90 ms. pLVAT was measured in lead aVL as a surrogate because of slurred R waves in leads V_4 to V_6. Abbreviations as in Figures 1 and 3.

conduction (Figure 3D). Lead-related complications were routinely tracked. Echocardiographic indexes, including LVEF, LV end-diastolic diameter (LVEDD), and LV volumes, were recorded pre-implantation and at 3- to 6-month follow-up. Change in NYHA functional class, any heart failure-related hospitalizations, and death of any cause were recorded.

Echocardiographic response was defined as a ≥5% increase in LVEF. Superresponse was defined as an absolute improvement in LVEF of ≥20% or improvement in LVEF to >50% (in patients with LVEFs ≤35%) between baseline and follow-up echocardiography (19). Clinical response to CRT was defined as an improvement in NYHA functional class by at least 1 class and no heart failure hospitalization (18). Heart failure hospitalization was defined as a hospital admission or an urgent care visit for intensive treatment for heart failure with intravenous diuretic agents or intravenous inotropic medications.

STATISTICAL ANALYSIS. Values are expressed as frequencies and percentages for categorical variables and as mean ± SD or median (interquartile range) for continuous variables. Descriptive statistics were reported for the full sample and stratified by various subgroups, such as type of cardiomyopathy, baseline conduction disease, and whether conduction system pacing was first-line or a bailout procedure. Comparison between groups was accomplished using

TABLE 1 Baseline Characteristics

	All Patients (N = 325)	Successful LBBP (n = 277)	Unsuccessful LBBP (n = 48)	p Value
Age	71 ± 12	70 ± 13	75 ± 8	0.03
Female	113 (35)	101 (36)	12 (25)	0.07
Medical history				
HTN	224 (69)	188 (68)	36 (75)	0.11
DM	113 (35)	100 (36)	13 (27)	0.08
CAD	161 (50)	126 (46)	35 (73)	0.01
AF	184 (57)	166 (60)	18 (38)	0.01
Ischemic cardiomyopathy	144 (44)	114 (41)	30 (63)	0.01
Baseline NYHA functional class III or IV	209 (64)	184 (68)	25 (52)	0.24
Baseline NYHA functional class	2.7 ± 0.7	2.7 ± 0.7	2.5 ± 0.7	0.92
Echocardiographic parameters				
LVEF	32 ± 12	33 ± 10	27 ± 10	0.06
LVEDD, mm	57 ± 10	56 ± 9	61 ± 9	0.03
LVESV, ml	115 ± 70	114 ± 68	124 ± 81	0.45
LVEDV, ml	170 ± 86	169 ± 84	175 ± 90	0.18
LA volume index, ml/m^2	58 ± 22	58 ± 23	59 ± 16	0.92
IVSD, mm	11.6 ± 3	11.4 ± 2	14 ± 3	0.04
Electrocardiographic parameters				
Baseline QRS duration, ms	154 ± 32	152 ± 32	169 ± 35	0.02
Baseline QRS duration >150 ms	198 (61)	168 (62)	30 (63)	0.86
LBBB	126 (39)	116 (42)	10 (21)	0.02
RBBB	54 (17)	48 (17)	6 (13)	0.81
IVCD	49 (15)	32 (12)	17 (35)	0.02
RV paced	48 (14.5)	36 (13)	12 (25)	0.06
Narrow	48 (14.5)	45 (16)	3 (6)	0.62

Values are mean ± SD or n (%).

AF = atrial fibrillation; CAD = coronary artery disease; DM = diabetes mellitus; HTN = hypertension; IVCD = intraventricular conduction delay; IVSD = interventricular septal diameter; LA = left atrial; LBBB = left bundle branch block; LVEDD = left ventricular end-diastolic diameter; LVEDV = left ventricular end-diastolic volume; LVEF = left ventricular ejection fraction; LVESV = left ventricular end-systolic volume; NYHA = New York Heart Association; RBBB = right bundle branch block; RV = right ventricular.

the chi-square or Fisher exact test and the 2-sample Student's *t*-test or Wilcoxon rank sum test. Comparisons of continuous variables within groups were carried out using the paired Student's *t*-test or Wilcoxon signed rank test. Univariate logistic regression analyses were used to estimate the odds ratios for achieving echocardiographic response as defined earlier for various baseline characteristics. Multivariate regression analysis was then performed on variables with odds ratios with p values <0.10. A backward stepwise regression method was then used to determine the final multivariate regression model. Statistical analysis was performed using SPSS version 25 (SPSS, Chicago, Illinois). A p value of <0.05 was considered to indicate statistical significance.

RESULTS

BASELINE CHARACTERISTICS. LBBAP was attempted in 325 patients at the 8 implanting centers. Baseline characteristics of the entire study population are shown in Table 1. The mean age of the patients was 71 ± 12 years (35% women). All patients had cardiomyopathy at baseline, with a mean LVEF of 32 ± 12% (68% with LVEFs ≤35%); 64% of patients were in NYHA functional class III or IV. Ischemic cardiomyopathy (ICM) and non-ischemic cardiomyopathy (NICM) were present in 44% and 56% of the patients, respectively; 39% had underlying LBBB, 46.5% had non-LBBB (14.5% had ventricular paced rhythm, 17% had right bundle branch block, 15% had intraventricular conduction defects), and the remaining 14.5% of patients had narrow QRS complexes. Baseline QRS duration was 154 ± 32 ms. Patients were followed for an average duration of 6 ± 5 months (median 5 months; range 1 to 23 months).

PROCEDURAL OUTCOMES. The approach to CRT was quite variable among the centers and also varied among the operators within centers. His bundle electrogram mapping and pacing were attempted prior to performing LBBAP in 133 patients (Figures 1 and 3). LBBAP was attempted as the primary approach to CRT in 157 patients. In 35 patients, LBBAP was used as a rescue attempt after failed coronary sinus lead placement.

Permanent LBBAP was achieved in 277 of 325 patients (85%) and was unsuccessful in 48 patients because of inability to penetrate the septum (21 patients) and inadequate electric resynchronization (27 patients). BVP with coronary sinus lead placement was performed in all but 4 patients who had LBBAP was unsuccessful. Patients in the unsuccessful group were older, had ICM, had larger LVEDDs, had thicker interventricular septa, had wider baseline QRS duration, and had intraventricular conduction defects (Table 1). The presence of LBBB (defined by Strauss criteria) predicted success with LBBAP (92%). LBBAP was successful in 32 of 35 patients (91%) who had coronary sinus lead placement was initially unsuccessful.

Procedural outcomes are noted in Table 2. In patients receiving CRT devices (58%), the LBBAP lead was connected to the LV port (LV-to-right ventricular offset was maximized to achieve functional right ventricular noncapture). In 5 patients with chronic atrial fibrillation and need for ICDs, the LBBAP lead was connected to the atrial port (the device was programmed to DDIR mode to prevent right ventricular pacing). In patients receiving dual-chamber pacemakers (n = 87 [31%]), the LBBAP lead was connected to the right ventricular port. In patients with LBBB and normal PR intervals (<200 ms), the atrioventricular delay was optimized to achieve fusion

correction of right bundle branch block pattern induced by LBBAP (Figure 3D).

The average procedure duration and fluoroscopy time were 105 ± 54 and 19 ± 15 min, respectively. The fluoroscopy time for LBBAP lead placement (when available; n = 153) was 15 ± 13 min (range 1.2 to 62 min).

LBB CAPTURE. Evidence for LBB capture was observed in 255 of 277 patients (92%). Electrocardiographic changes to suggest delayed right ventricular depolarization (rSR′ or qR pattern in lead V_1 or deep S in lead V_6) during LBBAP was observed in all but 10 patients. LBB potentials were observed in 98 of 277 patients (35%). In patients with LBBB, potentials were observed during corrective HBP (Figure 3 and Supplemental Figure S2C) or during premature ventricular complexes in 12 patients. During threshold testing, transition from nonselective to selective LBB capture at near threshold output was observed in 93 patients (Figures 1B and 3B), and transition from nonselective to LV septal capture (Figure 4) was observed in 55 patients. Programmed stimulation was used to prove conduction system capture in 49 patients. Mean stimulus to peak LV activation time during LBBAP was 83 ± 16 ms. Peak LV activation time >90 ms was observed in 62 patients, the majority of whom had underlying intraventricular conduction defects (Figure 5) or right ventricular pacing at baseline.

PACING OUTCOMES. Average LBBAP capture threshold and R-wave amplitudes at implantation were 0.6 ± 0.3 V at 0.5 ms and 10.6 ± 6 mV, respectively, and remained unchanged (0.7 ± 0.3 V at 0.5 ms and 12.5 ± 5.7 mV) during a mean follow-up duration of 6 ± 5 months. Pacing impedance decreased significantly from 674 ± 193 Ω at implantation to 530 ± 123 Ω during follow-up. Lead dislodgements into the right ventricular cavity were observed in 5 patients: in 3 patients lead dislodgements occurred within 24 h, and in 2 patients they were observed at 2-week follow-up. In 2 other patients, loss of LV septal/LBB capture (no right bundle branch block pattern) was noted within 24 h, while midseptal/right ventricular capture was still maintained. Pneumothorax was seen in 3 patients, pocket hematoma requiring evacuation in 2 patients, and device infection requiring system explantation in 2 patients. acute perforation of the lead into the LV cavity during implantation as determined by high capture threshold, low impedance, and small R waves was recognized in 10 patients. In these patients, the lead was removed and repositioned at a different location. No patient developed late perforation of the lead into the LV cavity or stroke during follow-up.

TABLE 2 Procedural Outcomes

Procedural outcomes			
Total number of successful cases		277 (85)	
Procedure duration (min)		105 ± 54	
Fluoroscopy duration (min)		19 ± 15	
LBBP lead fluoroscopy time (n = 153) (min)		16 ± 13	
Type of device			
CRT		162 (58)	
CRT pacemaker		56 (20)	
CRT defibrillator		106 (38)	
Dual-chamber defibrillator		5 (2)	
Dual-chamber pacemaker (DDD)		87 (31)	
Single-chamber pacemaker (VVI)		23 (8)	
Pacing characteristics	Baseline	Follow-up	p value
R-wave amplitude (mV)	10.6 ± 6	12.5 ± 5.7	0.06
Impedance (Ω)	674 ± 193	530 ± 123	<0.001
LBBP threshold (V at 0.5 ms)	0.6 ± 0.3	0.7 ± 0.3	0.17
Stimulus to peak LV activation time (ms)	83 ± 16		
Complications			
Pneumothorax		3 (1)	
Pericardial effusion		0	
Device infection		2 (0.7)	
Stroke		0	
LV perforation		0	
Lead dislodgement		7 (2.5)	
Loss of left septal capture		2 (0.7)	

Values are n (%) or mean ± SD.
CRT = cardiac resynchronization therapy; LBBP = left bundle branch pacing; LV = left ventricular.

ELECTROCARDIOGRAPHIC AND ECHOCARDIOGRAPHIC PARAMETERS. Overall, QRS duration decreased from 152 ± 32 ms at baseline to 137 ± 22 ms ($p < 0.01$) during LBBAP (Table 3). Patients with baseline LBBB had more dramatic QRS narrowing (from 162 ± 24 ms to 133 ± 22 ms; $p < 0.01$). The reduction in QRS duration in patients with non-LBBB (baseline right bundle branch block, intraventricular conduction defects, or right ventricular pacing) was less than that observed in patients with LBBB ($p < 0.01$) (Supplemental Table S1). Although QRS duration decreased in patients with ICM and NICM compared with baseline, this reduction was greater in patients with NICM ($p < 0.01$) (Supplemental Table S1).

Follow-up echocardiographic data were available for 202 of 277 patients (73%) (Table 3). Echocardiographic response (≥5% improvement in LVEF) was noted in 148 patients (73%) (68% of those with ICM and 77% of those with NICM) (Supplemental Table S1). Response rates were greater among patients with LBBB compared with those with non-LBBB (87% vs. 67%; $p < 0.01$). Overall, LVEF improved significantly from 33 ± 10% at baseline to 44 ± 11% at follow-up ($p < 0.01$). Improvement in LV function was

FIGURE 5 LBBAP in a Patient With an Intraventricular Conduction Defect

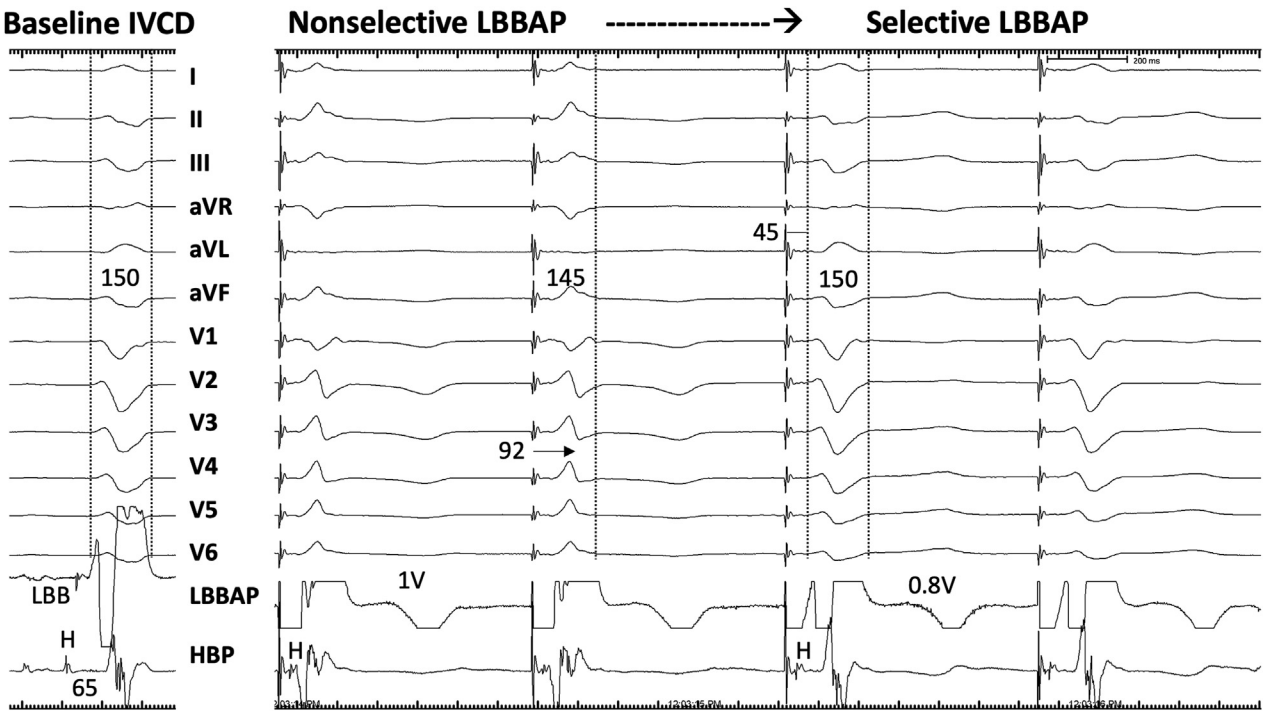

Electrograms from the LBBAP lead show an LBB potential in this patient with an LBBB-type intraventricular conduction defect (IVCD) and HV interval of 65 ms. LBBAP at 1 V demonstrated nonselective LBB capture with pLVAT of 92 ms and QRSd of 145 ms. Pacing at 0.8 V resulted in loss of left septal capture and demonstrated selective capture of the LBB with QRS configuration identical to native complex. LV ejection fraction improved from 36% at baseline to 44% during follow-up. Abbreviations as in Figures 1 and 3.

noted in patients with ICM and those with NICM and similarly in patients with LBBB and those with non-LBBB.

Among patients with LVEFs ≤35% (n = 131), LVEF increased from 27 ± 7% to 40 ± 121% ($p < 0.01$); 41 patients (31%) met the criteria for superresponse (18% of those with vs. 41% of those with NICM [$p < 0.01$], 38% of those with vs. 24% of those with non-LBBB [$p = 0.09$] (Supplemental Table S1). There were significant reductions in LVEDD (from 56 ± 9 mm to 54 ± 9 mm; $p < 0.01$), LV end-diastolic volume (from 169 ± 84 ml to 142 ± 69 ml; $p < 0.01$), and LV end-systolic volume (from 114 ± 68 to 83 ± 52 ml; $p < 0.01$).

PREDICTORS OF ECHOCARDIOGRAPHIC RESPONSE. Univariate analysis of the cohort with successful LBBAP and follow-up echocardiography (n = 202) showed that baseline LBBB, a wide baseline QRS complex, a greater reduction in QRS duration during pacing, and a shorter stimulus to peak LV activation time were predictive of echocardiographic response. Non-LBBB, narrow QRS configuration, and greater LVEDD at baseline were associated with a lower likelihood of echocardiographic response (Figure 6). There was a trend toward a tendency of response in women and patients with NICM. In a multivariate analysis, LVEDD and baseline LBBB remained predictors of echocardiographic response (odds ratios: 0.62 [95% confidence interval: 0.49 to 0.71] and 3.90 [95% confidence interval: 1.64 to 9.26], respectively; $p < 0.01$).

Univariate analysis identified reduction of paced QRS duration, LVEF, LVEDD, and NICM as predictors of echocardiographic superresponse to LBBAP. Multivariate analysis revealed that baseline LVEDD and reduced QRS duration with LBBAP pacing predicted echocardiographic superresponse (odds ratios: 0.66 [95% confidence interval: 0.50 to 0.86] and 1.29 [95% confidence interval: 1.14 to 1.49], respectively; $p < 0.01$) (Supplemental Table S2).

CLINICAL OUTCOMES. Clinical response (improvement by 1 NYHA functional class and no heart failure hospitalization) to LBBAP was noted in 157 of 207

TABLE 3 Clinical Parameters Before and After Pacing in Patients Who Underwent LBBAP

	All (N = 277)			ICM (n = 114)			NICM (n = 163)			LBBB (n = 116)			Non-LBBB (n = 116)		
	Baseline	LBBAP	p Value	Baseline	LBBAP	p Value	Baseline	LBBAP	p Value	Baseline	LBBAP	p Value	Baseline	LBBAP	p Value
Electrocardiographic response															
QRS duration, mm	152 ± 32	137 ± 22	<0.01	150 ± 34	143 ± 23	0.07	154 ± 31	133 ± 21*	<0.01	162 ± 24	133 ± 22†	<0.01	160 ± 28	143 ± 23	<0.01
Clinical response															
NYHA functional class	2.7 ± 0.7	1.8 ± 0.6	<0.01	2.7 ± 0.7	1.8 ± 0.7	<0.01	2.7 ± 0.7	1.7 ± 0.7	<0.01	2.8 ± 0.6	1.7 ± 0.7	<0.01	2.7 ± 0.7	1.8 ± 0.7	<0.01
Echocardiographic response															
LVEF	33 ± 10	44 ± 11	<0.01	33 ± 9	42 ± 11	<0.01	33 ± 10	45 ± 11	<0.01	30 ± 8	44 ± 11	<0.01	33 ± 10	43 ± 12	<0.01
LVEF (≤35% baseline)	27 ± 7	40 ± 11	<0.01	28 ± 6	38 ± 11	<0.01	27 ± 7	41 ± 12	<0.01	28 ± 6	42 ± 10	<0.01	27 ± 7	38 ± 12	<0.01
LVEF (36%–50% baseline)	42 ± 5	50 ± 8	<0.01	42 ± 5	49 ± 8	<0.01	42 ± 7	51 ± 7	<0.01	41 ± 5	52 ± 7	<0.01	43 ± 6	50 ± 8	<0.01
LVEDD	56 ± 9	54 ± 9	<0.01	57 ± 9	55 ± 9	0.13	56 ± 10	53 ± 9	0.02	57 ± 9	54 ± 9	0.01	57 ± 10	55 ± 9	0.12
LVESV	114 ± 68	83 ± 52	<0.01	119 ± 66	84 ± 55	<0.01	111 ± 70	82 ± 51	<0.01	123 ± 63	85 ± 56	<0.01	114 ± 76	83 ± 49	<0.01
LVEDV	169 ± 84	142 ± 69	<0.01	175 ± 84	140 ± 74	<0.01	165 ± 85	143 ± 66	0.03	181 ± 79	149 ± 78	<0.01	168 ± 92	139 ± 60	0.02

Values are mean ± SD. Values of $p < 0.05$ were considered to indicate statistical significance. Non-LBBB includes right bundle branch block, intraventricular conduction delay, and right ventricular pacing. *$p < 0.01$ compared with ICM. †$p < 0.01$ compared with non-LBBB.

ICM = ischemic cardiomyopathy; NICM = nonischemic cardiomyopathy; other abbreviations as in Table 1.

patients (72%) (80% of those with LBBB vs. 67% of those with non-LBBB [p = 0.03], 76% of those with ICM vs. 70% of those with NICM [p = 0.31]) (Supplemental Table S1). Overall, NYHA functional class improved from 2.7 ± 0.7 at baseline to 1.8 ± 0.7 on follow-up ($p < 0.01$). During follow-up, 15 patients were admitted with heart failure hospitalization (5.4%), and 11 patients (4%) died (cardiovascular causes in 6, noncardiovascular causes in 3, and indeterminate causes in 2).

DISCUSSION

The main findings of this retrospective, observational study are as follows: 1) CRT using LBBAP as an alternative approach is feasible in the majority of patients and is associated with few complications; 2) LBBAP resulted in changes in the cardiac variables of QRS duration, LVEF, LV dimensions and volumes, and NYHA functional class (**Central Illustration**); 3) LBBB at baseline and QRS duration reduction with pacing were independent predictors of echocardiographic response and superresponse, respectively; and 4) greater LVEDD was an independent predictor of a lower likelihood of echocardiographic response and superresponse.

Permanent HBP has been shown to achieve maximal electric resynchronization in patients with proximal LBBB and LV dysfunction and was associated with improved clinical outcomes in several small observational studies (10–12). In a small randomized, crossover study, Lustgarten et al. (10) showed equivalent clinical and echocardiographic improvements with HBP compared with BVP. Arnold et al. (20) compared HBP with conventional BVP in acute experiments performed in the same patients with LBBB and observed that HBP resulted in more effective ventricular resynchronization and hemodynamic performance. However, higher pacing thresholds and inability to correct distal LBBB or intraventricular conduction defects has been a major limitation of this approach, as demonstrated in a small randomized trial comparing HBP with BVP (21).

Huang et al. (13) recently developed a novel but simple and effective method to pace the proximal LBB. Since this initial description of LBBAP, several groups have reported on the feasibility and safety of LBBAP using the currently available SelectSecure pacing lead in short-term studies (13–16). Salden et al. (22) recently compared the acute electrophysiological and hemodynamic effects of transient LV septal pacing with BVP and HBP in 27 patients with LBBB. LV septal pacing was associated with larger reductions in QRS area compared with BVP and similar reductions to HBP. They found that LV septal pacing resulted in acute hemodynamic improvements comparable with BVP and HBP. The ability to capture the left conduction system in addition to LV septal pacing with LBBAP offers additional promise to improve electromechanical LV synchronization.

FEASIBILITY. Our study represents the first international, multicenter, real-world experience in a large series of patients undergoing CRT using LBBAP. The success rate of LBBAP was 85%, limited

FIGURE 6 Forest Plot of Predictors of Echocardiographic Response

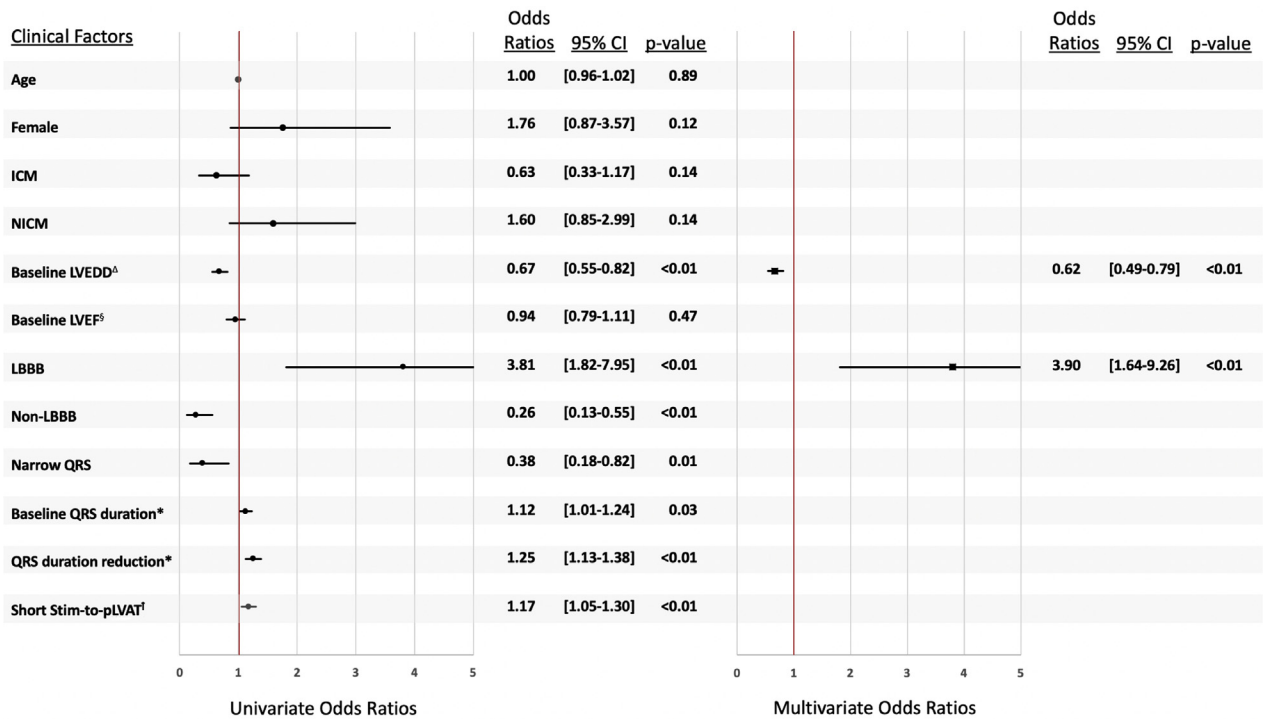

See text for description. CI = confidence interval; ICM = ischemic cardiomyopathy; LVEDD = left ventricular end-diastolic diameter; LVEF = left ventricular ejection fraction; NICM = nonischemic cardiomyopathy; other abbreviations as in Figure 1.

mainly by an inability to penetrate the septum, especially in patients with severely enlarged ventricles, and an inability to improve electric resynchronization in patients with intraventricular conduction defects (Supplemental Figure S3). LBBAP was successful in 92% of patients with LBBB compared with 71% of patients with intraventricular conduction defects. It is important to recognize that in several patients with electrogram-confirmed intraventricular conduction defects (presence of LBB potentials in the setting of intraventricular conduction defects), electric resynchronization was attributed predominantly to left septal endomyocardial capture with possible delayed engagement of arborizing Purkinje fibers (**Figure 5**). The overall success rates are comparable with those in a recent study by Huang et al. (23), who reported a success rate of 97% in a prospective, observational, multicenter study of 63 patients with NICM and LBBB. Compared with the success rates of HBP in this population, LBBAP appears to offer greater promise. Furthermore, the pacing thresholds achieved with LBBAP are lower than those reported in HBP studies to achieve bundle branch block correction (0.6 ± 0.3 V at 0.5 ms in our study vs. 1.89 ± 1.12 V at 0.5 ms and 3.8 ± 2.2 V at 0.7 ms) (10,12).

Fluoroscopy and procedural duration were significantly longer than previously reported for LBBAP and HBP studies (11-14,16). This likely reflects a learning curve at many of the participating centers in addition to the technical challenges posed by the limitations of the implantation tools in patients with advanced heart disease and severe ventricular dilatation.

OUTCOMES. This study demonstrates that LBBAP is associated with reduced paced QRS duration, translating into improved clinical and echocardiographic outcome. Patients with LBBB and/or NICM had significantly greater reductions in QRS duration and improved LVEF compared with patients with non-LBBB and/or ICM. Prior studies of BVP have demonstrated that reduced QRS duration is associated with improved clinical outcomes (24,25).

Echocardiographic response rates were greater in patients with LBBB compared with those with non-LBBB (87% vs. 67%; $p < 0.01$), while superresponse rates were higher in patients with NICM compared with those with ICM (41% vs. 18%; $p < 0.01$).

CENTRAL ILLUSTRATION **Left Bundle Branch Area Pacing for Cardiac Resynchronization Therapy**

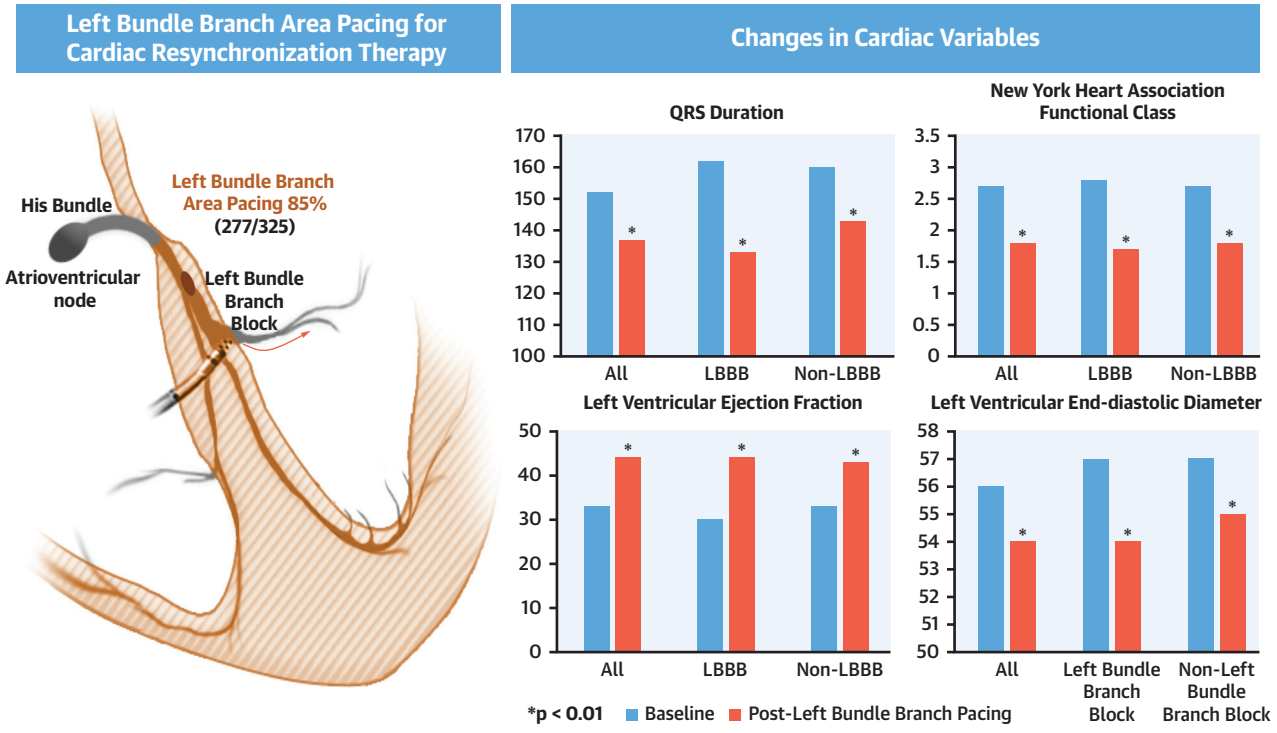

Vijayaraman, P. et al. J Am Coll Cardiol EP. 2021;7(2):135–47.

Left bundle branch area pacing (LBBAP) was successful in 85% of patients attempted. LBBAP resulted in significant reductions in QRS duration, New York Heart Association functional class, and left ventricular (LV) end-diastolic diameter along with significant improvement in LV ejection fraction in patients with left bundle branch block (LBBB) and non-LBBB. *p < 0.01. AV = atrioventricular; CRT = cardiac resynchronization therapy; HB = His bundle; LBBAP = left bundle branch area pacing; LBB = left bundle branch; LBBB = left bundle branch block; LBBP = left bundle branch pacing; LV = left ventricular; LVEDD = left ventricular end-diastolic diameter; NYHA = New York Heart Association.

Overall, significant improvements in electrocardiographic, echocardiographic, and clinical outcomes were achieved with LBBAP. In multivariate analysis, baseline LBBB (odds ratio: 3.96; 95% confidence interval: 1.64 to 9.26; $p < 0.01$) and reduction in paced QRS duration (odds ratio: 1.29; 95% confidence interval: 1.114 to 1.494; $p < 0.01$) were independent predictors of echocardiographic response and super-response, respectively, while larger LVEDD was predictive of lower likelihood of echocardiographic response. It appears as if the underlying disease substrate and the severity of electric dyssynchrony tend to predict outcomes in patients undergoing CRT. A recent mechanistic study by Upadhyay et al. (26) showed that about two-thirds of patients with LBBB had correctable conduction block in the His bundle or proximal left bundle. These patients are highly likely to benefit from permanent LBBAP at relatively low and stable pacing outputs. The benefit of LBBAP in patients with intraventricular conduction defects was less predictable in our study, with one-third of patients not achieving satisfactory electric resynchronization, translating into less impressive clinical and echocardiographic outcomes. Approximately 15% of patients had narrow QRS complexes in the study group. Requirements for ventricular pacing due to atrioventricular block or atrioventricular node ablation in the setting of LV dysfunction were the reasons for LBBAP. The major advantage is the low risk for LV dyssynchrony induced by LBBAP (16). Longer term, randomized controlled clinical trials comparing these different approaches to resynchronization therapy in different subgroups will be necessary to determine the individual applicability and feasibility of these effective therapeutic options.

STUDY LIMITATIONS. This was a nonrandomized, retrospective, observational study designed as an initial step to assess the feasibility and safety of permanent LBBAP in patients requiring CRT. This

study involved nonconsecutive patients with possible selection bias, and the results may not be applicable to all patients eligible for CRT. Because of the lack of a control group and heterogeneity of the study population, the results should be interpreted with caution. In addition, the high success rates of LBBAP achieved by operators experienced in HBP and LBBAP need to be replicated in prospective studies. Consensus criteria for LBB capture are lacking and need to be better characterized. Another major limitation of the study is the lack of a direct comparison with BVP or HBP. Carefully designed, large, randomized, controlled clinical trials comparing BVP are necessary to confirm the benefits of LBBAP in this population. The long-term electric performance of the deep-septal lead and potential risks associated with lead extraction from this site are unknown and need to be carefully studied.

CONCLUSIONS

LBBAP is feasible, safe, and potentially an alternative option for CRT. LBBAP provides remarkably low and stable pacing thresholds in short-term follow-up. Baseline LBBB and LVEDD were predictive of improved echocardiographic outcomes.

FUNDING SUPPORT AND AUTHOR DISCLOSURES

Dr. Vijayaraman has received honoraria, consulting fees, and research support from Medtronic; and has received consulting fees from Boston Scientific, Abbott, Biotronik, and Eaglepoint. Dr. Sharma has received honoraria from Medtronic; and has received consulting fees from Abbott, Biotronik, and Boston Scientific. Dr. Subsposh has received honoraria from Medtronic. Dr. Herweg has received honoraria and consulting fees from Abbott and Biotronik. Dr. Jastrzebski has received consulting fees and honoraria from Medtronic and Abbott. All other authors have reported that they have no relationships relevant to the contents of this paper to disclose.

ADDRESS FOR CORRESPONDENCE: Dr. Pugazhendhi Vijayaraman, Geisinger Heart Institute, Geisinger Wyoming Valley Medical Center, MC 36-10, 1000 East Mountain Boulevard, Wilkes-Barre, Pennsylvania 18711, USA. E-mail: pvijayaraman1@geisinger.edu.

PERSPECTIVES

COMPETENCY IN MEDICAL KNOWLEDGE: BVP is an effective therapy for CRT. Permanent LBBAP is a novel approach to conduction system pacing. LBBAP is feasible and safe and improves clinical and echocardiographic outcomes in patients requiring CRT.

TRANSLATIONAL OUTLOOK: LBBAP may provide a reasonable alternative to traditional BVP. Large randomized controlled clinical trials with long-term follow-up are necessary to confirm the clinical benefits of permanent LBBAP compared with BVP in patients requiring CRT.

REFERENCES

1. Cleland JG, Daubert JC, Erdmann E, et al. The effect of cardiac resynchronization on morbidity and mortality in heart failure. N Engl J Med 2005;352:1539–49.

2. Bristow MR, Saxon LA, Boehmer J, et al. Cardiac-resynchronization therapy with or without an implantable defibrillator in advanced chronic heart failure. N Engl J Med 2004;350:2140–50.

3. Abraham WT, Fisher WG, Smith AL, et al. Cardiac resynchronization in chronic heart failure. N Engl J Med 2002;346:1845–53.

4. Young JB, Abraham WT, Smith AL, et al. Combined cardiac resynchronization and implantable cardioversion defibrillation in advanced chronic heart failure: the MIRACLE ICD trial. JAMA 2003;289:2685–94.

5. Auricchio A, Stellbrink C, Sack S, et al. Long-term clinical effect of hemodynamically optimized cardiac resynchronization therapy in patients with heart failure and ventricular conduction delay. J Am Coll Cardiol 2002;39:2026–33.

6. Epstein AE, DiMarco JP, Ellenbogen KA, et al. 2012 ACCF/AHA/HRS focused update incorporated into the ACCF/AHA/HRS 2008 guidelines for device-based therapy of cardiac rhythm abnormalities: a report of the American College of Cardiology Foundation/American Heart Association Task Force on Practice Guidelines and the Heart Rhythm Society. J Am Coll Cardiol 2013;61:e6–75.

7. Singh JP, Klein HU, Huang DT, et al. Left ventricular lead position and clinical outcome in the Multicenter Automatic Defibrillator Implantation Trial-Cardiac Resynchronization Therapy (MADIT-CRT) trial. Circulation 2011;123:1159–66.

8. Kusumoto FM, Schoenfeld MH, Barrett C, et al. 2018 ACC/AHA/HRS guideline on the evaluation and management of patients with bradycardia and cardiac conduction delay. A Report of the American College of Cardiology/American Heart Association Task Force on Clinical Practice Guidelines and the Heart Rhythm Society. J Am Coll Cardiol 2018;74:e51–156.

9. Brugada J, Katritsis D, Arebelo E, et al. 2019 ESC guidelines for the management of patients with supraventricular tachycardia. Eur Heart J 2020;41:655–720.

10. Lustgarten DL, Crespo EM, Arkhipova-Jenkins I, et al. His-bundle pacing versus biventricular pacing in cardiac resynchronization therapy patients: a crossover design comparison. Heart Rhythm 2015;12:1548–57.

11. Sharma PS, Dandamudi G, Herweg B, et al. Permanent His-bundle pacing as an alternative to biventricular pacing for cardiac resynchronization therapy: a multicenter experience. Heart Rhythm 2018;15:413–20.

12. Huang W, Su L, Wu S, et al. Long-term outcomes of His bundle pacing in patients with heart failure with left bundle branch block. Heart 2019;105:137–43.

13. Huang W, Su L, Wu S, et al. A novel pacing strategy with low and stable output: pacing the left bundle branch immediately beyond the conduction block. Can J Cardiol 2017;33:1736.e1–3.

14. Vijayaraman P, Subzposh FA, Naperkowski A, et al. Prospective evaluation of feasibility, electrophysiologic and echocardiographic characteristics of left bundle branch area pacing. Heart Rhythm 2019;16:1774–82.

15. Zhang S, Zhou X, Gold MR. Left bundle branch pacing. J Am Coll Cardiol 2019;74:3039–49.

16. Hou X, Qian Z, Wang Y, et al. Feasibility and cardiac synchrony of permanent left bundle branch pacing through the interventricular septum. Europace 2019;21:1694–702.

17. Huang W, Chen X, Su L, Wu S, Xia X, Vijayaraman P. A beginner's guide to permanent left bundle branch pacing. Heart Rhythm 2019;16:1791–6.

18. Jastrzebski M, Moskal P, Kusiack A, et al. Programmed deep septal pacing for the diagnosis of left bundle branch capture. J Cardiovasc Electrophysiol 2020;31:485–93.

19. Ellenbogen KA, Huizar JF. Foreseeing super-response to cardiac resynchronization therapy: a perspective for clinicians. J Am Coll Cardiol 2012;59:2374–7.

20. Arnold AD, Shun-Shin MJ, Keene D, et al. His resynchronization versus biventricular pacing in patients with heart failure and left bundle branch block. J Am Coll Cardiol 2018;72:3112–22.

21. Upadhyay GA, Vijayaraman P, Nayak HM, et al. His corrective pacing or biventricular pacing for cardiac resynchronization in heart failure. J Am Coll Cardiol 2019;74:157–9.

22. Salden FCWM, Luermans JGLM, Westra SW, et al. Short-term hemodynamic and electrophysiological effects of cardiac resynchronization by left ventricular septal pacing. J Am Coll Cardiol 2020;75:347–59.

23. Huang W, Wu S, Vijayaraman P, et al. Cardiac resynchronization therapy in patients with non-ischemic cardiomyopathy utilizing left bundle branch pacing. J Am Coll Cardiol EP 2020;6:849–58.

24. Appert L, Menet A, Altes A, et al. Clinical significance of electromechanical dyssynchrony and QRS narrowing in patients with heart failure receiving cardiac resynchronization therapy. Can J Cardiol 2019;35:27–34.

25. Jastrzebski M, Baranchuk A, Fijorek K, et al. Cardiac resynchronization therapy-induced acute shortening of QRS duration predicts long-term mortality only in patients with left bundle branch block. Europace 2019;21:281–9.

26. Upadhyay GA, Cherian T, Shatz DY, et al. Intracardiac delineation of septal conduction in left bundle branch block patterns: mechanistic evidence of left intra-Hisian block circumvented by His pacing. Circulation 2019;39:1876–88.

KEY WORDS **biventricular pacing, bundle branch block, cardiac resynchronization therapy, His bundle pacing, left bundle branch area pacing**

APPENDIX **For supplemental figures and tables, please see the online version of this paper.**

Left bundle branch–optimized cardiac resynchronization therapy (LOT-CRT): Results from an international LBBAP collaborative study group

Marek Jastrzębski, MD, PhD,* Paweł Moskal, MD, PhD,* Wim Huybrechts, MD,† Karol Curila, MD, PhD,‡ Praveen Sreekumar, MBBS, MD, DM,§ Leonard M. Rademakers, MD, PhD,‖ Shunmuga Sundaram Ponnusamy, MBBS, MD, CEPS-A,¶ Bengt Herweg, MD, FHRS,# Parikshit S. Sharma, MD, MPH, FACC, FHRS,** Agnieszka Bednarek, MD, PhD,* Marek Rajzer, MD, PhD,* Pugazhendhi Vijayaraman, MD, FHRS††

*From the *First Department of Cardiology, Interventional Electrocardiology and Hypertension, Jagiellonian University, Medical College, Krakow, Poland, †Department of Cardiology, University Hospital Antwerp, Antwerp, Belgium, ‡Cardiocenter, Third Faculty of Medicine, Charles University, University Hospital Kralovske Vinohrady, Prague, Czech Republic, §Electrophysiology Unit, Department of Cardiology, Aster Medcity, Kochi, Kerala, India, ‖Department of Cardiology, Catharina Ziekenhuis, Eindhoven, The Netherlands, ¶Department of Cardiology, Velammal Medical College Hospital and Research Institute, Velammal Village, Madurai, Tamil Nadu, India, #Division of Cardiology, University of South Florida, Tampa, Florida, **Rush University Medical Center, Chicago, Illinois, and ††Geisinger Heart Institute, Wilkes-Barre, Pennsylvania.*

BACKGROUND Cardiac resynchronization therapy (CRT) based on the conventional biventricular pacing (BiV-CRT) technique sometimes results in broad QRS complex and suboptimal response.

OBJECTIVE We aimed to assess the feasibility and outcomes of CRT based on left bundle branch area pacing (LBBAP, in lieu of the right ventricular lead) combined with coronary venous left ventricular pacing in an international multicenter study.

METHODS LBBAP-optimized CRT (LOT-CRT) was attempted in nonconsecutive patients with CRT indications. Addition of the LBBA (or coronary venous) lead was at the discretion of the implanting physician, who was guided by suboptimal paced QRS complex, and/or on clinical grounds.

RESULTS LOT-CRT was successful in 91 of 112 patients (81%). The baseline characteristics were as follows: mean age 70 ± 11 years, female 22 (20%), left ventricular ejection fraction 28.7% ± 9.8%, left ventricular end-diastolic diameter 62 ± 9 mm, N-terminal pro–B-type natriuretic peptide level 5821 ± 8193 pg/mL, left bundle branch block 47 (42%), nonspecific intraventricular conduction delay 25 (22%), right ventricular pacing 26 (23%), and right bundle branch block 14 (12%). The procedure characteristics were as follows: mean fluoroscopy time 27.3 ± 22 minutes, LBBAP capture threshold 0.8 ± 0.5 V @ 0.5 ms, and R-wave amplitude 10 mV. LOT-CRT resulted in significantly greater narrowing of QRS complex from 182 ± 25 ms at baseline to 144 ± 22 ms ($P < .0001$) than did BiV-CRT (170 ± 30 ms; $P < .0001$) and LBBAP (162 ± 23 ms; $P < .0001$). At follow-up of ≥3 months, the ejection fraction improved to 37% ± 12%, left ventricular end-diastolic diameter decreased to 59 ± 9 mm, N-terminal pro–B-type natriuretic peptide level decreased to 2514 ± 3537 pg/mL, pacing parameters were stable, and clinical improvement was noted in 76% of patients (New York Heart Association class 2.9 vs 1.9).

CONCLUSION LOT-CRT is feasible and safe and provides greater electrical resynchronization as compared with BiV-CRT and could be an alternative, especially when only suboptimal electrical resynchronization is obtained with BiV-CRT. Randomized controlled trials comparing LOT-CRT and BiV-CRT are needed.

KEYWORDS Biventricular pacing; Cardiac resynchronization therapy; Left bundle branch area pacing; QRS narrowing; Heart failure

(Heart Rhythm 2021;■:1–9)

Funding sources: None. Disclosures: Drs Jastrzebski, Moskal, Huybrechts, and Curila have received consultant fees from Medtronic. Dr Herweg has received consultant fees from Abbott and Biotronik. Dr Sharma has received consultant fees from Abbott, Biotronik, Boston Scientific, and Medtronic. Dr Vijayaraman has received research and fellowship support as well as speaker and consultant fees from Medtronic. He has also received consultant fees from Abbott and Biotronik. The rest of the authors report no conflicts of interest. **Address reprint requests and correspondence:** Dr Marek Jastrzębski, First Department of Cardiology, Interventional Electrocardiology and Hypertension, Jagiellonian University, Jakubowskiego 2, 30-688 Kraków, Poland. E-mail address: mcjastrz@cyf-kr.edu.pl.

1547-5271/$-see front matter https://doi.org/10.1016/j.hrthm.2021.07.057

Introduction

Left bundle branch area pacing (LBBAP) is a promising physiological pacing technique with potential for application in both patients with bradyarrhythmia and those with heart failure.[1–4] However, proximal left bundle branch (LBB) pacing is inherently limited in its ability to restore physiological activation of the lateral wall of the left ventricle (LV) in patients with distal conduction delay in the distal LBB, LV Purkinje network, or myocardium. Moreover, perhaps in a significant percentage of patients in whom LBBAP was attempted, only left ventricular septal (LVS) myocardial capture was obtained, resulting in a small but potentially important nonphysiological delay in LV lateral wall activation.[4]

Conventional cardiac resynchronization therapy (CRT) using biventricular (BiV) pacing based on right ventricular (RV) pacing and coronary venous (CV) pacing is also limited in its ability to fully restore physiological activation of the LV. Limitations of BiV-CRT are related, among others, to the potentially desynchronizing impact of myocardial pacing with the RV lead, single area nonphysiological epicardial LV pacing, latency, and suboptimal LV lead position (paraseptal/apical) due to the unfavorable anatomy of the cardiac veins and/or LV scars.[5,6] Failure of BiV-CRT to restore physiological activation might express itself as QRS prolongation rather than narrowing. This is observed in one-third of patients who underwent BiV-CRT and related to poor prognosis.

Combining LBBAP and BiV pacing (Figures 1 and 2) might address some of the above-mentioned limitations of both techniques, providing narrower QRS complex and a more efficient form of CRT, especially in challenging cases and patients with more advanced heart failure.[7]

The aim of the study was to assess the feasibility and outcomes of CRT based on LBBAP (in lieu of the RV lead), combined with CV pacing, in an international multicenter study.

Methods

The data that support the findings of this study are available from the corresponding author on reasonable request. The study adhered to the Helsinki Declaration as revised in 2013; data collection was approved by respective institutional review boards.

Population and design

This was a prospective observational multicenter study that included 4 European sites, 3 American sites, and 2 Indian sites. LBBAP-optimized CRT (LOT-CRT) was attempted in a nonconsecutive series of patients qualified for CRT or in nonresponders to prior CRT. The selection of patients for this novel form of CRT, rather than for BiV-CRT or LBBAP alone, was at the discretion of the implanting physician, who was guided mainly by suboptimal paced QRS complex of either BiV pacing or LBBAP alone and/or by clinical reasoning, with an inclination to offer this form of CRT to patients with more advanced heart failure. Baseline data on New York Heart Association (NYHA) functional class, comorbidities, sex, age, echocardiographic parameters, electrocardiographic (ECG) parameters, and N-terminal pro–B-type natriuretic peptide (NT-proBNP) level were obtained.

Implantation procedure

All implanters had experience in permanent LBBAP and BiV pacing, and some also in His bundle pacing (HBP)–optimized CRT (HOT-CRT), the other CRT technique that is based on combining CV pacing and conduction system pacing. CV pacing was performed according to the established standards for BiV-CRT. The LBB implantation procedure was described by us and others elsewhere.[2,3] Briefly, LBBAP was performed using a thin (4.1-F), active helix, screw-in pacing lead (SelectSecure model 3830, 69 cm, Medtronic Inc., Minneapolis, MN) and dedicated delivery sheaths (C315HIS, C304, Medtronic Inc.). The His bundle potential (if recorded) and/or the tricuspid annulus appraised electrophysiologically and fluoroscopically were used as anatomical landmarks. We aimed at any basal to mid-interventricular septal site where proper deep septal lead deployment was possible. The area located ~1.5–2 cm apically from the distal His bundle or from the superior aspect of the tricuspid annulus site was targeted. At this initial site, paced QRS complex should be preferentially characterized by the normal axis in the frontal plane (R in lead I, R/Rs in lead II, and rS in lead III); this ensures that both high and low septal sites, that are further away from the proximal LBB, are avoided. Lead deployment was performed under fluoroscopic and ECG guidance to cross the septum, reach the subendocardial area on the left side of the interventricular septum, and avoid perforation into the LV cavity. Lead behaviors during deep septal deployment and fixation beats, characterized by us elsewhere, were used to guide lead positioning and fixation.[8–10] Constant or interrupted pacing from the lead was delivered to monitor change in the paced QRS morphology during fixation.[11] We aimed to obtain paced QRS complex with an r′ deflection in lead V_1 and features of LBB capture (see below). Attempts were made to obtain LBB capture, but LVS pacing was considered acceptable; the number of lead deployment attempts was at the discretion of the operator.

The following procedure-related data were recorded: fluoroscopy time, LBBAP capture threshold, CV LV capture threshold, sensing, acute complications, V-V interval programming, device type, and LBBAP lead connection used.

The following ECG-based data were obtained: LBBAP QRS duration and V_6 R-wave peak time (V_6RWPT), paced BiV-CRT QRS duration, paced LOT-CRT QRS duration, and presence of LBB capture.

Follow-up

Postimplantation follow-up was performed as per standards in each of the participating centers; data from the final follow-up visit were used for analysis. For clinical and

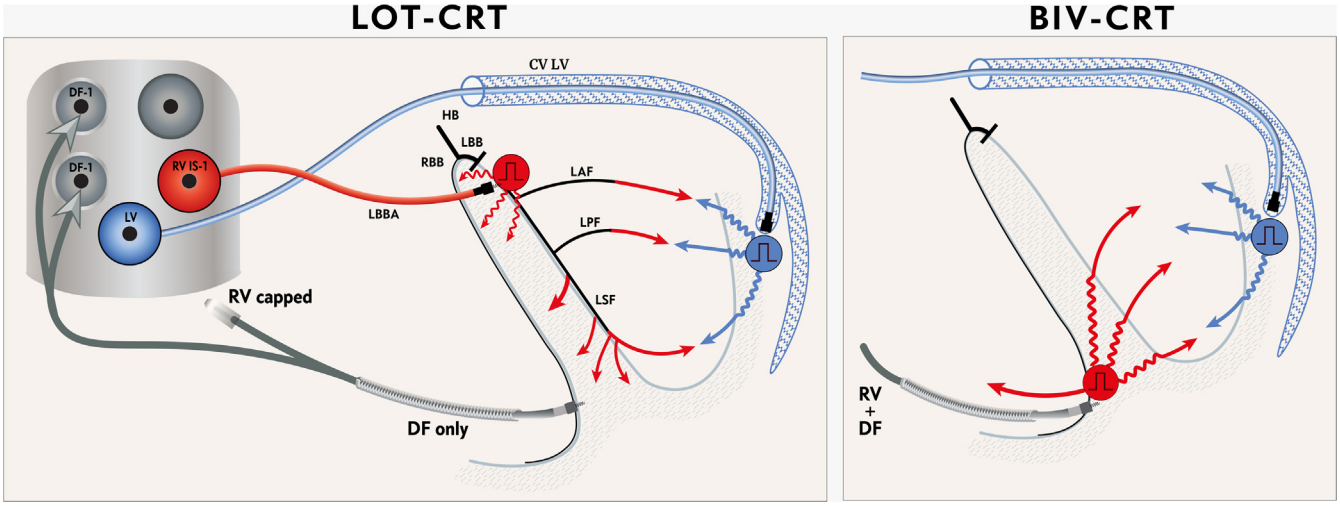

Figure 1 Schematic of pacing lead connection and left ventricular activation wavefronts of left bundle branch–optimized cardiac resynchronization therapy (LOT-CRT) compared with those of biventricular CRT (BiV-CRT). CV LV = coronary venous left ventricular; DF = defibrillation; LAF = left anterior fascicle; LBB = left bundle branch; LBBA = left bundle branch area; LPF = left posterior fascicle; LSF = left septal fascicle; LV = left ventricle; RBB = right bundle branch; RV = right ventricle.

echocardiographic response, a minimum follow-up of 3 months was adopted for the purpose of this study.

Definitions and measurements

LBB capture was diagnosed as per currently used criteria/methods, which include QRS morphology transition during the threshold test (to either selective LBB capture or LVS capture), paced V_6RWPT < 90 ms, and diagnostic response during programmed stimulation.[12]

The QRS duration, both for native and for paced QRS complexes, was obtained using the global QRS measurement method (from the earliest onset or pacing spike to the latest offset with all 12-lead ECGs recorded simultaneously). V_6RWPT was measured from the pacing stimulus to the

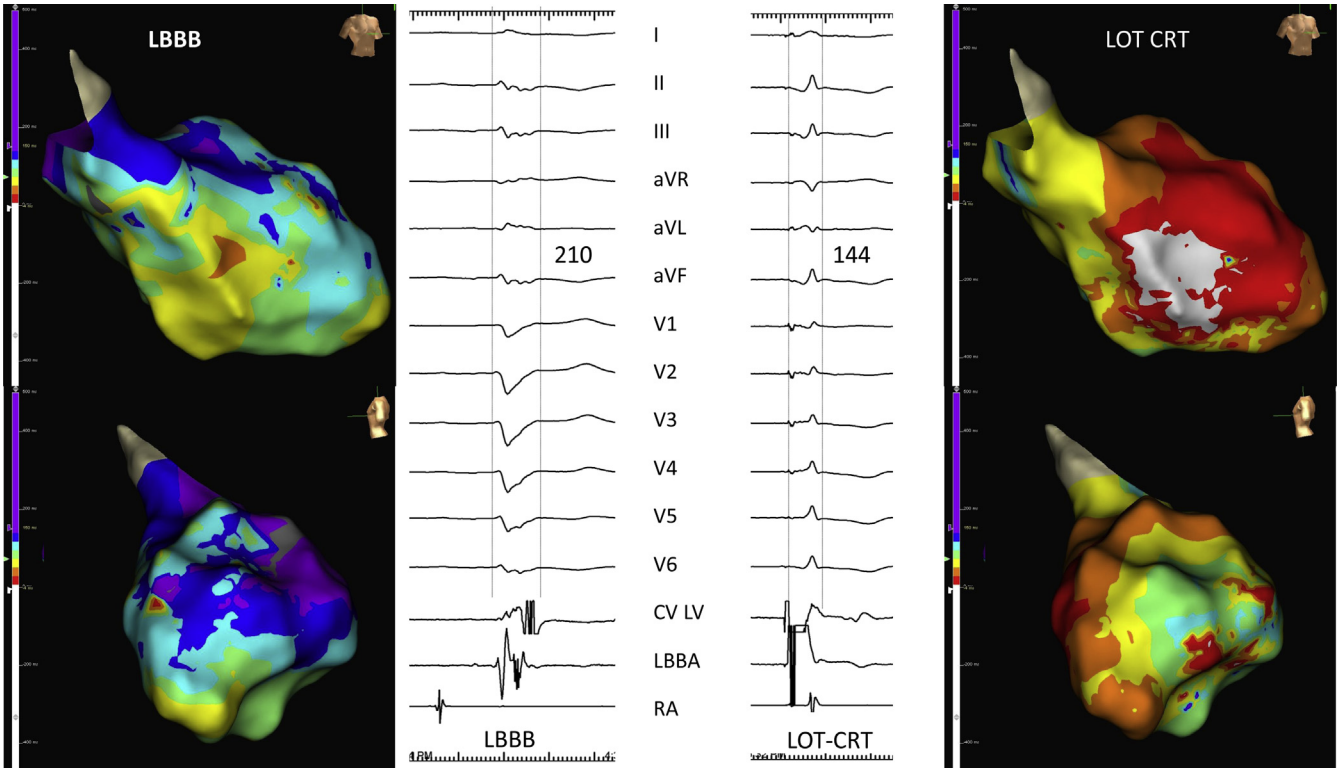

Figure 2 Electroanatomic mapping in left bundle branch–optimized cardiac resynchronization therapy (LOT-CRT). Baseline electrocardiogram and 3-dimensional electroanatomic map in a patient with ischemic cardiomyopathy are shown. With LOT-CRT, the QRS duration narrowed from 210 to 144 ms, with excellent electrical resynchronization of the left ventricle. LBBB = left bundle branch block.

peak of the R wave in lead V_6. QRS duration and V_6RWPT measurements were done with a fast sweep speed (100–200 mm/s) and digital calipers by using the electrophysiological recording system.

Echocardiographic examination was performed using a commercially available ultrasound system; 2-dimensional echocardiographic assessment included parasternal long- and short-axis views and apical 4-, 3- and 2-chamber views according to the American Society of Echocardiography recommendations.[13] Four consecutive cardiac cycles were recorded. The ejection fraction and LV volumes were calculated using the Simpson's biplane method. *Echocardiographic response* was defined as ≥5% increase in LV ejection fraction (LVEF). *Super-responder status* was defined as an absolute improvement in LVEF by ≥20% or an increase of LVEF to a value >50%.

Statistical analysis

Categorical variables were expressed as counts and percentages, and continuous variables were reported as mean ± SD. For continuous variables, differences in 2 groups were assessed using the *t* test and the Mann-Whitney test. For categorical variables, the Fisher exact test was used. Paired data were compared using the *t* test if normally distributed or Wilcoxon signed-rank test if nonparametric. Statistical analysis was performed using STATA 16.1 (StataCorp LLC, College Station, TX). A *P* value of <.05 was considered significant.

Results

Population

A total of 112 patients underwent LOT-CRT at 9 centers. Baseline group characteristics are summarized in Table 1. Briefly, the mean age of patients was 70.5 ± 11 years (20% female) and most patients had ischemic cardiomyopathy (61%) with a mean LVEF of 28.8% ± 9.8%. Seventy-two percent of patients were grouped under NYHA functional class III or IV. The mean follow-up duration in the study population was 7.8 ± 2.3 months. Because of the severe acute respiratory syndrome–related coronavirus disease 2019 pandemic, only a remote follow-up visit could be done for 12 patients.

Procedural outcomes

LOT-CRT was successful in 91 of 112 patients (81%). LBBAP in the septum could not be reached in 16 patients, and CS lead implantation failed in 4 patients. A BiV defibrillator device was implanted in 83 patients, while a pacemaker was implanted in the remaining 29 patients.

There were 5 early complications: 2 cases of early lead dislocation—1 LBBAP and 1 CV LV lead—both successfully repositioned; 1 intraprocedural septal perforation with the LBBAP lead, repositioned without any consequences; and 2 pocket hematomas. During follow-up, there was 1 infection and 1 case of increase in CV LV lead threshold and right atrial lead dislodgment.

In patients with preserved sinus rhythm, the LBBAP lead was connected to the RV port of the device; in cases where the CRT–defibrillator device was used, the IS-1 pin of the RV/defibrillation lead was capped. In patients with permanent atrial fibrillation, the LBBAP lead was connected either to the atrial (n = 14) or to the RV port.

The atrioventricular (AV) delay and V-V interval were set to pace with the LBBAP lead earlier than with the CV lead and to obtain maximal narrowing of paced QRS complex. In patients with quadripolar CV leads, different pacing configurations were explored for both BiV-CRT QRS complex and LOT-CRT QRS complex. In patients where the LBBAP lead was connected to the right atrial port, the V-V interval adjustment was limited by the minimal programmable AV delay interval (25–30 ms). The average programmed V-V delay in the whole group was 20 ± 18 ms.

The fluoroscopy duration for the whole procedure was 27.3 ± 22 minutes. The LBBAP capture threshold and R-wave amplitudes at implantation were 0.8 ± 0.4 V @ 0.5 ms and 10 ± 5 V mV, respectively, which remained stable during follow-up (0.7 ± 0.3 V @ 0.4 ms and 12 ± 5 mV).

ECG outcomes

LOT-CRT resulted in significant narrowing of QRS complex from 181 ± 26 to 144 ± 22 ms ($P < .0001$), which was better than narrowing obtained with BiV-CRT (170 ± 30 ms; $P < .0001$) or LBBAP (162 ± 23 ms; $P < .0001$) alone, as illustrated in Figure 3. Lack of QRS narrowing during BiV-CRT and LOT-CRT pacing was noted in 20.6% and 4.4% of patients, respectively. LBB capture and LVS capture per used criteria were diagnosed in 68 (75%) and 23 (25%) patients, respectively. The mean V_6RWPT during LBBAP was 99.6 ± 21 ms.

Echocardiographic outcomes

There was an increase in LVEF from 28.5% ± 9.9% at baseline to 37.2% ± 12% during follow-up ($P < .0001$), as well as a decrease in LV end-diastolic diameter (62.0 ± 8.9 vs 59.1 ± 9.1; $P = .0442$), LV end-diastolic volume (209.8 ± 99 vs 171.4 ± 83; $P < .0001$), and LV end-systolic volume (149.5 ± 84 vs 110.6 ± 69; $P < .0001$) (Figure 4). Echocardiographic response and super-response (Figure 5) were observed in 62.8% and 24.4% of patients, respectively.

Clinical and biochemical outcomes

Clinical response, defined as improvement by 1 NYHA functional class after LOT-CRT, was noted in 66 of 87 (76%) and 58 of 67 patients (87%) under baseline NYHA functional class III and IV, respectively. There was a significant improvement in overall NYHA functional class from 2.9 ± 0.6 at baseline to 1.9 ± 0.6 at follow-up ($P < .0001$). During follow-up, NT-pro-BNP levels decreased significantly (5668 ± 8249 pg/mL vs 2561 ± 3555 pg/mL; $P < 0.0001$). No long-term complications were noted. One patient was lost to follow-up, 1 patient died of heart failure,

Table 1 Baseline characteristics

Characteristic	All patients (N = 112)	Successful LOT-CRT (n = 91)	Failed LOT-CRT (n = 21)	*P*
Age (y)	70.5 ± 11.4	69.8 ± 11.7	73.1 ± 10	.11
Sex: female	22 (20)	18 (20)	4 (19)	.91
NT-proBNP level (pg/mL)	5821 ± 8193	6072 ± 8373	4880 ± 7660	.70
Medical history				
HTN	87 (78)	71 (78)	16 (76)	.85
DM	47 (42)	40 (44)	7 (33)	.37
Permanent AF	33 (29)	25 (27)	8 (38)	.34
Ischemic cardiomyopathy	68 (61)	56 (62)	12 (57)	.71
NYHA class III–IV	81 (72)	70 (77)	11 (52)	.13
Mean baseline NYHA functional class	2.8 (0.7)	2.9 (0.6)	2.6 (0.7)	.98
Echocardiographic parameters				
LVEF (%)	28.7 ± 9.8	28.5 ± 9.9	30 ± 9.5	.26
LVEDD (mm)	61.9 ± 8.6	62.0 ± 8.9	61.4 ± 6.6	.78
LVEDV (mL)	211 ± 101	210 ± 99	227 ± 126	.70
LVESV (mL)	149 ± 84	149 ± 84	146 ± 88	.93
Electrocardiographic parameters				
Baseline QRS duration (ms)	180 ± 24	182 ± 25	172 ± 24	.11
LBBB	47 (42)	40 (44)	7 (33)	.17
RBBB	14 (12.5)	11 (12)	3 (14)	
NIVCD	25 (22)	18 (20)	7 (33)	
RV paced	26 (23)	22 (24)	4 (19)	

Values are presented as mean ± SD or n (%).

AF = atrial fibrillation; DM = diabetes mellitus; HTN = hypertension; LBBB = left bundle branch block; LOT-CRT = left bundle branch–optimized cardiac resynchronization therapy; LVEDD = left ventricular end-diastolic diameter; LVEDV = left ventricular end-diastolic volume; LVEF = left ventricular ejection fraction; LVESV = left ventricular end-systolic volume; NIVCD = nonspecific intraventricular conduction delay; NT-proBNP = N-terminal pro–B-type natriuretic peptide; NYHA = New York Heart Association; RBBB = right bundle branch block; RV = right ventricular.

and 2 patients died of noncardiac causes (renal failure and coronavirus disease 2019).

Subgroup analysis according to the presence of LBB or LVS capture

LOT-CRT with confirmed LBB capture resulted in narrower paced QRS complex (141 ± 20 ms vs 152 ± 25 ms; *P* = .028), better LVEF improvement (11.1 ± 11.3 percentage points vs 4.7 ± 7.5 percentage points; *P* = .0196), higher percentage of echocardiographic response (71% vs 45%; *P* = .039), and higher percentage of clinical response (82% vs 61%; *P* = .035) than did LOT-CRT with LVS capture only. There was no difference in the decrease in NT-pro-BNP levels (3620 ± 6877 pg/mL vs 656 ± 663 pg/mL; *P* = .21).

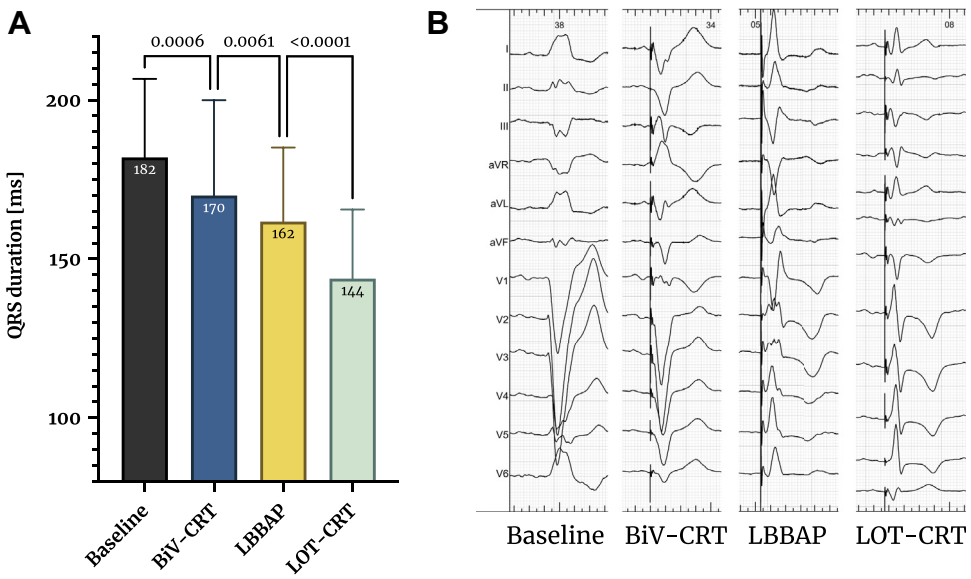

Figure 3 Comparison of the impact of conventional cardiac resynchronization therapy (biventricular CRT [BiV-CRT]) pacing and left bundle branch–optimized CRT (LOT-CRT) pacing on QRS duration. LBBAP = left bundle branch area pacing.

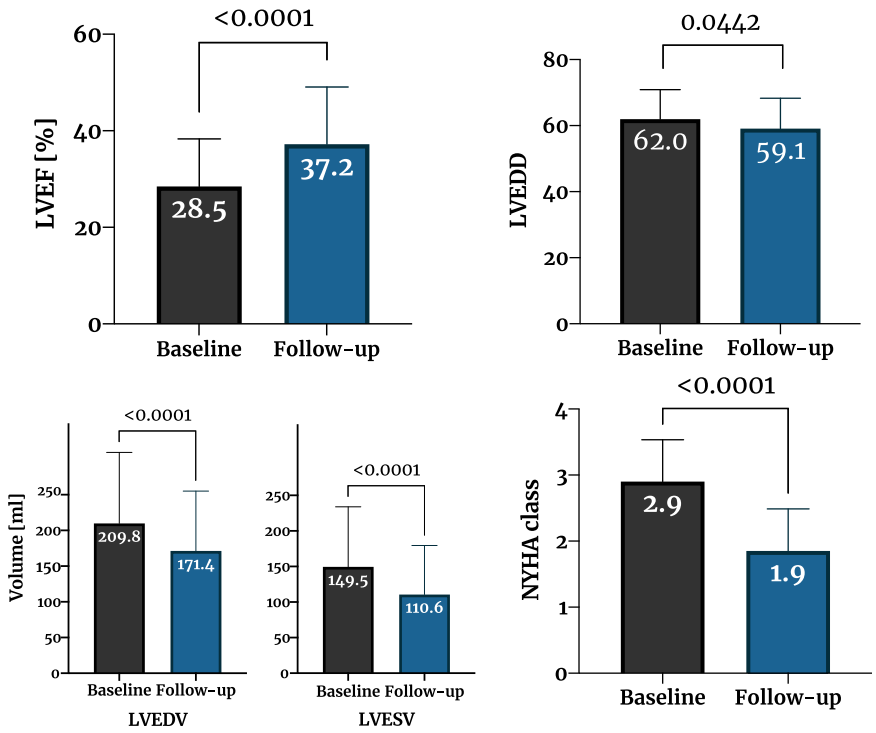

Figure 4 Echocardiographic response after left bundle branch pacing–optimized cardiac resynchronization therapy. LVEDD = left ventricular end-diastolic diameter; LVEDV = left ventricular end-diastolic volume; LVEF = left ventricular ejection fraction; LVESV = left ventricular end-systolic volume; NYHA = New York Heart Association.

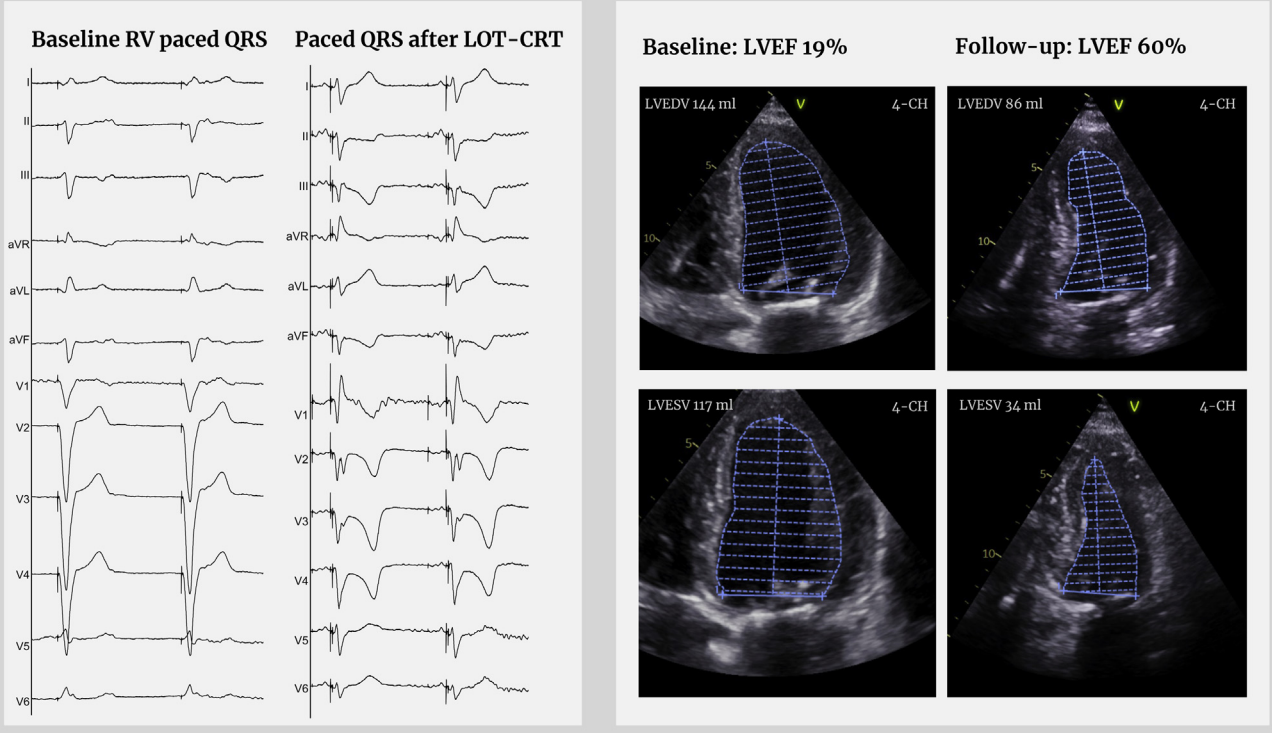

Figure 5 An example of super-response after left bundle branch pacing–optimized cardiac resynchronization therapy (LOT-CRT). Twelve-lead electrocardiograms before and after LOT-CRT are shown at 25 mm/s. Apical 4-chamber echocardiographic views demonstrate remarkable improvement in left ventricular end-diastolic volume (LVEDV) and left ventricular end-systolic volume (LVESV). 4-CH =four chamber view; LVEF = left ventricular ejection fraction; RV = right ventricular.

Discussion

This study presents multicenter experience with mid-term follow-up of the LOT-CRT technique in nonconsecutive patients with advanced heart failure and broad QRS complex. It addresses pertinent initial questions related to the rationale behind this new pacing method and provides data on its safety, feasibility, and outcomes.

Electrical synchrony

The major rationale behind replacing the RV lead with the LBBA lead was to obtain greater electrical synchrony due to (1) direct depolarization of the LV conduction system and (2) bypass the slow cell-to-cell conduction from the right to the left side of the interventricular septum.

The studied group had more advanced dysfunction of the conduction system/heart muscle as evidenced by the baseline QRS duration of 180 ms, which was broader than in many of the recent CRT studies. More advanced electrical asynchrony might be one of the justifications for this new pacing option. At 12 ms (182–170 ms), acute QRS narrowing obtained with BiV-CRT was comparable with the values in many other CRT studies (6–20 ms).[6,13–16] At 38 ms (182–144 ms), the acute electrical synchrony outcome obtained with LOT-CRT was 3 times greater, showing that this method compares well not only with BiV-CRT but also with the other new CRT modalities. Wireless stimulation endocardially for CRT, based on endocardial LV pacing, was reported to narrow QRS complex by 27.3 ms, while HOT-CRT, based on HBP and CV pacing, resulted in QRS narrowing by 60–63 ms.[17–19] The difference in QRS narrowing between LOT-CRT and HOT-CRT is probably related to the presence of RV activation delay (terminal R/r in lead V_1) during LOT-CRT but not during HOT-CRT. The impact of LOT-CRT on electrical synchrony might translate to favorable long-term clinical outcomes, as the degree of QRS narrowing in CRT was related to decreased long-term mortality while the degree of QRS prolongation was related to increased mortality.[20,21] In a study by Sweeney et al,[22] QRS narrowing $\geq$ 25 ms was associated with both response and super-response to CRT with an odds ratio of 2.35 and 2.75, respectively.

Although LBBAP alone can achieve electrical synchrony of the LV, as documented in a few mid-sized nonrandomized studies,[4,23] the following arguments support keeping the CV pacing lead in a CRT system in patients with advanced conduction system disease. First, delayed activation of the lateral wall of the LV in patients with heart failure might results not only from discrete lesion in LBB that can be bypassed by LBB pacing but also from widespread and/or distal delay in the conduction system. Electrical uncoupling, myocardial scars, or functional conduction block can lead to delay in LV lateral wall activation as well. Upadhyay et al[24] demonstrated that patients with left bundle branch block (LBBB) on ECG, even diagnosed according to the Strauss criteria that are considered as specific, might have intact septal LBB activation. Such conduction abnormality can be corrected/compensated for by CV pacing but not LBBAP. There is often a coexistence of both mechanisms (focal lesion and distal delay) in some patients with LBBB and wider QRS complex on ECG and advanced heart failure.

A further argument that LBBAP alone might not be able to fully restore physiological activation of the LV comes from studies that assessed the ECG marker of the LV lateral wall activation time—V_6RWPT.[25] During LBBAP in patients with narrow QRS complex and diseased His-Purkinje conduction system, V_6RWPT values differ. In patients with narrow QRS complexes, V_6RWPT closely follows intrinsic native activation times and, as expected, remains within the norm for the V_6 intrinsicoid deflection time (ie, 50–60 ms + LBB latency of 20–30 ms). In contrast, in patients with LBBB, nonspecific intraventricular conduction delay or asystole V_6RWPT values, despite confirmed LBB capture, are much longer and not infrequently greater than normal physiological LV lateral wall activation times.[25] In the present study, V_6RWPT during LBBAP was quite long—99.6 ms. This suggests that despite proximal LBB capture, additional LV conduction delay remained and CV LV pacing might have been needed to correct this.

Recently, HOT-CRT has been proposed as an alternative to achieve greater electrical resynchronization in patients with advanced conduction disease and severe heart failure.[17,19] A significant number of patients in the study by Vijayaraman et al[17] had permanent atrial fibrillation, allowing HBP lead connection to the atrial port. However, in patients with underlying sinus rhythm, this technique is significantly limited by the need to connect the HBP lead to the LV port and the bipolar LV lead to the RV port. The HBP lead should not be connected to the RV port because of the risk of atrial oversensing and ventricular undersensing. In LOT-CRT, the quadripolar LV lead can be used with the option of multipoint pacing if necessary and ventricular sensing/arrhythmia detection is normal. Additionally, in patients with intact AV conduction and nonspecific intraventricular conduction delay, HBP without any correction of LV conduction delay does not provide any advantage over adaptive LV-only pacing. In contrast, LBBAP provides additional LV resynchronization by early LV septal endocardial activation in addition to conduction system capture. Furthermore, HBP is often associated with higher pacing thresholds and potential risk of late rise in capture thresholds. LBBAP has consistently been shown to achieve low and stable capture thresholds with high R-wave amplitudes.

Echocardiographic, biochemical, and clinical response

Echocardiographic and clinical outcomes significantly improved, compared to baseline, in the group of patients with advanced conduction disease and severe heart failure. A clinical response of 87% was noted in patients with class III–IV heart failure, a value comparable to the outcomes (84%) reported by Vijayaraman et al[17] by using HOT-CRT in a feasibility study of 27 patients with class III–IV heart

failure. LVEF increased by ~9% in the present study compared with an average increase of 14% reported with HOT-CRT. Similar rates of super-response were observed in both study populations (24% vs 28%). Many of the operators in our study were well versed in HOT-CRT, and patient selection might likely have been biased toward a sicker population.

Clinical implications

There is a great diversity of both the extent and the location of conduction disorders that cause electromechanical delay. In patients eligible for CRT, empirical CRT based on BiV pacing without regard to the mechanism underlying electrical dyssynchrony may not fully achieve optimal clinical outcomes. LOT-CRT may provide an alternate, individualized, more tailored approach to CRT in patients with advanced peripheral conduction disease. This approach needs to be further studied in a randomized fashion.

This study suggests that LBB capture might be related to better outcomes than did LVS capture when combined with CV LV pacing and probably should be the preferred procedural goal in CRT candidates. Further studies are needed to clarify the clinical difference between LVS pacing and LBB pacing, especially in patients with heart failure.

Limitations

The major limitation of this observational study was the nonconsecutive patient design and lack of uniform criteria to select patients for LOT-CRT rather than for BiV-CRT or LBBAP alone, leading to potential selection and operator bias.

Lack of randomization and acute ECG-only comparison between LOT-CRT and BiV-CRT were other limitations. Our aim was to primarily demonstrate the feasibility of the LOT-CRT approach. Randomized studies with longer-term follow-up may be necessary to assess the value of this novel CRT concept in clinical practice.

One practical procedure-related limitation concerned the need to use an additional lead and capping of the RV pace/sense lead and loss of magnetic resonance imaging conditionality. In the future, it may be possible to use a defibrillation coil alone in the RV in order to eliminate the need for RV pace/sense capping.

In 15 of 29 patients with CRT–pacemaker devices, BiV-CRT QRS complex could not be obtained because of the lack of the RV pacing lead.

In some patients with significant septal scar, the LBBAP lead may be associated with smaller and fractionated electrograms. However, in this study, we did not observe any sensing issues related to this approach during follow-up, but this needs to be carefully considered during implantation.

Conclusion

LOT-CRT is feasible and safe and provides greater electrical resynchronization, compared with BiV-CRT, and could be an alternative to BiV-CRT, especially when only suboptimal electrical resynchronization is obtained with BiV-CRT. Randomized controlled trials comparing LOT-CRT and BiV-CRT are needed.

References

1. Huang W, Su L, Wu S, et al. A novel pacing strategy with low and stable output: pacing the left bundle branch immediately beyond the conduction block. Can J Cardiol 2017;33:1736.
2. Huang W, Chen X, Su L, Wu S, Xia X, Vijayaraman P. A beginner's guide to permanent left bundle branch pacing. Heart Rhythm 2019;16:1791–1796.
3. Ponnusamy SS, Arora V, Namboodiri N, Kumar V, Kapoor A, Vijayaraman P. Left bundle branch pacing: a comprehensive review. J Cardiovasc Electrophysiol 2020;31:2462–2473.
4. Vijayaraman P, Ponnusamy S, Cano O, et al. Left bundle branch area pacing for cardiac resynchronization therapy: results from the International LBBAP Collaborative Study Group. JACC Clin Electrophysiol 2021;7:135–147.
5. Herweg B, Ilercil A, Madramootoo C, et al. Latency during left ventricular pacing from the lateral cardiac veins: a cause of ineffectual biventricular pacing. Pacing Clin Electrophysiol 2006;29:574–581.
6. Jastrzebski M, Wilinski J, Fijorek K, Sondej T, Czarnecka D. Mortality and morbidity in cardiac resynchronization patients: impact of lead position, paced left ventricular QRS morphology and other characteristics on long-term outcome. Europace 2013;15:258–265.
7. Vijayaraman P. Left bundle branch pacing optimized cardiac resynchronization therapy: a novel approach [published online ahead of print July 21, 2021]. JACC Clin Electrophysiol. https://doi.org/10.1016/j.jacep.2021.04.005.
8. Jastrzebski M, Moskal P, Holda MK, et al. Deep septal deployment of a thin, lumenless pacing lead: a translational cadaver simulation study. Europace 2020; 22:156–161.
9. Jastrzebski M, Kielbasa G, Moskal P, et al. Fixation beats: a novel marker for reaching the left bundle branch area during deep septal lead implantation. Heart Rhythm 2021;18:562–569.
10. Ponnusamy SS, Ganesan V, Syed T, Balasubramanian S, Vijayaraman P. Template beat: a novel marker for left bundle branch capture during physiological pacing. Circ Arrhythm Electrophysiol 2021;14:e009677.
11. Jastrzebski M, Moskal P. Reaching the left bundle branch pacing area within 36 heartbeats. Kardiol Pol 2021;79:587–588.
12. Jastrzebski M. ECG and pacing criteria for differentiating conduction system pacing from myocardial pacing. Arrhythm Electrophysiol Rev 2021. In press.
13. Lang RM, Badano LP, Mor-Avi V, et al. Recommendations for cardiac chamber quantification by echocardiography in adults: an update from the American Society of Echocardiography and the European Association of Cardiovascular Imaging. J Am Soc Echocardiogr 2015;28:1–39.
14. Abraham WT, Fisher WG, Smith AL, et al. Cardiac resynchronization in chronic heart failure. N Engl J Med 2002;346:1845–1853.
15. Gold MR, Thebault C, Linde C, et al. Effect of QRS duration and morphology on cardiac resynchronization therapy outcomes in mild heart failure: results from the Resynchronization Reverses Remodeling in Systolic Left Ventricular Dysfunction (REVERSE) study. Circulation 2012;126:822–829.
16. Sweeney MO, van Bommel RJ, Schalij MJ, Borleffs CJ, Hellkamp AS, Bax JJ. Analysis of ventricular activation using surface electrocardiography to predict left ventricular reverse volumetric remodeling during cardiac resynchronization therapy. Circulation 2010;121:626–634.
17. Vijayaraman P, Herweg B, Ellenbogen KA, Gajek J. His-optimized cardiac resynchronization therapy to maximize electrical resynchronization: a feasibility study. Circ Arrhythm Electrophysiol 2019;12:e006934.
18. Reddy VY, Miller MA, Neuzil P, et al. Cardiac resynchronization therapy with wireless left ventricular endocardial pacing: the SELECT-LV study. J Am Coll Cardiol 2017;69:2119–2129.
19. Deshmukh A, Sattur S, Bechtol T, Heckman LIB, Prinzen FW, Deshmukh P. Sequential His bundle and left ventricular pacing for cardiac resynchronization. J Cardiovasc Electrophysiol 2020;31:2448–2454.
20. Jastrzebski M, Baranchuk A, Fijorek K, et al. Cardiac resynchronization therapy-induced acute shortening of QRS duration predicts long-term mortality only in patients with left bundle branch block. Europace 2021;21:281–289.
21. Kronborg MB, Nielsen JC, Mortensen PT. Electrocardiographic patterns and long-term clinical outcome in cardiac resynchronization therapy. Europace 2010;12:216–222.
22. Sweeney MO, Hellkamp AS, van Bommel RJ, Schalij MJ, Borleffs CJ, Bax JJ. QRS fusion complex analysis using wave interference to predict reverse remodeling during cardiac resynchronization therapy. Heart Rhythm 2014;11:806–813.

23. Huang W, Wu S, Vijayaraman P, et al. Cardiac resynchronization therapy in patients with nonischemic cardiomyopathy using left bundle branch pacing. JACC Clin Electrophysiol 2020;6:849–858.
24. Upadhyay GA, Cherian T, Shatz DY, et al. Intracardiac delineation of septal conduction in left bundle branch block patterns: mechanistic evidence of left intra-hisian block circumvented by His pacing. Circulation 2019; 139:1876–1888.
25. Jastrzebski M, Kielbasa G, Curila K, et al. Physiology-based electrocardiographic criteria for left bundle branch capture. Heart Rhythm 2021;18: 935–943.

Journal of Interventional Cardiac Electrophysiology
https://doi.org/10.1007/s10840-020-00899-4

CASE REPORTS

Concealed left bundle branch potential during physiological pacing

Shunmuga Sundaram Ponnusamy[1] · Pugazhendhi Vijayaraman[2]

Received: 6 October 2020 / Accepted: 19 October 2020

A 70-year-old gentleman presented to us with recurrent syncope, intermittent left bundle branch block (LBBB) (Fig. 1a) and left ventricular ejection fraction of 35%. He had undergone percutaneous coronary intervention for inferior wall myocardial infarction 5 months ago. Holter monitoring showed intermittent LBBB and high-grade AV block. A3830 Selectsecure^{tm} lead was deployed using C315-His sheath to capture the left bundle branch (LBB) [1]. Electrocardiography showed narrow QRS duration during the procedure. After 4 rapid rotations, LBB potential was noted (Fig. 2a) but the peak left ventricular activation time (pLVAT) at 2 V/0.5 ms pacing output was 93 ms. One more rotation resulted in negative LBB current of injury (LBB-COI) with disappearance of LBB potential (Fig. 2b) but pLVAT improved to 53 ms at 2 V/0.5 ms. Resurgence of concealed LBB potential was noted after 20 min. A predominant negative deflection followed by sharp high frequency biphasic potential was observed (Fig. 2c–f), which was different from the three types of LBB-COI described by Su et al. [2]. This type IV LBB-COI pattern concealing the LBB potential has to be considered before repositioning the lead due to sudden loss of LBB potential during deployment.

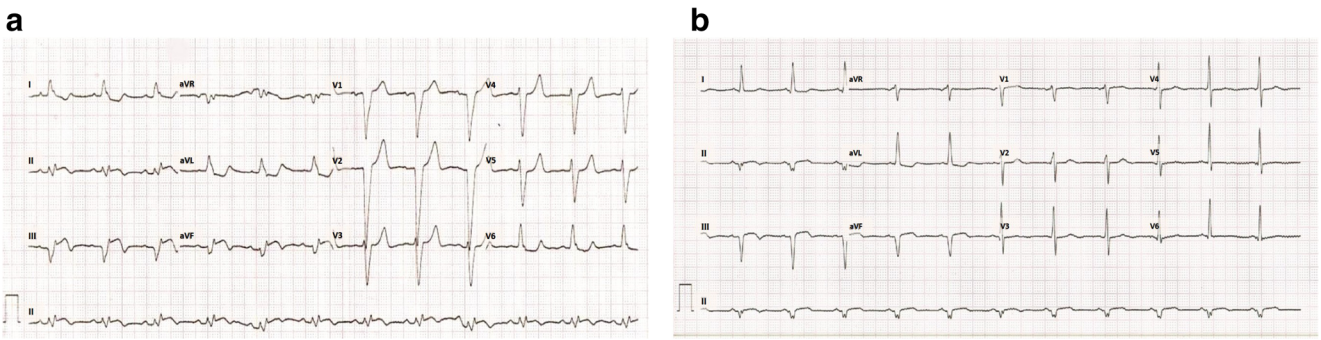

Fig. 1 **a** Baseline 12 lead electrocardiography showed complete left bundle branch block with Q waves in inferior leads. **b** Post LBBP ECG showed narrow paced QRS with duration of 108 ms

✉ Shunmuga Sundaram Ponnusamy
shunmuga.pgi@gmail.com

[1] Department of Cardiology, Velammal Medical College Hospital and Research Institute, Madurai, Tamilnadu, India

[2] Geisinger Commonwealth School of Medicine, Geisinger Heart Institute, MC 36-10, 1000 E Mountain Blvd, Wilkes-Barre, PA 18711, USA

Published online: 04 November 2020

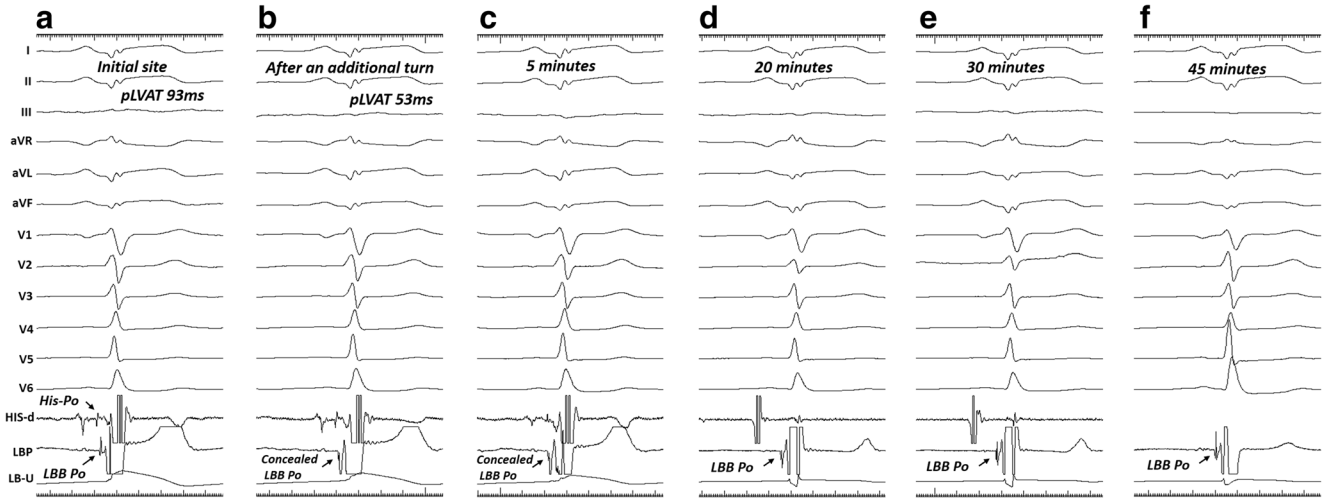

Fig. 2 Concealed left bundle branch potential. **a** After 4 rotations, LBB potential (LBB Po) was noted but pLVAT was 93 ms at 2 V/0.5 ms. **b** One more rotation was given resulted in LBB COI with disappearance of LBB potential with improvement in pLVAT to 53 ms at 2 V/0.5 ms. **c**–**f** Gradual resurgence from a predominantly negative deflection to sharp high frequency biphasic LBB potential after 45 min. His Po His bundle potential, COI current of injury, LBB CON concealed LBB potential within the current of injury

Authors' contribution SSP: Consultant: Medtronic

PV: Honoraria, consultant, research, fellowship support: Medtronic, consultant: Boston Scientific, Abbott, Biotronik, Eaglepoint LLC

Compliance with ethical standards

Ethical approval The study was conducted after getting the ethical committee approval.

Conflict of interest The authors declare that they have no conflict of interest.

The paper is not under consideration elsewhere. None of the paper's contents have been previously published. All authors have read and approved the manuscript.

References

1. Ponnusamy SS, Arora V, Namboodiri N, Kumar V, Kapoor A, Vijayaraman P. Left bundle branch pacing: a comprehensive review. J Cardiovasc Electrophysiol. 2020;31(9):2462–73.
2. Su L, Xu T, Cai M, Xu L, Vijayaraman P, Sharma PS, et al. Electrophysiological characteristics and clinical values of left bundle branch current of injury in left bundle branch pacing. J Cardivasc Electrophysiol. 2020;31:834–42.

JACC: CLINICAL ELECTROPHYSIOLOGY VOL. 7, NO. 10, 2021

PUBLISHED BY ELSEVIER

IMAGES IN ELECTROPHYSIOLOGY

Bundle Branch Re-Entrant Ventricular Tachycardia During Left Bundle Branch Pacing

Shunmuga Sundaram Ponnusamy, MD, DM,[a] Pugazhendhi Vijayaraman, MD[b]

A 58-year-old woman with left ventricular (LV) ejection fraction of 24% underwent cardiac resynchronization therapy with a defibrillator for recurrent heart failure, with episodes of nonsustained ventricular tachycardia. Electrocardiography showed left bundle branch block with a QRS duration of 200 ms and prolonged PR interval of 210 ms (**Figure 1A**). Diagnostic quadripolar catheters were placed at the His bundle region and right ventricle apex. Left bundle branch pacing (LBBP) was performed using a C315 sheath and Selectsecure lead (Medtronic) by premature ventricular complex-guided approach (1). Premature ventricular complexes generated during rapid lead deployment showed a prolonged V-H interval and induced bundle branch re-entrant ventricular tachycardia of left bundle branch block morphology (**Figure 1A**). The H-V interval during tachycardia was constant at 72 ms (baseline H-V interval: 68 ms), and change in the H-H interval preceded and predicted the change in the V-V interval (**Figure 1B**), suggesting bundle branch re-entrant tachycardia (2). Tachycardia could be easily induced by pacing the LBBP lead (**Figure 1B**). Retrograde left bundle potential was noted in the pacing lead electrogram (**Figure 1A**). The LBBP lead was connected to the LV port and the DF-1 defibrillator lead to the right ventricle port. Final electrocardiography showed a QRS duration of 116 ms after atrioventricular interval optimization. Device interrogation during the 3-month follow-up showed stable parameters (sensed R-wave: 7 mV) without any ventricular tachycardia and improvement in LV ejection fraction to 39%. Radiofrequency ablation of the right bundle branch was not considered because the patient had not demonstrated sustained ventricular tachycardia. Additionally, atrioventricular delay optimization (100 ms) and QRS duration normalization was achieved with fusion pacing, and a ventricular sense response algorithm was programmed to provide LBBP after a sensed- ventricular event.

FUNDING SUPPORT AND AUTHOR DISCLOSURES

The authors have reported that they have no relationships relevant to the contents of this paper to disclose.

ADDRESS FOR CORRESPONDENCE: Dr Shunmuga Sundaram Ponnusamy, Department of Cardiology, Velammal Medical College Hospital and Research Institute, Velammal Village, Madurai 625009, Tamilnadu, India. E-mail: shunmuga.pgi@gmail.com.

From the [a]Department of Cardiology, Velammal Medical College Hospital and Research Institute, Madurai, Tamilnadu, India; and the [b]Geisinger Commonwealth School of Medicine, Geisinger Heart Institute, Wilkes-Barre, Pennsylvania, USA.

The authors attest they are in compliance with human studies committees and animal welfare regulations of the authors' institutions and Food and Drug Administration guidelines, including patient consent where appropriate. For more information, visit the Author Center.

Manuscript received April 19, 2021; revised manuscript received June 4, 2021, accepted June 13, 2021.

ISSN 2405-500X/$36.00 https://doi.org/10.1016/j.jacep.2021.06.004

FIGURE 1 **Bundle Branch Re-Entrant Ventricular Tachycardia During LBBP**

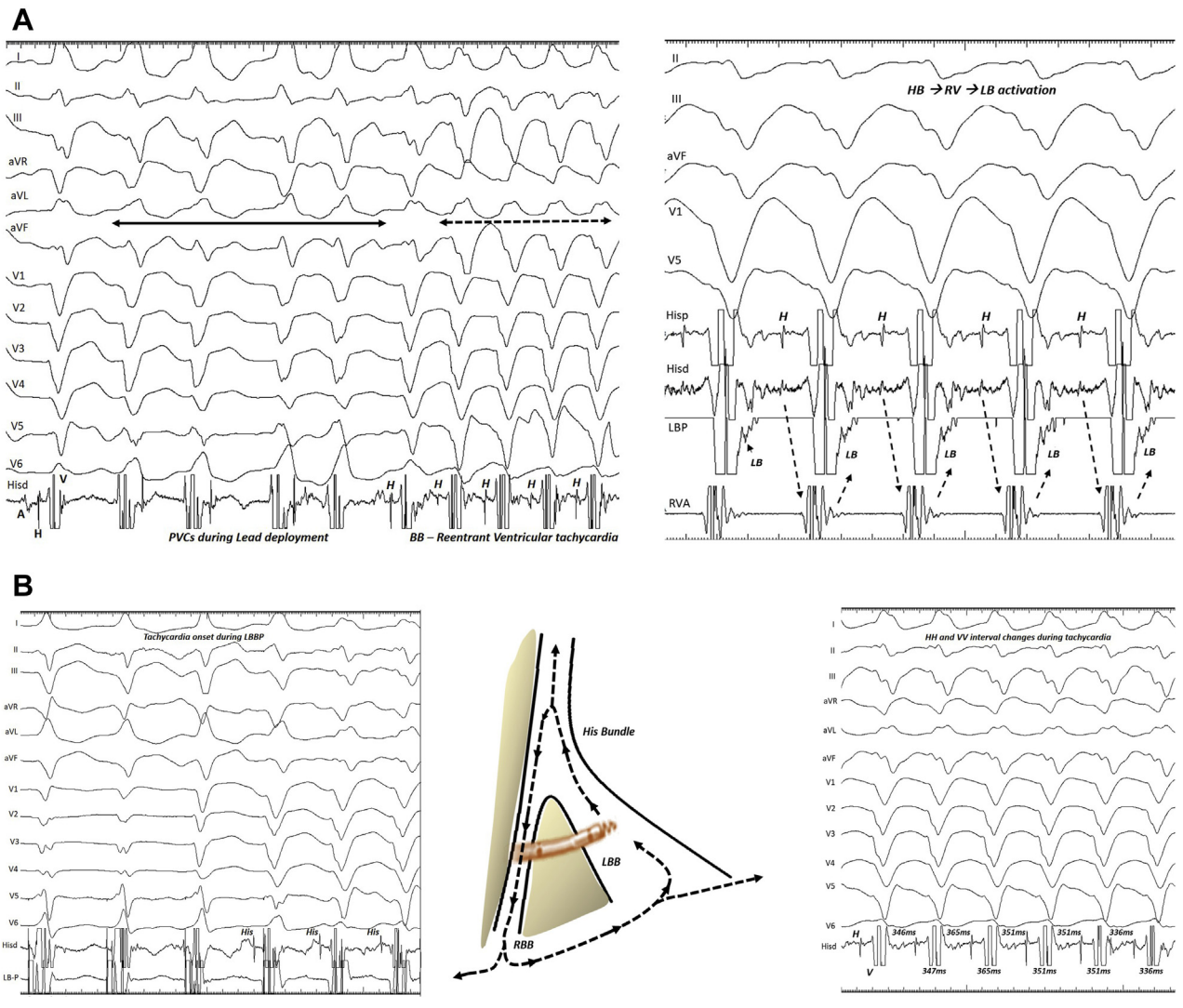

(A) Bundle branch re-entrant ventricular tachycardia was induced by premature ventricular complexes with a prolonged retrograde V-H interval. Right ventricle activation occurred after His potential, followed by the ventricular electrogram on the left bundle branch pacing lead with retrograde left bundle potential. **(B)** Tachycardia initiation during left bundle pacing with constant H-V interval after the onset. The H-V interval during tachycardia was 72 ms, with changes in the H-H interval preceding changes in the V-V interval. BB = bundle branch; HB = His bundle; LB = left bundle; LBBP = left bundle branch pacing; LV = left ventricle; PVC = premature ventricular complex; RBB = right bundle branch; RV = right ventricle.

REFERENCES

1. Ponnusamy SS, Vijayaraman P. Left-bundle-branch-pacing guided by premature-ventricular-complexes during implant. *Heart Rhythm Case Rep*. 2020;6(11):1–4.

2. Mazur A, Kusneic J, Strasberg B. Bundle-branch-reentrant ventricular tachycardia. *Indian Pacing Electrophysiol J*. 2005;5(2):86–95.

KEY WORDS bundle branch re-entrant ventricular tachycardia, heart failure, left bundle branch pacing, premature ventricular complex

Journal of Interventional Cardiac Electrophysiology
https://doi.org/10.1007/s10840-021-01028-5

CASE REPORTS

Unmasking of left bundle branch potential in left bundle branch block during physiological pacing

Shunmuga Sundaram Ponnusamy[1] · **Pugazhendhi Vijayaraman**[2]

Received: 5 April 2021 / Accepted: 24 June 2021

A 70-years-old lady had undergone left bundle branch pacing (LBBP) for left bundle branch block (LBBB) (Fig. 1A) with left ventricular ejection fraction of 35% using C315 sheath and 3830 SelectSecure^{tm} lead [1]. Both non-selective to selective (Fig. 1B) and non-selective to septal capture transition could be demonstrated by decreasing the pacing output. Left bundle branch potential (LBB-Po) during sinus rhythm was unmasked without performing dual lead technique by gap phenomenon (Fig. 1D and E). Unipolar threshold measurement by rapid pacing resulted in loss of LBB capture at 0.2 V/0.5 ms followed by a blocked P-wave which peeled away the refractoriness of LBB transiently (phase 3 block) [2]. The next beat showed antegrade activation of LBB resulting in narrow QRS duration (Fig. 2A) and appearance of LB potential on the lead electrogram. Subsequent beats were conducted through right bundle (RB) with LBBB pattern. Programmed deep septal stimulation showed change in QRS morphology and R-wave peaking time at 500 ms (S1) and 300 ms (S2) confirming loss of LBB capture (Fig. 2B). Final paced QRS after optimizing AV delay was 98 ms (Fig. 1C). Burst pacing of the LBB to peel away the refractoriness is an alternative option to dual lead technique to unmask the LBB potential in patients with complete LBBB. Careful evaluation by electrophysiology study is required to document the phase 3 block.

✉ Shunmuga Sundaram Ponnusamy
shunmuga.pgi@gmail.com

[1] Department of Cardiology, Velammal Medical College Hospital and Research Institute, Madurai, Tamilnadu, India

[2] Geisinger Commonwealth School of Medicine, Geisinger Heart Institute, MC 36-10, 1000 E Mountain Blvd, Wilkes-Barre, PA 18711, USA

Published online: 10 July 2021

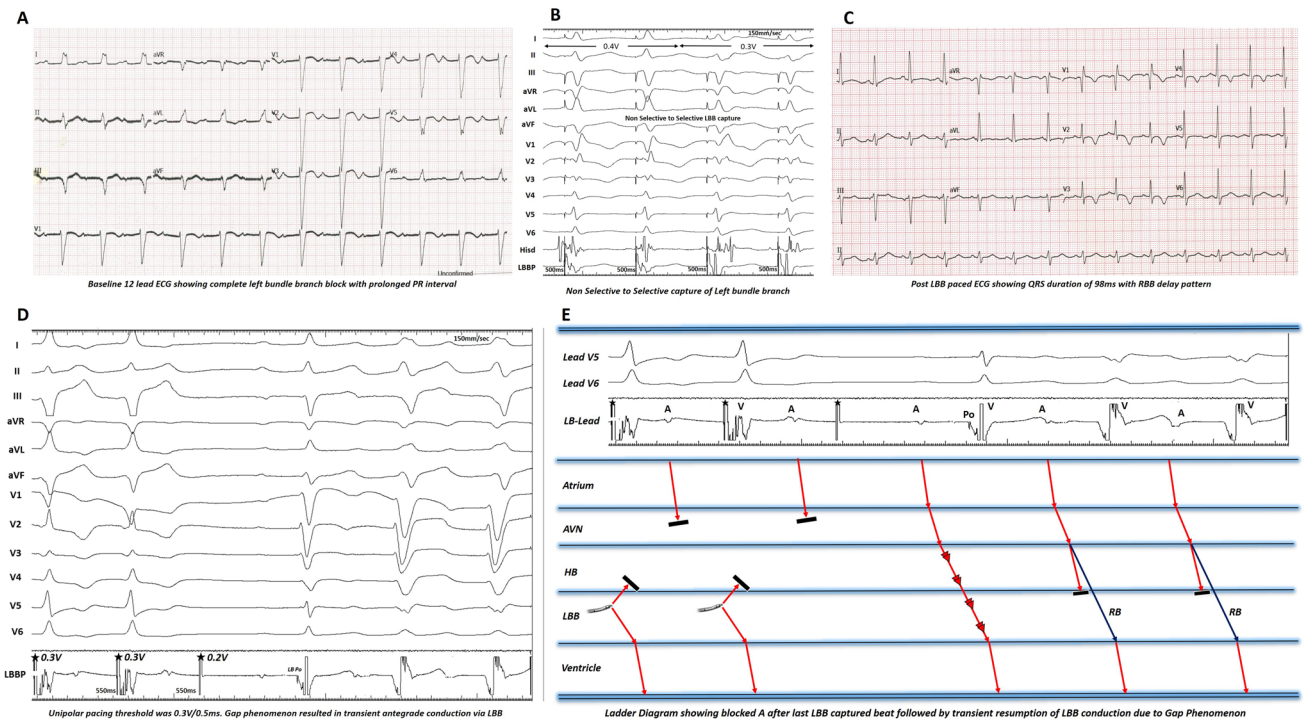

Fig. 1 **A** Baseline 12 lead ECG showing complete left bundle branch block. **B** Non-selective to selective capture transition during decremental unipolar pacing. **C** Post LBB paced QRS with duration of 98 ms. **D** Rapid pacing from LBBP lead. Unipolar pacing threshold was 0.3 V/0.5 ms. Gap phenomenon resulted in transient antegrade conduction via left bundle. **E** Ladder diagram showing blocked A after last LBB captured beat followed by transient resumption of LBB conduction due to gap phenomenon

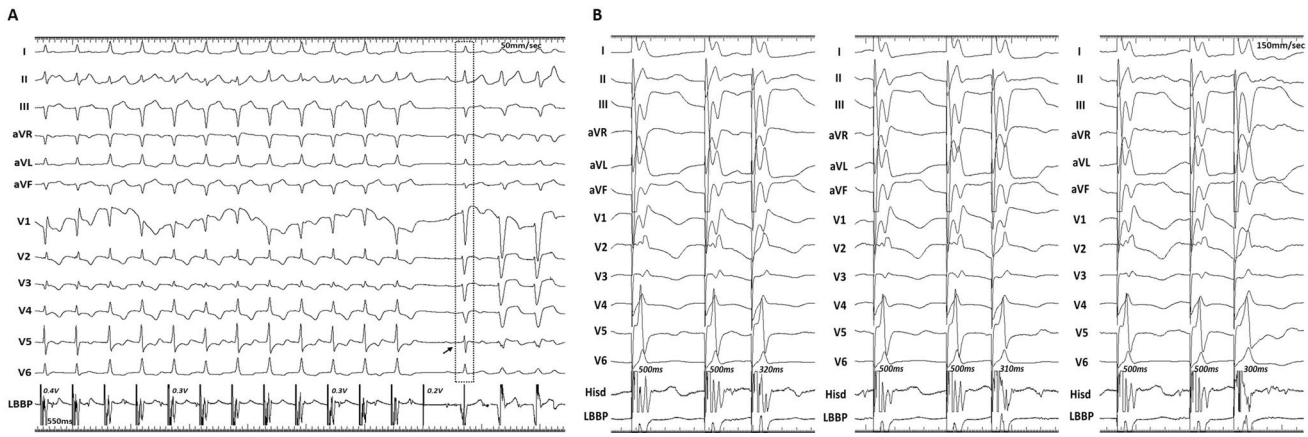

Fig. 2 **A** Rapid pacing from LBBP with decremental output resulted in progressive reduction in R-wave amplitude and loss of capture at 0.2 V followed by blocked P-wave which peeled away the refractoriness of LBB. The next beat (arrow head) showed narrow QRS duration with LBB potential on the pacing lead electrogram. **B** Programmed deep septal stimulation showed loss of R-wave in V1 at 300 ms with change in QRS morphology confirming loss of LBB capture

Author contribution All authors have read and approved the manuscript.

Declarations

Ethics approval The study was conducted after getting the ethical committee approval.

Conflict of interest SSP: Consultant, Medtronic. PV: Honoraria, consultant, research, fellowship support, Medtronic; consultant, Boston Scientific, Abbott, Biotronik, Eaglepoint LLC.

References

1. Ponnusamy SS, Arora V, Namboodiri N, et al. Left bundle branch pacing: a comprehensive review. J Cardiovasc Electrophysiol. 2020;31(9):2462–73.
2. El-Sherif N, Jalife J. Paroxysmal AV block: are phase 3 and phase 4 block mechanisms or misnomers? Heart Rhythm. 2009;6:1514–21.

Received: 19 May 2021 | Revised: 2 June 2021 | Accepted: 29 June 2021

DOI: 10.1111/jce.15155

CASE REPORTS

WILEY

Late dislodgement of left bundle branch pacing lead and successful extraction

Shunmuga Sundaram Ponnusamy MD, DM, CEPS[1] | Pugazhendhi Vijayaraman MD, FHRS[2]

[1]Department of Cardiology, Velammal Medical College Hospital and Research Institute, Madurai, Tamil Nadu, India

[2]Geisinger Commonwealth School of Medicine, Geisinger Heart Institute, Wilkes-Barre, Pennsylvania, USA

Correspondence
Shunmuga Sundaram Ponnusamy MD, DM, CEPS, Department of Cardiology, Velammal Medical College Hospital and Research Institute, Velammal Village, Madurai 625009, Tamil Nadu, India.
Email: shunmuga.pgi@gmail.com

Abstract

A 61-years-old male underwent left bundle branch pacing for nonischemic dilated cardiomyopathy with recurrent heart failure. Left bundle branch pacing (LBBP) resulted in reduction in QRS duration along with improvement in left ventricular ejection fraction (LVEF) to 64% during follow-up. Two years after implantation he had recurrence of symptoms along with decline in LVEF to 51%. Late lead dislodgement was diagnosed and re-do LBBP was planned. The lead was extracted en-masse without complication and a new 3830 lead was positioned deep inside the proximal septum to capture the left bundle. Postprocedure echocardiography showed no ventricular septal defect or damage to tricuspid leaflet.

KEYWORDS
late dislodgement, lead extraction, left bundle branch pacing

1 | INTRODUCTION

Left bundle branch pacing (LBBP) overcomes the limitation of His bundle pacing (HBP) as it provides stable pacing parameters at low capture threshold.[1] Though studies have shown the feasibility of LBBP as an alternative strategy for cardiac resynchronization therapy the long-term safety of LBBP is yet to be available.[2–4] A prospective study by Su et al.,[5] showed stable pacing parameters at mean follow-up of 2 years. Currently available tools for lead extraction may not be able to safely remove the deeply positioned LBBP lead in the proximal interventricular septum. In this paper we describe a case of late lead dislodgement of LBBP lead, 2 years after initial implantation for which successful manual extraction was done along with lead repositioning in LBB area.

1.1 | Case description

A 61-year-old male underwent LBBP for nonischemic cardiomyopathy, left bundle branch block (QRS duration 160 ms) with left ventricular ejection fraction (LVEF) of 25%. He was under treatment for obstructive airway disease. LBBP resulted in significant reduction in QRS duration to 108 ms with normal axis. Patient showed significant improvement in clinical symptoms and LVEF increased to 64% during 6-month follow-up. His heart failure medications were gradually reduced. During subsequent office visits electrocardiography (ECG) demonstrated LBB capture (Figure 1). Lead V1 showed rSR' pattern with narrow QRS duration. The QRS axis remained normal with rapid LV free wall activation as evidenced by short R-wave peaking time in lateral leads. After 2 years, he presented with exertional dyspnea along with decline in LVEF to 51%. ECG confirmed loss of LBB capture with QRS duration of 150 ms (Figure 1). Device interrogation showed right ventricular (RV) septal capture with threshold of 0.75 V at 0.5 ms pulse-width and unipolar pacing impedance of 620 ohms. Late dislodgement of LBBP lead was diagnosed and re-do cardiac resynchronization therapy was planned. Left anterior oblique fluoroscopy view confirmed lead dislodgment with the anode completely displaced out of the septum (Figure 1).

The lumen-less 3830 Selectsecure^{tm} lead (Medtronic) was removed en-masse (Figure 2B) from the proximal septum using manual traction within three cardiac cycles (video). There was no hemodynamic compromise during the procedure. LBBP was again performed 5 mm apical to the initial implantation site using a new 3830 pacing lead with C315His sheath. Deep septal placement of the lead captured the LBB with

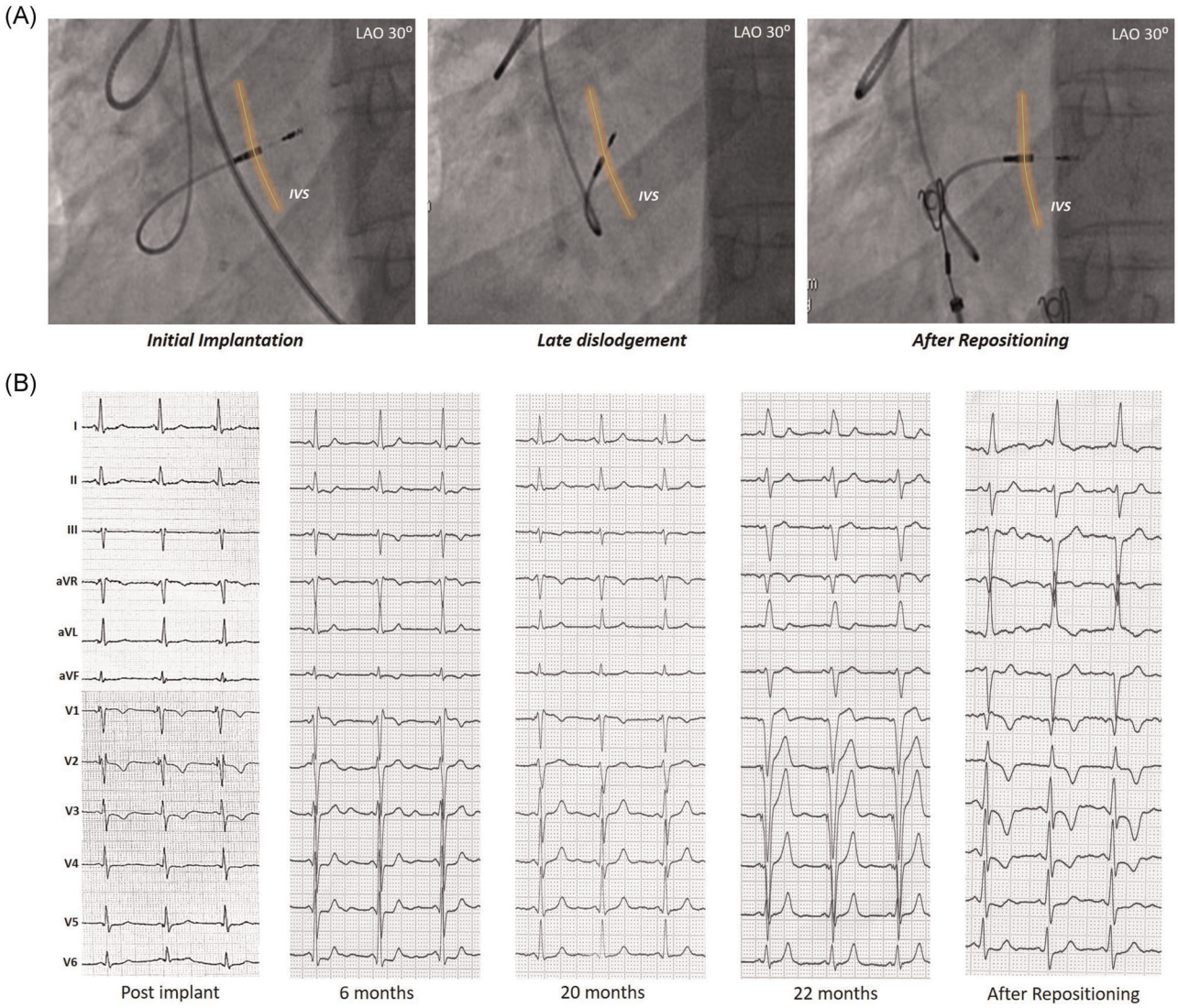

FIGURE 1 Late lead dislodgement and repositioning after LBBP. (A) Fluoroscopic image in left anterior oblique view showing the lead position after initial implantation, dislodgement and repositioning. (B) Serial change in electrocardiography at immediate postimplantation, follow-up in device clinic and after repositioning. Note: at 22 months after implantation, the lead was capturing the septum with LBBB pattern and wide QRS (150 ms). LBBP, left bundle branch pacing

reduction in QRS duration to 90ms after optimizing the atrio-ventricular delay (Figure 1). The capture threshold was 0.3 V at 0.5 ms pulse-width with unipolar pacing impedance of 580 ohms. LBBP lead was connected to the ventricular port of the same dual chamber pulse-generator. Post-procedure echocardiography showed no evidence of ventricular septal defect (from lead extraction) and the location of the new lead placed 13 mm inside the septum (Figure 2B). Patient had an uneventful hospital stay and was discharged on the next day.

2 | DISCUSSION

Huang et al.[2] first described LBBP as an alternative to HBP and bi-ventricular pacing to achieve cardiac resynchronization therapy. LBBP is done by using C315 His sheath and 3830 Selectsecure^{tm} lead (Medtronic).[1] The lead is placed deep inside the proximal inter-ventricular septum 1–1.5 cm below the His bundle along an imaginary line connecting distal His signals with RV apex by 4–5 rapid rotations. It is important to differentiate LBBP from LV septal pacing as conduction system capture is essential for electrical and mechanical synchrony.

Though several studies have shown feasibility and safety of the procedure along with stable pacing parameters during follow-up,[3,4] lead dislodgment could still occur due to lack of effective anchoring mechanism. Su et al.[5] reported increase in capture threshold by >3 V or loss of capture in 1% (6/618) of patients. No late lead dislodgement was noted though two patients required lead revision due to acute dislodgement on the next day. In our patient consistent capture of LBB could be demonstrated till 20 months after implantation with stable pacing threshold and unipolar pacing impedance (Figure 2D).

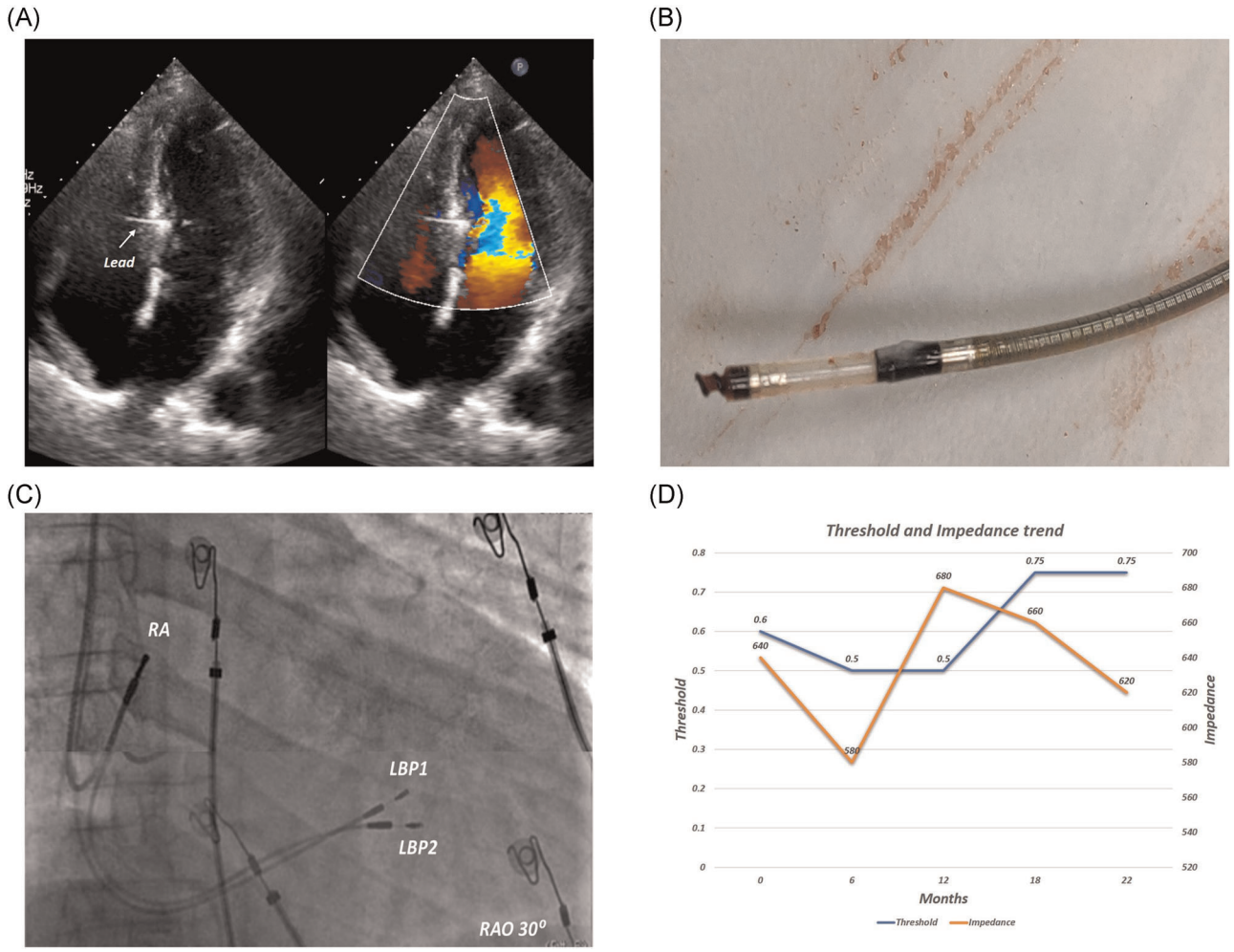

FIGURE 2 (A) Echocardiography showing the depth of the pacing lead and intact ventricular septum after repositioning. (B) Extracted lead with intact helix and ring electrode. (C) Superimposed fluoroscopy image in right anterior oblique (RAO) view showing pacing lead location during initial implantation (LBP1) and after reimplantation (LBP-2). (D) Threshold and pacing impedance trend from the time of implantation

The loss of LBB capture was accompanied by reoccurrence of symptoms and decline in EF to 51% after 2 months. The reason for late lead dislodgement in our patient is not known but could be due to old age, recent weight loss resulting in tissue laxity in the pocket and chest physiotherapy received for his obstructive airway disease.[6,7] Though the septal capture threshold was <1 V at 0.5 ms pulse-width, as LBB capture could not be demonstrated even at high output it was decided to reposition the lead. Controlled traction was applied manually which removed the lead en-masse without damaging the interventricular septum (Video S1). The extracted lead showed intact helix and ring electrode without insulation damage (Figure 2B). A new 3830 selectsecure lead was implanted 5 mm apical to the initial implantation site (Figure 2C) and QRS had leftward shift in the axis (Figure 1). Paced QRS during initial implantation showed normal axis with Rs in lead aVF as compared to the QRS after re-do procedure which showed leftward shift in axis and rS in lead aVF (Figure 1). Alternatively, dislodged lead could have been extracted after completing the implantation procedure of the new lead to avoid going through the same septal location.

Concerns regarding the feasibility and consequences of extraction of the lead from its deep septal location remain. The need for lead revision is less as compared to HBP. Teigeler et al.,[8] showed loss of His bundle capture was seen in 17% during mean follow-up of 22.8 ± 19.5 months. 11% (31 patients) underwent lead revisions for unacceptable high threshold. Su et al.,[5] showed 0.32% (2/618 patients) lead revision rate for lead dislodgement after LBBP during mean follow-up of 18.6 ± 6.7 months. Previously successful manual extraction of the LBBP lead, 1 year after implantation had been reported.[9] Here we have described an unusual case of late dislodgement of LBBP Lead and successful manual extraction of the lead, 2 years after initial implantation.

3 | CONCLUSION

LBBP is a novel technique in the armamentarium of conduction system pacing which provides stable pacing parameters at low capture threshold. Long-term safety of LBBP is yet to be established.

Lead extraction of LBBP lead can be attempted safely provided there is no major venous adhesions along its course.

CONFLICT OF INTERESTS

Shunmuga Sundaram Ponnusamy: Consultant Medtronic. Pugazhendhi Vijayaraman: Speaker, Consultant, Research, Fellowship support (Medtronic), Consultant (Biotronik, Boston Scientific, Abbott, Eaglepoint LLC); patent—His delivery tool.

DATA AVAILABILITY STATEMENT

The data that support the findings of this study are available from the corresponding author upon reasonable request. The data underlying this article are available in the article and in its online Supporting Information material.

ORCID

Shunmuga Sundaram Ponnusamy https://orcid.org/0000-0002-7059-425X

Pugazhendhi Vijayaraman https://orcid.org/0000-0003-2230-100X

REFERENCES

1. Ponnusamy SS, Arora V, Namboodiri N, Kumar V, Kapoor A, Vijayaraman P. Left bundle branch pacing: a comprehensive review. *J Cardiovasc Electrophysiol*. 2020;31:1-12. https://doi.org/10.1111/jce.14681
2. Huang W, Su L, Wu S, et al. A novel pacing strategy with low and stable output: pacing the left bundle branch immediately beyond the conduction block. *Can J Cardiol*. 2017;33:1736.e1-3.
3. Vijayaraman P, Ponnusamy SS, Cano O, et al. Left bundle branch area pacing for cardiac resynchronization therapy: results from international LBBAP collaborative study group. *J Am Coll Cardiol EP*. 2021;7(2):135-147.
4. Ponnusamy SS, Muthu G, Kumar M, Bopanna D, Anand V, Kumar S. Mid-term feasibility, safety and outcomes of left bundle branch pacing—single center experience. *J Interv Card Electrophysiol*. 2021;60(2):337-346. https://doi.org/10.1007/s10840-020-00807-w
5. Su L, Wang S, Wu S, et al. Long-term safety and feasibility of left bundle branch pacing in a large single-center study. *Circ Arrhythm Electrophysiol*. 2021;14:e009261.
6. Tseng AS, Shipman JN, Lee JZ, et al. Incidence, patterns, and outcomes after transvenous cardiac device lead macrodislodgement: insights from a population-based study. *Heart Rhythm*. 2019;16(1):140-147.
7. Espliguero RA, Dominguez JFO, Mejuto EC, et al. Late displacement of a ventricular pacing lead after respiratory theapy. *Pacing Clin Electrophysiol*. 2001;24(11):1693-1695.
8. Teigeler T, Kolominsky J, Vo C, et al. Intermediate-term performance and safety of His-bundle pacing leads: a single-center experience. *Heart Rhythm*. 2021;18(5):743-749.
9. Vijayaraman P. Extraction of left bundle branch pacing lead. *J Am Coll Cardiol Clin Electrophysiol*. 2020;6(7):903-904.

SUPPORTING INFORMATION

Additional Supporting Information may be found online in the supporting information tab for this article.

How to cite this article: Ponnusamy SS, Vijayaraman P. Late Dislodgement of Left Bundle Branch Pacing Lead and Successful Extraction. *J Cardiovasc Electrophysiol*. 2021;32:2346-2349. https://doi.org/10.1111/jce.15155

Journal of Interventional Cardiac Electrophysiology
https://doi.org/10.1007/s10840-021-01014-x

CASE REPORTS

Segmental fascicular block during physiological pacing

Shunmuga Sundaram Ponnusamy[1] · **Pugazhendhi Vijayaraman**[2]

Received: 27 April 2021 / Accepted: 23 May 2021

A 63-year-old male underwent left bundle branch pacing (LBBP) for symptomatic atrio-ventricular (AV) block. Using C315 His sheath a 3830 SelectSecure™ lead was placed deep inside the septum 1.5 cm apical to the distal His bundle signal with monitoring of paced QRS morphology and unipolar pacing impedance. Intracardiac electrograms showed AH block with HV interval of 54 ms. Left posterior fascicle was captured (Fig. 1A) resulting in right bundle branch delay pattern in lead-V1, left axis deviation with short and constant left ventricular activation time [1]. Distal His bundle pacing was excluded based on paced QRS morphology and fluoroscopic position of the lead. Unipolar pacing with decremental output showed non-selective to selective capture transition with appearance of potential after the pacing spike on the 3830 lead electrogram. The interval from potential to QRS onset during pacing was less (29 ms) as compared to native rhythm (49 ms) (Fig. 1B). Additionally, there was a reversal of polarity of the left bundle branch potential during pacing compared to native rhythm (Fig. 1C). The left posterior fascicle is extensively arborized and has numerous ramifications with interconnections [2]. The observed phenomenon may be explained by block in one of the segmental branches of the left posterior fascicle with conduction circling around the zone of block (Fig. 2A). Despite local conduction block, final paced QRS duration was narrow (Fig. 2B) due to extensive septal arborization of left bundle. Hence, LBBP could be considered even in patients with fascicular block as it can effectively correct distal conduction system disease.

✉ Shunmuga Sundaram Ponnusamy
shunmuga.pgi@gmail.com

[1] Department of Cardiology, Velammal Medical College Hospital and Research Institute, Madurai, Tamilnadu, India

[2] Geisinger Commonwealth School of Medicine, Geisinger Heart Institute, MC 36-10, 1000 E Mountain Blvd, Wilkes-Barre, PA 18711, USA

Published online: 02 June 2021

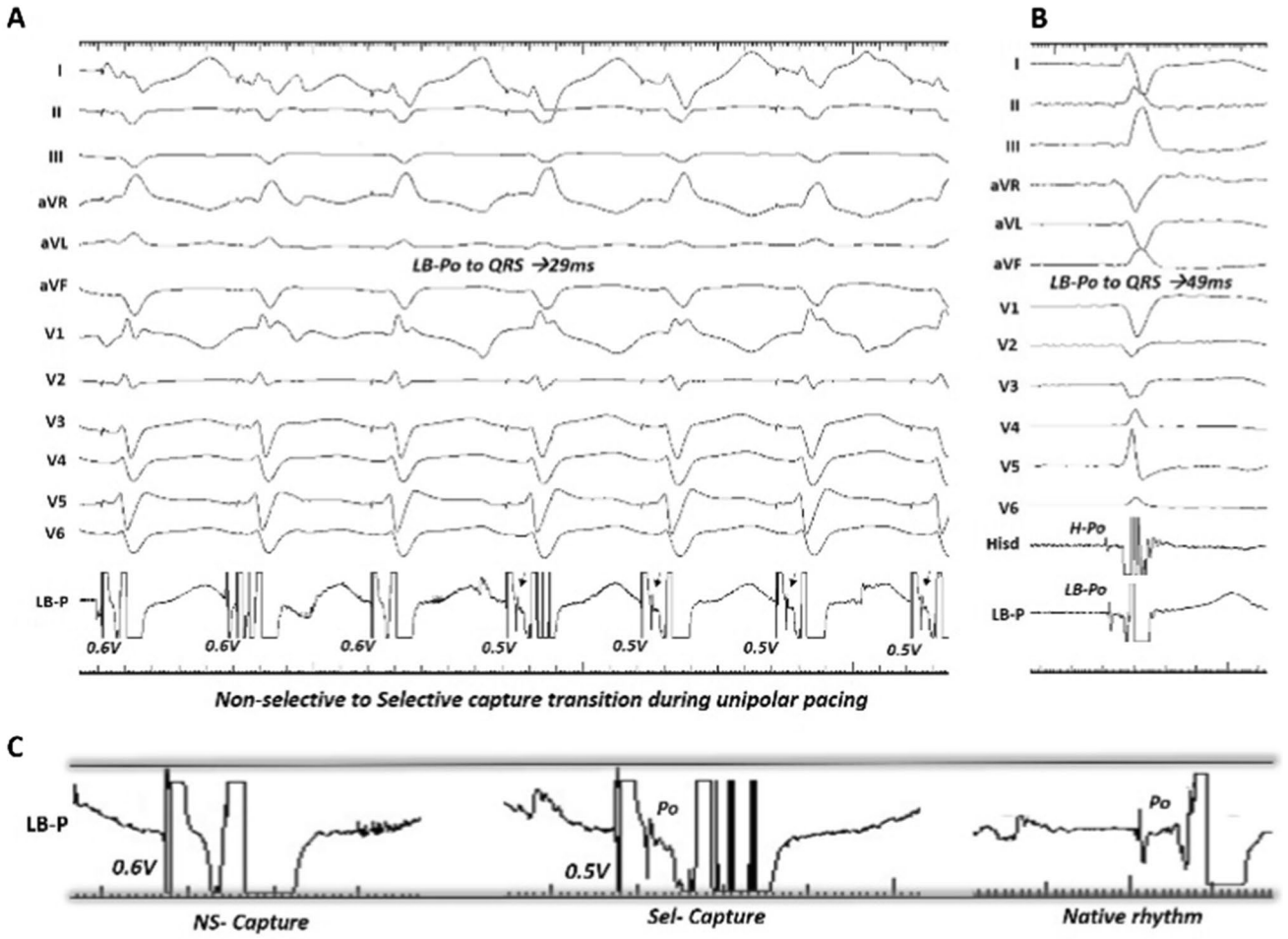

Fig. 1 **A** Non-selective to selective capture transition. Note the appearance of potential (black arrow) after the pacing artefact during selective capture. **B** Electrogram during native rhythm showing HV interval of 54 ms and potential to QRS interval of 49 ms. **C** Magnified view of lead electrogram during non-selective capture, selective capture and during native rhythm. *H-Po* His bundle potential, *LB-Po* left bundle potential, *NS* non-selective

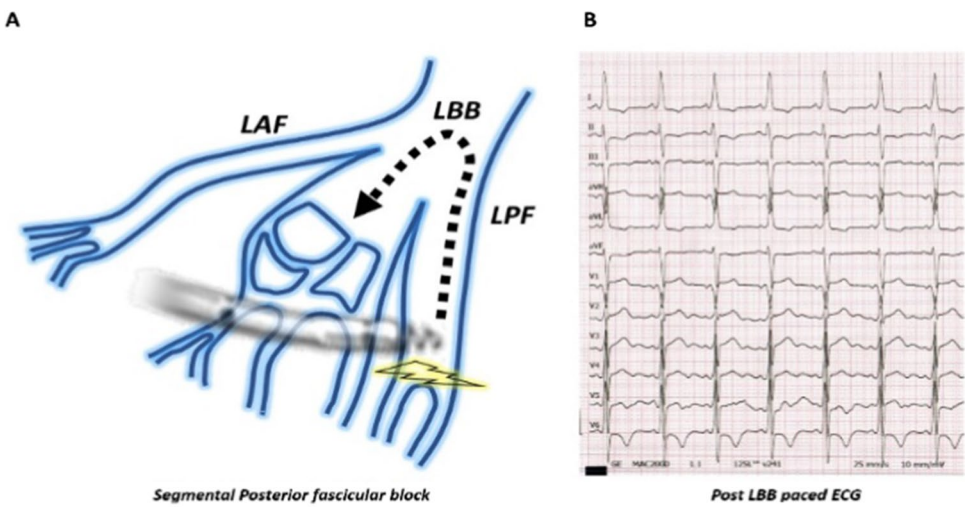

Fig. 2 **A** Diagrammatic representation of segmental fascicular block. **B** Final paced QRS after LBBP with duration of 126 ms. LBB, left bundle branch; LAF, left anterior fascicle; LPF, left posterior fascicle

Authors' contribution All authors have read and approved the manuscript.

Declarations

Ethics approval The study was conducted after getting the ethical committee approval.

Conflict of interest SSP: Consultant: Medtronic.
PV: Honoraria, consultant, research, fellowship support (Medtronic), consultant (Boston, Scientific, Abbott, Biotronik, Eaglepoint LLC).

References

1. Ponnusamy SS, Arora V, Namboodiri N, et al. Left bundle branch pacing: a comprehensive review. J Cardiovasc Electrophysiol. 2020;31(9):2462–73.
2. Tawara S. Das Reizleitungssystem des Saügetierherzens. Jena: GustavFischer; 1906:135–8 [149].

J Innov Cardiac Rhythm Manage. 2021;12(5):4493–4496

The Journal of Innovations in Cardiac Rhythm Management™

DOI: 10.19102/icrm.2021.120506

CARDIAC PACING

IMAGES IN CARDIAC EP

CASE REPORT

Left Posterior Fascicular Pacing

SHUNMUGA SUNDARAM PONNUSAMY, MD, DM, PDF (EP), CEPS,[1] THABISH SYED, DNB (MED), DNB (CARD),[1] and SURYA KUMAR, MBBS[1]

[1]*Department of Cardiology, Velammal Medical College Hospital and Research Institute, Madurai, Tamil Nadu, India*

ABSTRACT. *Left bundle branch pacing (LBBP) is emerging as an alternative to His bundle pacing that overcomes the latter's limitations. Several studies have reported on the safety, efficacy, and electrophysiological properties of LBBP, while postoperative success rates range from 80.5% to 94%. The left posterior fascicle is composed of broad bands of fibers coursing inferiorly and posteriorly toward the papillary muscle, while the anterior fascicle is a thin, tendon-like structure. We report a case of a 70-year-old man in whom left posterior fascicular pacing was done after LBBP failed. We were able to demonstrate all the features of left posterior fascicular capture, including fascicular potential and a left anterior hemiblock pattern, using surface 12-lead electrocardiography. Left posterior fascicular pacing could be an alternative technique when attempts to deploy LBBP fail.*

KEYWORDS. *Left bundle pacing, posterior fascicle, peak left ventricular activation time.*

ISSN 2156-3977 (print)
ISSN 2156-3993 (online)

Introduction

His bundle pacing (HBP) has emerged as an excellent alternative to right ventricular (RV) apical pacing wherein the cardiac conduction system is captured directly. However, although the use of HBP avoids RV pacing–related complications, its use is also limited by technical challenges, high capture threshold, lead dislodgement, and the need for redo procedures.[1] Huang et al. reported an alternative strategy to HBP that involves direct capture of the LBB.[2] LBB pacing (LBBP) provides a low and constant threshold with excellent lead stability and reported success rates that vary between 80.5% and 94%.[3,4] In this report, we describe the case of a 70-year-old man with symptomatic sinus node dysfunction for whom left posterior fascicular pacing was performed after a failure to deploy LBBP.

The authors report no conflicts of interest for the published content. Manuscript received August 14, 2020. Final version accepted October 12, 2020.
*Address correspondence to: Shunmuga Sundaram Ponnusamy, MD, DM, PDF (EP), CEPS, Department of Cardiology, Velammal Medical College Hospital and Research Institute, Madurai 625009, Tamil Nadu, India. Email: shunmuga.pgi@gmail.com.

Case presentation

A 70-year-old male with symptomatic sinus node dysfunction and normal coronaries **(Figure 1)** presented to us for permanent pacemaker implantation. He had recurrent episodes of unprovoked syncope. Echocardiography showed normal left ventricular function and 24-hour Holter monitoring recorded multiple sinus pauses of greater than three seconds.

After obtaining informed consent from the patient for the procedure, LBBP was attempted. Continuous recording of a 12-lead electrocardiogram (ECG) and intracardiac electrograms (EGMs) were recorded using an electrophysiology (EP) system (Abbott, Chicago, IL, USA). As atrial pacing showed atrioventricular Wenchebacking at 110 bpm, a dual-chamber pacemaker was considered. A 4.1-French lumenless 3830 SelectSecure™ lead and a C315 sheath (Medtronic, Minneapolis, MN, USA) were used to capture the left bundle. An attempt to deploy this at a site 1.5 cm below the His bundle along the imaginary line joining the distal His bundle signal to the RV apex failed. A sheath-in-sheath technique using a coronary sinus sheath to provide additional support was also tried without success. Subsequently, a C315 sheath was

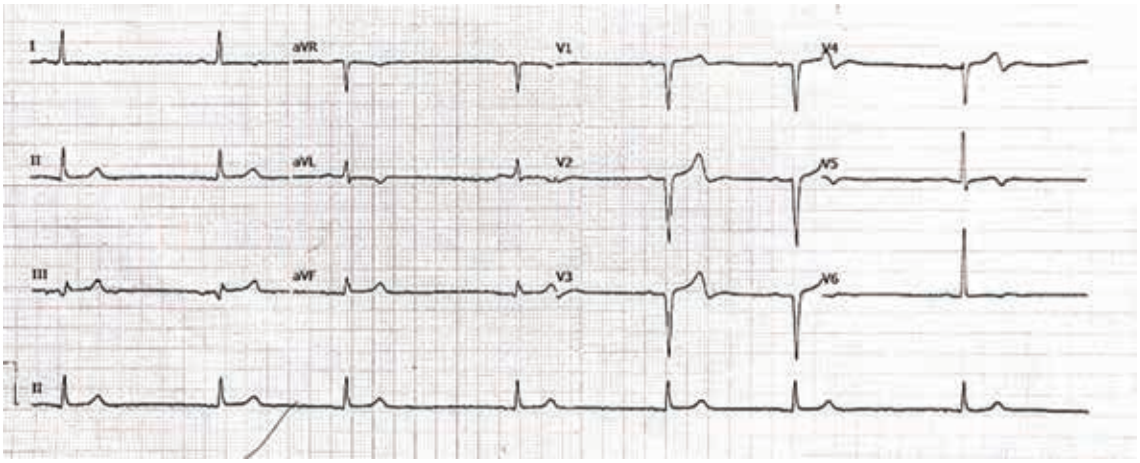

Figure 1: Baseline 12-lead ECG showing sinus bradycardia with normal QRS duration.

positioned 2 cm inferior to the previously attempted site toward the RV apex **(Figure 2A)**. From here, the pacing lead could be positioned deep inside the septum using five rapid turns. The lead-tip EGM showed a sharp fascicular potential preceding the local ventricular signal **(Figure 2B)** with the potential to surface QRS duration of 18 ms. Unipolar pacing showed qR in lead V1, a peak left ventricular activation time of 63 ms in lead V5, and a QRS duration of 115 ms **(Figure 3A)**. Finally, a 12-lead ECG showed rS in inferior leads and a deep S-wave in lead V6 suggestive for left anterior fascicular conduction delay.

Together, the abovementioned features suggested successful capture of the left posterior fascicle by the pacing lead, resulting in a sharp fascicular potential preceding the local ventricular EGM during sinus rhythm and a left anterior hemiblock pattern in the surface ECG. The unipolar pacing impedance was 680 Ω, and the capture threshold was 0.5 V at a 0.6-ms pulse width. The sensed R-wave was 10 mV. The atrial lead was positioned at the right atrial appendage. The final paced ECG showed qR in lead V1 and a left anterior hemiblock pattern with a QRS duration of 115 ms **(Figure 3B)**. The patient recovered well and was discharged the next day without any

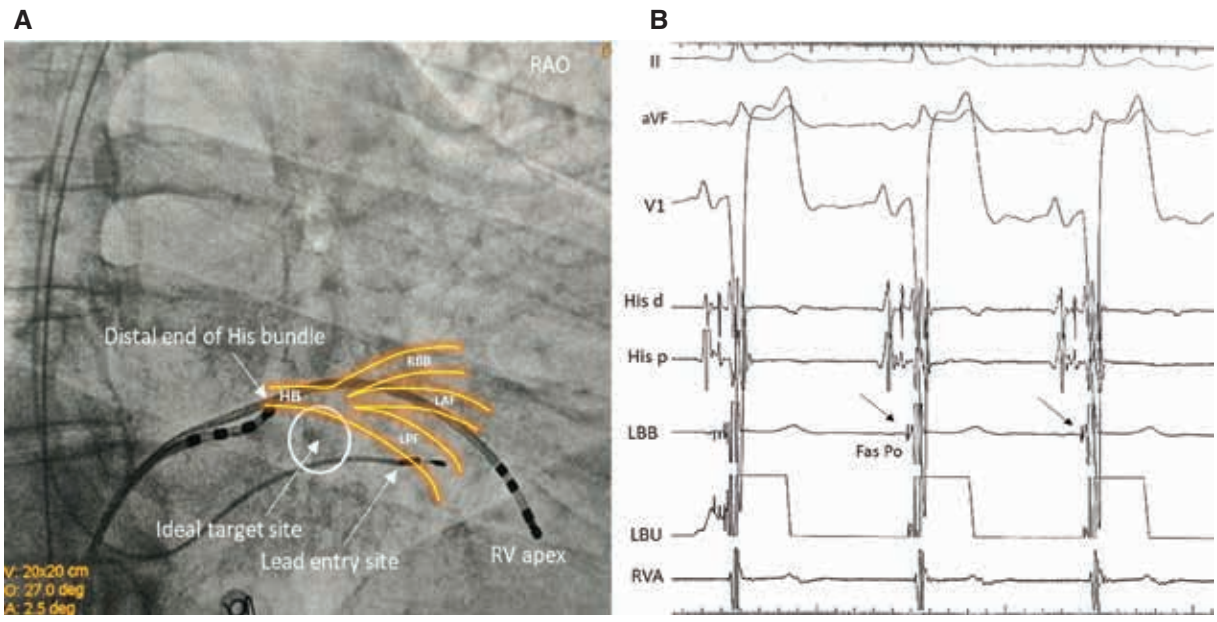

Figure 2: Left posterior fascicular pacing. **A:** A right anterior oblique 30° fluoroscopic view showing the ideal target site (white circled area) and the actual placement of the lead to capture the posterior fascicle. RV: right ventricle. **B:** Intracardiac pacing lead EGMs recorded during sinus rhythm showing a sharp fascicular potential (black arrow) preceding the local ventricular EGM. LBB: left bundle branch pacing lead EGM; His d and His p: His bundle EGM distal and proximal; RAO: right anterior oblique; RVA: right ventricular activation distal EGM; Fas Po: fascicular potential; RBB: right bundle branch; LAF: left anterior fascicle: LPF: left posterior fascicle.

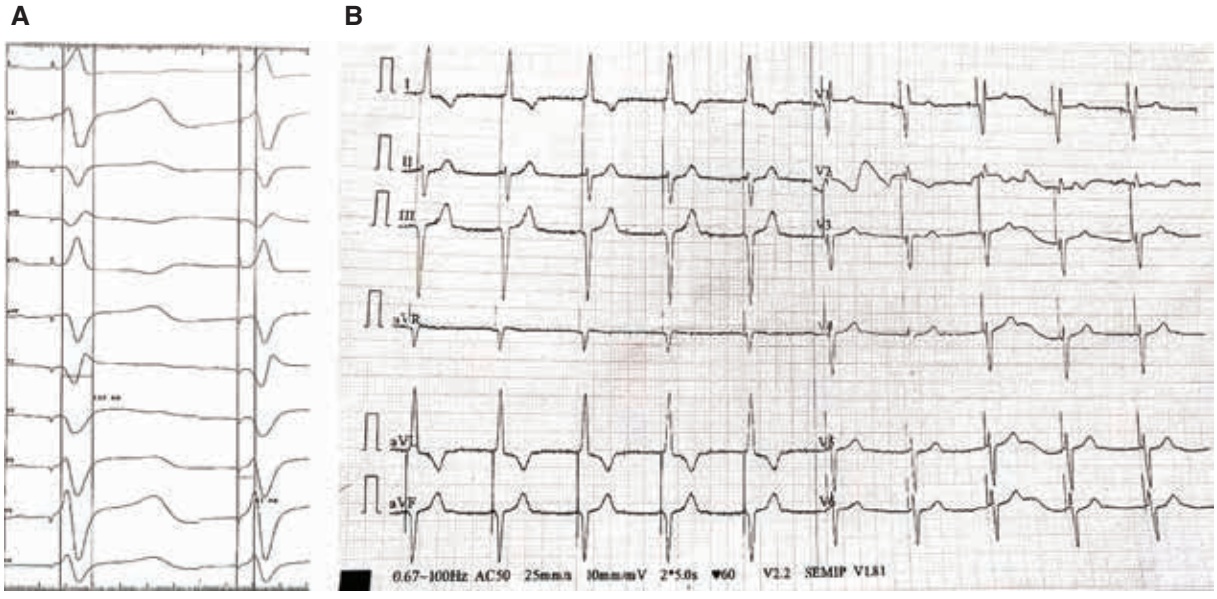

Figure 3: A: The peak left ventricular activation time as measured from lead V5 was 63 ms and the paced QRS duration was 115 ms. **B:** A 12-lead ECG showing qR in lead V1, rS in inferior leads, and a deep S-wave in lead V6 suggestive of left posterior fascicular capture manifesting as left anterior hemiblock.

complications. Three months later, the pacing parameters remained stable with the pacing threshold at 0.5 V at a 0.6-ms pulse width and a sensed R-wave of 9.5 mV. No episodes of syncope occurred following pacemaker implantation.

It is believed that the difficulty encountered in this case was likely due to an inappropriate sheath–septum orientation and the inability of the lead to penetrate sufficiently deep enough into the septum. In such cases, left posterior fascicular pacing can be attempted to capture the conduction system.

Discussion

Huang et al. first described direct capture of the LBB by deep septal pacing.[2] Since then, many studies have suggested the feasibility, safety, and electrophysiological properties of left bundle pacing for the management of symptomatic bradyarrhythmias.[4] The left bundle separates from the branching portion of the His bundle underneath the membranous septum. It gives rise to two branches, the anterior and posterior fascicles, each heading toward the corresponding papillary muscle.[5] The left posterior fascicle is composed of multiple fibers distributed over a broad area in contrast with the anterior fascicle, which is essentially a thin tendon.

Li et al.[3] reported a success rate of 80.5% for LBBP in patients with bradycardia. These authors provided several explanations for the possible failure of left bundle capture, including (1) the inability of the lead to penetrate sufficiently deep enough into the septum; (2) existence of a malpositioned sheath so that the lead cannot go perpendicularly; and (3) a failure of the lead tip to advance due to local hypertrophy. In patients with ischemic cardiomyopathy, a septal scar is an additional factor to consider in unsuccessful positioning of the LBBP lead.

If the left bundle cannot be captured, then posterior fascicular pacing can be attempted by placing the lead 2 cm inferiorly toward the RV apex. This will increase the success rate of conduction system capture. In patients without infra-Hisian complete heart block and complete LBBB, sharp fascicular potentials can be demonstrated preceding the local ventricular EGM during sinus rhythm, as shown in our case. The interval between the fascicular potential to the surface QRS will be less than 20 ms. The paced QRS will have a short LVAT (63 ms in our case) and a left anterior hemiblock pattern.

Conclusion

Although LBBP has a better learning curve than HBP, certain factors limit the capacity to achieve successful lead placement with the latter. In patients in whom the LBB cannot be captured, left posterior fascicular pacing can be attempted before opting for alternative strategies. With further innovations in tools and techniques, the success rate and efficacy of conduction system pacing are expected to increase.

References

1. Zanon F, Ellenbogen KA, Dandamudi G, et al. Permanent His-bundle pacing: a systematic literature review and meta-analysis. *Europace*. 2018;20(11):1819–1826.

2. Huang W, Su L, Wu S, et al. A novel pacing strategy with low and stable output: pacing the left bundle branch immediately beyond the conduction block. *Can J Cardiol*. 2017;33(12): 1736.e1731–1736.e1733.
3. Li Y, Chen K, Dai Y, et al. Left bundle branch pacing for symptomatic bradycardia: implant success rate, safety and pacing characteristics. *Heart Rhythm*. 2019;16(12):1758–1765.
4. Ponnusamy SS, Arora V, Namboodiri N, et al. Left bundle branch pacing: a comprehensive review. *J Cardiovasc Electrophysiol*. 2020;31(9):2462–2473.
5. Rosenbaum MB, Elizari MV, Lazzari JO. *The Hemiblocks: New Concepts of Intraventricular Conduction based on Human, Anatomical and Clinical Studies*. Olsmar, FL: Tampa Tracings; 1970.

Journal of Interventional Cardiac Electrophysiology
https://doi.org/10.1007/s10840-020-00861-4

CASE REPORTS

Unmasking Of pathologic Q waves by left bundle branch pacing

Shunmuga Sundaram Ponnusamy[1] · Pugazhendhi Vijayaraman[2]

Received: 17 August 2020 / Accepted: 4 September 2020

A 61-year-old man with left ventricular ejection fraction of 25% was referred for cardiac resynchronization therapy. He had undergone percutaneous coronary intervention to right coronary artery (RCA) for inferior wall myocardial infarction 3 years ago. Electrocardiography (ECG) showed complete left bundle branch block with QRS duration of 174 ms (Fig. 1a). Coronary angiography confirmed patent stent in RCA. Left bundle branch pacing (LBBP) was done using C315 sheath and 3830 Selectsecure™ lead (Medtronic, Minneapolis, MN) [1] (Fig. 2a). Nonselective to selective capture of left bundle could be demonstrated at near pacing threshold value. Paced ECG showed rSR pattern in lead V1 with QRS duration of 108 ms (Fig. 2b) and peak left ventricular activation time of 65 ms. Inferior leads showed resurgence of Q wave (> 40 ms) corresponding to the old inferior wall myocardial infarction(Fig. 1b and 2b). ECG diagnosis of myocardial ischemia during right ventricular pacing and native left bundle branch block can be difficult as non-physiological activation would result in masking of pathological Q waves and ST segment changes [2]. LBBP restores the physiological activation of the ventricle thereby unmasking the pathological Q waves.

✉ Shunmuga Sundaram Ponnusamy
shunmuga.pgi@gmail.com

[1] Department of Cardiology, Velammal Medical College Hospital and Research Institute, Madurai, Tamil Nadu, India

[2] Geisinger Commonwealth School of Medicine, Geisinger Heart Institute, MC 36-10, 1000 E Mountain Blvd, Wilkes-Barre, PA 18711, USA

Published online: 12 September 2020

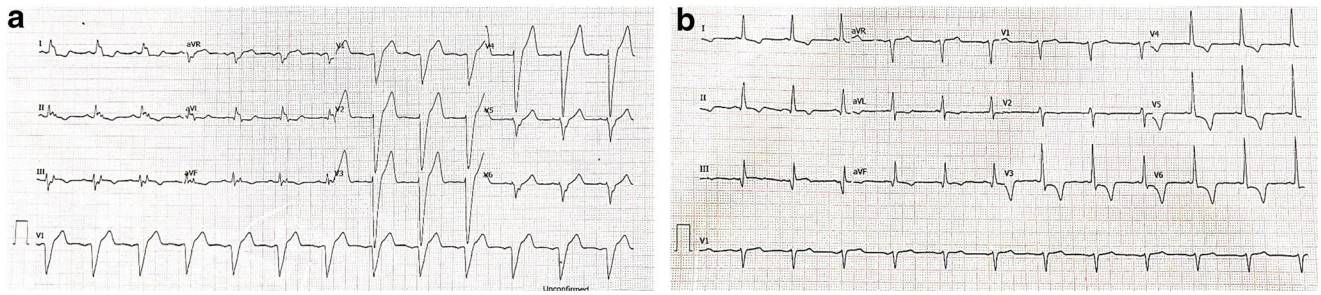

Fig. 1 **a** Baseline 12 lead ECG showing complete LBBB with QRS duration of 174 ms without Q wave in inferior lead. **b** Post-LBBP paced ECG showing narrow QRS (duration 102 ms) with pathological Q in inferior leads and T-wave memory. Right bundle branch delay due to LBBP was corrected by optimizing the AV delay

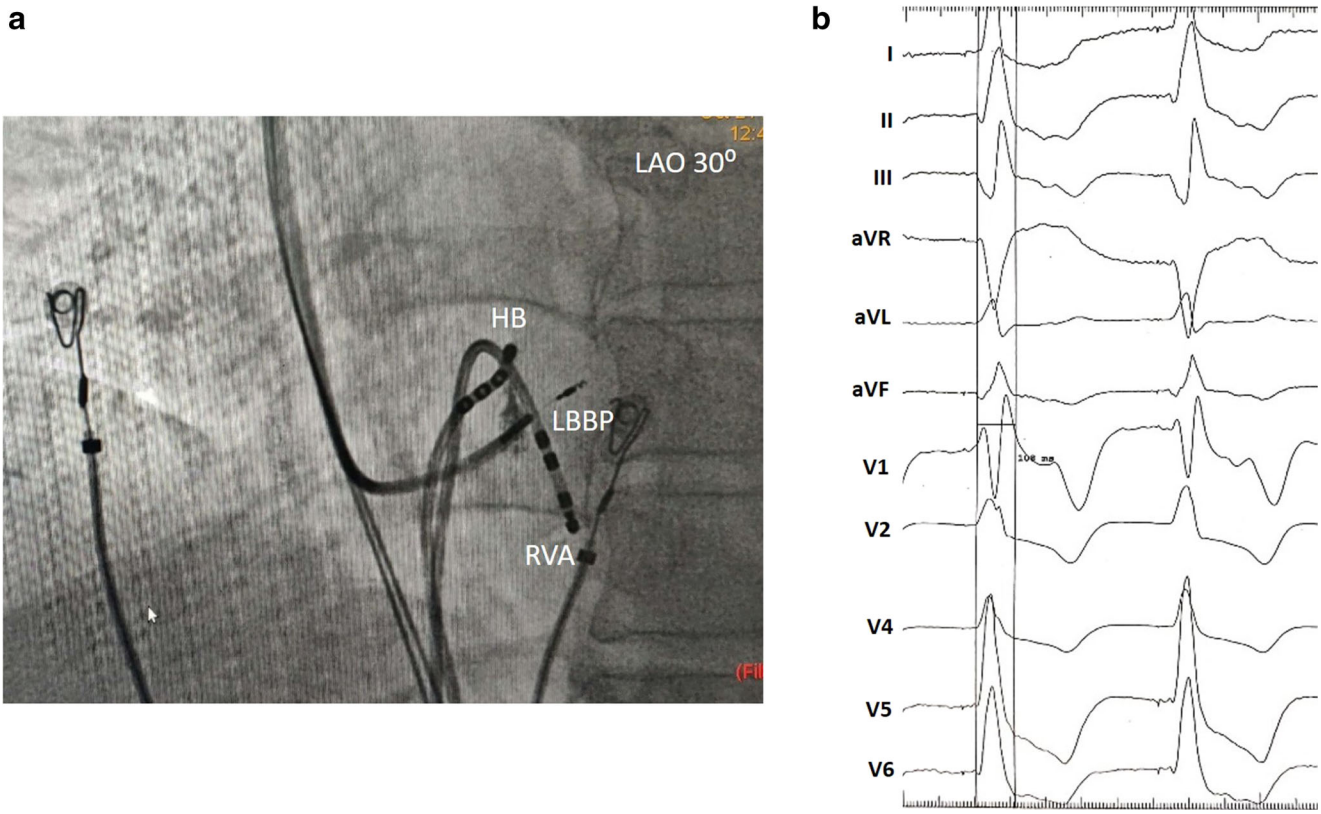

Fig. 2 **a** Fluoroscopic view in left anterior oblique view showing the depth of 3830 pacing lead inside the proximal septum. **b** Unipolar paced ECG showing rSR in lead V1 with rapid left ventricular activation time (65 ms). Note the distinct isoelectric interval between pacing spike and onset of QRS complex. Pathological Q wave (> 40-ms duration) noted in inferior leads. HB, his bundle; RVA, right ventricular apex; LBBP, pacing lead

Compliance with ethical standards

The study was conducted after getting the ethical committee approval. The paper is not under consideration elsewhere. None of the paper's contents has been previously published. All authors have read and approved the manuscript.

Conflict of interest The authors declare that they have no conflict of interest.

References

1. Ponnusamy SS, Arora V, Namboodiri N, Kumar V, Kapoor A, Vijayaraman P. Left bundle branch pacing: a comprehensive review. J Cardiovasc Electrophysiol. 2020;31:2462–73. https://doi.org/10.1111/jce.14681.
2. Herweg B, Marcus MB, Barold SS. Diagnosis of myocardial infarction and ischemia in the setting of bundle branch block and cardiac pacing. Herzschrittmacherther Elektrophysiol. 2016;27:307–22.